Studies on Polylactic Acid based Nanocomposites for Improved Dispersion and Sensor Applications

Thesis submitted in partial fulfilment of the requirements for the degree of

DOCTOR OF PHILOSOPHY

By

Gourhari Chakraborty

(Roll No. 136107009)

Department of Chemical Engineering

Indian Institute of Technology Guwahati

Guwahati-781039

Assam, India

November, 2019

Dedicated to

My Beloved Grandparents

Late Jagabandhu Ghoshal

and

Smt. Kamalarani Ghoshal

Department of Chemical Engineering

Indian Institute of Technology Guwahati

DECLARATION

The research work in the thesis entitled "**Studies on Polylactic Acid based Nanocomposites for Improved Dispersion and Sensor Applications**" has been carried out by me in the Department of Chemical Engineering at Indian Institute of Technology Guwahati under the supervision of Prof. Vimal Katiyar and Prof. G. Pugazhenthi. The results documented in this thesis have been achieved by me and has not been submitted to any other university or institute for the award of any degree or diploma. I declare that I have faithfully acknowledged and given credits to the research workers wherever their works have been cited in this thesis. I further declare that I have not wilfully copied any other work, paragraph, text, data, result, etc., reported in journals, books, magazines, reports, dissertations, thesis, etc., or available in websites and have not included them in this thesis or presented them as my own work.

(**Gourhari Chakraborty**)

Roll No.: 136107009

Department of Chemical Engineering

Indian Institute of Technology Guwahati

Guwahati-781039, India

Department of Chemical Engineering

Indian Institute of Technology Guwahati

CERTIFICATE

This is to certify that the research work in the thesis entitled "**Studies on Polylactic Acid based Nanocomposites for Improved Dispersion and Sensor Applications**" being submitted by Gourhari Chakraborty for the award of Ph.D. degree has been carried out by him in the Department of Chemical Engineering at Indian Institute of Technology Guwahati under our guidance and supervision. The work documented in this thesis has not been submitted to any other university or institute for the award of any degree or diploma.

(**Prof. Vimal Katiyar**)
Professor
Department of Chemical Engineering
Indian Institute of Technology Guwahati
Guwahati-781039, India

(**Prof. G. Pugazhenthi**)
Professor
Department of Chemical Engineering
Indian Institute of Technology Guwahati
Guwahati-781039, India

Acknowledgment

With heartfelt pleasure and sincere gratitude, I take this opportunity to convey my sincere thanks to the persons who directly or indirectly helped me to conduct my research work. Firstly, I bid my respect and gratitude to my grandfather, **Late Jagabandhu Ghoshal** who was the main source of inspiration and knowledge throughout my life. He and my grandmother, **Smt. Kamalarani Ghoshal** with their immense greatness had taken care of me, my knowledge and my development from childhood till Ph.D. Then comes the contributions of my respected supervisors, **Prof. Vimal Katiyar and Prof. G. Pugazhenthi** whose constant support, supervision, guidance and encouragement helped me to build my every single step in this Ph.D. journey. I am grateful to my respected supervisors for their kind help and valuable suggestions. I would like to thank my Doctoral Committee members **Prof. Bishnupada Mandal, Dr. Amit Kumar** and **Prof. Gopal Das** for their continuous support, meaningful criticisms and valuable suggestions during my every progress evaluation seminar. Execution of this research work only became possible and smooth because of the sophisticated instruments and equipments provided by **the Centre of Excellence for Sustainable Polymers (CoE-SusPol)** and **Central Instruments Facility (CIF), IIT Guwahati**. I am really indebted to CoE-SusPol, CIF and Department of Chemical Engineering for providing the necessary analytical facilities. I am thankful to the Head and all departmental authorities including technical and non-technical staff of the Department of Chemical Engineering. I am also thankful to **Deep Jyoti Sinha, Sailen Das, Ritumoni Kalita, Jayanta Kumar Mout, Dr. Lukomoni Borah, Harsaraj Biswanath, Dipak Kumar Barman, Debojit Borah, Pankaj Sekhar Baruah** and **Bhagya Boro** for helping me whenever required. I am thankful to **Narendran S, Dr.**

Ravibabu Valapa, Dr. Arvind Gupta, Dr. Prodyut Dhar and Sayan Bhattacharjee for spending their valuable time and helping me during the tenure of my research work. My thanks are also due to my lab mates including seniors, juniors, friends and staff, especially **Narendren S, Shasanka Sekhar Borkotoky, Monika, Melaku Tesfaye, Surendra Singh Goud, Siddharth Mohan Bhasney, Riddhi Mahansaria, Medha Mili, Naba Kalita, Kiran Kumar Gali, Chetna M, Neha Mulchandani, Tabli Ghosh, Pankaj Boruah, Kona Mandal, Mohammed Modu Aji, Munmi Das, Doli Hazarika, Deepshikha Das, Bhanupriya Das, Victor Sharma, Sourav Pratim Kashyap, Dr. Purabi Bhagabati, Dr. Prasanta Baishya, Dr. Akhilesh Pal, Dr. Rahul Patwa, Dr. Neelima Tripathi, Dr. Arbind Prasad** and **Lakhya Dhar Boro** for their help in the lab. I would like to thank **Ranganath Bhaiya** and **Sachin** for helping me in a part of my work. I am also thankful to my close friends **Atanu Kumar Paul, Basudhrity Banerjee, Pradip Das** and **Sonali Ghosh** who supported me during this journey. Last but not the least, I would like to thank my **parents and family members,** especially my maternal uncle, **Prof. Aloke Kumar Ghoshal**, for their continuous encouragement and support. In the end, I would like to thank one and all who have helped me in any form at any time for the successful completion of my Ph.D. I am thankful to the **Almighty** for blessings.

[Gourhari Chakraborty]

Abstract

Polylactic acid (PLA) is one of the leading bio-based and biodegradable polymers with thermoplastic nature, moderate processing temperature window, good mechanical property and hydrophobic character. However, one of the major limitations of PLA is its nonconductive nature, which prevents it to be applicable for conductive applications, particularly as electrochemical and biochemical sensors. Incorporation of carbon allotropes can improve the electrical mobility of the composite and in the presence of additives, its performance can be enhanced. Incorporation of carbon allotropes can improve the electrical mobility of the composite and in the presence of additives, its performance can be enhanced. Hence, it was inferred that very less work had been conducted to improve the dispersion of carbon fillers without altering its chemical structure, particularly for melt processing. Studies on the conductive application of PLA in combination with carbon allotrope like graphene is very limited. Studies on the applicability of PLA composite system in combination with different additives for sensing of different stimuli like organic solvents, carbohydrates, amino acids and metal ions have not been explored much. Compatibility of PLA with magnetic nanoparticles and extending its application towards sensing of organic vapour has been studied very little. In general, studies on the effect of dispersion on different properties of PLA for different applications using the same filler by modifying the processing route and the compatibility investigation for the application of magnetic particle based PLA composites have not been explored much.

In view of the above, the present doctoral work is targeted to study different dispersion techniques to promote uniform dispersion of graphene in the PLA matrix in case of melt processing. In order to accomplish this, solvent coating and non-covalent master-

batch approaches were adopted without any structural changes of GR. Secondly, PLA and GR nanocomposites were made for the detection of different molecules like organic solvents, glucose, glycine and metal ions. Different additives like iron decorated cellulose nanocrystal (Fe-CNC), albumin, ethylenediaminetetraacetic acid (EDTA) and silk nanocrystal (SNC) were used in order to improve the sensitivity of PLA/GR composites towards the targeted electrochemical or biosensing applications. Finally, in order to utilize PLA for vapour sensing, carbon templated magnetic nanoparticles were incorporated into PLA and a 3D printed gas chamber along with interdigital electrode based sensing set up was constructed and applied to test ethanol vapour detection. The present doctoral thesis work has been arranged in eight chapters as follows:

The First Chapter of the thesis briefly introduces polylactic acid (PLA) and its characteristics; nanocomposites in general and PLA based nanocomposites, with a focus on its applicability as a conductive material; various dispersion techniques; and merits and demerits of PLA based conductive nanocomposites for application as sensors. Then, it discusses the scope and structure of the thesis. The chapter then presents a thorough review of literature in the areas pertinent to the thesis and highlights the gap areas for future research. The chapter ends with discussion about the motivation behind the work and objectives of this research work.

In Chapter 2, effect of dispersion of graphene (GR) was investigated in melt-processed PLA, fabricated by solvent coating of GR over PLA prior to extrusion. The effect of melt processing on different graphene loaded composites (PLA-M-0.05GR and PLA-M-0.2GR) was studied. X-ray diffraction (XRD) study and morphological analyses confirmed the formation of well-dispersed composite. Thermo-gravimetric analysis and kinetic study revealed significant improvement in thermal stability. Improvements in crystallinity, melting point and crystallization point were found from differential

scanning calorimetric (DSC) analysis. Crystallization kinetic study was carried out and the nucleation effect of GR on crystallization of PLA chain was determined. Tensile properties and dynamic mechanical properties were also investigated. Melt rheology and solution viscosity measurements were carried out to study the structural and flow nature of the composites. Pristine polymer (PLA-M) and its composites (PLA-M-0.05GR and PLA-M-0.2GR) showed shear thinning behavior. Excellent dispersion of GR and single-phase nature of the composites were noticed by studying Han plot, Cole-Cole plot and van Grup-Palmen's plot.

The work in Chapter 3 attempted to improve the dispersion of graphene through coating of master-batch (MB) on PLA before melt processing. In situ polycondensation reaction of lactic acid oligomer was utilized to prepare the MB of exfoliated graphene (GR). MB dispersed composites of PLA were fabricated by melt extrusion of MB coated PLA. One normal coated composite without MB (PLA-M-0.2GR) was fabricated for comparison purpose. XRD analysis, Raman spectroscopy and morphological studies revealed better compatibility, dispersion and interaction of GR in case of MB diluted composite as compared to normal coated composite. Thermal stability, crystallization properties and mechanical properties of the composites were examined and the effect of short PLA chains in case of MB diluted composites was studied. Melt rheology nature of the composites was examined. Cole-Cole plot and Han plot suggested uniform distribution of graphene. PLA-MB-0.05GR showed improved modulus and elongation at break, better dispersion of GR and comparable thermal stability with high activation energy.

Chapter 4 demonstrates the utilization of exfoliated graphene (GR) for the fabrication of conductive PLA/GR nanocomposites, which were characterized by XRD, field emission scanning electron microscopy (FESEM) and impedance analysis. Optimum

loading was found to be 1.7 wt.% GR. A new concept of equivalent polymer length was introduced for the impedance behavior of the composites. Composite containing 2.5 wt. % GR loading showed the most stable conductivity and was taken as the model composite film, which yielded good sensitivity and high selectivity for ethanol detection. The composites showed good reusability and reproducibility. Sensitivity and detection behaviour of PLA/GR composite towards other alcohols like methanol, isopropanol, isobutanol and organic solvents having different functionality were also examined in this chapter.

In Chapter 5, iron oxide decorated cellulose nanocrystal (Fe-CNC) was incorporated into PLA and exfoliated graphene (GR) system (PLA-S-2.5GR) to investigate the impact of Fe-CNC inclusion on the various properties of PLA/GR composite system and to optimize the Fe-CNC loading. Thermal, mechanical, morphological and impedance analyses of different iron-loaded composites were conducted. Fe-CNC loading of 0.5 wt.% (PLA-S-2.5GR-0.5Fe) was found to have comparable thermal stability, better dispersion, better mechanical strength and unaltered GR networks inside the composite. Then, PLA-S-2.5GR-0.5Fe was utilized as ethanol sensor. Recycle study, reusability study and repeatability study, followed by stability analysis of the composite after use were conducted. The PLA based composite film, possibly for the first time, was successfully used as an electrode for the detection of biomolecules such as D-glucose and glycine.

Chapter 6 attempted the fabrication of thin-film based metal ion sensor, where PLA was used as the matrix with the aim to detect copper ion as the representative metal ion. GR was used as the reinforcement material to impart high conductivity in the PLA/GR composite. A comparison of concentration detection with commercial conductivity meter was also carried out. Dependency of current in different metal ions and different

anionic environment was also studied. Different materials such as EDTA, albumin and SNC, having bonding property with metal ions, were also incorporated into the PLA/GR system in order to improve the sensitivity and selectivity towards copper ion chosen for this work. Basic characteristics like morphology, thermal stability, crystallization property and dynamic mechanical strength of the composite films were investigated before use as a sensor.

Chapter 7 includes the synthesis of magnetic nanoparticle from graphene oxide (GO) and oxidized carbon fiber (CF). Co-precipitation technique was adopted to prepare magnetic materials like GO-Fe, GO-FC and CF-Fe. These magnetic materials were found to have good ferromagnetic properties. Impact on different properties like morphology, thermal stability, crystallization nature, magnetic rheological behaviour and impedance was analysed using fabricated PLA based composites of 0.5-2 wt.% filler loading. An ethanol vapour detection set up was fabricated by combining 3D-printing and interdigital electrode. Representative materials were tested for ethanol vapor sensing under nitrogen flow environment. Response was found to be increasing within 10 seconds. A comparison of performance for ethanol sensing was carried out between the present and the previously used composites.

Chapter 8 presents the findings and conclusions of the research work and also indicates the future direction of the research.

Contents

List of Figures

List of Tables

Nomenclature

Abbreviations

ASTM	American society for testing and materials
ATR	Attenuated total reflectance
CNC	Cellulose nanocrystal
CF	Carbon fiber
CF-Fe	Iron decorated carbon fiber
CNT	Carbon nanotube
CNW	Cellulose nanowhiskers
DCC	N, N' di-cyclohexyl carbodiimide
DCM	Dichloromethyelene
DMA	Dynamic mechanical analysis
DSC	Differential scanning calorimetric
EB	Elongation at break
EDTA	Ethylenediaminetetraacetic acid
FESEM	Field emmision scanning electron microscope
FTIR	Fourier transform infrared spectroscopy
GNS	Graphene nanosheet
GNP	Graphene nanoplatelets
GO	Graphene oxide
GR	Exfoliated graphene
HDPE	High density polyethylene
LDH	Layard double hydroxide
LLDPE	Linear low density polyethylene
MB	Master batch

MC	Methylated Cellulose
MMT	Montmorillonite
MWCNT	Multiwall carbon nanotube
NCC	Nanoparticle calcium carbonate
PE	Polyethylene
PP	Polypropylene
PLA	Polylactic acid
PLLA	Poly L-lactic acid
PCL	Poly caprolactone
PEG	Poly ethyelene glycole
PET	Polyethylene terephthalate
PHB	Poly hydroxybutyrate
PGA	Polyglycolic acid
PS	Polystyrene
ROP	Ring opening polymerization
SNC	Silk nanocrystal
SWCNT	Single wall carbon nanotube
TGA	Thermogravimetric analysis
THF	Tetrahydrofuran
TEM	Transmission electron microscope
TRG	Thermally reduced graphene
TS	Tensile strength
XRD	X-ray diffraction

Notations

A/ A°	Pre-exponential factor
E_a/E	Activation energy

I	Current
n	Avrami exponent
R	Universal gas constant
T_g	Glass transition temperature
T_m	Melting Temperature
T_{cc}	Cold crystallization temperature
T_{onset}	Onset degradation temperature
T_{50}	Temperature at 50% degradation
T_{max}	Temperature at maximum degradation rate
R_{rel}	Relative change in response
V	Voltage
Z	Impedance

Greek letters

α	Degree of conversion
β	Heating rate
η	Intrinsic viscosity
η^*	Complex viscosity
ρ	Resistivity
θ	Diffraction angle
σ	Ultimate tensile strength
ε	Elongation at break

Chapter 1

Introduction and Literature Review

Abstract

This chapter of the thesis briefly introduces polylactic acid (PLA) and its characteristics; nanocomposites in general and PLA based nanocomposites with a focus on its applicability as a conductive material; various dispersion techniques; and merits and demerits of PLA based conductive nanocomposites for application as sensors. Then it discusses the scope and structure of the thesis. This chapter also presents a thorough review of literature in the areas pertinent to the thesis and highlights the gap areas for future research. The chapter ends with the motivation behind the work and objectives of this research work.

Parts of this chapter has been published as the following book chapters:

G. Chakraborty, P. Bhagabati and V. Katiyar, Author's viewpoint on the developments of biodegradable polymers to improve their versatility in food packaging, Biobased plastics for food packaging applications, Smithers Pira, 2017, (eBook ISBN: 978-1-91024-259-9, Hardback: 978-1-91024-258-2)

G. Chakraborty, V. Katiyar, Biobased Polymeric Conductive Materials for Advanced Applications, Advances in sustainable polymers: Processing and Applications, Springer (Press)

1.1 Introduction

Manufacturing of cost-effective product with versatile applicability is always a desirable target for its commercialization. A large number of conventional products made up of metals and ceramics is nowadays replaced by polymeric substances. Incorporation of polymer not only adds to quality and area of application but also makes the production more profitable. As a result, polymeric products are becoming inevitable in every section of society (Flory, 1953; Kumar & Gupta, 2018). However, in spite of several inherent advantages, most of the petroleum based plastics are associated with certain serious issues such as disposal of solid waste and scarcity for raw material. In particular, the solid waste generated by petrochemical-based polymers serves as environmental hazards, which causes a major threat for the survival of living organisms due to uncontrolled disposal of solid polymeric waste and emission of CO_2 and toxic substances upon open-air burning of such polymeric waste. In view of limited resources of petroleum feedstock, researchers are looking for renewable resource-based polymers as alternatives. Thus, non-availability of feed and degradation issues of disposals are the main reason for the rising demand for bio-based and biodegradable polymeric products (Babu et al., 2013; Reddy et al., 2013b).

Hence, biodegradable polymer based products have originated as an obvious alternative to the non-renewable polymer based materials. The biopolymers derived from renewable resources find commercial value particularly in short-period packaging applications and commonly used disposable goods, which include plates, cups, food item wrappers, utensils, trash bags, beverage containers, medical devices, etc. Most of the biodegradable materials are manufactured from bio-based feedstocks and easily degradable by microorganisms under controlled environmental conditions. Biodegradable thermoplastic polymers such as polylactic acid (PLA),

polyhydroxyalkanoate (PHA) and polycaprolactone (PCL) have the capability to fulfil the commercial needs along with environmental sustainability (Auras et al., 2004; Ojijo & Ray, 2013a; Rhim et al., 2013a).

PLA, a potential thermoplastic polymer, having biocompatible and biodegradable nature has become a widely used bio-plastic material. Ring-opening polymerization (ROP) of lactide or direct polycondensation is the synthesis routes for the production of PLA from lactic acid. PLA possesses the remarkable properties to be used as a product for even direct food contact packages. Many industries have already commercialized cups, cutlery and food containers made of PLA. The latter can also be used to laminate paper and paperboard by extrusion coating to enhance its application as packaging material (Auras et al., 2004). Other major application areas where nowadays PLA is being used as basic ingredient for commodity production include biomedical, electronics and drug delivery (Drumright et al., 2000; Raquez et al., 2013b).

PLA exhibits comparable Young's modulus and impact strength with commodity polymers, like polyethylene (PE), polypropylene (PP), polystyrene (PS), and polyethylene terephthalate (PET) (Nampoothiri et al., 2010). However, the thermal stability of PLA is low and thus shows rapid loss of molecular weight because of random main-chain scissions. This molecular weight loss becomes higher above the melting point of PLA. The post-production application of the polymer for casting into products involves processing operations like injection moulding, extrusion and blow moulding, which cause decrement of properties because of such loss in molecular weight. Therefore, PLA having low melting point grades can have narrow processing window. Eventhough PLA is highly useful and attractive material for commercialization, improvement in barrier properties, mechanical properties and

processing stability are required for high temperature application and for replacement of petroleum-based plastics (Taubner & Shishoo, 2001).

Several strategies have been reported in literature to regulate PLA properties by changing processing technology or modifying chemical composition and components. Reinforcement of PLA with various fillers like carbon fillers, clays, inorganic compounds and biomaterials (cellulose nanocrystals, cellulose whiskers and bio fibers) has been reported (Lim et al., 2008; Murariu & Dubois, 2016). It was found that the incorporation of filler materials has significantly contributed to improve the properties of PLA, especially when the filler dimension is in nanometre range (Jamshidian et al., 2010; Raquez et al., 2013b). Recently, various carbon allotropes such as graphene oxide, graphene nanoplatelets, expanded graphite and reduced graphene oxide have drawn interest as fillers for PLA nanocomposites due to their exceptional electrical, thermal, optical and mechanical properties (Norazlina & Kamal, 2015). Exfoliated graphene (GR) has emerged as novel filler to improve the mechanical properties of PLA. However, agglomeration of graphene is still a problem for exfoliated graphene reinforced PLA composites (Valapa et al., 2015a). Melt processing of PLA composites is always associated with phase separation, degradation of polymeric substrate and non-uniform distribution of filler (Murariu et al., 2010). Therefore, it is necessary to overcome the challenges that underlie in dispersion of GR into PLA matrix by extrusion so as to come up with commercially viable plastic materials. In this perspective, novel approach is being used to promote the dispersion of GR in the PLA matrix prior to melt extrusion.

Along with dispersion and industrial-scale production of PLA/GR nanocomposite, diversity of application of nanocomposites also needs to be focused. GR with high electrical conductivity can add conductive nature to the fabricated PLA/GR

nanocomposites (Singh et al., 2011). Conductive material finds several types of applications such as sensor, battery, semiconductor, etc (Feig et al., 2018; Mai et al., 2013). Electrochemical sensors and biosensors have nowadays become important devices to detect diseases and quantify particular component in the biomedical field for proper diagnosis (Gan & Hu, 2011; Liu et al., 2013). Different modification strategies of GR and PLA/GR nanocomposites can therefore be incorporated to enhance the application range.

1.1.1 Polylactic acid (PLA)

PLA is one of the leading biodegradable polymers with wide range of application domains because of comparable properties similar to commercial polymers like polyethylene, polypropylene, polystyrene, etc. Bio-based nature, biocompatibility, thermoplasticity, various synthesis options and ecofriendliness have made PLA lucrative and prominent alternative to conventional commodity materials (Södergård & Stolt, 2002). PLA can be synthesized from lactic acid by direct polycondensation or ring-opening (ROP) of lactide. Lactic acid is optically active. Hence, both D and L type molecules can combine in multiple combinations during polymerization to generate multiple varieties of PLA starting from homopolymeric to block and stereo complex PLA (Fig. 1.1). Different metallic compounds such as aluminum, zinc, tin are utilized as catalyst for the production of PLA. ROP of lactide is carried out to get higher molecular weight PLA instead of direct melt polycondensation. Along with conventional heating, microwave assistance is also taken nowadays for fast production of PLA. PLA possesses –OH and –COOH as terminal groups, which give possibility of co-polymerization with similar class of polymers or grafting with other polymers giving copolymers with application oriented properties (Nampoothiri et al., 2010; Xiao et al., 2012).

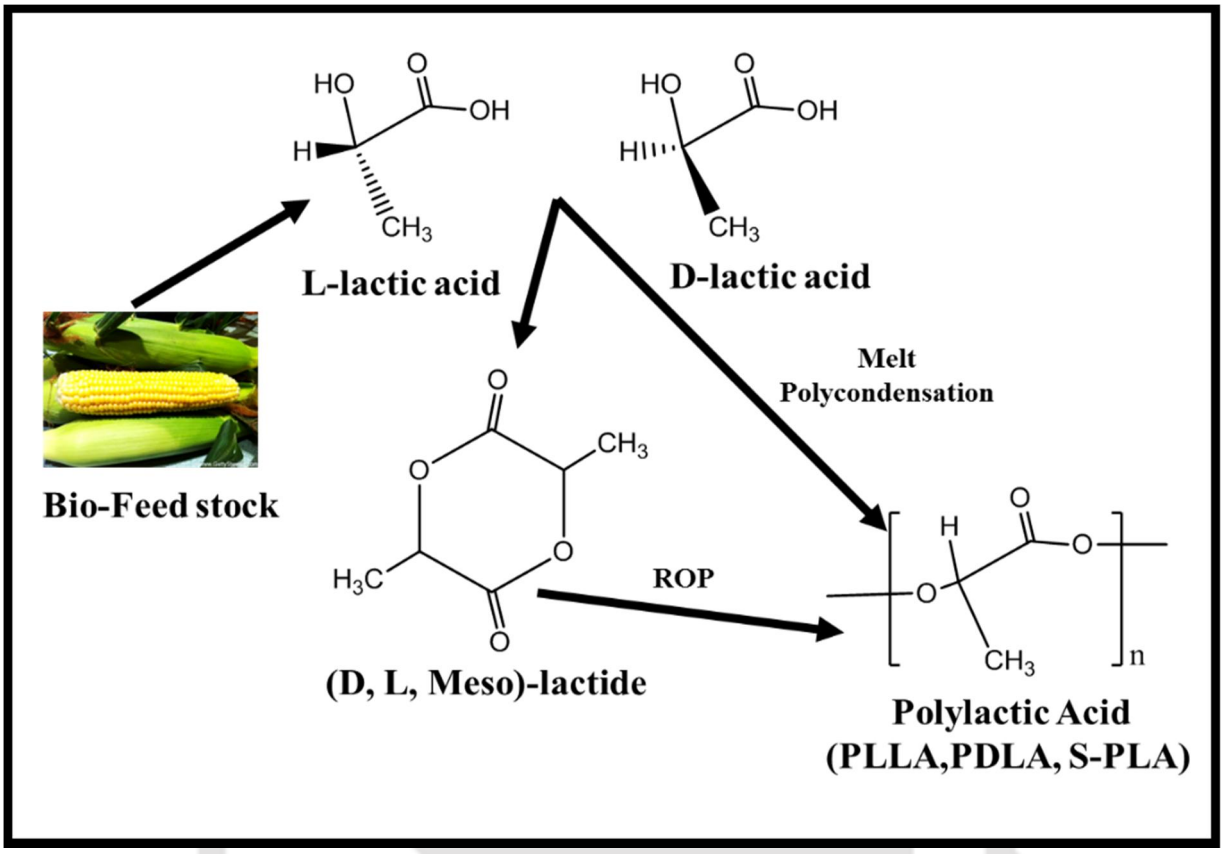

Fig. 1.1 Synthesis routes of PLA

Properties of the PLA depend on the crystalline nature, molecular weight and monomer unit during synthesis. Thermal properties depend on the type of monomer unit of the PLA. Glass transition temperature varies between 51 to 63 °C and melting temperature varies between 180 to 210 °C depending upon the optical activity of the monomer unit of PLA. Stereo complex PLA generally has higher density and crystallization nature compared to homopolymeric PLA. Amorphous PLA has density ~ 1.25 g/cm^3 and crystalline PLA can have density in the range of 1.35-1.49 g/cm^3. Rheological behavior conveys linear chain nature and pseudoplastic behavior of PLA. PLA is hydrophobic in nature and soluble in solvents like chloroform, dichloromethane, tetrahydrofuran (Drumright et al., 2000). Some of the properties of different grades of PLA are presented in Table 1.1.

Table 1.1 Properties of different types of PLA (Mehta et al., 2005)

PLA	Tensile Strength (MPa)	Elongation at break (%)	Glass transition Temperature (°C)	Melting Temperature (°C)
L-PLA (M.W.-50000)	28	6	54	170
L-PLA (M.W.-100000)	50	3.3	58	159
L-PLA (M.W.-300000)	48	2	59	178
D,L-PLA (M.W.-107000)	29	6	51	-
D,L-PLA (M.W.-550000)	35	5	53	-

PLA possesses comparable properties similar to conventional polymers to be applied to almost all applications like packaging, biomaterial, etc. However, some properties such as poor melt strength, low processing window, low heat deflection temperature and thermal degradation during melt processing are the obstacles towards its wide applicability (Kopinke et al., 1996). Biomedical application needs moderate hydrophilicity, controllable degradation nature at different pH and casting uniformity, which are not satisfied by virgin PLA (Lasprilla et al., 2012). PLA is not conductor of heat and electricity. This restricts its application in the area of conductive biomaterials. Packaging application requires improved barrier property towards oxygen, water vapour and aroma, which are lacking in case of PLA. Along with the melt processing, melt casting of PLA causes drastic reduction in the molecular weight. This is associated with defects like necking, shrinking and crack, because of its brittle nature and less melt stability at higher temperatures. Apart from the above drawbacks, synthesis routes also lead to high production cost of PLA, which makes it expensive for commercial

production. In order to utilize PLA as commercially viable material, modification or improvement of the properties is necessary. Modification of synthesizing route, nanocomposite fabrication and blend preparation are some of the techniques being used to improve the properties of PLA and extend its application in multiple directions with reduced cost or towards value-added products (Castro-Aguirre et al., 2016).

1.1.2 PLA-nanocomposites

Nanocomposites are engineered materials utilized for versatile applications with desired effectiveness (De Azeredo, 2009). Different inorganic substances and biomaterials are reinforced to PLA to fabricate nanocomposites, which improves the properties of PLA or extends its application to versatile dimension. PLA based nanocomposites can be the replacement for conventional commodities as cost-effective, better quality, lightweight and easy to handle composite materials. Nanocomposite fillers with high aspect ratios increase interaction between matrix and reinforcing substances and thus enhance the strength and modulus. Depending upon the filler type and application, thermal stability, conductivity, barrier property, surface nature, crystallization and degradability of PLA based nanocomposites can be improved (Raquez et al., 2013b).

Typical reinforcing substances include,

- *Particulate material*: CNT, silicates, graphene, etc (Kuilla et al., 2010; Sinha Ray et al., 2003).
- *Fiber material*: carbon nanofiber, aramid fiber, boron fiber, naturally occurring cellulose fibers, etc (Faruk et al., 2012; Silvestre, Duraccio, & Cimmino, 2011).

Some of the reinforcing agents along with properties are presented below-

- *Graphene/Graphene-based substances*: Graphene is a new attractive carbon material with a honeycomb and one atom thick structure having carbon-carbon distance of 0.142 nm (Fig. 1.2). It covers a wide range of compounds with different structure and surface nature such as graphite, expanded graphite, graphene oxide (GO) and thermally reduced graphene (Singh et al., 2011). These materials have excellent mechanical and physicochemical properties. Graphene is a zero-gap semiconductor with high thermal conductivity (> 5000 $Wm^{-1}K^{-1}$) and Young's modulus (1TPa). Graphene is used to increase the electrical conductivity, thermal stability, barrier and mechanical property. Sensors, capacitors and conducting films can be made using graphene-based compounds. GO is hydrophilic and biocompatible in nature because of available surface functionalities. It is used directly and in some cases, functional groups of GO are utilized to prepare hybrids with advanced properties (Lü et al., 2012; Sun, Wu et al., 2013).

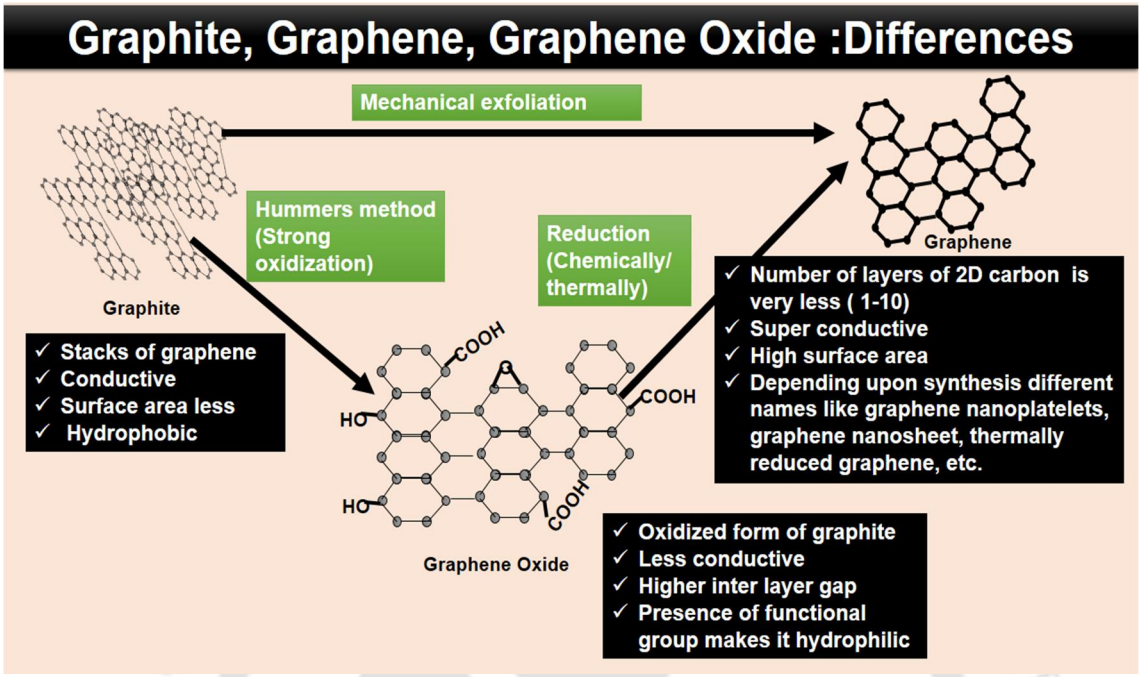

Fig. 1.2 Synthesis and property difference of graphite, graphene oxide and graphene

- *CNT (Carbon nanotube)*: CNT is the rolled tubular form of 2-D graphene sheet. Dome-shaped caps close the extreme ends of the CNTs. It possesses high specific surface area. For instance, SWCNT (single-wall carbon nanotube) is typically having surface area of 1315 m^2/gm and decreases with no of layers. The aspect ratio also lies in the range of 1000, Young's modulus and tensile strength of SWCNT are~1054 GPa and ~75 GPa, respectively. Electrical conductivity of SWCNT is very high. CNTs are used to prepare biosensors, conductive scaffold, conductive films, etc (Hirsch, 2002).
- *Clays*: Clays are layered silicates where tetrahedral silicon and octahedral metallic (Mg/Al) sheets are fused together. Charge of layers depends on cation exchange capacity. Interlayer spacing depends on type of the clay. Based on surface modification, clays can be of two types such as unmodified clay and organically modified clay. Clays have good barrier properties and flame

retardant properties. Clays are mostly utilized as reinforcement into polymeric substances for their good barrier property towards oxygen essential for food packaging applications (Neppalli et al., 2014; Sanchez-Garcia et al., 2010).

- *Bio-fillers*: Different naturally occurring substances are also used as fillers during fabrication of nanocomposites. Cellulose nanocrystal (CNC), cellulose whiskers, cellulose fibrils, bamboo fiber, jute fiber, chitosan, silk, etc. are typical examples of bio-fillers. CNC having high aspect ratio and flaks like morphology similar to clay improves the oxygen barrier. All the PLA based bio-composites are 100% biodegradable and thus reduces the disposal problem and adds value to some of the agricultural wastes. PLA based biocomposites are used in packaging applications (Faruk et al., 2012) (Oksman et al., 2003).

PLA and PLA based composites cover a wide range of applications. Some of them are presented below.

- *Packaging*: Permeability is considered to be the most important parameter in the case of packaging applications. Nano clay incorporation enhances the barrier property most. Oxygen and water vapour barrier properties are improved by 15-48% and 40-50% for PLA-clay nanocomposites, respectively compared to that for PLA. Therefore, PLA based nanocomposites are attractive packaging materials (Auras et al., 2004; Rhim et al., 2013a).
- *Electronics, Sensors, and Energy Application*: Flexible and post usage degradable electronics materials are more desirable in today's context of environmental awareness. As a result, nanocomposites have drawn extensive attention (Feig et al., 2018). However, PLA itself is an insulator material, but incorporation of different reinforcements (carbon fillers and metal oxides) into

the PLA matrix makes it suitable for advanced applications like sensor, electrode, capacitor, etc. PLA/MWCNT and PLA/graphene composites can be used for detection of solvents, vapours, glucose (Mai et al., 2013; Norazlina & Kamal, 2015). Electromagnetic shielding devices, thermo electronic systems and photovoltaic cells can also be produced by such PLA based nanocomposites.

- *Medical applications*: The essential features of biomaterials are biocompatibility in case of medical application and the ability of proper functionality in the human body to come up with desired clinical outcome without causing negative/side effects. Recognition of PLA is increasing as biocompatible material for clinical use. Hydroxyapatite, carbon nanotube and graphene oxide are some of the reinforcements incorporated inside PLA in order to improve the biocompatibility of PLA for different applications like orthopedic transplants, tissue engineering and nerve regeneration (Lasprilla et al., 2012).

PLA based nanocomposites are usually prepared using three main techniques namely, (i) in-situ polymerization, (ii) solution casting and (iii) melt processing. Recently, other preparation techniques such as electrospinning and processing under supercritical conditions (e.g., supercritical carbon dioxide foaming) have gained interest (Lim et al., 2008).

i) *In-situ polymerization*: In this technique, the nanoparticles are premixed with the liquid monomer or monomer solution. Then polymerization is initiated either by heat, radiation or suitable initiators. In this process, no solvent is required. The separation of PLA from reactor can be done easily as solvent recovery is not associated. But it is not applicable for large scale production. L-lactic acid and D-lactic acid based in-situ

polymerization have been carried out by different research groups in the presence of fillers like chitosan, cellulose, GO (Li et al., 2014; Pal & Katiyar, 2016) in order to prepare well dispersed composites where direct mixing with PLA generates lots of agglomeration of filler in polymer matrix and phase separation because of non-homogeneity of surface property (Zheng et al., 2004).

ii) *Solution casting*: In solution casting process, one solvent is used to dissolve the polymer and separate suspension/solution of filler is prepared with the same solvent. Then these two solutions are mixed well and the films are fabricated by solvent evaporation. Organic solvents like chloroform, DCM, THF are used depending on solubility parameters, boiling point and type of polymer and filler. Advantage of this technique is that lab-scale investigation can be done without much processing complexity. Good dispersion can be achievable. However, it is not applicable for large scale production. PLA based solution cast films with different fillers like clay, CNT and bio fillers showed excellent uniformity up to some level of filler loading (Rizvi et al., 2010).

iii) *Melt Processing*: In the melt processing technique, the nanoparticles are mixed with the polymer in the molten state. The formation of PLA based nanocomposites via polymer melt intercalation depends upon the thermodynamic interaction between the polymer and the nanoparticle. For clays, this interaction also depends upon the transport/diffusion of polymer chains from the bulk melt into the silicate interlayers. The polymer needs to be sufficiently compatible with the nanoparticle surface to ensure proper dispersion. This technique is applicable for large scale production. Dispersion of filler and possibility of degradation of PLA are the major problems in this case. Different types of melt processing such as micro compounding, extrusion, injection molding, blow molding, thermoforming, melt spinning are nowadays carried out to

fabricate PLA based nanocomposites (Murariu & Dubois, 2016). Melt processing also has the liberty to extend variety in composition, however, compatibility, local phase separation and drastic thermal degradation are the associated problems (Murariu et al., 2010).

Uniform/desired dispersion of the nanofillers within the PLA matrix is the biggest problem. As most of the inorganic fillers are hydrophilic and PLA is hydrophobic, hence, the interaction between the filler and matrix is poor and particles tend to agglomerate due to van der Waal's force. As a result, phase separation takes place and various defects within the polymer occur (Chaudhry & Castle, 2011). In case of continuous processing, residence time for proper mixing is very much difficult to achieve as it causes degradation of the matrix and reduces the fillers property in some cases. Control of the bio fillers loading during the fabrication of composites is very difficult, especially for fibers. Alignment of fibers is one of the biggest challenges. Tunnelling effect and percolation network construction are the major problems for CNT based composites (Ojijo & Ray, 2013a). Advance applications of PLA based nanocomposites need further modifications and incorporation of active reinforcements (Appendini & Hotchkiss, 2002; Sanchez-Garcia et al., 2010). Thus, the dispersion of filler and extension of applicability of PLA based composites in the area directions, like electrochemical sensing, biosensing, etc. need extensive research in the said areas.

1.1.3 Dispersion technique

Nanocomposite efficiency depends on the type of filler as well as the orientation and distribution of filler within polymer matrix. Uniform dispersion reduces the amount of filler incorporation within the matrix, processability of local phase separation and defects. Surface nature and aspect ratio are some of the properties of the filler, which

influence the dispersion alongside processing condition. In order to achieve good dispersion, some of the techniques presented below are followed universally.

- *Physical processes*: Physical processes like sonication, mechanical stirring, homogeniser and magnetic stirring are used to promote filler into polymer matrix. However, in case of systems where polymer and the filler have different surface nature, application of these processes does not solve the agglomeration and phase separation problems.
- *Covalent functionalization followed by grafting***:** This technique is mainly dependent on the transformation of the surface nature of reinforcements by functional group conversion in order to promote filler dispersion in matrices. There are cases where fillers like CNC, chitosan and cellulose fiber that possess functional groups and in some cases, functional group creation is required prior to surface modification (Pal & Katiyar, 2016). Compounds such as graphene, CNT are oxidized by strong oxidizing agent to create groups, like –COOH, -OH, etc. Then polymer is grafted on functionalized filler in order to produce surface-modified filler. The latter is then dispersed within PLA (Yoon et al., 2010). In-situ polymerization of lactic acid or oligomer in presence of such fillers can generate master-batch (MB) consisting surface modified with PLA, which is then processed directly or in combination with other polymers. Then by MB dilution technique or by direct extrusion, well-dispersed nanocomposite can be made (Tripathi & Katiyar, 2016a). Grafting also can be done with the help of click-chemistry (single-step modification by conversion of functional groups) to get modified filler (Fig. 1.3) (Chen et al., 2014). In some cases, a similar polymer is grafted to improve compatibility. This is effective for hydrophilic fillers like clay, cellulose and chitosan to get well dispersed PLA

based nanocomposites. In some cases, initial functionalization reduces some of the properties like electrical conductivity, thermal conductivity and mechanical strength of fillers like CNT and graphene. Hydrophilic fillers like CNC, cellulose fiber and GO are dispersed into PLA matrix using covalent grafting approach (Lei et al., 2012; Li et al., 2014).

- *Non-covalent wrapping*: This technique is used for filler which doesn't have any functional group on the surface or surface functionalization of such filler deteriorates properties like mechanical, electrical conductivity, thermal stability and morphology. During this process, fillers are wrapped with some polymers to keep intact the original property of the fillers and only coating on surface of these polymers takes place. Further, processing of these modified fillers (MB) mixing with same polymer or other polymer having similar properties are carried out (dilution) for better dispersion. Fillers like graphene and CNT are these types where non-covalent wrapping approach can be used. In situ polymerization in the presence of fillers is carried out to get MB and is usually conducted prior to processing for this type of dispersion technique (Chieng et al., 2014; Hirsch, 2002).
- *Π-Π stacking*: This type of grafting is possible where free electrons are available on the surface of fillers like CNT, graphene, etc. Aromatic compounds are used to coat fillers in order to obtain better dispersion. In the presence of aromatic moiety, dispersion of these kinds of fillers becomes stable for long time, which helps for better dispersion during solvent casting (Tong et al., 2013).

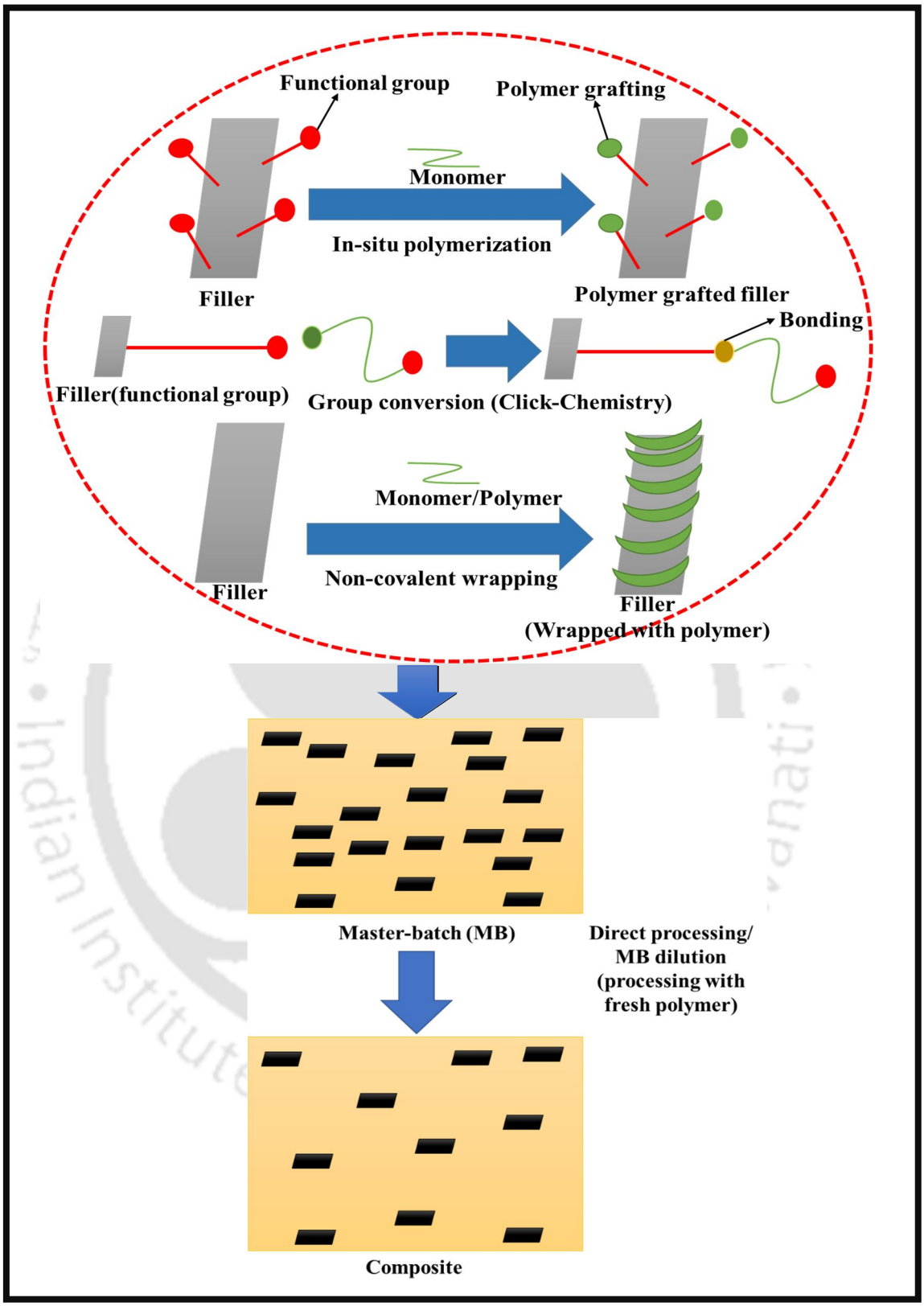

Fig. 1.3 Different dispersion techniques (covalent and non-covalent approach)

1.1.4 Sensor application

Application of biodegradable polymers as conductive material is limited because of its inherent insulating characteristics. Low thermal stability and poor mechanical stability after mechanical operation are also the shortcomings of PLA to be applicable as insulator (Drumright et al., 2000). Nanocomposites containing conductive fillers like CNT, graphene and metallic compounds can reduce the effective resistance of the PLA and makes it suitable as conductive material (Mai et al., 2013). The conductive application domains of PLA based composites are dielectrics, capacitors, electrochemical and biosensors, battery applications (Feig et al., 2018; Llorens et al., 2013).

Application as a sensor is one of the lucrative areas where PLA based nanocomposites are utilized replacing the conventional metallic or other conductive polymer based sensors. In this case, the conductive composite is used as a detector and is able to generate responses in presence of liquids, gases or biomolecules. The sensor application can be of two types; (i) Electrochemical sensor and (ii) Biosensor.

The journey of the electrochemical sensor was started long back in 1950 in order to monitor oxygen. Presently, many electrochemical sensors are used for sensing liquids, vapours, and gases in both stationary and portable device form. These types of devices are used in monitoring environment and detecting small molecules. A good electrochemical sensor should have the following characteristics: fast sensing, high selectivity, high sensitivity, multiple time usability and a well-defined usable range (Qureshi et al., 2009). In addition to the above, if the material is degradable and consists of bio-based component/components that addresses the waste disposal problems also. The two commonly used sensor set up uses the materials as sensing element between a

two probe detection system (Fig. 1.4(a)) and as working electrode in a three-electrode system (Fig. 1.4(b)) (Bakker & Telting-Diaz, 2002; Gan & Hu, 2011).

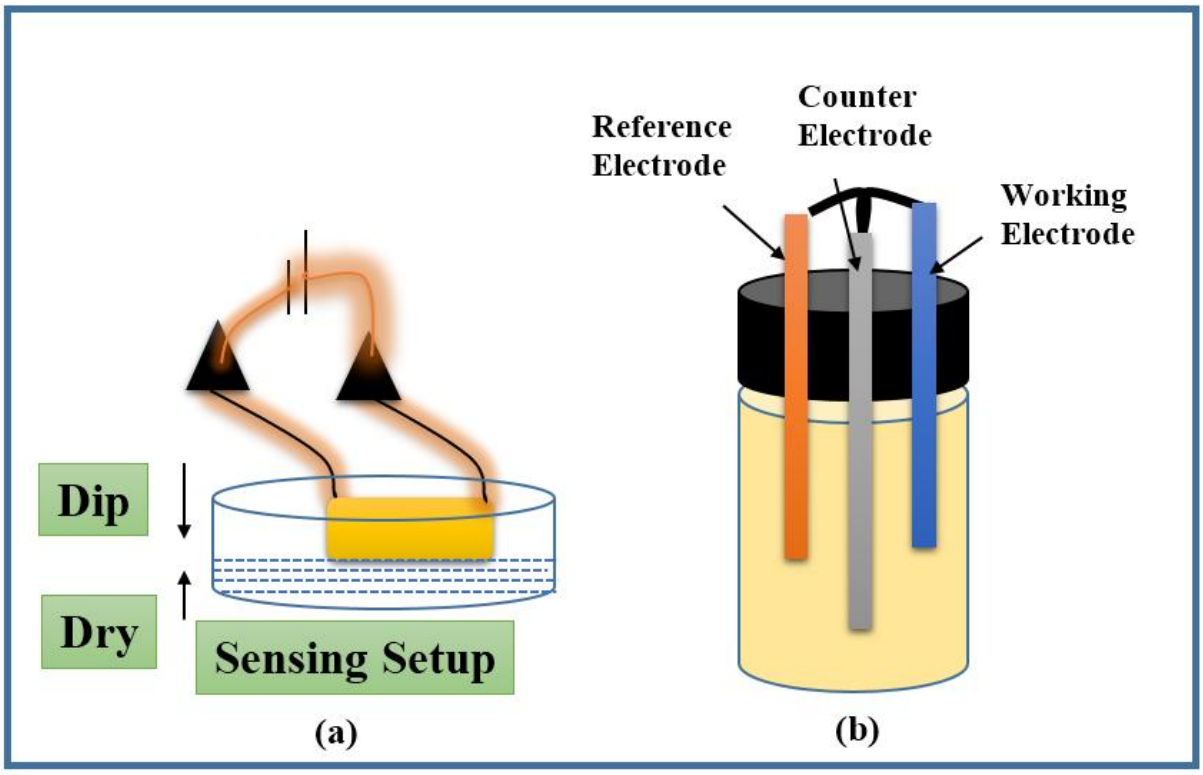

Fig. 1.4 Different types of electrochemical sensor

Detection of biomolecules likes proteins, glucose, amino acids, antibodies, antigens using enzyme or targeted binder as sensor comes under the category of biosensor (Mohanty & Kougianos, 2006). Bio-based polymers are utilized presently for the detection of biomolecules in combination with metallic or organic binder site embedded onto it (Han et al., 2013; Li et al., 2015). Figure 1.5 is a representative scheme of functionality of biosensor where red marked active site works as active binding site towards the biomolecules and generate particular current-voltage response conveying information about specific binding as well as quantitative presence of the biomolecule. PLA based nanocomposites along with specific binding sites are not exercised in this

regard and therefore this needs thorough investigation in order to explore its potential in this area.

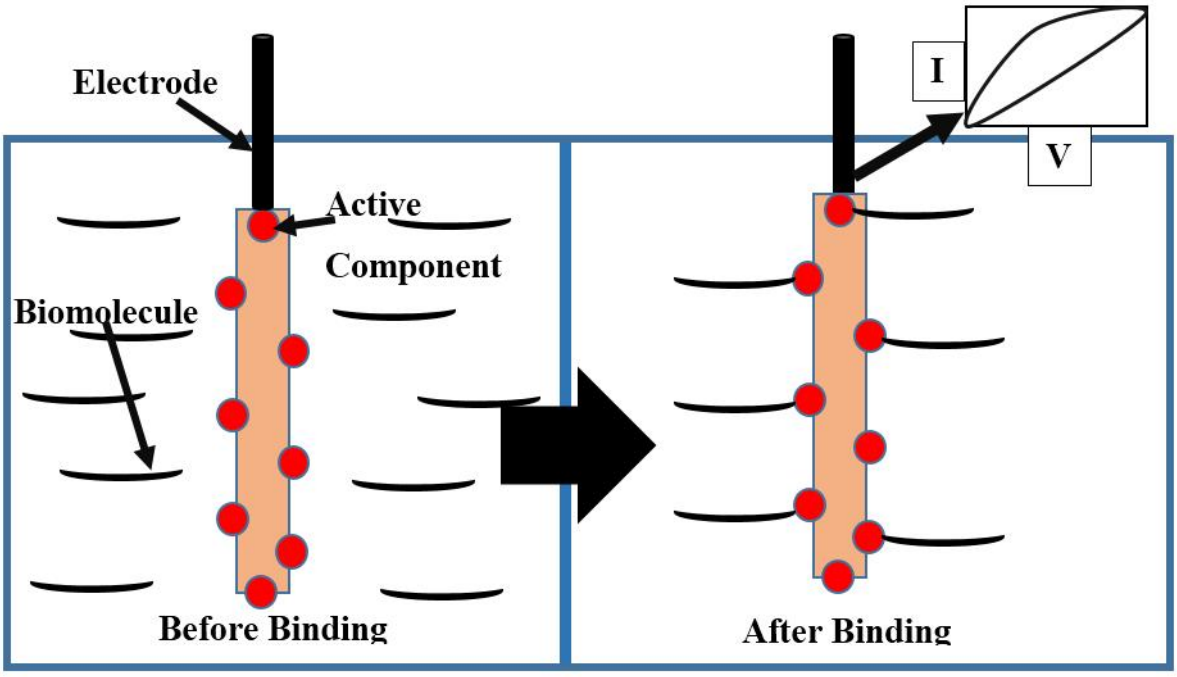

Fig. 1.5 Representative scheme of biosensor functionality

PLA has also typical drawbacks to be applied as conductive biomaterial (Fig. 1.6) that includes reproducibility, chemical stability, etc. (Han et al., 2013; Pötschke et al., 2010). However, with suitable modification, certain characteristics of PLA based nanocomposites can be further improved to make it suitable in the area of sensor application. For example, incorporation of active component can effectively increase the response towards biomolecules (Rahman et al., 2010; Yáñez-Sedeño et al., 2017; Yogeswaran & Chen, 2008). Thus, there is a lot of scope for PLA based conductive composites in the area of flexible electrode based sensing applications.

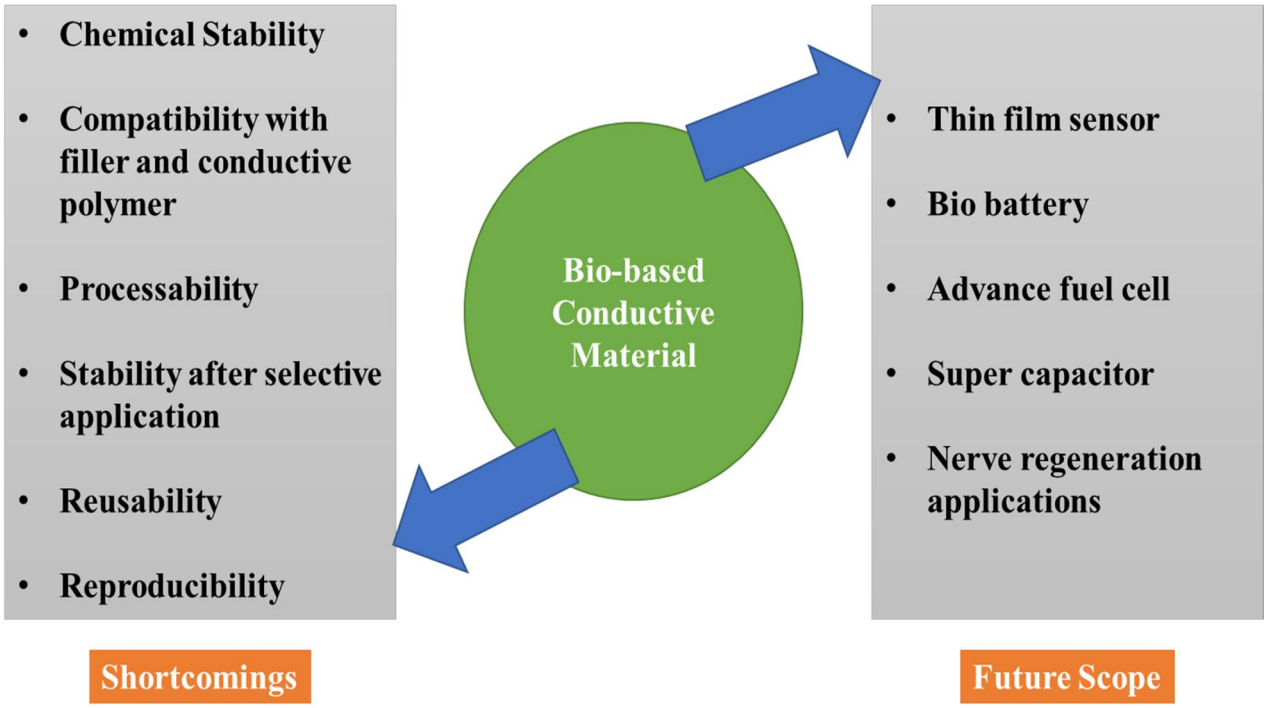

Fig. 1.6 Shortcomings and future scope of bio-based conductive materials

1.2 Literature review

Polylactic acid (PLA) is the most promising biopolymer to be utilized in various fields of applications like packaging, tissue engineering, orthopedics transplants, drug delivery, etc. because of its thermoplastic nature and mechanical strength. Along with biodegradability nature, it is a bio-based and non-toxic polymer. However, industrial-scale utilization of PLA is being hindered because of low processing window, low melt strength, low heat distortion temperature and brittleness. So, in order to address these shortcomings, researchers have adopted different techniques like nanocomposites fabrication, blend preparation, coating. Reinforcement materials like clays, silicates, carbon fiber, carbon nanotube, graphene, bio-based fibers, and cellulose nanocrystals are utilized in different cases to improve selective properties of PLA. Graphene is an

allotrope of carbon with two-dimensional array having high electrical, mechanical and thermal stability. Reinforcement of graphene into the PLA matrix can improve the mechanical strength, thermal stability and electrical conductivity of the PLA. Therefore, a comprehensive literature survey has been carried out for understanding of researches in this area.

The entire literature review is classified on the basis of effect of reinforcement type on the properties of PLA upon composite fabrication; types of processing; special dispersion techniques in order to fabricate PLA nanocomposites; improvement of properties of PLA/graphene based nanocomposites fabricated using various techniques; utilization of graphene based materials in the sensor and electrode applications; and modifications of graphene and graphene oxide (GO) for advanced applications.

1.2.1 PLA based nanocomposites: Different reinforcement materials

Nanotechnology in the area of polymer was first introduced by Toyota Company in 1988, which had a path-breaking impact on conventional polymer technology (Okada et al., 1988). Reinforcement of nanomaterial enhances the interfacial compatibility between the matrix and the filler. Depending upon the reinforcement material various properties of the nanocomposites such as morphology, chemical composition, thermal stability, mechanical strength and electrical conductivity can be modified and enhanced. Reinforcement material can be particulate, fibrous, layered, spherical and tubular, depending on the origin and synthesis route. Layered materials such as clay, silicates and graphene have capability to improve the gas barrier properties of PLA, which is one of the prime requirements for packaging application. Rhim et al., (2009) developed PLLA nanocomposites with organically modified MMT (Closite20A & Closite30B) and unmodified MMT by solution processing using chloroform as a

solvent. They found that the tensile strength was decreased with addition of clay and for PLA/Closite20A nanocomposite, the decrease was the least. The films they processed became brittle and brittleness was increased with an increase in the clay content. The water vapour permeability (WVP) was decreased with increasing clay content for the nanocomposites. Only PLA/Cloisite 30B nanocomposite showed bacteriostatic activity against *L. monocytogenes* and others were inactive (Rhim, Hong, & Ha, 2009). Molinaro et al., (2013) reported that apart from morphological characteristics, clay modification also has an impact on oxygen and water vapour barrier properties. Incorporation of Closite 30B showed barrier effect towards oxygen transmission and reduced the oxygen transmission rate (OTR) up to 50% as compared to pristine polymer (Molinaro et al., 2013). Similarly, Ravi babu et al., (2015) used graphene as reinforcement for PLA nanocomposites preparation and reduced oxygen percolation by 22% was noticed with incorporation of 0.1 wt. % exfoliated graphene (Valapa et al., 2015a). Barrier property is primarily influenced by the two factors viz. gas solubility and diffusion through the polymer matrix. Some bio-based fillers like sucrose palmitate (Valapa.,2015b), cellulose nanocrystal (Dhar et al., 2015), gum (Tripathi & Katiyar, 2016a) and chitosan (Pal & Katiyar, 2016) were also reported to be effective to reduce transmission of oxygen. The requirement for improvement of mechanical, crystallization and thermal properties is dependent upon the application of the PLA based nanocomposites. Compounds that possess fiber-like morphology showed significant improvement in the tensile strength. Lee et al., (2006) prepared biocomposites by taking PLA and poly butylene succinate (PBS), separately with bamboo fiber. Kneading temperatures adopted for the process were 180 ^{o}C and 140 ^{o}C for PLA and PBS respectively. Improvement of strength and modulus were very high upon use of L-lysine diisocyanate (LDI) as compatibilizer. The composite without LDI

absorbed higher water. Melting point did not change and degradation temperature was decreased (Lee & Wang, 2006). Okubu et al., (2009) prepared microfibrilled cellulose (MFC) and PLA composites using three-roll mill. They reported no change of melting point and melt enthalpy. Elastic modulus and tensile strength of the composite were increased with MFC loading (Okubo et al., 2004). Bondeson et al., (2007) fabricated PLA and cellulose nanowhiskers (CNW) composites by extrusion in the temperature range of 170-200 ^{o}C at screw speed of 150 rpm. Before the addition of CNW, it was treated with polyvinyl alcohol (PVA). Both dry and wet feeding conditions in the extruder were studied. Better tensile modulus, tensile strength and elongation at break were observed for both wet and dry feeding conditions. FESEM images indicated that CNW were preferably present in PVA than in PLA (Bondeson & Oksman, 2007).Yu et al., (2010) did surface treatment of Ramie fiber in various ways (alkali, silane I and silane II) and reinforced into PLA by two roll plastic mill at 140 °C for 5 min. Tensile strength was increased because of good compatibility. Maximum strength obtained was 64.24 MPa. Improvement in mechanical property was better in case of alkali-treated fiber composites. Flexural strength and impact strength were also increased with incorporation of the fiber. Vicat softening temperature and degradation temperature were increased for surface treated fibers than unmodified (Yu et al., 2010). Particulate materials are also observed to improve the tensile properties of PLA composites. Murariu et al., (2007) prepared PLA and $CaSO_4$, 0.5 H_2O composites in presence of ester like plasticizer namely, glyceryl triacetate,bis(2-ethylhexayl adipate) by Barbender bench-scale kneader at 190 °C and the mixture melt was processed for 3 minutes. T_g value was decreased from 62 °C to around 39-45 °C with addition of plasticizer; however, crystallinity was increased. Incorporation of $CaSO_4$, 0.5 H_2O enhanced the thermal stability of the composite. Tensile strength and Young's modulus

values were increased and elongation at break was decreased with the incorporation of filler (Murariu et al., 2007). Jiang et al., (2007) synthesized PLA with montmorillonite (MMT) clay and nanoparticle of calcium carbonate based composites separately by melt extrusion. Nano-sized precipitated calcium carbonate (NPCC) showed ordered arrangement and in case of clay, intercalated structure was found. Storage modulus value for PLA/MMT was higher than PLA/NPCC. Elongation at break was also increased with incorporation of NPCC. Young's modulus value was higher for MMT composites (Jiang et al., 2007). Carbon based materials like graphene, carbon nanotube and carbon fiber were utilized to improve thermal stability and impart electrical conductivity on the PLA matrix. Murariu et al., (2010) prepared PLA and expanded graphite (EG) composites using melt blending. Due to addition of EG, reduction in molecular weight was obseved. At 12 % EG addition, thermal stability was increased by 10 ºC (Murariu et al., 2010). Kobashi et al., (2008) fabricated PLLA, multiwall carbon nanotube (MWCNT) (90% pure, l_{av}=1.5µm and D=9.5nm) composites by melt compounding for liquid sensing application. Volumetric resistivity was decreased from 10^{16} Ω cm to less than 10^{2} Ω cm with an increase in the MWCNT content from 0 to 2 wt. %. Thinner sample was leading to sharper response i.e., change of resistance was affected by surface area/volume. Resistance was increased significantly for good solvents of PLA (Toluene, Chloroform, THF and DCM) and decreased with time. Response for n-hexane was good and reversibility was observed. Small change in resistance was observed for ethanol whereas no significant change was noticed for water (Kobashi et al., 2008). Buys et al., (2010) blended PLA and polymethyl methacrylate (PMMA) in the 70:30 ratio and incorporated carbon black (CB) (~28 nm diameter), vapour grown carbon fiber (VGCF) (~140 nm diameter and 10 µm length) and MWCNT (~10-20 nm diameter and 5-20 µm) length using two-roll mill at 180 °C

separately and studied the effect of these fillers on the properties before and after alkaline hydrolysis of composites. Percolation threshold depends on shape and aspect ratio. High aspect ratio material such as VGCF and CNT, constructs conductive network within the matrix, hence a decrease of volume resistivity was sharp with VGCF and CNT filler content. From SEM image, no macroscopic phase separation was located. After hydrolytic degradation, it was observed that PLLA/CNT was contained on the surface whereas PLLA/PMMA/CNT was contained in the bulk. Surface roughness of CB composites was higher (Buys et al., 2010). Some of the literature discussed in this section are summarised in Table 1.2.

Table 1.2 Summary of representative literatures of section 1.2.1

Reinforcement in PLA	Morphology	Processing	Key-points	Reference
MMT (Closite 20A and 30B)	Platelet	Solution	WVP decreased significantly	Rhim et al., 2009
Graphene	Layered	Solution	Oxygen percolation reduced by 22% on 0.1 wt. % graphene loading. Agglomeration of graphene was observed in higher loading.	Valapa et al., 2015a
MWCNT	Tubular	Solution	Volumetric resistivity decreased to 10^2 Ω in incorporation of 2 wt. % of MWCNT	Kobashi et al., 2008
Carbon fiber	Fibrous	Melt	Volumetric resistivity was decreased Phase separation was located	Buys et al., 2010
Bamboo fiber	Fibrous	Melt	Tensile strength and modulus was increased Compatibilizer was used to reduce the interfacial force.	Lee et al., 2006
Ramie fiber	Fibrous	Melt	Flextural strength and impact strength were increased Different surface treatment impoverd the compatibility between matrix and the filler	Yu et al., 2010
Microfribilled Cellulose (MFC)	Fibrous	Melt	Tensile strength was increased with MFC loading	Okubo et al., 2004
CNC	Needle-like, rice grain-like	Solution	Young's modulus improved by ~72%	Dhar et al., 2015
Calcium sulphate	Particulate	Melt	Thermal stability was increased. Tensile strength and young's modulus significantly increased	Murariu et al., 2007

1.2.2 PLA based nanocomposites: Different dispersion techniques

Despite introduction of nanomaterial that enhances different properties of PLA matrix, agglomeration and phase separation are not completely removed yet for the particulate materials. In case of fibrous material also, different micro and macro-scale defects are noticed like breakage, crack formation and bundle formation because of less interfacial adhesion and compatibility. In order to improve the distribution of reinforcement material in PLA matrix, both non-covalent and covalent modifications of pristine substances have been carried out (Hirsch, 2002). Yoon et al., (2010) grafted PLA in acid functionalized carbon nanotube (MWCNT-COOH) by ring-opening polymerization. The chain length of PLA was controlled by weight ratio between lactide and MWCNT-COOH. For PLA/MWCNT-g-PLA, a better dispersion was achieved. Tensile strength was increased depending on grafted chain length. For PLA/MWCNT-g-PLA530, tensile strength and modulus were increased by 44 % and 44 %, respectively. Due to increase in chain length, the dispersion was increased which caused increment in resistivity (Yoon et al., 2010). Boncel et al., (2013) introduced β-D-uridine as linker between MWCNT-COOH and PLA and prepared composites MWCNT-CO–(Oβ-Ur)–(R)-PLA by ring-opening polymerization. Treatment with β-D-uridine changed the appearance into glossy-black crystalline from porous matt black films. Morphology did not show any difference between MWCNT-COOH and MWCNTs-CO–(OβUr). It was observed that the homopolymer material was continuously porous and amorphous. Nanotube produces 3D network and enhances the alignment of polymer fibrils. The molecular weight of grafted PLA was found to be 116,700 Da. T_m value of the nanocomposite didn't not change but T_g was increased to 60.3ºC from 57.8ºC (Boncel et al., 2013). Lei et al., (2012) reported grafting of PMMA on the surface of GO, prepared by Hummer's method, via admicellar polymerization.

Graphene nanosheet (GNS) was also prepared from GO by reduction with hydrazine hydrate. Polymer functionalized graphene (PFG) and PLA composites were fabricated by melt compounding. Conductivity of PFG/PLA was increased with increasing wt. % of PFG. With incorporation of 5 wt. % PFG, conductivity of PLA (10^{-14} S/cm) was increased to 2.58 $\times 10^{-4}$ S/cm. Young's modulus value was increased for PFG/PLA on loading at 1% concentration and improvement was 22% from a value of 0.96 GPa to 1.17 GPa. Tensile strength was increased from 59.88 MPa to 65.02 MPa and elongation at break was decreased (from 6.22% to 4.05%) with an increase in the loading of filler from 0 to 5 wt. %. Agglomeration was found at higher loading of PFG (Lei et al., 2012). In case of clay-based composites also, different organic modifications showed better dispersion and compatibility with PLA matrix. Li et al., (2009) reported melt extrusion of PLA with organically modified rectonite (OR) clay at 170 ºC -190 °C and a screw speed of 90 rpm. Both intercalated and exfoliated structure were present in the composites. Incorporation of OR did not alter the crystal structure of PLA. Clays acted as nucleating agent for the growth of the crystal structure. Elongation at break was increased to 209.7% from 7.9% due to the incorporation of 1 wt. % clay. Modulus was increased and strength was decreased with increasing clay content (Li et al., 2009). Araujo et al., (2014) reported the fabrication of PLA/clay nanocomposites via melt mixing technique using Closite 30B, Closite 15A and Dellite 43B clay along with PLA. Better dispersion was achieved in case of Closite30B and Dellite 43B at 3 wt. % loading and Dellite 43B showed better thermal stability (Araújo et al., 2014). Similarly, other techniques to improve dispersion including usage of different compatibilizers for bamboo fiber was reported by Lee & Wang, (2006). PVA treatment of cellulose nanowhiskers before melt processing (Bondeson & Oksman, 2007), 1-Pyrene methanol stabilization of thermally reduced graphene and fabrication of thermally stable and high

strength composite (Tong et al., 2013) were reported. Non-covalent technique was also adopted for the substances, which don't have functional groups on the surface or having different surface properties as compared to matrix PLA. In this regard, wrapping of reinforcement material with suitable polymer needs to be done prior to composite fabrication. Another approach to eliminate agglomeration problem is Π-Π stacking. Especially for substances having high Π electron moiety like carbon nanotube, graphene, etc. can be dispersed uniformly using aromatic compounds (Tong et al., 2013). Few literatures discussed in this section are summerized in Table 1.3.

Table 1.3 Summary of representative literatures of section 1.2.2

Materials	Dispersion technique	Key-points	Reference
PLA, acid functionalized MWCNT	Covalent grafting	Tensile strength and modulus improved by 44% for both the cases. Improved dispersion increased the resistivity	Yoon et al., 2010
PLA, acid functionalized MWCNT	β-D-uridine linker was used prior to ROP	High molecular weight PLA was achieved. Thermal properties almost similar to normally synthesized PLA	Boncel et al., 2013
PLA,GO, GNS	Admicellar polymerization was carried out PMMA over the filler prior to melt mixing with PLA	Young's modulus improved by 22% on 1wt. % loading of polymer functionalized graphene.	Lei et al.,2012
PLA, Clay	Surface treatment of clay prior to melt mixing with PLA	Among Closite 30B, Closite 15A and Dellite 43B Dellite 43B showed better thermal stability	Araujo et al., 2014
PLA, Chitosan	Covalent grafting of lactic acid over chitosan (in-situ polymerization) Master batch dilution for composite preparetion	Better dispersion improved oxygen barrier property by 10 fold. Glass transition temperature decresed significantly	Pal & Katiyar., 2016
PLA, Thermally reduced graphene (TRG)	1-pyrenemethanol was used for stabilization of TRG	Tensile strength inceased because of better dispersion. Electrical conductivity also increased in the incorporation of TRG.	Tong et al., 20 13

1.2.3 PLA/Graphene nanocomposites: Dispersion, property and applications

In this thesis, graphene is utilized as reinforcement material to fabricate PLA based nanocomposites. Graphene-based compounds include graphite, expanded graphite, graphene oxide (GO) and graphene. Graphene can be synthesized from graphite either by chemical treatment or by thermal exfoliation. Incorporation of graphene into PLA matrix can improve the mechanical, thermal and electrical properties. However, as graphene is a particulate material, uniform dispersion is difficult to achieve for PLA/graphene-based nanocomposites. GO is one of the graphene based material which are used as reinforcement of PLA. Shen et al., (2012) prepared graphene oxide (GO) by Staudenmaier method and reduced it chemically by glucose and polyvinyl pyrrolidone (PVP). Reduced GO/PLA composites were fabricated using DMF solvent and compared with thermally reduced GO/PLA composites. Thermal stability and electrical conductivity found to be increased with incorporation of reduced GO. T_{50}, the 50% decomposition temperature was higher for rGO-g (245 ºC) than rGO-p (235 ºC) and GO (232 ºC). Electrical conductivity of PLA/ rGO-g (2.2 S/m) was high due to better reduction of GO than rGO-p/PLA (4.67×10^{-8} S/m) and GO/PLA (6.47×10^{-13} S/m) at 1.25 vol% loading (Shen et al., 2012).

Pinto et al., (2012) produced GO from graphite by modified Hummer's method and dispersed in PLA matrix using chloroform solvent with 0.4 % concentration of GO to check relative improvement in biocompatibility with respect to graphene nano-platelet (GNP). Cell proliferation inhibition index (CPII) in protein (mouse embryo fibroblast) adhesion culture after 24 hours was 17 % for PLA/GO and that was 31 % for PLA/GNP. GNP composites showed less complexity in post-operative application. Fluorescence study indicated PLA/GO as nontoxic material (Pinto et al., 2013). Li et al., (2014) attempted to graft PLLA on GO which was prepared from graphite by improved

Hummer's method, and dispersed in PLA matrix by solution processing using chloroform as solvent to achieve better dispersion and property improvement. It was reported that T_g and T_m values were increased to 60.2 ºC and 169.1 ºC respectively for PLLA /GO-g-PLLA, whereas the values for PLLA/GO were reported to be 59.4 ºC and 167.1 ºC, respectively. Breaking strength values for PLLA/GO-g-PLLA (120 MPa) and GO/PLLA (109 MPa) were greater than that of PLLA (56 MPa). Tensile strength was increased by 51.4 % and 105.7 % for GO/PLLA and PLLA/GO-g-PLLA, respectively. Elongation at break was also increased to 114.3 % and 196.8 % for GO/PLLA and PLLA/GO-g-PLLA, respectively as compared to PLLA (3.68 %) (Li et al., 2014).

Similarly, Lei et al., (2012) reported grafting of PMMA on the surface of GO, prepared by the Hummer's method through admicellar polymerization. Tensile strength and elongation at break were increased by incorporation of graphene. In order to promote the dispersion of GO and to make composites of improved electrical conductivity, Tong et al., (2013) used 1-pyrene methanol to stabilize thermally reduced graphene (TRG) in DMF solution and prepared TRG/PLA/Py-PLA by solution processing using DMF as solvent and Han et al., (2013) reported modification of GO with methylene diphenyl diisocyanate (MDI) in the presence of 1, 4-butanediol to produce GO-MDI-OH. GO-g-PLA was prepared by mixing GO-MDI-OH, PLA and hydrated toluene in proper proportion following the necessary steps and found singnificant improvent in properties for respective cases. GO was also incorporated into PLA based blends using different techniques.

Yoon et al., (2011) fabricated nanocomposites using PLA, polyglycolic acid (PGA) and GO by electrospinning method. GO was prepared by Modified Hummer's method. Tensile modulus was increased by 172.8 % and 204.9 % respectively for PLGA/GO (1 wt. %) and PLGA/GO (2 wt. %). Storage modulus value was increased with loading.

Glass transition temperature was increased to 66.7 ºC for 2 wt. % composite compared to that of PLGA and PLGA/GO (1 wt. %) composites and the values were 32 ºC and 33 ºC. Biocompatibility and cytotoxicity analysis showed positive results for the composites (Yoon et al., 2011). GO also used for promoting crystallization of PLA.

Wang et al., (2012) studied isothermal and non-isothermal crystallization kinetics of GO/PLLA composites prepared by solution processing. They reported that degree of crystallinity was increased with GO loading. It was maximum at 1 wt. % of GO and further increase in the loading yielded agglomareted structure. Isothermal crystallization mechanism was similar for all the different composites having different GO with similar Avrami exponent (n) value ~2.3. They concluded that graphene only acted as a nucleating agent for crystallization of PLA (Wang & Qiu, 2012).

Wang et al., (2011) in another paper reported the crystallization behavior of GO/PLLA composites from amorphous state. Cold-crystallization peak temperature was decreased upon loading. GO loading showed no influence on T_g (around 61 ºC). Time for 50 % crystallization ($t_{0.5}$) was decreased with increasing heating rate as well as GO loading at a particular temperature (Wang & Qiu, 2011). Graphene also incorporated into PLA in different forms like sheet, platelet, etc., and also from different synthesis routes to increase the properties like thermal stability, electrical conductivity.

Sabzi et al., (2013) fabricated PLA/graphene nanoplatelets based nanocomposites by solution casting method. Two types of graphene nanoplatelets were utilized namely, xGn-M25 (thickness of graphene sheet ~10 nm) and N002-PDR (thickness less than 1nm). The conductivity of the composites was increased from 10^{-13} S/m to 0.1 S/m due to the loading of 0.059 and 0.01 vol% of xGn-M25 and N002-PDR, respectively. It was also reported from the rheological study that because of larger aspect ratio of N002-

PDR, it showed lower percolation threshold as compared to that of xGn-M25 (Sabzi et al., 2013).

Valapa et al., (2015) studied the effect of thermal exfoliation of expanded graphite and synthesis of graphene was optimized at 750 °C. PLA based nanocomposite was fabricated using chloroform as solvent and after 30 min sonication of graphene. Exfoliated nature of the graphene was observed in the composite. For 0.5 wt. % graphene loaded composite an improvement of 6 °C was observed in the case of T_{onset} of PLA. A reduction of 53 % in the transparency was noticed due to the incorporation of graphene into PLA matrix. Tensile strength of nanocomposite was found to be 40 MPa for 0.1 wt. % graphene loading (Valapa et al., 2015a).

Xu et al., (2013) fabricated PLLA based nanocomposites using graphene nanosheet (GNS) and multiwall carbon nanotube (CNT) as reinforcement material. The composites were fabricated by coagulation followed by moulding of the coagulates at 180 °C for 10 min. With the increase of CNT loading from 0.05 wt. % to 0.1 wt. %, $t_{0.5}$ was decreased from 15 min to 11 min, which was indicative of the nucleation effect of CNT. It was also showed that induction ability of GNS was weaker as compared to that of CNT. Considering the size dependent-soft epitaxy (SSE) mechanism effect of filler, dimension on the crystal growth was explained (Xu et al., 2010).

Chieng et al., (2014) used reduced graphene oxide (rGO) and graphene nanoplatelets (xGnP) to fabricate PLA based nanocomposites with plasticized PLA using Berbender mixer at 170 °C and 50 rpm keeping loading at 0.3 wt.%. poly (ethylene glycol) (PEG). Epoxidized palm oil (EPO) was used as plasticizer. In case of PLA/EPO/rGO, the tensile strength was increased from 41.07 to 42.62 MPa and elongation at break was increased by 53.9% for rGO reinforcement as compared to xGnP.

Similarly, Cao et al., (2010) prepared graphene nanosheet (GNS) by reducing graphene oxide (GO) using hydrazine as a reducing agent followed by lyophilization. PLA/GNS nanocomposites were fabricated by the coagulation method using DMF as solvent. Storage modulus was improved to 3385 MPa as compared to pure PLA (2862 MPa) due to incorporation of 0.2 wt. % GNS. Graphene also found to improve the crystallization of PLA (Valapa et al., 2015). Summary of few representative literatures is presentated in Table 1.4.

Table 1.4 Summary of representative literatures of section 1.2.3

Materials	Methods	Key-points	Reference
PLA, GO	Solution casting using DMF solvent	Reduction of GO was found to be better using glucose In incorporation of reduced GO by glucose (rGO-g) conductivity was increased upto 2.2 S/m	Shen et al., 2012
PLA, GO	Covalent grafting of PLLA on GO. Solution casting with PLA	Elongation at break was increased up to 196.8% compared to pure PLA (3.68%)	Li et al., 2014
PLLA, GO	Solution casting	GO observed to be acted as nucleating substance towards crystallization of PLLA	Wang et al., 2012
PLA, Graphene nanoplatelets	Solution casting	Conductivity of the composite was improved to 0.1 S/m in very low loading of graphene	Sabzi et al., 2013
PLA, rGO, graphene nano platelets	Melt mixing PEG and EPO used as plasticizers.	10 ^{o}C improvement in T_{50} was observed EPO plasticized PLA/rGO composite	Chieng et al., 2014
PLA, GNS	Coagulation method using DMF solvent	Thermal stability of the composite was improved. Tensile strength and Young's modulus were improved by 26 % and 18 % as compared to PLA, respectively	Cao et al., 2010

1.2.4 Graphene applications: Sensors and electrodes

Graphene is highly electrically conductive material because of the availability of free electrons on its surface. Considering its conductive nature, it can be applicable in the field of electrochemical and biosensor applications (Lu et al.,2009; Ramachandran et al., 2013). Sometimes graphene acts as a 'plain sensor' i.e., direct deposition over glassy

carbon electrode enhances the conductivity and gas sensing ability. This type of sensor is used for different gases and organic liquid vapour. This gives distinct responses for electron-withdrawing and electron-donating molecules. In other types of electrochemical sensors, modified graphene oxides are used for sensing. Functional groups of GO need to be modified based on the type of sensing (Kochmann, 2014). In most of the cases, metal oxides are used to enhance gas sensing properties. Graphene has the capability to absorb gas and organic vapours (Arsat et al., 2009). Yuan et al., (2013) used sulfonated and ethylenediamine modified reduced graphene oxide to detect NO_2 gas. Conductance was found to be increased with an increase in the NO_2 gas concentration and exposure time (Yuan et al., 2013). Similarly, reduced graphene oxide was used for H_2, O_2, water and other gas sensing (Chung et al., 2012; Dua et al., 2010; Russo et al., 2012). Biosensor applications using graphene molecules are also increasing utilizing both conductive nature as well as functionalities. Keeley et al., (2010) fabricated graphene nanosheet (GNS) immobilized pyrolyzed photoresist film (PPF) electrode to detect ascorbic acid. From cyclic voltammetry analysis, detection range was found to be 0.4 to 6 mM with 0.12 mM detection limit (Keeley et al., 2010). Other compounds like hydrazine (Wang et al., 2010), dopamine (Chen et al., 2011), and hydrogen peroxide (Mani et al., 2014) were also detected using graphene-based electrode. In case of electrochemical sensing of liquids, two probe or four-probe methods are followed using Multimeter and responses are recorded either in terms of change in resistance or relative change in resistance. In some cases, change in current is recorded as response. Selection of procedure depends on the type of sensing element and nature of the stimuli to detect. In some cases, three-electrode system was used, which measures the current-voltage response. Biosensing of any stimuli is associated with oxidation/reduction or coupling of any component depending on the type of the

modification of graphene surface. This generates distinct peak in current-voltage response, which is indicative of selectivity, sensitivity and selection range (Yu et al., 2014). Thin film stretchable sensor utilizing graphene is very limited. PMMA/graphene was utilized as novel strain sensor by Chen et al., (2007). Digital printing technique was utilized in some of the cases in order to cast electrode for making sensor. Table 1.5 presents the summary of few literatures discussed in this section.

Table 1.5 Summary of representative literatures of section 1.2.4

Sensing element	**Type of sensor**	**Key-points**	**Reference**
GO attached with dye labelled DNA	Bio sensing	GO successfully acted as platform for biosensing Flrurosence is higher for human thrombin compared to other proteins.	Lu et al., 2009
rGO, chemically modified graphene	NO_2 gas sensor	Sensor has good sensitivity, selectivity and reversibility Sensor response is linear up to low concentaration of NO_2	Yuan et al., 2013
GO	Photo induced charge transfer based biosensor of Dopamine	Sensitivity range 0-50 µM with linear relationship	Chen et al., 2011
GNS	Pyrolyzed photoresist film electrode for ascorbic acid sensing	Cyclic voltametric analysis revealed detection range 0.4- 6 mM Detection limit was 0.12 mM	Keeley et al.,2010
rGO/PET	Vapour sensor	Inkjet-printed sensor found to be responsive towards different gases like Cl_2, NO_2 and organic vapours like chloroform, methanol.	Dua et al., 2010

1.2.5 Modification of graphene and graphene oxide: Advanced applications

Graphene utilization is being further extended in different advanced applications like supercapacitors, biosensors, electrodes, etc. by fabricating novel nanocomposites with metal oxide, conductive polymer and carbon materials via different modification techniques. Magnetic graphene oxide is one of the emerging materials, which can impart stimuli controlled properties into composites (Yu et al., 2014). Improved properties of composites such as optical transparency and sensing nature and smart electronics application of magnetic particles are successful features nowadays, particularly due to the use of carbon template magnetic nanomaterial (Yáñez-Sedeño et al., 2017). GO is one such promising candidate to be modified as a magnetic material for variety of applications. He et al., (2010) prepared Fe_3O_4-GO hybrid by covalent bonding and used this hybrid for dye removal purpose. Adsorption capacity of the synthesized material was observed to be 190.14 and 140.79 mg/g towards methylene blue and neutral red, respectively. Lu et al., (2010) fabricated graphene film over graphitic substance by screen printing technique. ZnO and SnO_2 modification of graphene was carried out by ultrasonic spray pyrolysis technique. Current density vs. potential response indicated that graphene in modification with metal was transformed into an improved capacitor. Graphene-ZnO showed higher capacitance value 61.7 F/g. Similarly, Zhang et al., (2009) also used ZnO decorated graphene for fabrication of capacitor. GO preparation from graphite by Hummers method followed by deposition of ZnO and heat treatment generated the hybrid. The modified graphene showed significant improvement in capacitive behavior of the substance. Kassaee et al., (2011) fabricated Fe_3O_4-GO hybrid by co-precipitation technique and fabricated magnetically active polystyrene film by solution casting method. Bose et al., (2010) synthesized conductive composite of polypyrrole (PPy) by incorporating chemically reduced

graphene from GO. Improvement in conductivity was reported from 0.19 S/cm to 1.64 S/cm due to incorporation of graphene in PPy matrix. Shayeh et al., (2015) used polyaniline and gold nanoparticle in combination with graphene in order to make super capacitor. Similarly Gomez et al., (2011) utilized polyaniline and graphene for fabrication of supercapacitor by chemical precipitation technique. Application of graphene was also extended in some of the advanced areas like flexible electrode (Gwon et al., 2011; Jang et al., 2016) and conductive ink (Huang et al., 2011) etc. Table 1.6 presents the summary of few literatures discussed in this section.

Table 1.6 Summary of representative literatures of section 1.2.5

Material	**Modification**	**Application**	**Reference**
GO	Magnetization by co-precipitation	Dye removal of methylene blue and neutral red	He et al., 2010
Graphene	ZnO, SnO_2 modification by ultrasonic spray pyrolysis	Capacitor	Lu et al., 2010
GO	ZnO modification by heat deposition	Capacitor	Zhang et al., 2009
GO	Magnetic GO by co-precipitation followed by film preparation with PMMA	Magnetic field active composite	Kassaee et al., 2011
r-GO	Conductive composite using polypyrrole	High conductive composite	Bose et al., 2010
Graphene	Modification with polyaniline and gold nanoparticle	Super-capacitor	Shayeh et al., 2015
Graphene	Printing technique	Flexible electrode	Jang et al., 2016
Graphene	Sonication and filtretion	Conductive Ink	Huang et al., 2011

1.3 Gaps in the Prior Art

From the above literature study, it is observed that the main goal of the researchers was to have better dispersion of filler in the polymer matrix in order to achieve enhanced properties. Accordingly, several researchers have performed grafting of fillers. Surface treatment of fillers and used compatibilizer for better interaction between the filler and the matrix. However, the synthesized composites contained agglomeration when the higher fraction of filler was present. In most of the cases, melt processing led to non-uniform dispersion of filler, particularly for those filler materials which don't have functional groups like CNT, graphene, etc. Except covalent grafting, no other technique is reasonably achieved better dispersion. Information on large scale production using extruder for composites having functionalized fillers is found to be inadequate. In order to use these nanocomposite materials for various applications, improvement in crystallization kinetics, rheological properties especially melt rheology, degradation temperature, mechanical properties and barrier properties as compared to existing literature data are essential requirement. It is also found that little work has been carried out for the fabrication of polymer composites with exfoliated graphene by melt processing. Potential applicability of the graphene in combination with biodegradable polymer like PLA in conductive products like sensor, capacitor is not explored adequately. Application of biodegradable polymer like PLA in the field of thin-film electronics is very limited.

1.4 Motivation

Motivation of the present work is to fabricate biodegradable PLA based nanocomposite with improved dispersion of filler and without alteration of the structure. Exfoliated graphene is taken as the reinforcement material.

Secondly, exploration of the applicability of the PLA based nanocomposites containing graphene-based material in areas like electrochemical sensing and biosensing.

Finally, fabrication of an effective sensing set up for detection of ethanol vapour with the help of such PLA based nanocomposites.

1.5 Research objectives

The main aim of the thesis is to fabricate and characterize graphene-based PLA nanocomposites with and without combination of different fillers and to examine their potential for various applications. This is achieved through three major objectives.

(1) The first objective of this work is to make better dispersion of graphene in the PLA/GR nanocomposites in case of melt processing. In order to accomplish this, the following steps are adopted:

- Fabrication of PLA and graphene-based potential biodegradable thermoplastic nanocomposites by facile coating technique followed by extrusion.
- Development of master-batch (MB) using one step polycondensation reaction of PLA from its oligomer.
- Melt extrusion of the MB diluted nanocomposites.
- Characterization and comparison of the nanocomposites fabricated.
- Study and comparison on the melt rheology behavior of the composites prepared from both the processes.

(2) In order to enhance the application domain of PLA nanocomposites, the second objective is designed to synthesis of PLA/graphene/metallic compound nanocomposites for sensor application. The following research works are taken up in order to meet the objective.

- Fabrication of conductive PLA/GR nanocomposites by solution casting and evaluation of applicability as sensor.
- Fabrication of PLA/GR/Fe-CNC nanocomposites for application as sensor for organic molecules.
- Enrichment of PLA/GR composites by suitable additives for metal ion detection.

(3) The final objective is to explore the applicability potential of magnetic particle reinforced PLA nanocomposites as a sensor. The following steps are used to meet this objective.

- Preparation of ferromagnetic particles by co-precipitation method.
- Fabrication and application of PLA-magnetic particle nanocomposites for ethanol vapour sensing.

1.6 Organization of the Thesis

In this chapter benefits and shortcomings of PLA and PLA based nanocomposites are discussed in detail. Dispersion of reinforcements into PLA matrix is still a challenge to overcome specifically in case of melt processing for both particular and fiber reinforcement. Covalent grafting, non-covalent wrapping and π-π stacking are some of the dispersion techniques to fabricate composite with improved uniformity.

Application of PLA based nanocomposites covers almost all the fields like packaging, biomedical, tissue engineering, etc. However, the possibility of application in the area of conductive material after reinforcements with graphene, carbon fiber, carbon nanotube, etc. is emerging areas nowadays. Among other conductive applications like capacitor, electrode, energy application and sensor application of bio-based conductive

substances containing PLA is able to generate stable and distinct response towards different stimuli.

Therefore this PhD research work is aimed at the utilization of bio-based and biodegradable polymer PLA for advanced applications in combination with graphene-based filers and magnetic fillers. Dispersion of fillers specifically particulate material like graphene is difficult during melt processing with PLA, which is addressed first and secondly utilization of PLA based conductive nanocomposite for conductive application in particular as sensor for various stimuli like ethanol and other alcohols, formic acid and acetone are carried out. Further, different functional materials like Fe-CNC, EDTA, and Albumin are incorporated into PLA-graphene system for improvement of sensing capacity towards alcohol, biomolecules and metal ions in different cases. Finally, the magnetic nanomaterial of different aspect ratio is incorporated to fabricate PLA based vapour sensor. The thesis is organized in the form of eight Chapters. The significant findings are arranged in Chapters 2-7 of this thesis. The thesis organization and title of the individual chapter are presented below:

Chapter 1

Introduction and Literature Review

Chapter 2

Investigatigating the Properties of Polylactic acid/Exfoliated Graphene (GR) based Nanocomposites Fabricated by versatile Coating approach

Chapter 3

Facile Dispersion of Exfoliated graphene/PLA Nanocomposites via in situ Polycondensation cum Melt Extrusion Process and its Rheological Studies

Chapter 4

Exfoliated Graphene Dispersed Polylactic acid based Nanocomposite Sensors for Liquid Solvent Detection

Chapter 5

Applicability of Fe-CNC/GR/PLA Composite as Potential Sensor for Detection of Biomolecules

Chapter 6

Enrichment of PLA/GR Nanocomposites by suitable additives for the Detection of Metal Ions

Chapter 7

Synthesis of Magnetic Nanomaterials and Studies on Magneto rheological behavior and Vapour Sensing behavior of PLA based Nanocomposites

Chapter 8

Conclusions and Future Scope

1.7 Graphical Abstract of the Thesis

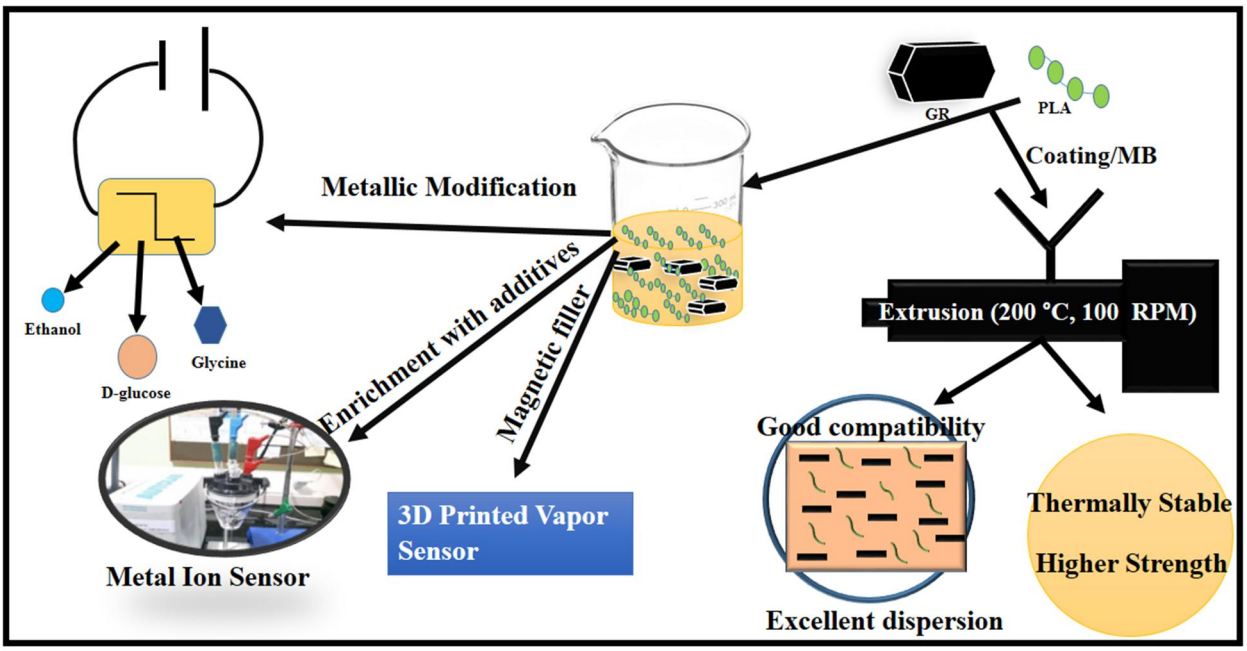

Chapter 2

Investigating the Properties of Polylactic acid/Exfoliated Graphene Based Nanocomposites Fabricated by Versatile Coating Approach

Abstract

In this chapter effect of dispersion of graphene (GR) was investigated in melt processed PLA, fabricated by solvent coating of GR over PLA prior to extrusion. The effect of melt processing on different graphene loaded composites (PLA-M-0.05GR, PLA-M-0.2GR) was studied. XRD and morphological analyses confirm the formation of well dispersed composite. Thermo-gravimetric analysis and kinetic study reveal significant improvement in thermal stability. Improvement in crystallinity, melting point and crystallization point are found from DSC analysis. Crystallization kinetic study was carried out and nucleation effect of the GR on crystallization of PLA chain was noticed. Tensile properties and dynamic mechanical properties were also investigated. Melt rheology and solution viscosity measurements were carried out to study the structural and flow nature of the composites. Pristine polymer (PLA-M) and its composites (PLA-M-0.05GR and PLA-M-0.2GR) show shear thinning behavior. Excellent dispersion of GR and single phase nature of the composites is noticed by studying Han plot, Cole-Cole plot and van Grup-Palmen's plot.

Part of this research work has received scientific recognition as follows:

Chakraborty, G., Valapa, R. B., Pugazhenthi, G., & Katiyar, V. (2018). Investigating the properties of poly (lactic acid)/exfoliated graphene based nanocomposites fabricated by versatile coating approach. ***International Journal of Biological Macromolecules***, 113, 1080-1091.

Graphical Abstract

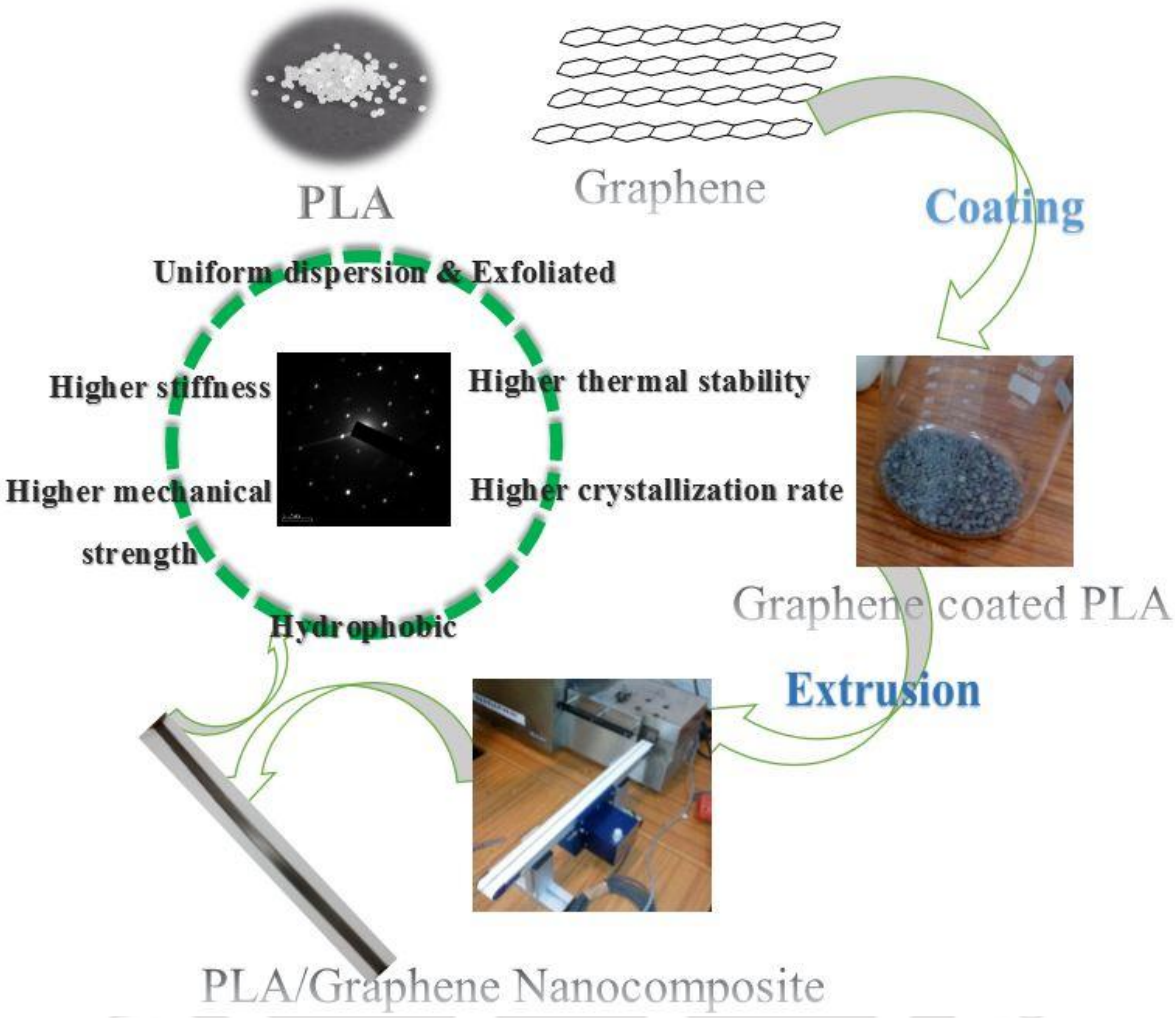

2.1 Introduction

In this contemporary period, majority of the practical applications are directly or indirectly associated with polymers. This is owing to the fact that thermoplastic polymers exhibit the properties like lightweight, thermal stability, tuneable gas as well as water vapour barrier properties and good printability. All of these properties make polymers as versatile materials suitable for product manufacturing such that they are extensively being utilized for automobile, packaging, agriculture, and biomedical applications. In spite of several inherent advantages, most of the petroleum feed stock based plastics are associated with certain serious issues such as disposal of solid waste, and scarcity for raw material. In particular, the solid waste generated by petrochemical based polymers serve as environmental hazards, which cause major threat to the survival of living organisms (Lim et al., 2008).

Biodegradable polymer based products originated as an obvious alternative to the non-renewable polymer based materials. The biopolymers derived from renewable resources find commercial value particularly in short-period packaging applications and commonly used disposable goods, which include plates, cups, food item wrappers, utensils, trash bags, beverage containers, and medical devices, etc. Most of the biodegradable materials are manufactured from bio-based feedstocks and easily degradable by microorganisms under controlled environmental conditions. Biodegradable thermoplastic polymers like poly (lactic acid) (PLA), polyhydroxyalkanoate (PHA) and polycaprolactone (PCL) have the capability to fulfill the commercial needs along with environmental sustainability (Rhim et al., 2013b).

Among the biopolymers, PLA emerged as a potential and widely used thermoplastic polymer, which exhibits both biocompatibility and biodegradability characteristics. PLA is produced from lactic acid source via synthetic routes such as direct

polycondensation or ring-opening polymerization (ROP) of lactide (Jem et al., 2010). PLA possesses the properties to be used as storage product for even direct contact with food containing aqueous, acidic and fatty acids. Several industries have already started producing cups, cutlery and food containers made of PLA. The PLA biopolymer can also be used to laminate paper and paperboard by extrusion coating to enhance its application as packaging material (Auras et al., 2004; Reddy et al., 2013a). The other major applications where PLA has been excitingly utilized as basic ingredient for commodity production are biomedical (Lasprilla et al., 2012; Lopes et al., 2012) , electronics (Reddy et al., 2013a) and drug delivery (Babu et al., 2013). PLA exhibits comparable Young's modulus and tensile strength with commodity polymers, like polystyrene (PS), different grades of polyethylene (PE), polypropylene (PP), and polyethylene terephthalate (PET). However, thermal stability of PLA is low and thus shows rapid loss of molecular weight because of random chain scissions. Therefore, when PLA is subjected to post processing operations like extrusion, injection and blow moulding, decrement in terms of properties become prominent due to loss in molecular weight. The reduction in molecular weight actually lowers the melting point and results in narrow processing window for PLA. Even though PLA is highly useful and attractive material for commercialization still improvement in terms of processing ability, barrier and mechanical properties for PLA are essential for high temperature application and in order to replace petrochemical based plastics (Carrasco et al., 2010; Mori et al., 2004; Norazlina & Kamal, 2015).

Several strategies have been reported to regulate PLA properties by changing processing technology or modifying chemical composition and components. Reinforcement of PLA with various fillers like carbon fillers (Pinto et al., 2013; Wang et al., 2008; Wu et al., 2008), clays (Li et al., 2009; Neppalli et al., 2014; Zaidi et al.,

2010; Zhao et al., 2008), inorganic compounds (Xu et al., 2007; Xu et al., 2006) and biomaterials (cellulose nanocrystals, cellulose whiskers and bio fibres) (Bondeson & Oksman, 2007; Dhar et al., 2015; Lee & Wang, 2006; T. Yu et al., 2010) has been reported. It is found that the incorporation of filler materials has significantly contributed to improve the properties of PLA, especially when the filler dimension is in the nanometre range (Duncan, 2011; Raquez et al., 2013a; Valapa et al., 2015b). Recently, various carbon allotropes such as graphene oxide (Yoon et al., 2011), graphene nanoplatelets (Sabzi et al., 2013), expanded graphite (Mortazavi et al., 2013), reduced graphene oxide (Shen et al., 2012) have drawn interest as fillers for PLA nanocomposites due to their exceptional electrical, thermal, optical, and mechanical properties (Singh et al., 2011). Exfoliated graphene (GR) has emerged as a novel filler for PLA to upgrade mechanical properties. However, agglomeration of graphene is still the problem for exfoliated graphene reinforced PLA composites (Valapa et al., 2015a). Melt processing of PLA composites is always associated with phase separation, degradation of polymeric substrate and non-uniform distribution of filler (Taubner & Shishoo, 2001). Exfoliated graphene is very lightweight material and like other nanoparticles, open-air handling of this material always will be associated with material loss and can cause air pollution. Nanomaterial rich air causes breathing problems and sometimes due to long-time exposure, it creates serious deceases like asthma, emphysema, and lung cancer (Buzea et al., 2007; Slezakova et al., 2013; Terzano et al., 2010). Therefore, it is necessary to overcome the challenges that underlie in dispersion of GR into PLA matrix by extrusion so as to come up with commercially viable plastic materials (Murariu et al., 2010; Ojijo & Ray, 2013b). In this perspective, versatile approach is used to promote the nanofiller (GR) dispersion within the PLA matrix prior to melt extrusion. In the present chapter, a facile coating technique is followed with an

aim to obtain uniform layer of GR over PLA pellets. This approach helps to disperse GR in the PLA matrix while subjected to melt extrusion and improve the properties of PLA/GR nanocomposite. The GR loading is fixed to be below 0.5 wt. % for the fabrication of PLA/GR nanocomposite. This is to avoid agglomeration problem resulted in the earlier report when 0.5 wt. % of GR was reinforced in the PLA matrix (Valapa et al., 2015a). Investigation on the structural, morphological, surface wettability, thermal, mechanical and crystallization characteristics for the melt processed PLA/GR nanocomposites is carried out in detail.

2.2 Materials and Methods

2.2.1 Materials

2003D grade of poly (L-lactic acid) (PLA) from NatureWorks® LLC (USA) was used for this present investigation. Exfoliated graphene EXG 750 (GR) used for fabrication of composites was synthesised in lab (Valapa et al., 2015a). Methanol (extra pure AR) required for coating of graphene over PLA pellets was provided by SISCO research laboratories (SRL Chemicals, India).

2.2.2 Experimental Section

2.2.2.1 Fabrication of PLA/GR nanocomposites by solvent coating approach

PLA/GR nanocomposites with 0.05 and 0.2 wt. % of GR content were fabricated as follows. Appropriate amount of GR was weighed with respect to 20 g of PLA in order to prepare PLA-GR nanocomposites of different compositions. Initially, GR was added into a beaker containing 50 mL methanol and subjected to sonication in order to disperse GR in methanol solvent. The sonication process was carried out for 45 min until the methanol solution became uniformly black ensuring that no residue was left at the bottom of the flask. Thereafter, PLA pellets was added into GR/methanol

mixture and stirred for 10 min followed by drying at 50 °C for overnight to obtain uniform coating of GR onto PLA pellets.

The PLA and PLA-GR nanocomposite strips were fabricated using a mini extruder (Make: Thermo Scientific Model: Haake Minilab II). The schematic representation of the steps followed for coating of GR onto PLA and subsequent fabrication of PLA-GR nanocomposites is shown in Fig. 2.1. The PLA and its composites were extruded at 200 °C at a speed of 100 rpm. With further increase in temperature beyond 200 °C, decrement in terms of molecular weight (M_n) for PLA was noticed. The M_n value for PLA at 200 and 210 °C were determined to be 62372 and 54274 Da, respectively. On the other hand, the flow of PLA during extrusion was restricted when the temperature condition was maintained below 200 °C. Therefore, the temperature condition of 200 °C was maintained as appropriate for extrusion process in case of both PLA and its composites. The thickness and width of PLA and PLA-GR nanocomposite strips obtained after extrusion process were 0.5 mm and 4 mm, respectively. The strips fabricated via extrusion were designed as PLA-M, PLA-M-0.05GR and PLA-M-0.2GR for neat PLA, PLA melt-processed with 0.05 wt. % of GR content and PLA melt-processed with 0.2 wt. % of GR content, respectively.

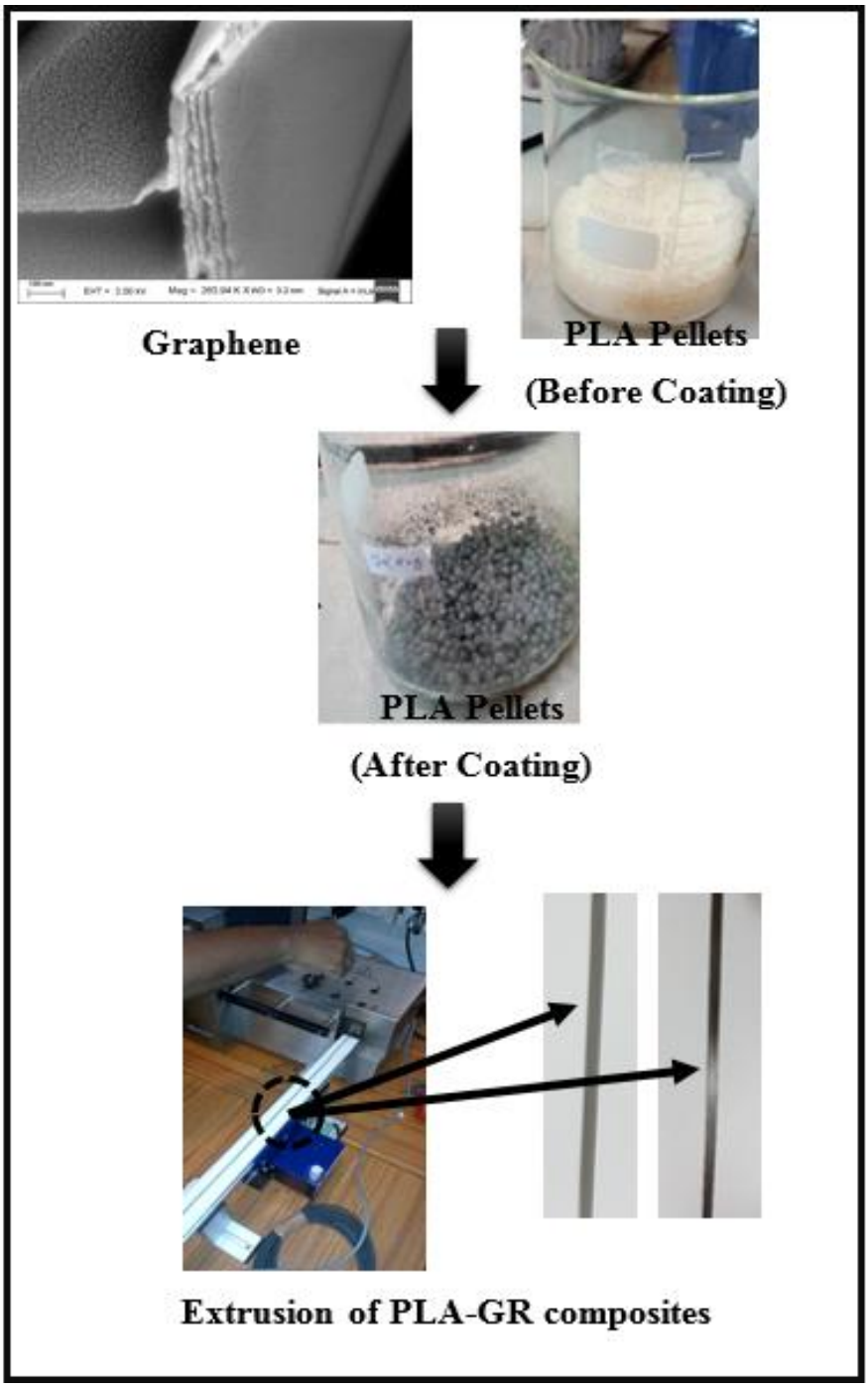

Fig. 2.1 Schematic representation for the fabrication of PLA-M-GR nanocomposites

2.2.3 Characterization

2.2.3.1 X-ray diffraction analysis (XRD)

The diffraction patterns of GR, PLA and the nanocomposites were obtained using an advance diffractometer (Make: Bruker, Model: D8). The analysis was carried out in an air atmosphere under room temperature and in the presence of radiation source Cu-Kα (λ= 0.15406 nm). The instrument was acted at 40 kV and 40 mA during the analysis. The diffraction data were recorded maintaining step size of 0.5 s, 2θ range of 1-50° and scanning rate of 0.05 s^{-1}.

2.2.3.2 Fourier transform infrared spectroscopy (FTIR)

The spectral analysis of GR, PLA and the nanocomposites were carried out using a FTIR spectrometer (Perkin Elmer, Model: Frontier). The FTIR spectrum was obtained for GR under diffuse reflectance mode (DRM), whereas attenuated total reflectance mode (ATRM) was used for the PLA-M and nanocomposite strips. The FTIR spectra of all the samples were acquired within the wavenumber region 4000-400 cm^{-1}. Resolution setting was 4 cm^{-1} and scan speed was 16 spectra per second during the characterization.

2.2.3.3 Gel permeation chromatography (GPC)

The molecular weight measurement of PLA samples melt-processed at different temperature conditions (200 and 210 °C) was carried out using a high-performance liquid chromatography (Make: Shimadzu, Model: LC-20A). The instrument was equipped with PLgel 5 µm mixed D columns (Agilent) along with standards of polystyrene (M_W range 300–500,000). For calibration of molecular weight, chloroform (HPLC grade) was used as eluent at a flow rate of 1mL/min under room temperature. Appropriately, 2 mg of PLA-M samples was dissolved in chloroform before injecting the solution into the column.

2.2.3.4 Raman spectroscopy

Raman spectra of PLA-M and its nanocomposites were carried out using a spectrometer (Make: Lab Ram HR Model: Horiba Jobin Vyon) equipped with a Nd: YAG diode-pumped laser (1W, 1064 nm) and operated at an excitation wavelength of 514 nm. The materials were scanned in the wavenumber ranging from 3000 to 500 cm^{-1}.

2.2.3.5 Thermogravimetric analysis (TGA)

Thermogravimetric analyzer (Make: Perkin Elmer, Model: TGA4000) was utilized to acquire the thermal degradation pattern of PLA nanocomposites. The samples (7.5±0.3 mg) were subjected to TG analysis in the temperature ranging from 25 to 700 °C at a heating rate of 10 °C/min. Nitrogen gas flow of 20 mL/min was maintained during the analysis.

2.2.3.6 Differential scanning calorimetry (DSC)

The investigation of thermal properties of PLA and the nanocomposites was carried out using a differential scanning calorimeter (Make: NETZSCH, Model: DSC204 F1). The samples (7.5±0.5 mg) were subjected to DSC analysis in the temperature ranging from 25 to 180 °C at 10 °C/min heating rate in presence of nitrogen atmosphere. After the first heating cycle, in order to remove the thermal history, an isothermal condition of 180 °C was maintained for 5 min. Thereafter, 10 °C/min cooling rate was applied to cool the samples down to 25°C and then followed by a second heating cycle i.e. 25 °C to 180 °C at 7.5 °C/min heating rate. The glass transition temperature (T_g), melting temperature (T_m), crystallization temperature (T_{cc}) and percentage crystallinity (%X_c) were determined from the thermal profile obtained from the second heating cycle.

2.2.3.7 Mechanical property analysis

The mechanical properties such as tensile strength, elongation at break (%) and

Young's modulus were determined using a Universal Testing Machine (Make: Kalpak instruments, Model: KIC-2-050-C, India). A load cell of 50 kN with a crosshead speed of 5 mm/min were applied on the specimen (60 mm x 4 mm x 0.5 mm) under standard conditions for thin films following ASTM D 882. Five different samples were carried out and average value is reported in the results.

2.2.3.8 Hardness analysis

The harness test of PLA and the nanocomposite samples was carried out using a Durometer (Make: Hiroshima, Model: GGR 30). ASTM standard 2240 was followed to calculate the shore hardness for all the samples during analysis. The analysis was carried out in minimum five different places of the composites and the average value of the results are reported.

2.2.3.9 Dynamic mechanical analysis (DMA)

The storage modulus and tan δ values of PLA and the nanocomposites were obtained using a dynamic mechanical analyser. (Make: NETZSCH, Model: DMA 242E). The dimension of the samples used for analysis is 5 mm x 4 mm x 0.1 mm. The analysis was conducted using tension mode under the temperature condition of 25 to 100 ^{o}C with a 3 ^{o}C/min heating rate. The dynamic mechanical properties were obtained at three different frequency conditions such as 1, 5 and 10 Hz.

2.2.3.10 Contact angle analysis

The contact angle measurements of PLA-M and PLA-M-GR nanocomposites were performed using a goniometer (KRUSS goniometer) via sessile drop method. The contact angle was measured within 60 s after 5 µL droplet of water was detached from the injector. The measurement was carried out at five different locations and the average value was reported.

2.2.3.11 Impedance analysis

The impedance analysis of PLA-M and the nanocomposites were investigated using Autolab (Metrohm). Potentiostatic frequency response analysis was carried out in the frequency range of 0.1 to 10^5 Hz. Resultant impedance was compared in three different frequency points, namely 0.1, 10 and 21544 Hz.

2.2.3.12 Morphology analysis

The morphology and selected area diffraction (SAED) pattern of PLA-M and the nanocomposites were pictoriated using a transmission electron microscopy (TEM) (Make: JEOL, Model: JEM 2100). The instrument was operated at 200 kV during analysis. The TEM sample was prepared by solution casting over the carbon-coated TEM grid. The topography of the samples and their corresponding fractured specimens was visualized using a Field emission scanning electron microscopy (FESEM) (Make: Zeiss, Model: Sigma). Gold sputtering over the samples were maintained for 180 s before subjecting to FESEM analysis and the instrument was operated between 2-3 kV.

2.2.3.13 Melt rheology analysis

The rheological measurements of PLA and the nanocomposites were carried out by using a controlled stress rheometer (Make: Anton Parr, Model: MCR 102) having parallel plate arrangement (50 mm in diameter) in the melt state. The temperature range was so chosen in order to operate above the melting temperature of PLA. Residual thermal histories of the test samples were eliminated by heating for 5 min. The dynamic frequency sweep test was performed with a strain level of 5% in the linear viscoelastic region (LVE) which was predetermined experimentally by the amplitude sweep test.

2.2.3.14 Solution viscosity measurement

The solution viscosity of the samples was measured by using DIN-Ubbelohde viscometer (Make: SI Analytics, Model: CT 72/2) in order to investigate the effect of

GR on viscosity average molecular weight of PLA. A stock solution of 12 mg/mL was initially prepared by dissolving weighed amount of strip in chloroform. Solutions of different dilution were made from the stock solution by adding suitable amount of chloroform. For the composites, the solutions were filtered using 0.2 µm PTFE filter (AXIVA syringe filter). All the investigations were carried out at 25 °C.

2.3 Results and Discussion

2.3.1 XRD analysis

XRD analysis for neat GR, PLA-M and PLA-M-GR nanocomposites were accomplished to experience the diffraction pattern by which the crystallographic nature of the PLA and composites can be interpreted. For GR, a sharp diffraction peak is observed at 26.52^{o}, which corresponds to graphitic carbon structure of (0 0 2) plane arrangement (R. B. Valapa et al., 2015a). Diffractograms recorded (Fig. 2.2) for melt processed PLA shows a broad peak of scattered pattern close to 2θ ~16.7°, which corresponds to the (1 1 0) and (2 0 0) planes of PLA (Krikorian & Pochan, 2003; Murariu et al., 2010; Valapa et al., 2015a) . This intense broad peak indicates the presence of orthorhombic PLA crystals. Due to rapid cooling after extrusion (200 °C to room temperature in air), count of the crystalline regime becomes less. In PLA-M-0.05GR and PLA-M-0.2GR composites, broad spectrum close to 2θ ~16.7° resembles same crystal structure for PLA still after incorporation of graphene. The absence of peak at 2θ ~26.52° for PLA-M-0.05GR indicates complete exfoliation of graphitic carbon structure within the composite. A small peak in PLA-M-0.2GR at 2θ ~26.35° reveals the presence of graphene stacks in the composite with small decrement in 2θ. An increment in ‘d’ spacing for the graphene moiety is due to the incorporation of PLA chains between the graphene layers (Al-Mulla et al., 2011). Thus, PLA-M-0.05GR can be termed as exfoliated PLA/ graphene composite while PLA-M-0.2GR can be termed

as intercalated PLA/graphene composite.

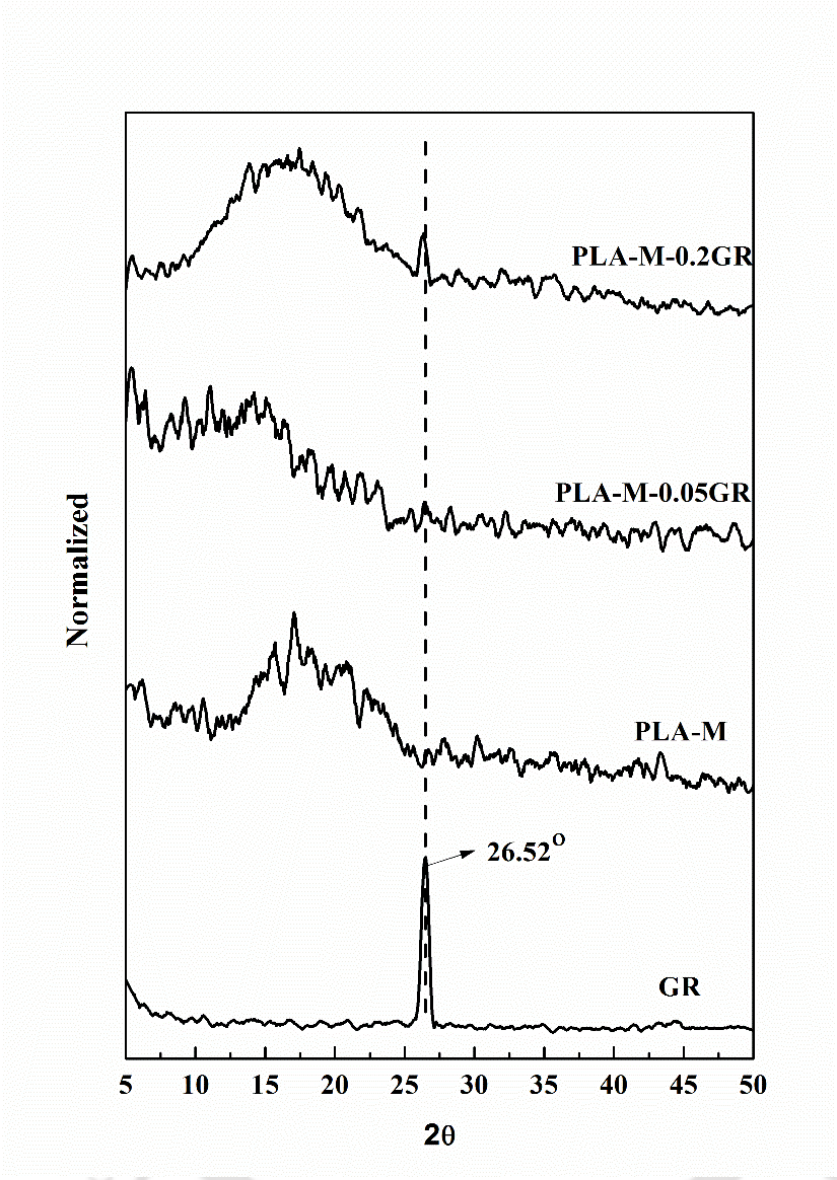

Fig. 2.2 XRD pattern for GR, PLA-M, PLA-M-0.05GR and PLA-M-0.2GR nanocomposites

2.3.2 Morphological analysis

Graphene dispersion within the PLA-M matrix in case of the composites was investigated using FESEM and TEM images. It can be visualized in Fig.2.3 (b) and 2.3 (c) that agglomeration is less in case of PLA-M-0.05GR as compared to PLA-M-0.2GR. This observation indicates uniformity in graphene distribution in PLA-M-0.05GR compared to PLA-M-0.2GR. The FESEM image obtained for fractured surface of PLA-

M-0.2GR suggests material pull out when subjected to failure (Fig. 2.3(d)). The SAED (selected area electron diffraction) pattern as well as morphology obtained for PLA-M-0.2GR are shown in Fig. 2.3(e) and 2.3(f), respectively. These images display the presence of layered graphene within the PLA matrix.

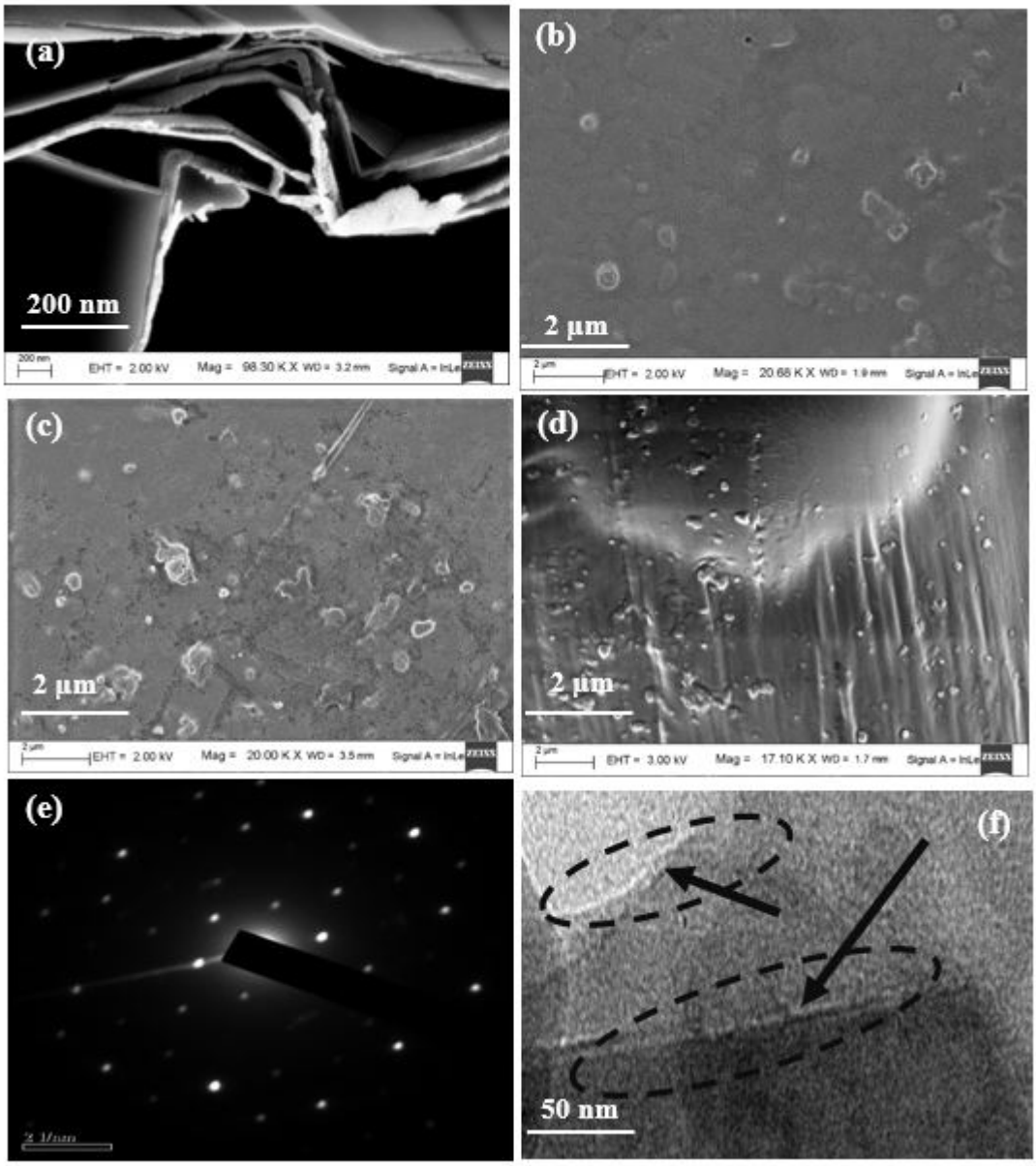

Fig. 2.3 Morphological analysis (a) FESEM image for GR, (b) FESEM image for PLA-M-0.05GR, (c) FESEM image for PLA-M-0.2GR, (d) FESEM image for PLA-M-0.2GR (fractured surface), (e) SEAD pattern for PLA-M-0.2GR and (f) TEM image for PLA-M-0.2GR

2.3.3 FTIR analysis

FTIR spectra of GR, PLA-M, PLA-M-0.05GR and PLA-M-0.2GR composites can be seen from Fig. 2.4 In the FTIR spectrum of GR, the appearance of bands at 1645 and 1585 cm^{-1} corresponds to C=C and C-C stretching of carbon backbone. Appeared peak at 3437 cm^{-1} in GR implies presence of stretching vibration due to functional group –OH. The presence of OH functionalities might be due to external adsorbed moisture or unreduced OH groups still present in GR after thermal exfoliation of expandable graphite into exfoliated graphite (Zheng et al., 2004). For PLA-M, the presence of bands at 1746 and 1452 cm^{-1} is because of the stretching of C=O, C-CH_3 bonds, respectively and the peaks at 1182, and 1079 cm^{-1} correspond to stretching of -C-O present in PLA, respectively (Tripathi & Katiyar, 2016b). The FTIR spectra of PLA-M-GR composites are same as that of PLA-M and remains unaltered except for the presence of peak at 1645 cm^{-1}, which confirms the incorporation of GR in the PLA matrix (Yoon et al., 2011).

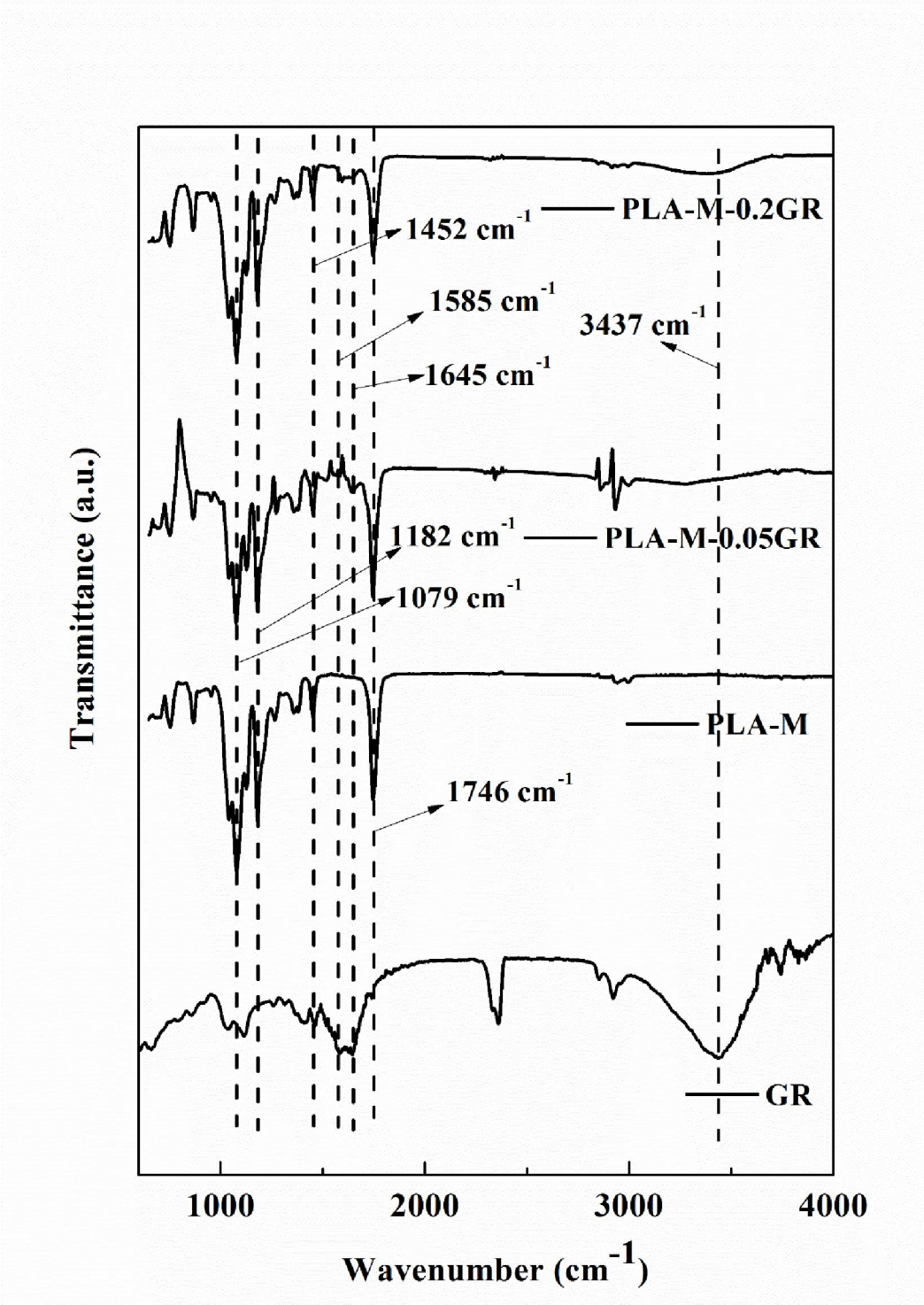

Fig. 2.4 FTIR spectra for GR, PLA-M, PLA-M-0.05GR and PLA-M-0.2GR nanocomposites

2.3.4 Raman spectroscopy

Raman spectrum is one of the major parameters to characterize graphene and graphene based composites. The Raman spectra obtained for GR, PLA-M, and PLA-M-0.2GR are depicted in Fig. 2.5 The I_G band corresponding to 1582.47 cm^{-1} is indicative of sp^2 carbon moiety present in GR and according to literature reports, peak corresponding to 1587 cm^{-1} is indicative of single layer graphene (Wall, 2011a). The stacked layers are calculated (Wall, 2011a) from wave number corresponding to I_G and is found to be 4.58 i.e. ~5. It can be seen from Fig. 2.5, the spectra obtained for PLA-M and PLA-M-0.2GR show several peaks in the wavenumber region ranging from 1000 to 2200 cm^{-1} which correspond to PLA chain vibration. In case of GR, the G-band is noticed at 1582.47 cm^{-1}, which is shifted to 1584.63 cm^{-1} in case of PLA-M-0.2GR. It reveals the presence of graphene inside the composite. The separation of graphene layers may be due to sonication effect and incorporation of polymer chains inside the graphene layers.

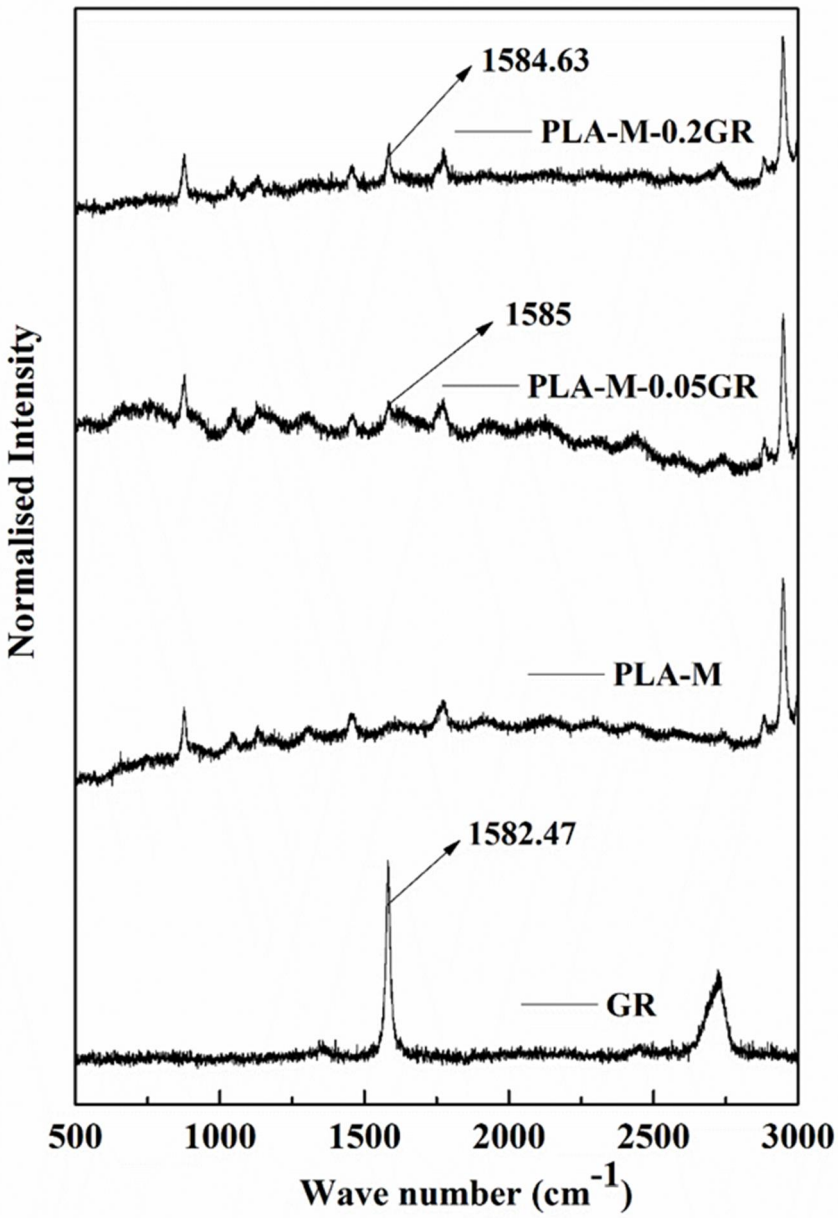

Fig. 2.5 Raman spectra for GR, PLA-M, PLA-M-0.05GR and PLA-M-0.2GR nanocomposites

2.3.5 TGA

Thermal stability assessment for PLA-M, PLA-M-0.05GR, and PLA-M-0.2GR was carried out using TGA analysis and the corresponding thermographs are presented in Fig. 2.6. The onset degradation temperature (T_{onset}) is indicative of temperature at which degradation of substances is initiated i.e. indicator of threshold limit of stability towards

heating. It can be noticed from Table 2.1 that for PLA-M, PLA-M-0.05GR and PLA-M-0.2GR, the onset degradation temperatures are 337.2, 350, and 345 °C, respectively. The temperature at which 50% weight loss takes place (T_{50}) for PLA-M, PLA-M-0.05GR and PLA-M-0.2GR are noticed to be 351.4, 367.6, and 363.9°C, respectively. The maximum degradation temperature (T_{max}) i.e. temperature at which rate of weight loss for samples is the maximum and found to be 360.2, 371.8 and 365.6 °C, respectively for PLA-M, PLA-M-0.05GR, and PLA-M-0.2GR nanocomposites. The thermal analysis results reveal that the incorporation of graphene enhanced the thermal stability of PLA significantly, which can be the result of barrier effect of layered morphology of graphene towards emission of gases and heat transmission, the governing parameters for thermal degradation of substances (Murariu et al., 2010; Valapa et al., 2015a). In case of PLA-M-0.05GR, thermal stability is noticed to be higher than that of PLA because of better dispersion that enhanced compatibility between PLA and graphene. In case of higher loading of GR, thermal stability for the composites decreases due to agglomeration. Thermal stability of nanocomposites depends on the dispersion state, interfacial interaction between filler and matrix, filler dimension, polymer molecular weight, and crystallinity. Extrusion process is associated with some extent of non-uniformity of filler dispersion due to formation of agglomerates within polymer matrix particularly at higher loading. Such agglomerates can cause local phase separation and reduction in interfacial adhesion, which leads to generation of local thermal stress and thereby enhancing the thermal degradation. The above situation is reflected in this present work where PLA-M-0.2GR with higher loading of GR shows lesser thermal stability as compared to the relatively better dispersed composite PLA-M-0.05GR with lower loading of GR. Similar trend is reported by Wen et al., (2010) for PLA/SiO_2

nanocomposites and Kim et al., (2009) for polylactide/Exfoliated graphite composite (Kim & Jeong, 2010; Wen et al., 2011).

The T_{onset} and T_{max} values for PLA-M-0.05GR are significantly higher than that of PLA and are found to be about 13 and 12 °C higher than neat PLA, respectively. In a study based on solution casting approach, for 0.5 wt.% of GR reinforcement in the PLA matrix, improvement in the T_{onset} and T_{max} values was reported to be 6 and 2 °C, respectively (Valapa et al., 2015a). Improvement in terms of T_{onset} obtained in the present work is better than expanded graphite (EXG) reinforced PLA composites fabricated by compression moulding technique, where 10 °C enhancement in T_{onset} value was achieved at 12 wt. % loading of filler (Murariu et al., 2010). In the present study, coating of GR on PLA followed by small scale extrusion allowed better dispersion of nanofiller GR in the PLA matrix and exhibited a remarkable improvement in terms of thermal stability.

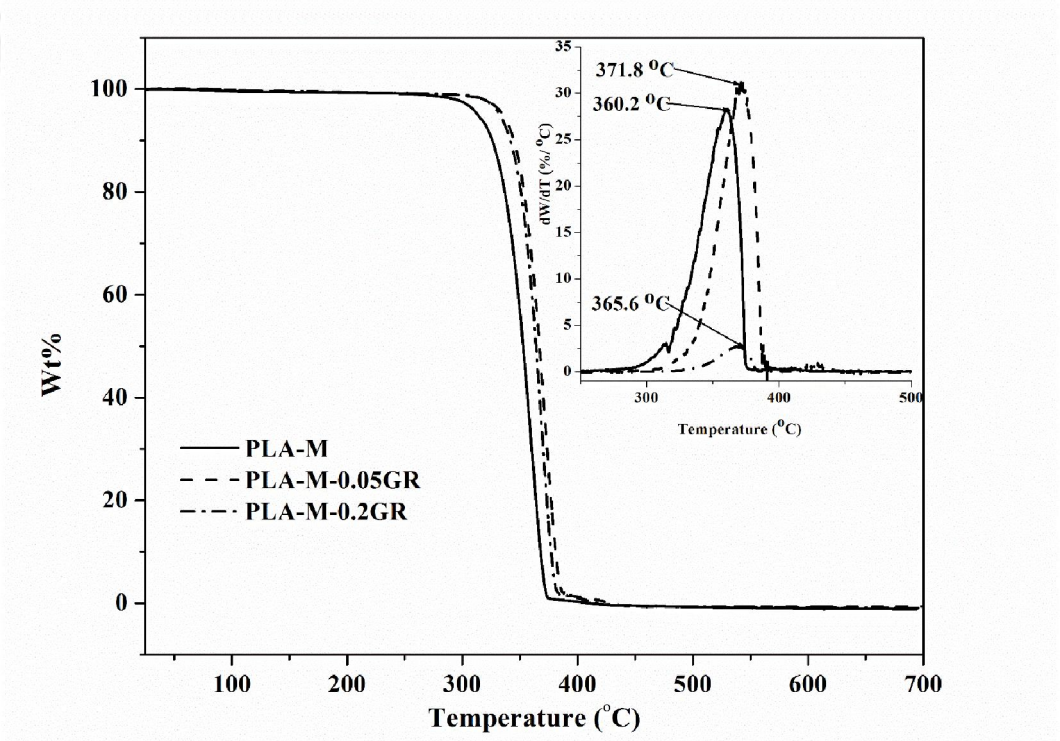

Fig. 2.6 TGA profile of PLA-M, PLA-M-0.05GR and PLA-M-0.2GR (DTG spectrum is in the inset)

Table 2.1 Thermal properties of PLA-M, PLA-M-0.05GR and PLA-M-0.2GR

Sample	T_{onset} (°C)	T_{50} (°C)	T_{max} (°C)	T_m (°C)	T_c (°C)	T_g (°C)	$E_{Friedman}$ (kJ/mol)	$E_{F\text{-}W\text{-}O}$ (kJ/mol)
PLA-M	337.2	351.4	360.2	151.6	120.4	62	153.8	151.4
PLA-M-0.05GR	350	367.6	371.8	152.6	128.3	63	164.3	154.3
PLA-M-0.2GR	345	363.9	365.6	152.7	126	63	195.1	178.9

2.3.6. DSC analysis

DSC analysis was executed to investigate non-isothermal cold crystallization nature of PLA-M and PLA-M-GR nanocomposites. Glass transition point (T_g) of the PLA-M-0.05GR and PLA-M-0.2GR (63 °C) is noticed to be almost similar to that of PLA-M (62 °C), which reveals no significant formation of lower molecular weight PLA chains on processing with graphene (Fig. 2.7) (Valapa et al., 2015a). The melting temperature of PLA-M-0.05GR and PLA-M-0.2GR composites is slightly increased which may be due to the incorporation of graphene that forms more stable and uniform crystals of PLA. Crystallization temperature significantly increased by 7.9 °C and 5.6 °C for PLA-M-0.05GR and PLA-M-0.2GR, respectively compared to PLA-M. This may be due to effect of graphene on nucleation of PLA crystals and hindrance created by the graphene towards diffusion of PLA chains to nucleus surface. Second heating cycle data was used to calculate the degree of crystallinity of PLA and composites. It suggests that because of immediate cooling of the melt processed composites from 200°C to room temperature, crystalline zone is very small. Even though low crystallinity is present in melt processed PLA, due to the inclusion of filler (GR)

crystallinity increases to 0.361% and 1.16% from 0.287% for PLA-M-0.05GR and PLA-M-0.2GR, respectively. It is reported in literature that reinforcing substances can act as nucleating agent, which provides surface for heterogeneous crystallization of polymer and because of this nucleating effect, melting temperature, crystallization

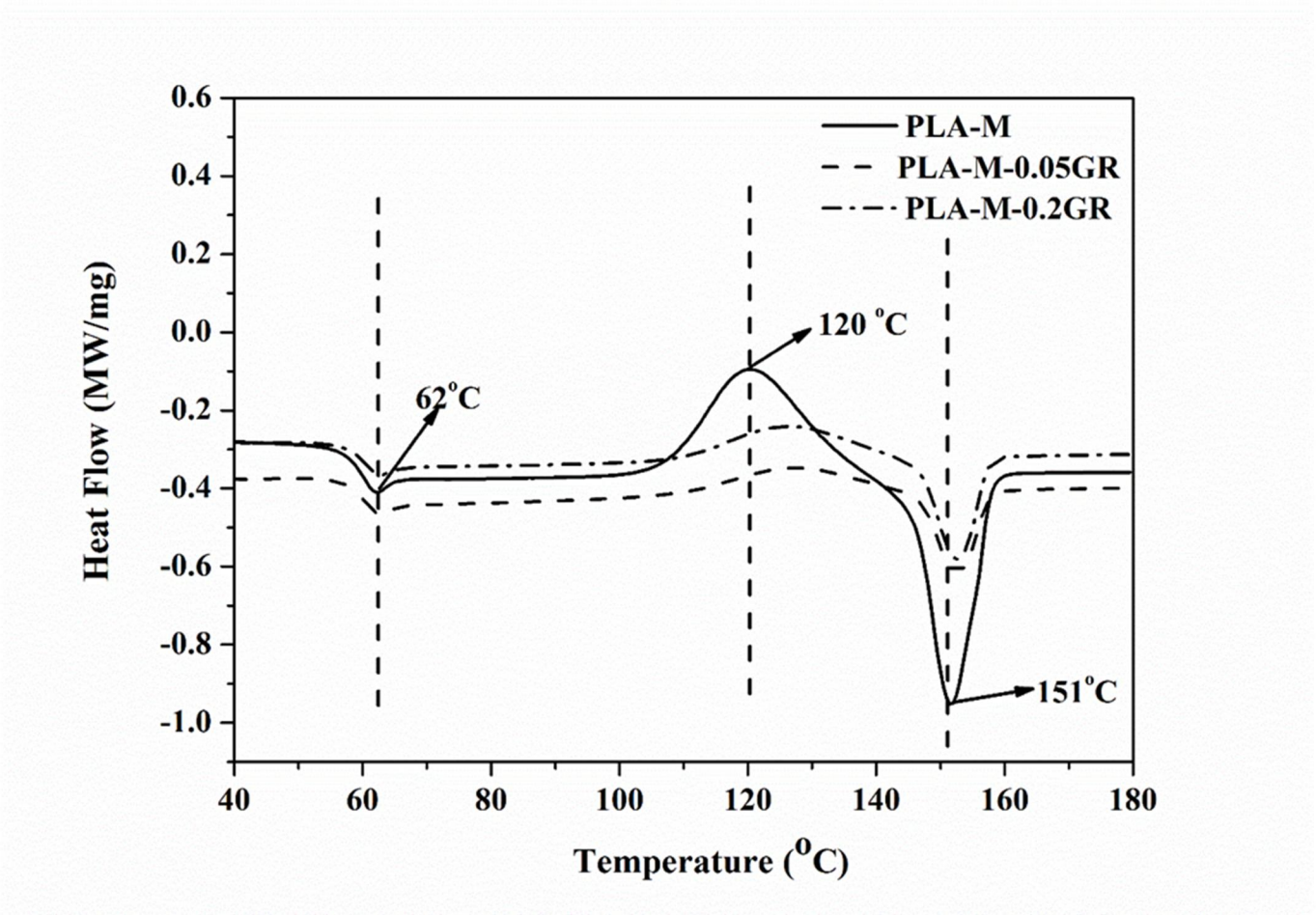

Fig. 2.7 DSC thermogram for PLA-M, PLA-M-0.05GR and PLA-M-0.2GR

2.3.7 Contact angle analysis

Wettability nature of the surface of PLA and its composites is determined by analyzing contact angle values. The contact angle value along with the standard deviation for PLA-M, PLA-M-0.05GR, and PLA-M-0.2GR is found to be 78.7^0 (2.9), 88.5^0 (2.8) and 84.2^0 (2.3) respectively. The enhancement observed in contact angle value for PLA composites is due to the hydrophobic nature of GR (Pinto et al., 2013). However, the decrement in contact angle for PLA-M-0.2GR is observed with respect to PLA-M-

0.05GR. This is because of the increased surface roughness of PLA with higher loadings of GR (Hernández et al., 2007; Misra et al., 2007), leading to reduced contact angle (Borkotoky et al., 2018).

2.3.8 Hardness analysis

The hardness analysis for melt processed PLA-M, PLA-M-0.05GR and PLA-M-0.2GR was carried out using a durometer. The hardness values are determined under the shore hardness scale regime ranging from 0-100. The average value for hardness is evaluated to be 78, 84 and 84 in the durometer scale for PLA-M, PLA-M-0.05GR, and PLA-M-0.2GR, respectively. The results obtained indicate that the presence of GR enhances the deformation resistance of PLA when subjected to external force.

2.3.9 Mechanical properties analysis

Tensile strength, Young's modulus and (%) elongation at break analyses provide the information about plasticity, brittleness and toughness characteristics of PLA and its composites (Table 2.2). It can be seen from the Table 2.2 that PLA-M-0.05GR and PLA-M-0.2GR composites exhibit ~19% and ~6% improvement in terms of tensile strength properties as compared to that of unfilled PLA-M. The lower tensile strength exhibited by PLA is due to the low crystalline content present in the melt processed PLA. It can be noticed from the Table that Young's modulus value is also found to be enhanced by ~32% and ~7% for PLA-M-0.05GR and PLA-M-0.2GR, respectively as compared to that of neat PLA-M. Elongation-at-break (%) value is not affected much for the composites and observed ~ 15% and ~12% for PLA-M-0.05GR and PLA-M-0.2GR, respectively with respect to neat PLA-M (13%). The improvement in all the above mentioned mechanical properties exhibited by the composites is due to better dispersion of GR within the matrix PLA-M. The results indicate that GR acted as an effective reinforcement in improving the mechanical properties of PLA-M. However,

the decrement in mechanical properties exhibited by PLA-M-0.2GR as compared to that of PLA-M-0.05GR may be due to the agglomeration effect pronounced at higher loading of GR.

Table 2.2 Ultimate tensile properties analysis results

Sample	UTS (N/mm^2)	Young modulus (N/mm^2)	Elongation at break (%)
PLA-M	29.51	4.30	12.93
PLA-M-0.05GR	35.08	5.66	14.47
PLA-M-0.2GR	31.34	4.58	11.74

2.3.10 DMA

The storage modulus (E) result obtained for PLA-M, PLA-M-0.05GR, and PLA-M-0.2GR is depicted in Fig.2.8. At 25 °C, the storage modulus value for PLA-M and its composites is noticed to be 3048 and 3838 MPa, respectively. With increasing temperature, the storage modulus value for both PLA and its composites decreases. With increase in temperature from 25 to 55 °C the storage modulus reduces to 2511, 3287 and 3226 MPa for PLA-M, PLA-M-0.05GR and PLA-M-0.2GR, respectively. These results are indicative of good interaction of GR with the PLA matrix (Joseph et al., 2003). Thereafter, drastic reduction in the storage modulus can be noticed for both PLA-M and its composites in the temperature range of 55 to 60 °C. This reduction in the storage modulus is due to the transition of PLA from elastic to viscous state. The tan δ plot for PLA and its composites is shown in the inset of Fig.2.8. The glass transition temperature (temperature that corresponds to maximum tan δ) for PLA-M and its composites is noticed to be ~ 65 ^{0}C. This implies that the addition of GR does

not influence the primary relaxation of PLA chains. Otherwise, reinforcement of GR does not show any effect on the folding pattern of PLA chains. Due to this fact, transition pattern of polymeric chains from elastic to viscous state is experienced to be similar in nature for both PLA and its composites. It can be noticed that the T_g values obtained for both PLA and its composites using DSC analysis is lower as compared to the result obtained via DMA. This is because primary chain movement of PLA is driven by direct heat flow in DSC analysis whereas DMA makes use of thermomechanical force as the governing factor. Figure 2.9 indicates the storage modulus as a function of frequency for PLA-M-0.05GR. The tan δ plot for the corresponding composite can also be seen from the inset of Fig.2.9. With respect to shift in frequency from 1 Hz to 10 Hz, the enhancement in the storage modulus is noticed for PLA-M-0.05GR composite. The glass transition temperature also shifts to higher values with increasing frequency. This may be due to the delay in PLA chain relaxation at higher frequency condition.

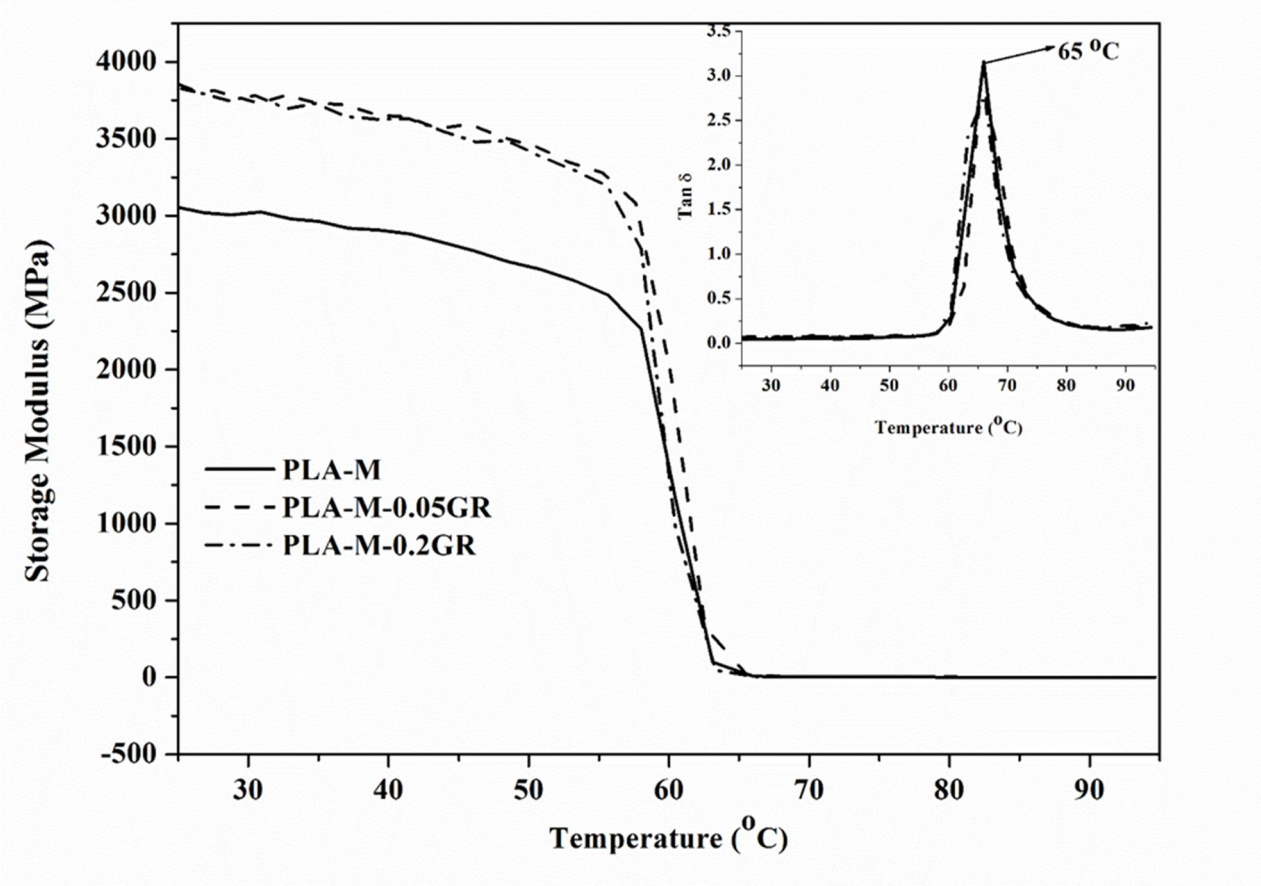

Fig. 2.8 Storage modulus and Tan δ plot (inset) for PLA-M, PLA-M-0.05GR and PLA-M-0.2GR at 1 Hz frequency

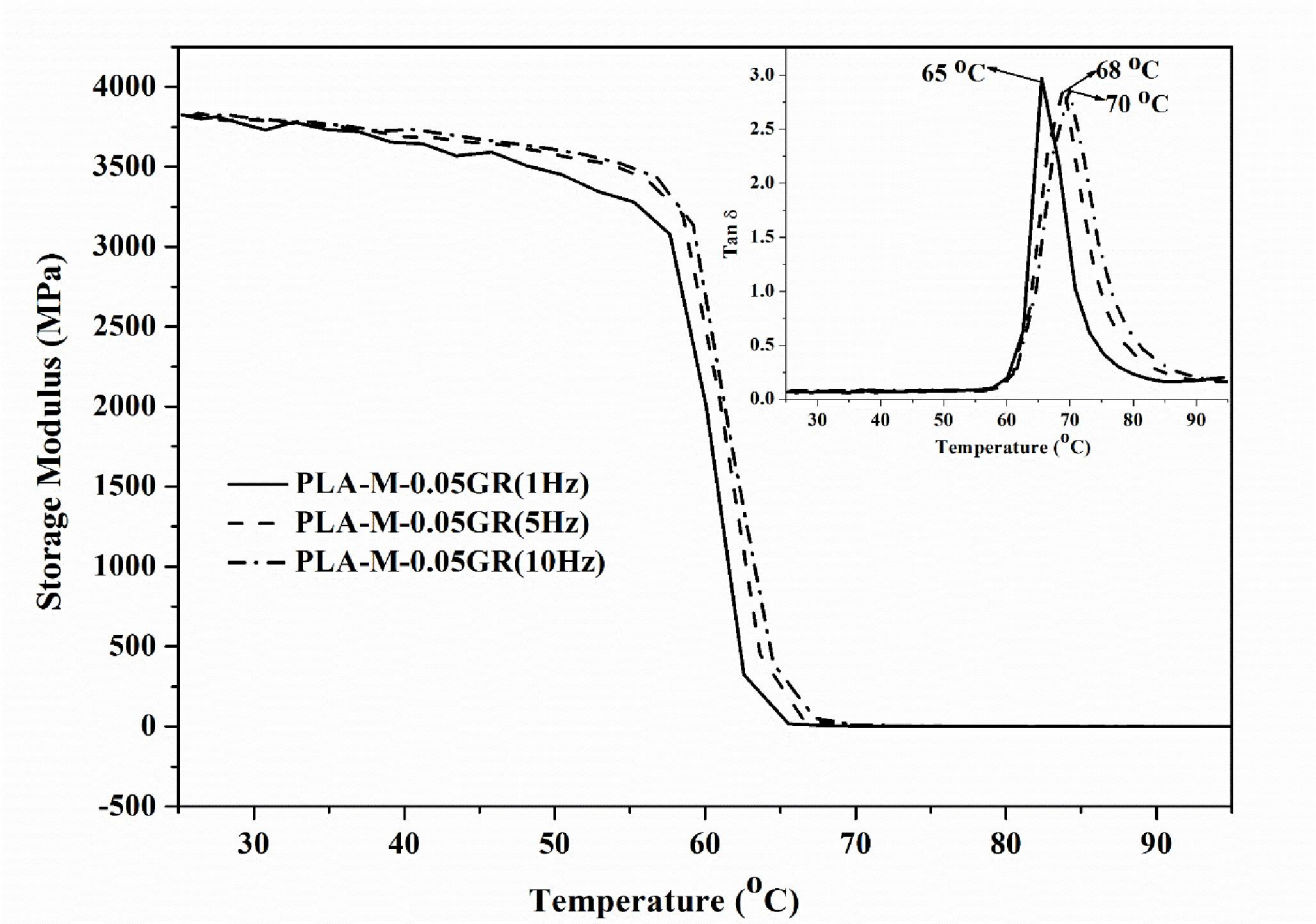

Fig. 2.9 Storage modulus and Tan δ plot (inset) for PLA-M-0.05GR at different frequencies (1 Hz, 5Hz and 10Hz)

2.3.11 Impedance analysis

The influence of GR on the electrical conductivity of PLA is examined using impedance analysis. The incorporation of GR in the PLA-M decreases the impedance values of PLA with rise in frequency conditions. At a frequency condition of 10 Hz, impedance is found to be decreased by 73.7% and 94.2% for PLA-M-0.05GR and PLA-M-0.2GR, respectively, in comparison to that of pure PLA-M (Fig. 2.10). In general, the desired value of impedance of conductive materials is well below the synthesized composites (range in the order of 10^9 Ohm). Therefore, the addition of graphene shows a positive effect on conductivity and still the values are not lucrative

for application like electrode, sensor, etc.(Wang et al., 2012). It can be concluded that the inclusion of graphene forms conductive network within PLA matrix, which increases with graphene loading. However, even 0.2 wt. % loading of GR appears insufficient to achieve good conductive channel by this processing.

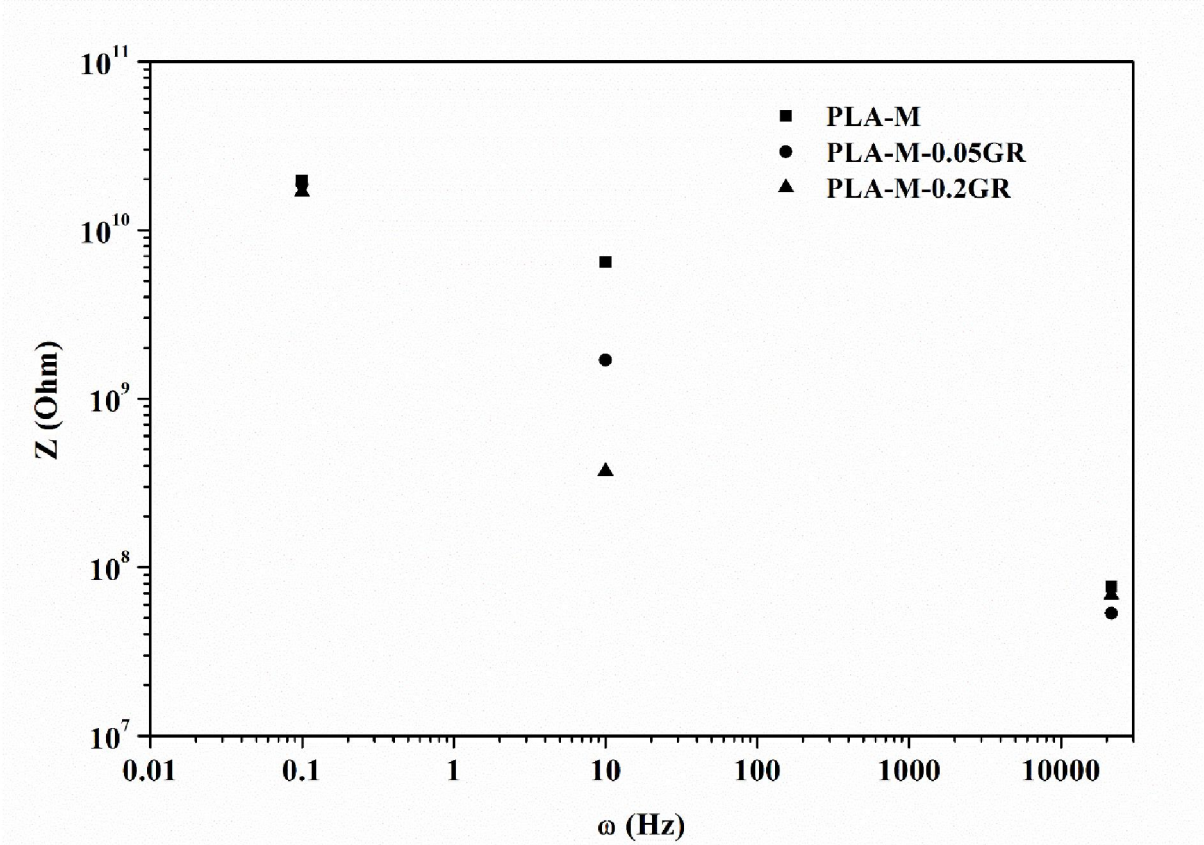

Fig. 2.10 Plot of impedance vs. frequency for PLA-M, PLA-M-0.05GR and PLA-M-0.2GR at the frequencies of 0.1 Hz, 10 Hz, and 21544 Hz

2.3.12 Thermal degradation kinetics of PLA and PLA/GR nanocomposites

The effect of GR on the thermal properties of PLA-M is studied using thermal degradation analysis. The kinetic parameters such as order (n), rate constant (k), activation energy (E), and pre-exponential factor (A) are determined by performing thermal degradation kinetic analysis of both PLA and its composites.

The rate of reaction is generally expressed by the following Arrhenius equation

$$\frac{d\alpha}{dt} = k \times f(\alpha) \quad \textbf{(2.1)}$$

$$\frac{d\alpha}{dt} = A \times EXP(-E / RT) \times f(\alpha) \quad \textbf{(2.2)}$$

Where $\frac{d\alpha}{dt}$ is the rate of reaction, 'A' is pre-exponential factor, 'E' is activation energy, and 'α' is degree of conversion. Now considering 'β' as heating rate, Eq.2.2 can be expressed as

$$\frac{d\alpha}{dT} = (A / \beta) \times EXP(-E / RT) \times f(\alpha) \quad \textbf{(2.3)}$$

In general, two different approaches are practiced to solve the above differential equation and get the kinetics data namely, (i) model fitting method and (ii) model free method. Model fitting method depends on the statistical fitting of data, whereas no modelistic assumptions are required in case of model free method (Apaydin-Varol et al., 2014). In the present study, thermal degradation kinetic analysis is carried out using model free method. Friedman equation is derived from Arrhenius equation by taking logarithm on both sides and is expressed as Eq.2.4 (A. Al-Mulla & Shaban, 2008). Flynn Wall Ozawa's expression is given by Eq. 2.6 and is derived using Doyle's approximation (Aboulkas & El Harfi, 2008; Gorghiu et al., 2004; Yuzay et al., 2010).

$$\ln \frac{d\alpha}{dt} = \ln A + n \ln(1-\alpha) - E / RT \quad \textbf{(2.4)}$$

Flynn Wall Ozawa method is based on integral approach

$$g(\alpha) = \frac{A}{\beta} \int_{T_0}^{T} \exp(-\frac{E}{RT}) dT \quad \textbf{(2.5)}$$

$$\text{Or, } g(\alpha) = \frac{AE}{\beta R}\int_{x}^{\infty}\frac{\exp(-\mathrm{x})}{x^2}dx, \quad \text{where x is E/RT}$$

$$\text{Or, } g(\alpha) = \frac{AE}{\beta R}\mathrm{p(x)}$$

$$\ln p(\mathrm{x}) = -5.331 - 1.052\frac{E}{RT} \text{ (Doyle's approximation)}$$

$$\ln\beta = \ln[(\mathrm{A}\times\mathrm{E})/(\mathrm{R}\times\mathrm{g}(\alpha))] - 5.331 - 1.052E/RT \quad \textbf{(2.6)}$$

In the present work, Friedman and Flynn Wall Ozawa's methods are applied to derive the activation energy in case of thermal degradation of PLA-M and its composites. The activation energy is calculated from slope of the plot derived using Friedman and Flynn Wall Ozawa methods. The thermal degradation profiles obtained at 5, 10, 20 and 30 °C/min heating rates are used to determine kinetic parameters of PLA and its composites.

The kinetic plots obtained for PLA-M and its composites using Friedman and Flynn Wall Ozawa methods are depicted in Fig. 2.11 and Fig. 2.12, respectively. The activation energy value obtained by the Friedman method for PLA-M, PLA-M-0.05GR, and PLA-M-0.2GR is found to be 154, 164 and 195 kJ/mol, respectively. Similarly, the activation energy value obtained by Flynn Wall Ozawa method for PLA-M, PLA-M-0.05GR and PLA-M-0.2GR is found to be 151, 154 and 179 kJ/mol. The activation energy obtained for PLA-M and its composites by both the methods show increasing trend with respect to increase in GR content. This is indicative of improvement in thermal stability of the PLA-M nanocomposites with the incorporation of GR within the matrix of PLA-M. This reveals the fact that GR acts as an effective reinforcement by increasing the thermal stability of PLA composites.

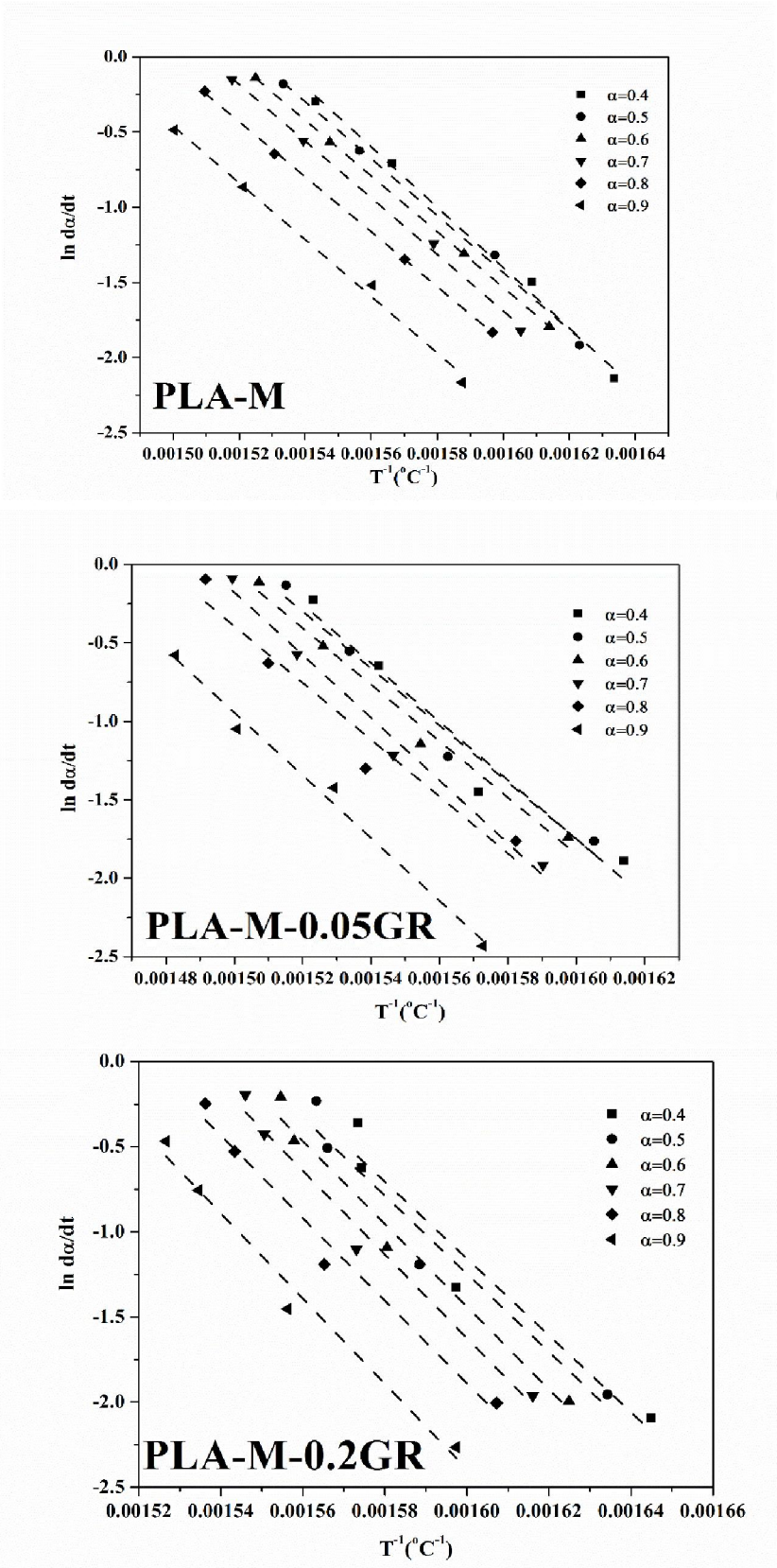

Fig. 2.11 Friedman analysis plot for PLA-M, PLA-M-0.05GR and PLA-M-0.2GR

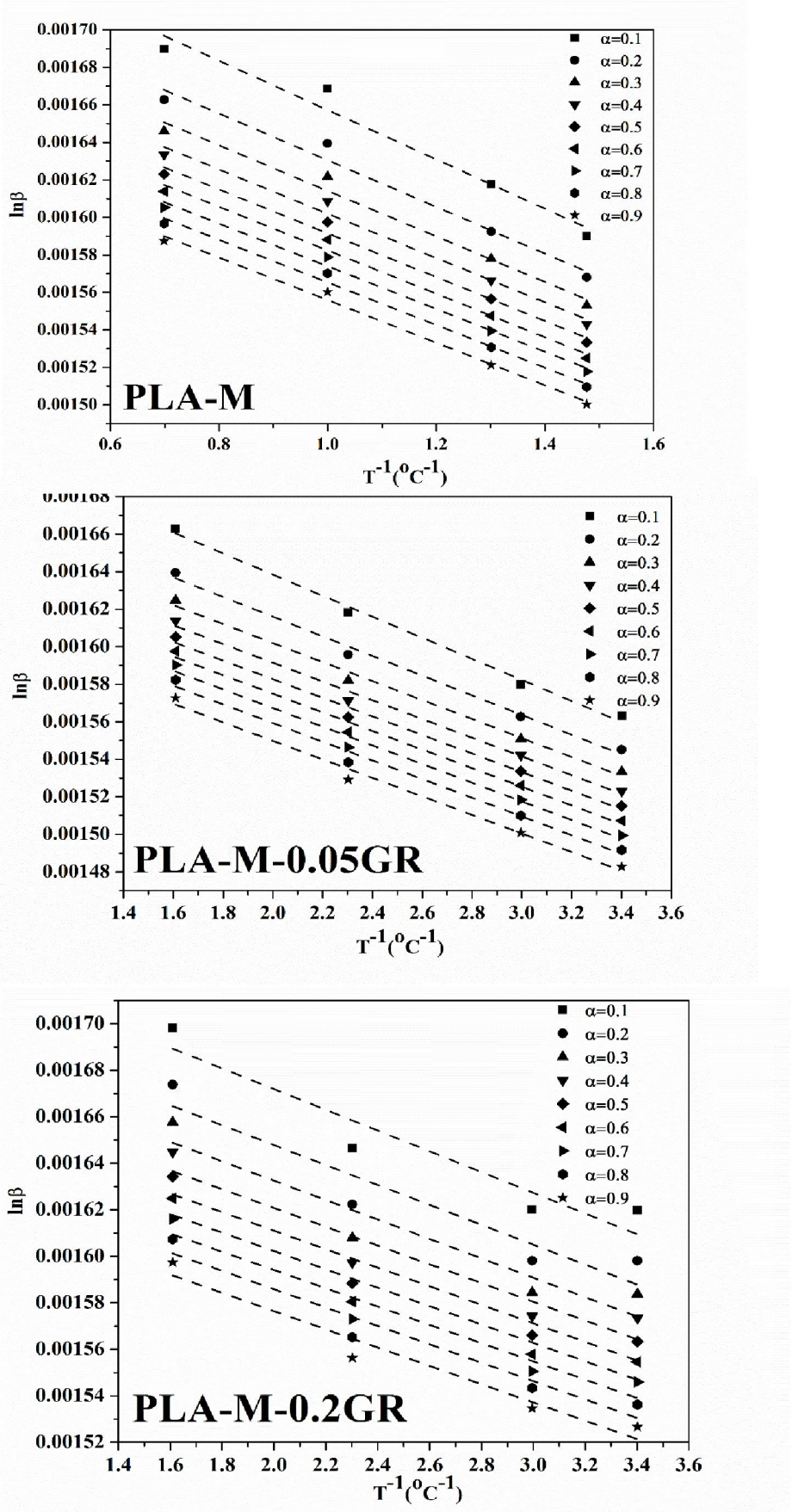

Fig. 2.12 Flynn-Wall-Ozawa analysis plot for PLA-M, PLA-M-0.05GR and PLA-M-0.2GR

The activation energy derived from Flynn Wall Ozawa method is plotted as a function of conversion and is presented in Fig 2.13. It can be seen from the Figure that activation energy for PLA-M and PLA-M-0.2GR increases continuously as a function of conversion but in the case of PLA-M-0.05GR the trend is increasing followed by a flat region after'α'value of 0.4.This may be due to the difference in degradation mechanism. In case of PLA, thermal degradation may be due to random nucleation and in case of GR loaded PLA, both random nucleation and nucleation and growth mechanism are taking place (Valapa et al., 2015a). Due to better dispersion of GR, in case of PLA-M-0.05GR, similar type of degradation reaction takes place after conversion 0.4 whereas in case of PLA-M-0.2GR, due to presence of agglomeration, degradation mechanism is different. The variation of activation energy with respect to conversion visualized indicates that thermal degradation of PLA and its composites occurs through complex

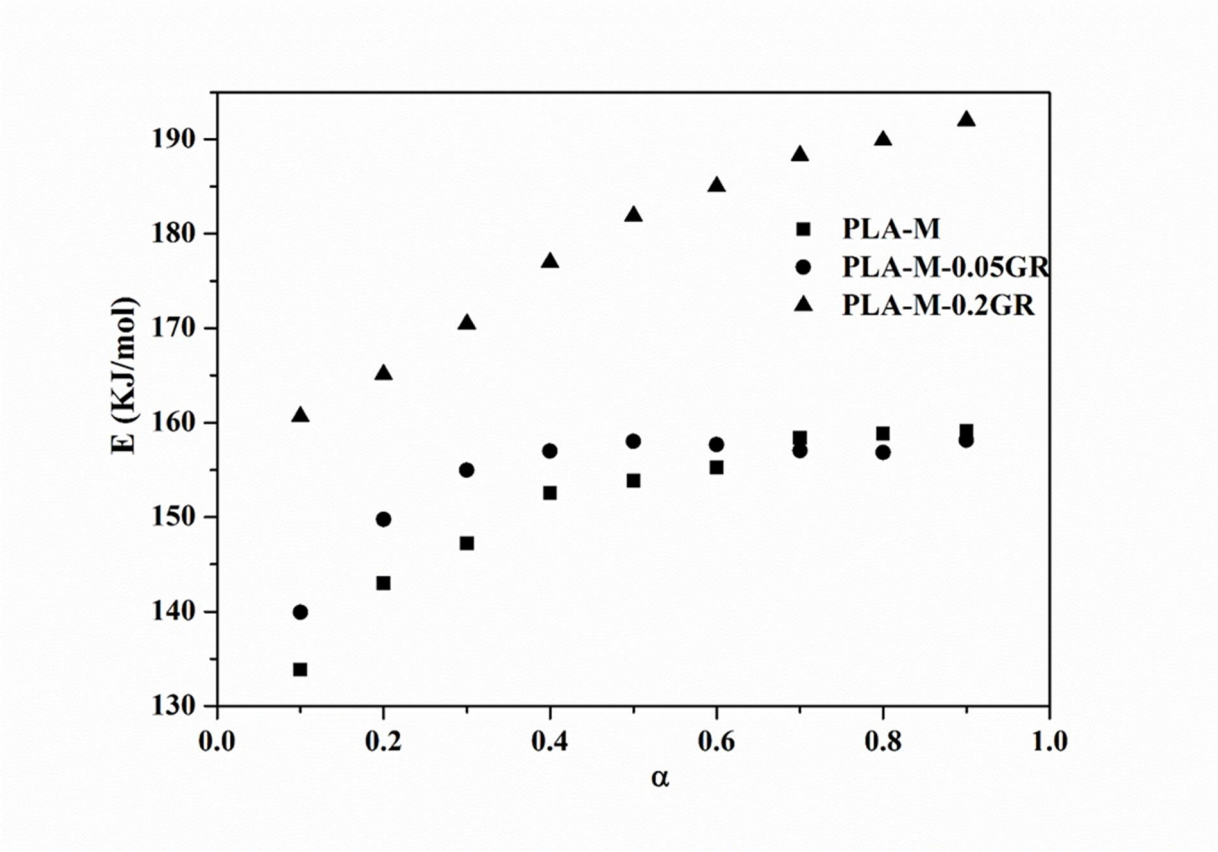

Fig. 2.13 Activation energy as a function of conversion obtained from Flynn-Wall-Ozawa plot

2.3.13 Crystallization kinetics of PLA-M and PLA-GR nanocomposites

Crystallization of PLA is associated with a specific arrangement of polymer chains. The morphology of reinforcements is shown to affect the nucleation rate, crystallization temperature, crystallinity and spherulite size of polymer (Battegazzore et al., 2011b). Therefore, the influence of GR on the crystallization properties of melt processed PLA is examined in the present work. The non-isothermal cold crystallization kinetics for PLA-M and its composites is carried out using the DSC data obtained at different heating rates such as 2.5, 5 and 10 °C/min. Avrami equation is used to study the non-isothermal crystallization kinetics for PLA as well as its composites and is denoted by Eq. (2.7) and (2.8). Avrami constant 'n' signifies nucleation mechanism and growth geometry while the crystallization rate constant is denoted by 'Z' (Miyata & Masuko, 1998; Q. Yuan, Awate, & Misra, 2006).

$$1 - X(t) = EXP(-Zt^n) \quad \textbf{(2.7)}$$

$$\log[-\ln(1 - X(\mathrm{t}))] = \log \mathrm{Z} + n \log \mathrm{t} \quad \textbf{(2.8)}$$

Instantaneous changes of temperature affect the Avrami parameters 'n' and 'Z' and thus this equation was modified by Ozawa considering nonisothermal nature. Cooling rate 'β' was introduced to generate the modified equation (Eq 2.9).

$$\log[-\ln(1 - X(\mathrm{T}))] = \log \mathrm{P}(\mathrm{T}) - m \log \beta \quad \textbf{(2.9)}$$

Mo equation (Eq 2.10) was developed by combining factors from the two processes discussed above. Therefore, consideration of relative crystallinity, heating rate, and crystallization temperature is taken into account. The modified equation (Eq 2.10) contains kinetic factor 'α',which is the ratio of the exponents 'n' and 'm' corresponding to Avrami and Ozawa equations.

$$\ln \beta = \ln F(t) - \alpha \ln t \quad \textbf{(2.10)}$$

For this present study, Tobin equation (Eq 2.11) is also used to investigate non-isothermal kinetics of PLA-M and its composites in which relative crystallinity (X_t) is expressed as a function of time, exponent (n_t), and rate constant (k_t).

$$\log[X_t / (1 - X_t)] = \log k_t + n_t \log t \quad \textbf{(2.11)}$$

Activation energy for crystallization (Δ E) is calculated using Kissinger method (Eq. 2.12) where 'β' is heating rate (°C/min), 'T_P' is peak crystallisation temperature and 'R' is universal gas constant.

$$d[\ln(\beta / T_P^2)] / d(1 / T_P) = -\Delta E / R \quad \textbf{(2.12)}$$

Relative crystallinity plot for PLA and its composites is presented in Fig 2.14. From Table 2.3, it can be seen that'$t_{0.5}$' values decrease with an increase in the heating rate for PLA-M and the composites. This indicates the improvement in rate of crystallization with respect to rise in heating rate. This trend of rate can be compared with 'Z' obtained from Avrami plot. From Avrami plot (Fig.2.15), it can be observed that 'n' value ~3 for pure PLA and PLA composites suggests a spherulitic growth from nuclei initiated at time zero or with plate-like growth from nuclei initiated over time (Wu et al., 2007).The 'n' factor ~2.3 signifies two dimensional nucleation and growth of crystals (Battegazzore et al., 2011b).Nonlinear deviation from the linear part is indication of secondary crystallization mechanism. Ozawa plot of PLA-M and PLA-M-0.05GR is mostly linear (Fig. 2.16). Nonlinear Ozawa plot of PLA-M-0.2GR is symbolic of secondary crystallization of PLA. Table 2.3 shows 'α' values from Mo plot (Fig. 2.17) for PLA-M, PLA-0.05GR and PLA-M-0.2GR and are found to be 1.91-3.26, 1.16-1.32, and 1.04-1.14 in different degrees of crystallization indicating, the

change of crystallization mechanism from PLA-M to PLA-M-GR nanocomposites. An increase of 'F (t)' values with increasing crystallization implies higher heating rate is required to achieve higher crystallinity. In the same crystallinity, PLA-M-0.2GR has lower 'F (t)' value than PLA-M-0.05GR and PLA-M, indicating that rate of crystallization is higher for PLA-M-0.2GR than the other two. For this system, it can be noticed that Mo plot is linear for all the cases and thus, assumption of this model does match with this study. Tobin plot (Fig. 2.18) suggests the presence of linear and nonlinear zones signifying the presence of both primary and secondary crystallization mechanisms. It can be noticed from Table 2.3 that the activation energy change ΔE (J/mol) for crystallization of PLA-M (83.7 kJ/mol) is lower than PLA-M-0.2GR (174 kJ/mol) indicating that presence of graphene hinders the folding of PLA chains and thus the change in activation energy becomes higher.

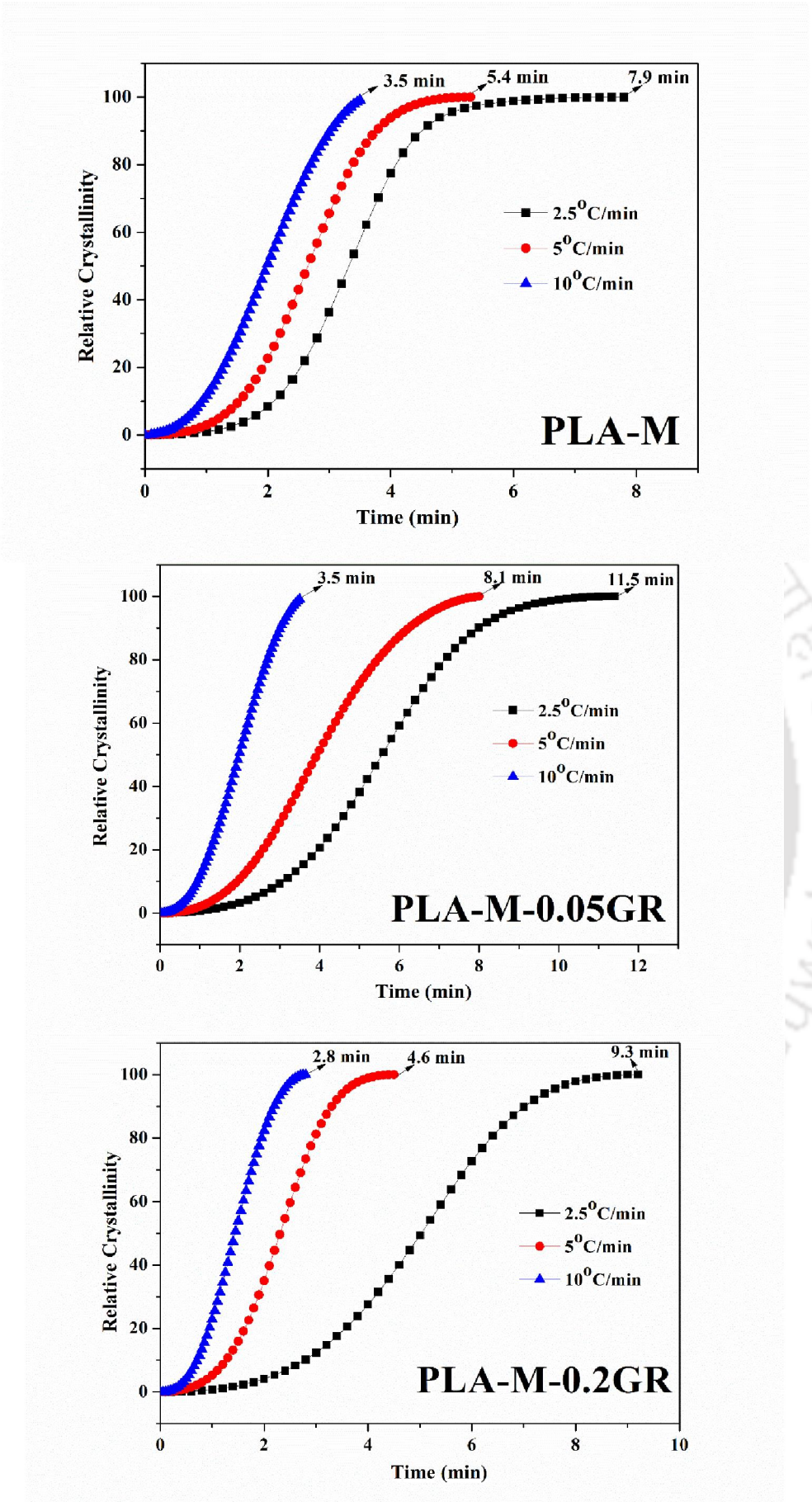

Fig. 2.14 Relative crystallinity plot for PLA-M, PLA-M-0.05GR and PLA-M-0.2GR

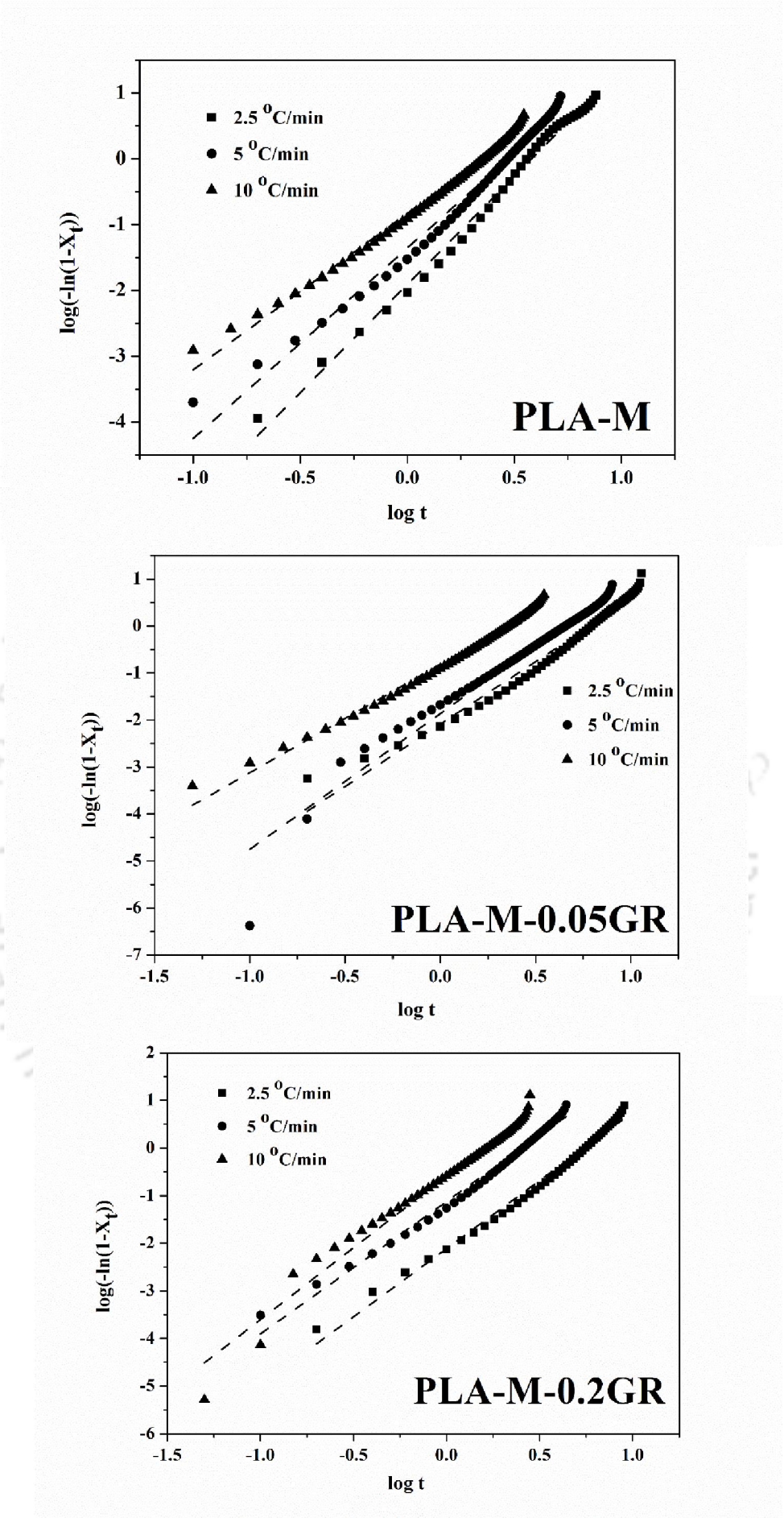

Fig. 2.15 Avrami plot for PLA-M, PLA-M-0.05GR and PLA-M-0.2GR

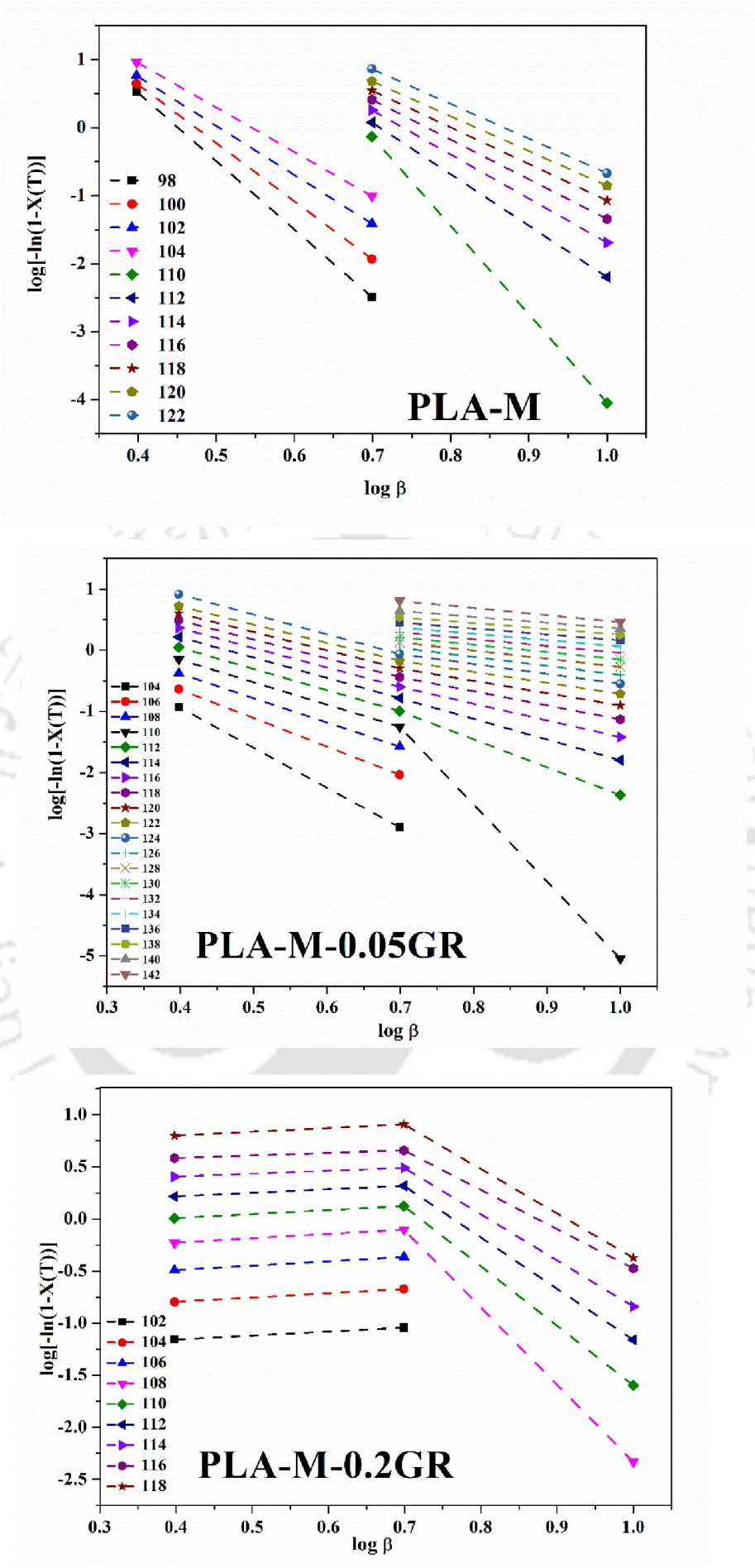

Fig. 2.16 Ozawa plot for PLA-M, PLA-M-0.05GR and PLA-M-0.2GR

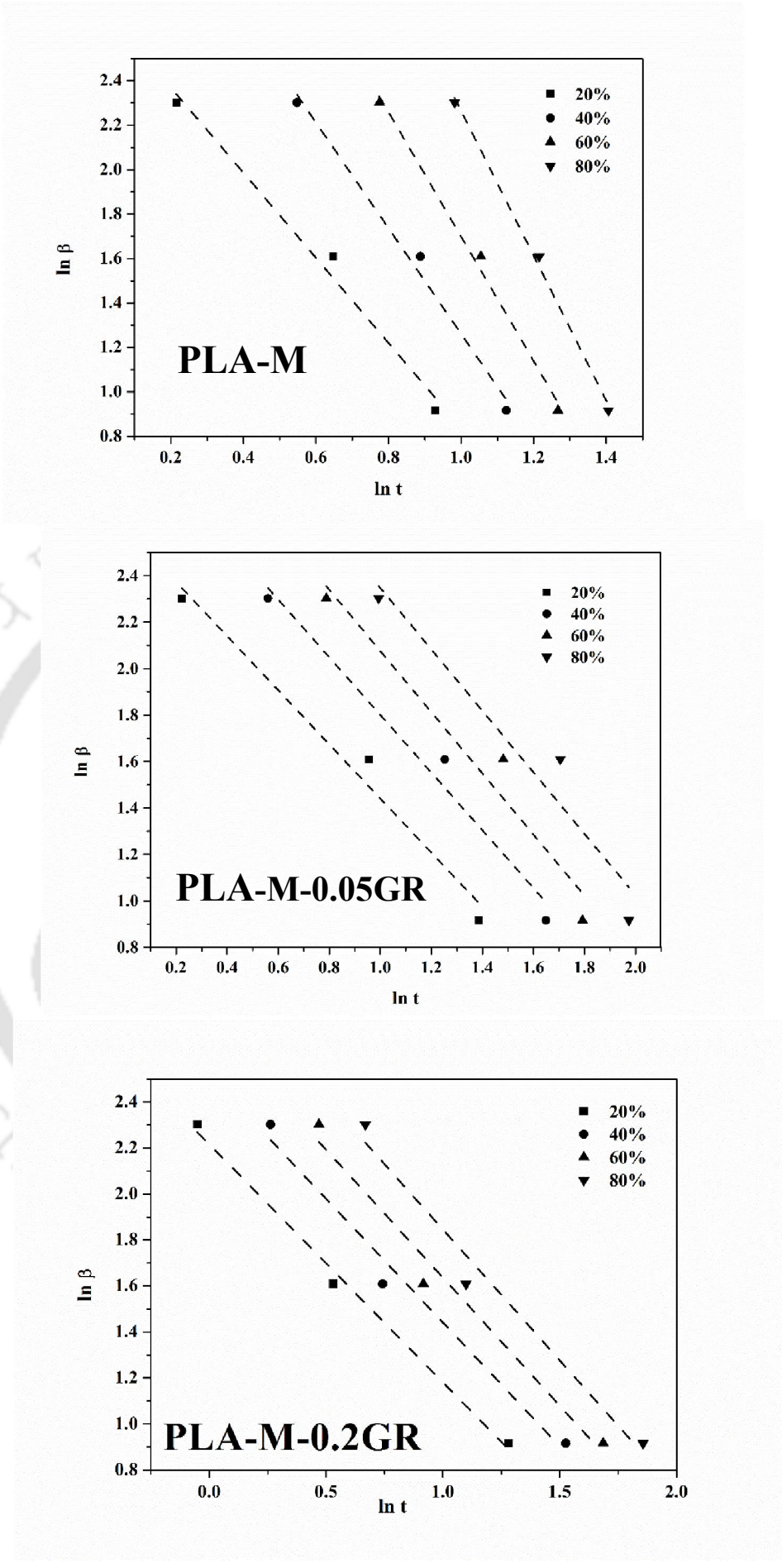

Fig. 2.17 Mo plot for PLA-M, PLA-M-0.05GR and PLA-M-0.2GR

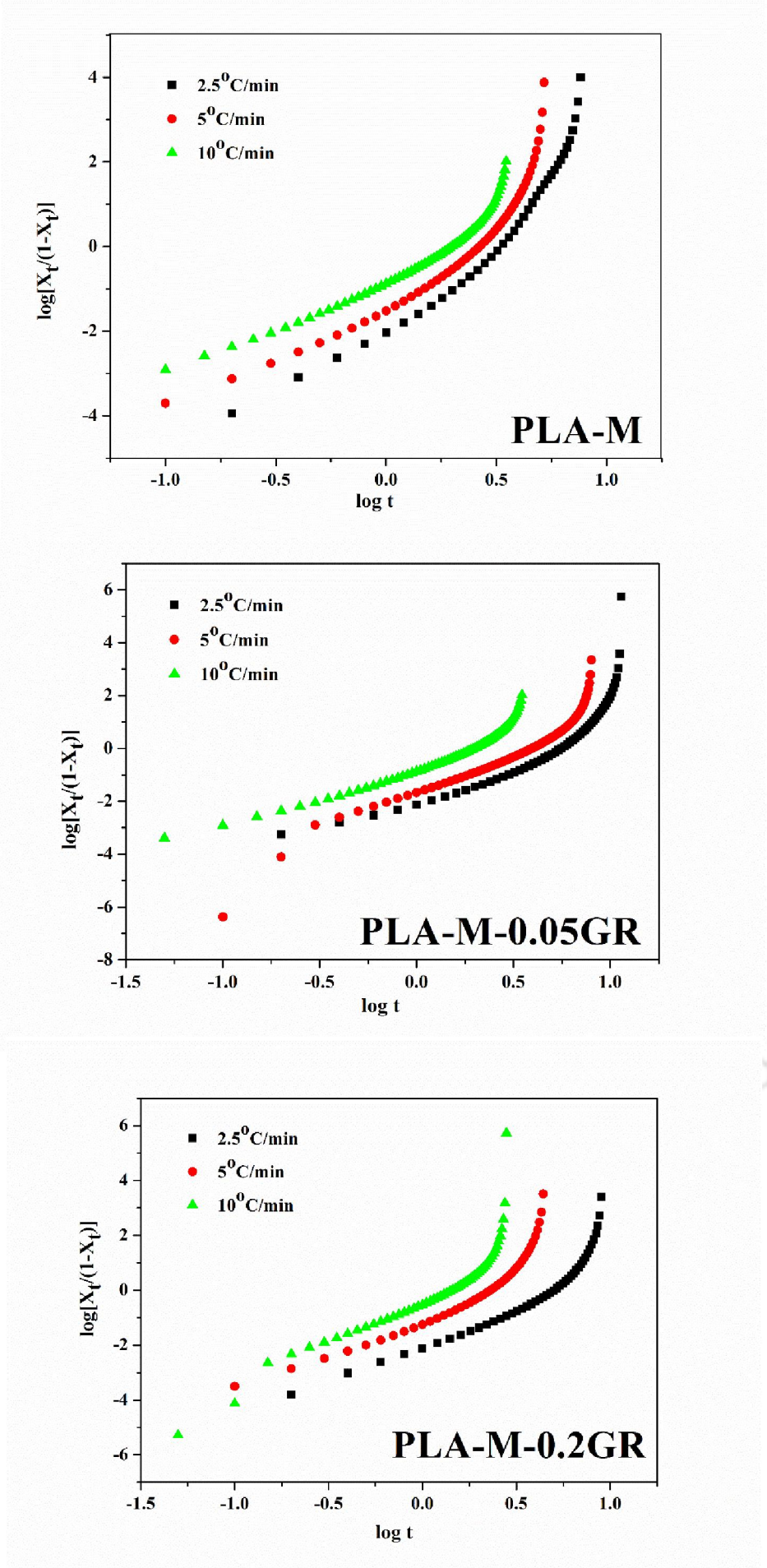

Fig. 2.18 Tobin plot for PLA-M, PLA-M-0.05GR and PLA-M-0.2GR

Table 2.3 Crystallization parameters from the Avrami, Mo and Kissinger analysis

Sample	Heating Rate (°C/min)	$t_{0.5}$ min	n	Z	X_t%	α	F(t)	ΔE (kJ/mol)
PLA-M								
	2.5	3.31	3.28	0.0123	20	1.91	15.67	
	5	2.65	2.89	0.0440	40	2.38	38.05	83.7
	10	1.96	2.37	0.1477	60	2.80	89.83	
					80	3.26	250.51	
PLA-M-0.05GR								
	2.5	5.56	2.65	0.0081	20	1.16	13.54	
	5	3.92	2.89	0.0137	40	1.24	20.95	
	10	1.96	2.31	0.1534	60	1.32	29.77	53.3
					80	1.32	39.29	
PLA-M-0.2GR								
	2.5	5.01	2.86	0.0077	20	1.04	9.17	
	5	2.31	2.78	0.0754	40	1.08	12.39	
	10	1.42	3.02	0.2596	60	1.11	15.64	174
					80	1.14	19.75	

2.3.14 Melt rheology analysis

Rheogram of PLA-M and GR reinforced composites of 0.05 wt. % and 0.2 wt. % GR loading at 180 °C is shown in Fig 2.19 Increase of storage modulus (G′) and loss modulus (G″), (Fig 2.19(a)) with angular frequency (ω) is smooth and continuous. At lower frequency region, much higher magnitude of G″ compared to that of G′, reveals more liquid like nature (Pluta et al., 2007). Increasing value of modulus with ω is due to stress relaxation. The extent of stress relaxation decreases with an increase in ω and becomes almost negligible at very high value of ω (ω ≥100 rad/s). From Fig. 2.19(b) it can be seen that crossover frequency for the composites is shifted towards higher frequency, indicating drop in relaxation time compared to PLA-M (Narimissa et al., 2014).

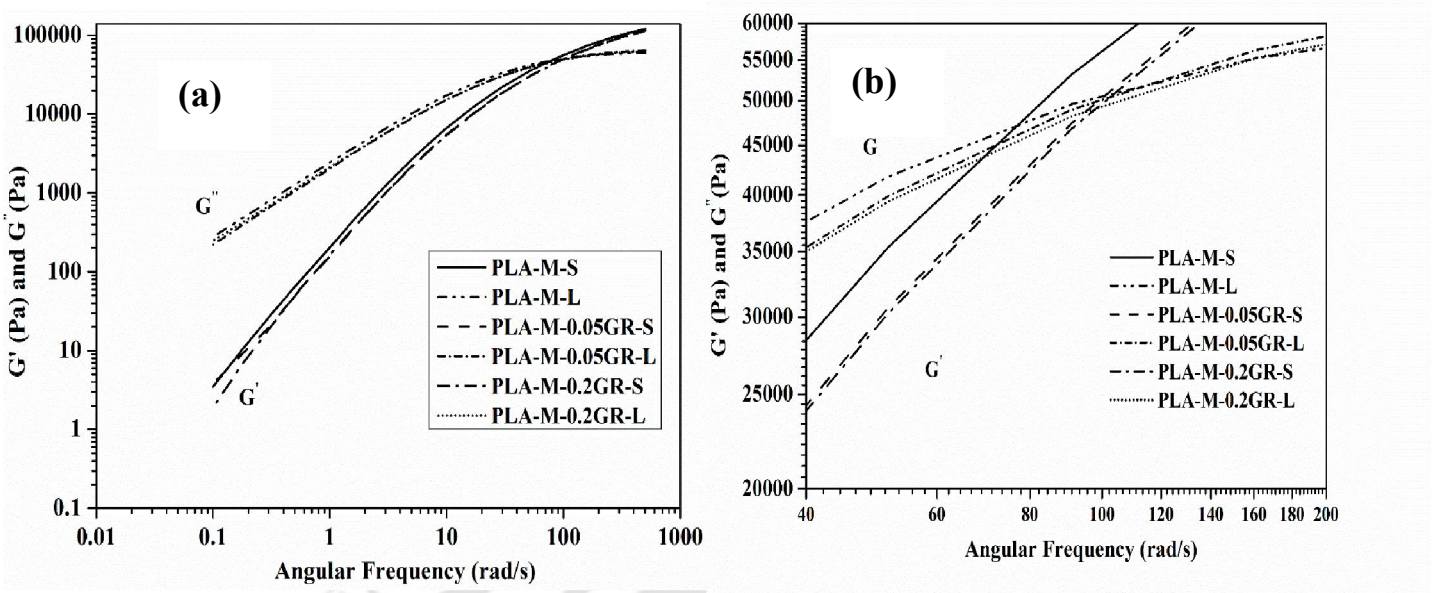

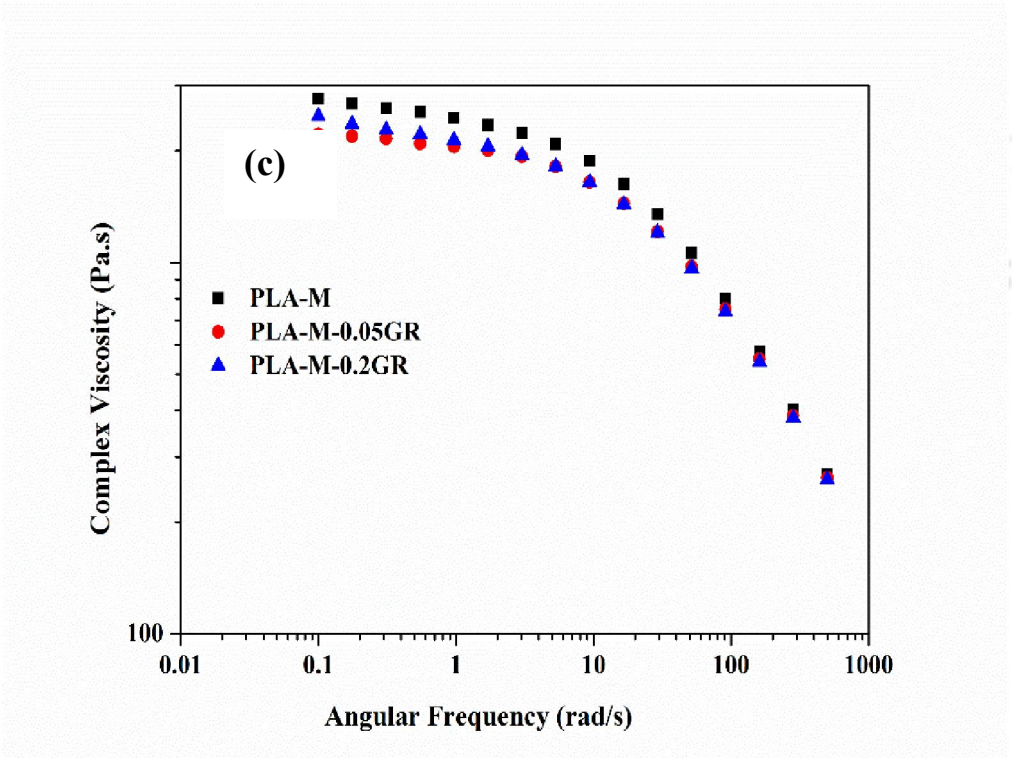

Fig. 2.19 (a) Storage modulus (G') and loss modulus (G'') with frequency ('S' indicates storage modulus and 'L' indicates loss modulus, (b) expanded view of crossover point and (c) complex viscosity plot with respect to angular frequency of PLA-M, PLA-M-0.05GR and PLA-M-0.2GR at 180 °C

Complex viscosity (η^*) is found to be decreased with an increase in ω and it can be divided into two zones namely solid-like region (ω≤1 rad/s) where η^* is nearly independent of ω and liquid-like non-Newtonian (Power law) region (ω>1 rad/s), where η^* is dependent on ω (Fig. 2.19(c)). With an increase in ω, η^* decreases showing shear thinning and homopolymer like terminal flow behavior of the polymer (S Sinha Ray & Okamoto, 2003). The shear-thinning behavior as observed is because of the effect of shear on the entanglements. With increasing shear rate, the chains begin to orient to the direction of flow and disentangle from one another resulting in drop in viscosity. In the low-frequency region, complex viscosity of the composites decreases when compared to PLA-M. This is because of reduced chain entanglement in the PLA due to the presence of GR. whereas in the power law region the trend is similar for all the components. This happens because of reduction of the effect on entanglement at higher ω.

According to expectation, composites should possess homopolymer like characteristics in the terminal flow region. It means components should follow Power law equation i.e. storage modulus proportional to the square of angular frequency (ω^2) and loss modulus proportional to angular frequency (ω) (Ahmed et al., 2010b; S Sinha Ray & Okamoto, 2003). The slope of ln G′ vs ln ω and ln G″ vs ln ω in the low frequency region (0.01≤ ω ≤10 rad/sec) is presented in Table 2.4.The values of the composites are close to PLA-M and is near to 2 (ln G′ vs ln ω) and 1 (ln G″ vs ln ω) as like homopolymer at all the studied temperatures (180 °C, 185°C and 190 °C).

2.3.14.1 Activation energy

In Fig. 2.20(a), a representative plot of complex viscosity (η^*) with temperature is shown for PLA-M-0.05GR. It can be seen that viscosity decreases for the samples when the temperature increases. Effect of GR reinforcement on the flow activation energy of

the extruded PLA strips is evaluated using the Arrhenius equation (Eq. 2.13) (Ahmed et al., 2010b; Al-Itry et al., 2014).

$$\eta = A^{\circ} \times EXP\left(-E_a / RT\right) \quad \text{..... (2.13)}$$

'η' is dynamic viscosity at ω= 0.18 rad/s, which is taken as reference, 'E_a' , '$A°$','R' and 'T' are the activation energy corresponding to flow of polymer, pre-exponential factor, universal gas constant (8.314 J/mol K) and temperature (K), respectively. Figure 2.20(b) is a plot of ln η against 1/T for the temperatures 180,185 and 190 ˚C. Activation energy values are calculated from Fig. 2.20(b). It is found that activation energy value decreases on GR loading. For 0.05 wt. % and 0.2 wt. %, the values are 61.70 kJ/mol and 85.78 kJ/mol as compared to PLA (158.09 kJ/mol).

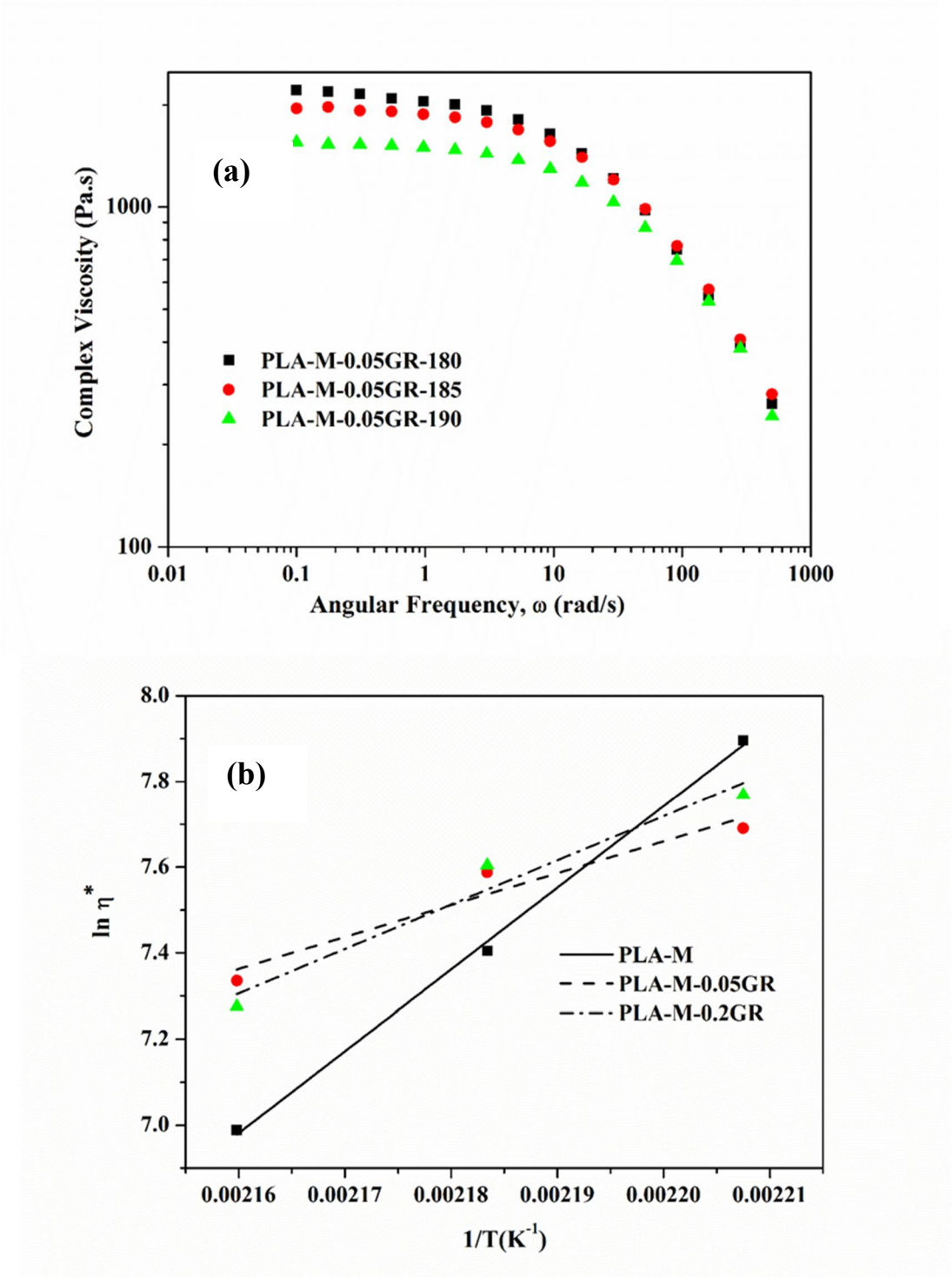

Fig. 2.20 (a) Complex viscosity plot of PLA-M-0.05GR at different temperatures and (b) Activation energy plot for PLA-M, PLA-M-0.05GR and PLA-M-0.2GR

Activation energy value depends on the short-chain and long-chain branching present within the polymer, which governs the chain entanglement of the polymer. The decrement of activation energy value for the composites is corroborating the earlier discussion i.e. better flowability of the composites compared to PLA-M due to the reduction in chain entanglement of the composites (Ahmed et al., 2010a; Al-Itry et al., 2014).

2.3.14.2 Han plot

Phase separation, if any, due to incorporation of GR within the PLA matrix is investigated using the Han plot of the components. The Han curve is linear in nature for the homogeneous polymeric system and it is independent of the temperature (Chen et al., 2013). In the present case, the Han plot is obtained by plotting G′ vs. G″ in the logarithmic scale for all the components at 180 ºC (Fig. 2.21) (Antić et al., 2010; Chen et al., 2013; Walha et al., 2016). It can be seen from the figure that, the Han curve is linear for all the PLA-M, PLA-M-0.05GR and PLA-M-0.2GR indicating no phase separation i.e. homogeneous single phase. Thus, reinforcement of GR is not creating any phase separation in the composites. Relaxation time of the polymer chain segments is reflected by the Han plot in the higher frequency region. From the curves in Fig. 2.21(a), it can be concluded that relaxation time is not much affected due to GR loading. Slopes of the Han curves are found to be comparable for all the components and the values are 1.87, 1.79 and 1.88 for the samples neat PLA, 0.05 and 0.2 wt. % GR loaded composites, respectively. Fig. 2.21(b) is a representative plot to examine the effect of temperature for PLA-M-0.05GR. It shows that the composite maintains homogeneous single-phase behavior even with temperature increment up to 190 °C. With the rise in temperature from 180 °C to 190 °C for PLA-M-0.05GR, the slope of the curve does not change significantly. This also indicates that polydispersity of the PLA system is not

affected much due to incorporation of the GR (Y. Chen et al., 2013) and the relaxation time is also not affected much with an increase in temperature up to 190 °C.

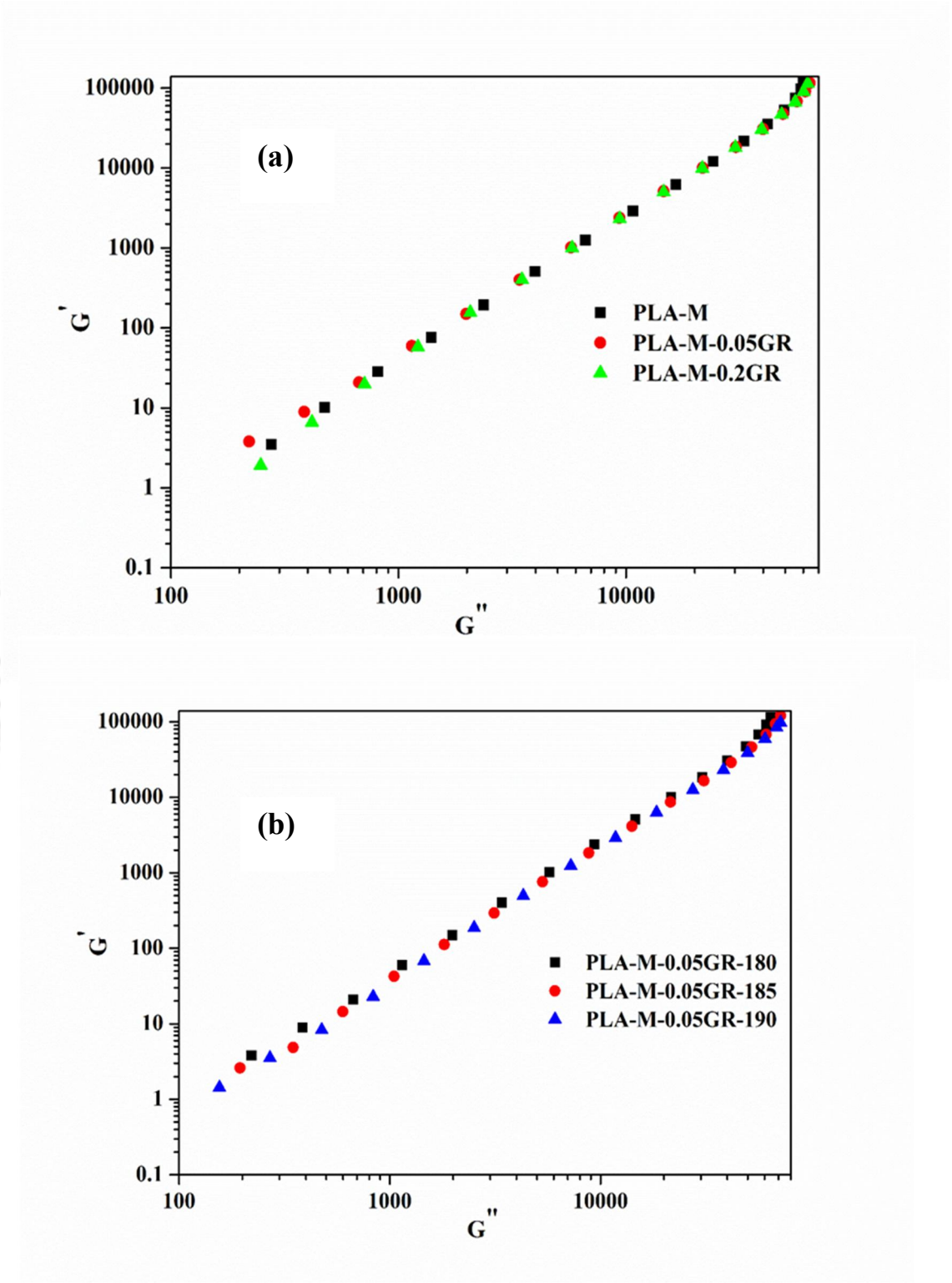

Fig. 2.21 (a) Han plot of PLA-M, PLA-M-0.05GR and PLA-M-0.2GR at 180 ºC and (b) Han plot of PLA-M-0.05GR at different temperatures

2.3.14.3 Cole-Cole plot

Cole-Cole plot is a plot between imaginary viscosity (η'') and real viscosity (η'). This is indicative of the interaction between reinforcement and the matrix (Chen et al., 2013; Tesfaye et al., 2017). The semi-circular nature of the curves of the Cole-Cole plot in Fig 2.22(a) for the samples reveals good compatibility and dispersion of GR within the PLA matrix (Y. Chen et al., 2013). For 0.05 wt. % GR loaded composite, the Cole-Cole plot at different temperatures of 180 ^{o}C, 185 ^{o}C, and 190 ^{o}C are shown in Fig 2.22(b). The nature of the curves remain independent of temperature. However, the shift of the peak of the curve towards the lower η'' value with an increase in temperature suggests an increase in the loss modulus with increasing temperature.

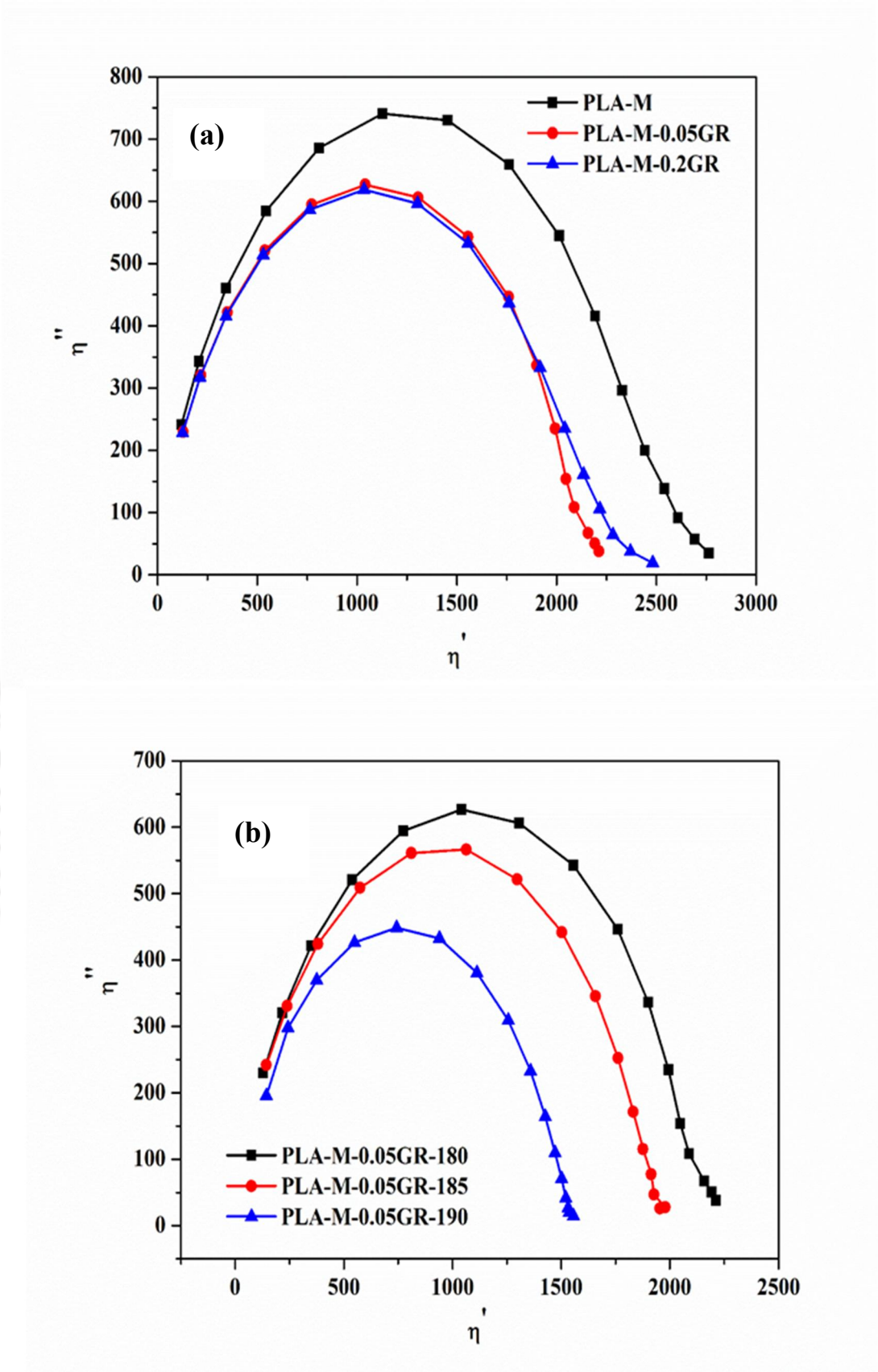

Fig. 2.22 (a) Cole-Cole plot of PLA-M, PLA-M-0.05GR and PLA-M-0.2GR at 180 ºC and (b) Cole-Cole plot of PLA-M-0.05GR at different temperatures

2.3.14.4 van Gurp-Palmen Plot

Van Gurp Palmen's plot is a well-known model to verify the temperature dependency of rheological behavior based on time-temperature superposition (TTS) technique. Following the Van Grup-Palmen model 'δ' ($\delta=\tan^{-1}(G''/G')$) is plotted against dynamic modulus 'G^*' [$G^*= (G'^2 + G''^2)^{1/2}$] (Van Gurp & Palmen, 1998). From Fig. 2.23(a), it can be seen that at 180 °C, TTS of the components is almost identical and the TTS is not deviating from the homopolymer for GR loaded composites (Fig. 2.23a). This is due to good mixing and compatibility of GR with the PLA matrix leading to less interfacial tension between the reinforcement and the matrix for the composites (Van Gurp & Palmen, 1998). Temperature effect on TTS of PLA-M-0.05GR is plotted at three different temperatures (180 °C, 185 °C and 190 °C). It is found that the value of 'δ' increases marginally with an increase in the temperature and the enhancement is more at higher modulus (Fig. 2.23b). This is because of the marginal reduction in G′ and increase in flowability that takes place due to increase in G″ with an increase in temperature to 190 °C. With reduction in temperature, stiffness of the chain increases resulting in shift of the TTS towards lower value.

2.3.14.5 Cox-Merz approximation

Shear-thinning behavior of the PLA-M and composites are examined through the Power law model. Power law model is fitted in the transition region between Newtonian and non-Newtonian range considering Cox–Merz approximation ($|\eta^*(\omega)| = \eta^*(\dot{\gamma})$, $\dot{\gamma} = \omega$) (Bair et al., 2014). Non-Newtonian nature of the components is determined from the slope (n-1) of the plot of '$|\eta^*|$' against 'ω' in the log-log scale. The value of 'n' indicates the deviation from Newtonian behavior of the melts. It can be seen from Table 2.4 that values of 'n' for PLA-M, PLA-M-0.05GR, and PLA-M-0.2GR are 0.43, 0.46, and 0.46, respectively at 180°C, which are typically similar to the shear-thinning

polymer. The incorporation of GR is not affected much the flow behavior of the PLA chains. For all the components, 'n' is enhancing with an increase in the temperature, which indicates improvements in flow behavior of the PLA chains with increasing the temperature.

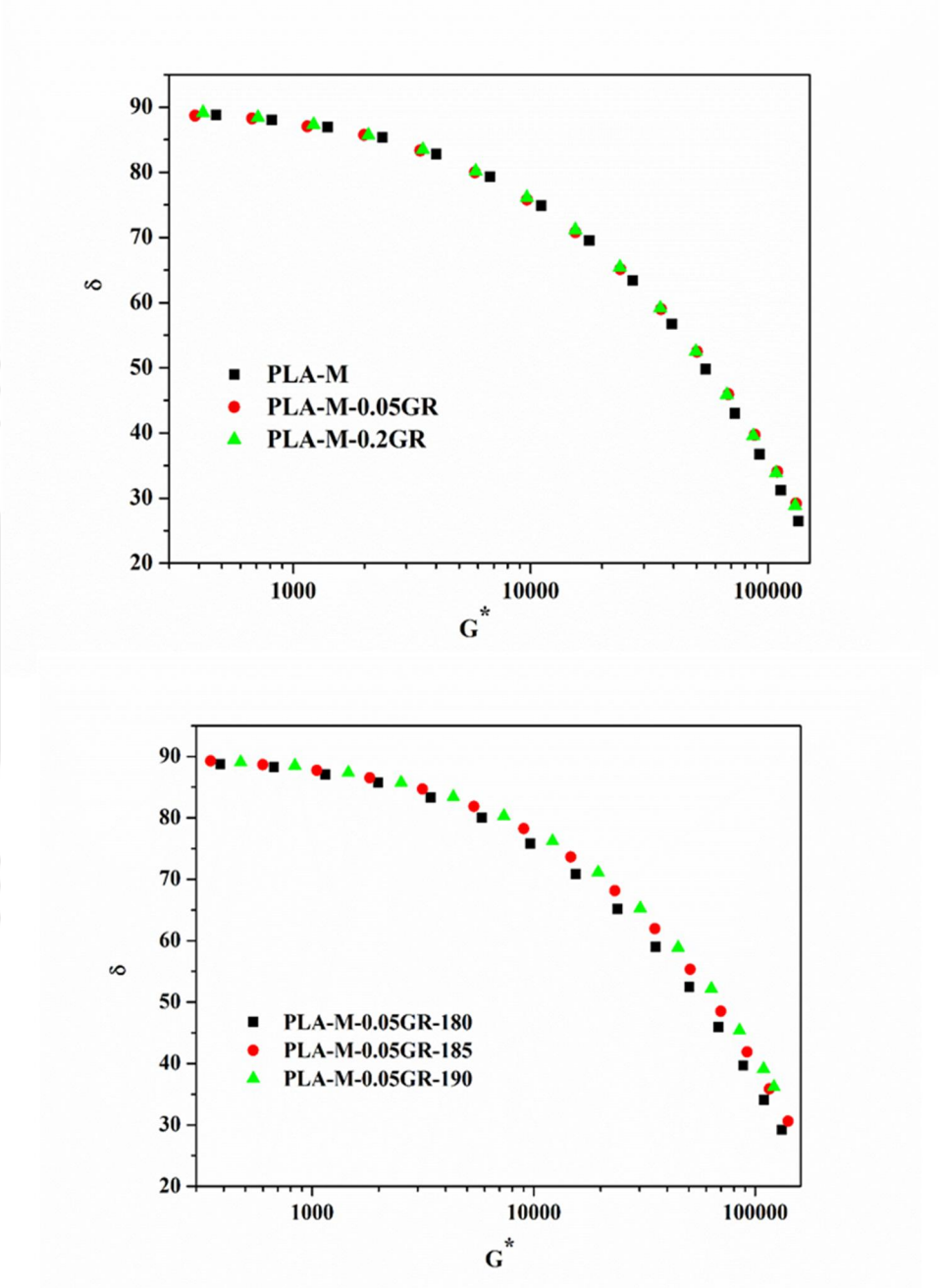

Fig. 2.23 (a) Phase angle as a function of dynamic modulus plot of PLA-M, PLA-M-0.05GR and PLA-M-0.2GR at 180 ºC and (b) Phase angle with respect to dynamic modulus of PLA-M-0.05GR at different temperatures

Table 2.4 Rheological properties analysis results

Sample	Temperature (°C)	Slope (ln G'Vs ln ω)	Slope (ln G"Vs ln ω)	'n' of Cox–Merz model	E (kJ/mol)
PLA-M	180	1.65	0.91	0.43	
	185	1.51	0.87	0.46	158.09
	190	1.61	0.84	0.48	
PLA-M-0.05GR	180	1.62	0.93	0.46	
	185	1.68	0.95	0.49	61.70
	190	1.71	0.96	0.50	
PLA-M-0.2GR	180	1.73	0.91	0.46	
	185	1.73	0.94	0.51	85.78
	190	1.82	0.94	0.53	

2.3.15 Solution viscometry and physicochemical/structural properties

Molecular weight is one of the major parameters, which govern the properties of a polymer. Melt processing of PLA can affect its molecular weight. Depending on the type of reinforcement, extent of shear and the value of process temperature, molecular weight might change. This change of molecular weight can have impact on the stability and rheological properties of the PLA. Viscosity average molecular weights of PLA and the composites are, therefore, calculated in this work with the help of intrinsic viscosity [η] values.

$$[\eta] = \lim_{C \to 0} \frac{\eta_{sp}}{C} \quad \text{..... (2.14)}$$

Where 'η_{sp}' is polymer's specific viscosity, 'C' is concentration of polymer and 'η_{sp}/C' is the reduced viscosity. Huggins equation is utilized to calculate intrinsic viscosity for the present work (Eq 2.15) (Tesfaye et al., 2017).

$$\eta_{sp}/C = [\eta] + k_H * [\eta]^2 * C \quad \text{(2.15)}$$

Huggins constant ('k_H') is specific for polymer, solvent, and temperature of the study (Table 2.5). [η] is found to be increased for the GR reinforced composites. Values of [η] for the composites PLA-M-0.05GR and PLA-M-0.2GR are 145.6 and 123.6, respectively and are higher than PLA-M (106.9) (Fig. 2.24(a) representative plot for PLA-M-0.2GR). The viscosity average molecular weight (M_v) of the PLA-M and the composites are calculated using the Mark-Howink-Sakurada (M-H-S) equation (Eq 2.16) (Al-Itry et al., 2014; Tesfaye et al., 2017).

$$[\eta] = K * M_v^{a} \quad \text{(2.16)}$$

'K' and '*a*' are M-H-S parameters and value of these parameters depends on the polymer system. 'K' and '*a*' are equal to 0.0221 mL/g and 0.77 for the PLA system at 25 °C (Al-Itry et al., 2014). Molecular weight is found to be increased for the composites PLA-M-0.05GR (91.04 kg/mol) and PLA-M-0.2GR (73.61 kg/mol) with respect to PLA-M (61 kg/mol) (Table 2.5). Hydrodynamic radius is an indicator of interaction between polymer chains and solvent molecule. In a good solvent, hydrodynamic radius becomes higher compared to theta solvent due to better mobility of the chains (Lewandowska, Staszewska, & Bohdanecký, 2001; Ma & Pawlik, 2007). The hydrodynamic radius of the PLA chains is found to be increased for the composites PLA-M-0.05GR (14.7 nm) and PLA-M-0.2GR (12.9 nm), with respect to PLA-M (11.6 nm). The relation between hydrodynamic radius and molecular weight is found to be $R_H = 1.015 \times M_v^{0.59}$ (Fig. 2.24(b)). It is quite similar to the homopolymeric system of PLA (Al-Itry et al., 2014).

Table 2.5 Huggins constant, intrinsic viscosity and viscosity average molecular weight values of the samples

Samples	Huggins constant (k_H)	Intrinsic viscosity ([η])	M_v(Kg/mol)
PLA-M	1.66	106.9	61.0
PLA-M-0.05GR	0.79	145.6	91.0
PLA-M-0.2GR	0.78	123.6	73.6

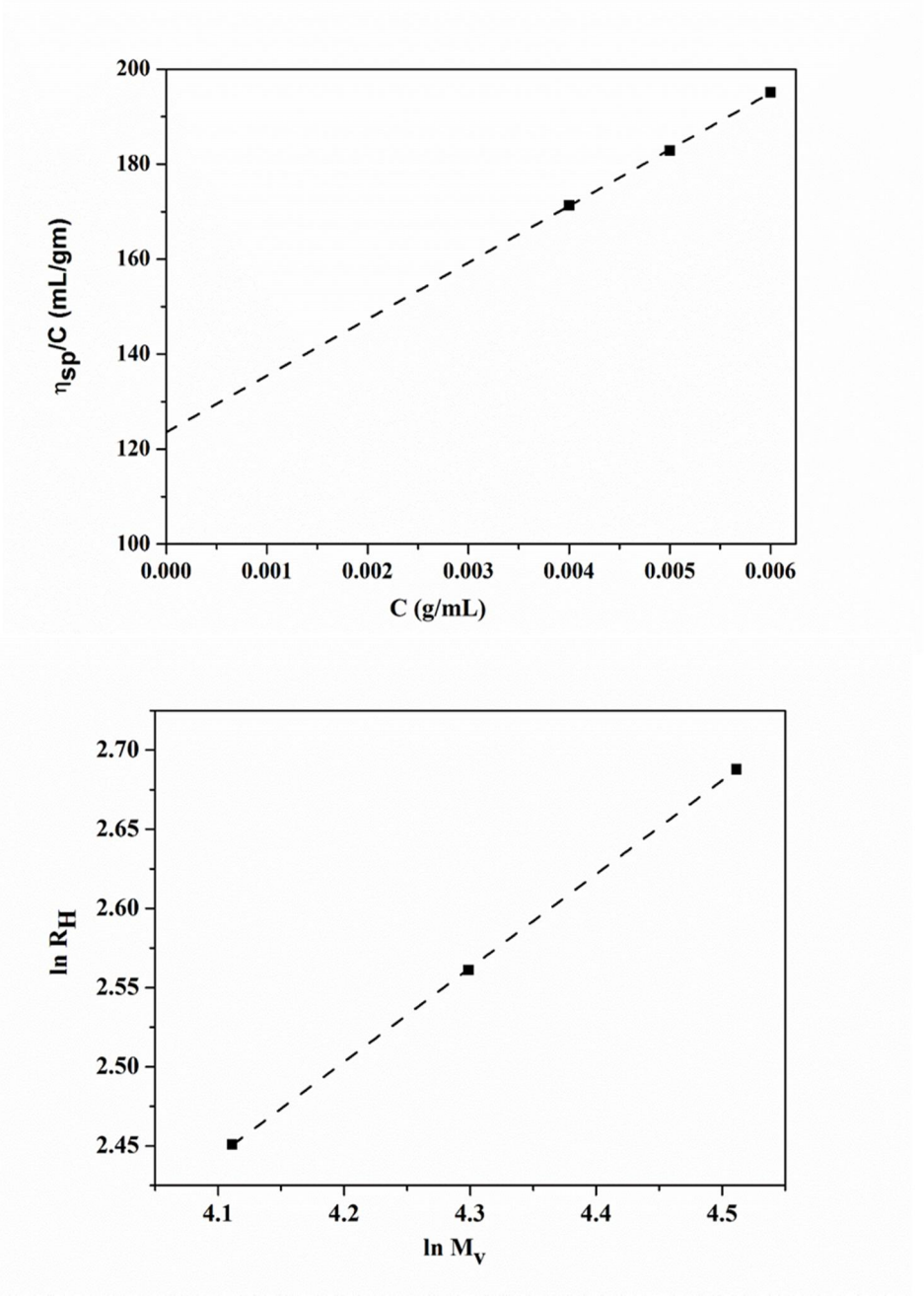

Fig. 2.24 (a) Representative plot of reduced viscosity with respect to concentration of PLA-M-0.2GR (b) Hydrodynamic radius with respect to molecular weight of PLA

2.4 Summary

In this chapter, versatile coating technique was applied prior to extrusion of PLA to overcome air pollution due to exfoliated graphene and successfully executed. The effect on the dispersion due to reinforcement of graphene has been studied by fabricating two different types of composites and was confirmed with XRD. Melt processing has significant effect on the dispersion of the graphene that was examined using FESEM. Incorporation of graphene has improved the thermal stability, hydrophobicity, mechanical strength, storage modulus of the composites significantly as compared to PLA-M. It is also confirmed that better dispersion of exfoliated graphene in PLA-M-0.05GR sample has significant impact on the properties. The thermal stability of the nanocomposite is improved significantly in case of PLA-M-0.05GR (Onset degradation temperature improved by 13 ^{o}C when compared to PLA-M) as compared to both PLA-M and PLA-M-0.2GR. Electrical conductivity improved marginally for the composites. So in order to achieve significant increase in conductivity, change of the processing technique or loading of nanofiller could be the possible option. Thermal degradation kinetics study demonstrated that the degradation stability of the composites increases due to incorporation of graphene. Crystallization kinetics revealed that at higher heating rate, crystallization rate is faster for PLA-M-0.2GR. The presence of nonlinear part in Avrami and Tobin kinetics indicates presence of both primary and secondary crystallization. Overall, the fabricated PLA/GR composites are thermally stable and mechanically strong as compared to PLA.

From the melt rheology of the melt extruded PLA and PLA/GR composites, it is observed that storage modulus (G′) is found to be lower than loss modulus (G″) for the PLA-M and composites but storage modulus value is higher for the GR loaded composites (PLA-M-0.05GR and PLA-M-0.2GR) as compared to PLA-M. Complex

viscosity (η^*) is found to be a little lower for the composites as compared to PLA-M. With rise in the temperature from 180 °C to 190 °C, complex viscosity decreases. PLA-M and its composites show shear thinning behavior. Flow activation energy decreases for the composites indicating increased flow property of the composites due to the reduction in chain entanglements. Excellent dispersion of GR in PLA-M and single phase behavior of the composites are observed from the Han plot, and the same is corroborated by Cole-Cole plot and Van Gurp-Palmen's plot. Polydispersity of PLA is not disturbed much due to incorporation of GR as reinforcement. Viscosity average molecular weight is found to be increased for the composites. Hydrodynamic radius is found to be increased with $M_v^{0.59}$, which is similar to the homopolymer system of PLA. The solution viscosity measurement results also support the melt rheology investigation that revealing the fact of good compatibility of GR with PLA system. Overall, the PLA/GR composites have similar rheological nature with respect to non-modified PLA within the temperature range 180 °C to 190 °C but with better flowability. In case of 0.05 wt. % (PLA-M-0.05GR), GR dispersion and its compatibility are better with the PLA system.

Chapter 3

Facile Dispersion of Exfoliated Graphene/PLA Nanocomposites via *in situ* Polycondensation cum Melt Extrusion Process and its Rheological Studies

Abstract

This work attempted on improved dispersion of graphene through coating of masterbatch (MB) on PLA before melt processing. In situ polycondensation reaction of lactic acid oligomer was utilized to prepare masterbatch (MB) of exfoliated graphene (GR). MB dispersed composites of PLA were fabricated by melt extrusion of MB coated PLA. One normal coated composite without MB (PLA-M-0.2GR) was fabricated for comparison purpose. X-ray diffraction, Raman spectroscopy, and morphological studies revealed better compatibility, dispersion and interaction of GR in case of MB diluted composite as compared to normal coated composite. Thermal stability, crystallization properties, mechanical properties of the composites were examined and effect of short PLA chains in case of MB diluted composites was observed. Melt rheology nature of the composites was examined. Cole-Cole plot and Han plot suggested uniform distribution of graphene. PLA-MB-0.05GR showed improved modulus and elongation at break. It also showed better dispersion of GR, comparable thermal stability, good miscibility, chain mobility, and high activation energy.

Part of this research work has received scientific recognition as follows:

Chakraborty, G., Gupta, A., Pugazhenthi, G., & Katiyar, V. (2018). Facile dispersion of exfoliated graphene/PLA nanocomposites via in situ polycondensation with a melt extrusion process and its rheological studies. ***Journal of Applied Polymer Science***, 135(33), 46476.

Graphical Abstract

3.1 Introduction

In the last few decades, though petroleum-based polymers, which are non-degradable in nature have been extensively utilized in the plastic material fabrication for a wide range of applications, these non-degradable plastics have become the prime source of waste disposal problems. Increase in awareness of environmental sustainability leads to the development of efficient solutions for producing new class of environment friendly or biodegradable polymers in the last decades (Chenet al., 2009; Lim et al., 2008; Ojijo & Ray, 2013b; Reddy et al., 2013a). However, some inherent properties of biodegradable polymers, such as brittleness, low melt viscosity, high gas and vapour permeability and low heat distortion temperature have restricted the use of these polymers for a variety of applications (Reddy et al., 2013a). Polylactic acid (PLA) is the glorious example of an aliphatic biodegradable polyester that has the potential to replace the conventional commodity plastics in almost all the fields of applications (Auras et al., 2004; Lasprilla et al., 2012; Lopes et al., 2012). Commercialization of PLA as a packaging material requires extensive improvement in the major properties like mechanical, thermal and barrier properties (Babu et al., 2013). Toyota Company in 1988 was the pioneer to introduce fabrication of composites specially nanocomposites with significantly improved properties compared to matrix polymer (Gao et al., 2004; Maniaret al., 2004). After this, different nano dimension material based composites were started to be manufactured with different polymeric systems. Reinforcement of fillers like carbon nanotubes (Lin et al., 2013), graphene (Norazlina & Kamal, 2015; Pinto et al., 2013) , cellulose nanocrystals (Borkotoky et al., 2017; Dhar et al., 2016; Dhar et al., 2015), and clays (Neppalli et al., 2014; Zaidi et al., 2010; Zhao et al., 2008) into PLA can lead to the formation of nanocomposites having properties essential for packaging applications. Uniform dispersion of the filler and interfacial adhesion are the

governing parameters that dictate the properties of the composite materials. Thus, the dispersion of reinforcements within the matrix is crucial problem to resolve in order to improve the nanocomposites properties (Li et al., 2014). Certain techniques like sonication (Valapa et al., 2015a) covalent grafting (Seligra et al., 2013) with some polymers were tested in different cases to improve the filler dispersion. In situ polymerization approach was also applied for better reinforcement of filler in matrix for graphene oxide (Li et al., 2014), and functionalized carbon nanotube (Yoon et al., 2010). Graphene is an allotrope of carbon with hexagonal honeycomb like dense lattice structure in a two-dimensional array. It has high thermal stability, mechanical strength, and electrical conductivity and because of such novel properties, it is used to fabricate nanocomposites for different applications like packaging, electrochemical and biosensors, and energy storage devices (Kuilla et al., 2010; Singh et al., 2011). The dispersion of graphene in polymer matrix leads to imperfect nanocomposites because of less interfacial stability. However, exfoliated graphene based nanocomposites were observed to have high tensile strength along with thermal stability and the agglomeration of filler was noticed in both solution processing and melt extrusion (Valapa et al., 2015a). Uniform dispersion of exfoliated graphene is also a challenging task in order to enhance the properties of the composites specially, at higher loading condition. So, in order to improve the dispersion of graphene, a new approach has been explored in the present study where in-situ polycondensation of oligomeric PLA was carried out in the presence of exfoliated graphene (GR) in order to prepare masterbatch (MB). Then the MB was coated over the PLA pellets prior to extrusion. The objective of the in situ polycondensation of oligomeric PLA in the presence of graphene is to deposit film of short PLA chains on the graphene surface. Thereafter, solvent based coating was applied over PLA pellets in order to obtain uniform coating of diluted MB

of different dilution followed by melt extrusion. Finally, the impact of the synthesized composites on different properties namely structural, morphological, mechanical, thermal, wettability and rheological properties were investigated in order to examine the improvement of dispersion as well as graphene compatibility with the PLA matrix. Subsequently, comparison of dispersion and properties among the MB diluted composites and that of MB-composite (0.2 wt. % graphene) with composite fabricated by normal coating technique (M) of same loading were also executed in the present work.

3.2 Materials and Methods

3.2.1 Materials

2003D grade of PLA purchased from NatureWorks® LLC, USA, was used for the fabrication of films. Lab synthesized exfoliated graphene EXG 750 (GR) was used as reinforcement substance. Methanol and chloroform required for coating were purchased from Sisco Research Laboratories (SRL Chemicals, India). L-lactic acid was purchased from Purac, Netherland. Stannous chloride ($SnCl_2$) and p-toluene sulfonic acid (PTSA) were purchased from Sigma Aldrich, USA.

3.2.2 Experimental Section

3.2.2.1 Preparation of oligomer from L-lactic acid

L-lactic acid was taken in a three-neck flask and kept under microwave (domestic) system equipped with condenser and receiver and then heating was carried out at 20% power of the microwave for 45 min under nitrogen gas flow. After cooling down to room temperature, the required amount of oligomer was taken for next stage polycondensation.

3.2.2.2 Preparation of MB

In order to prepare the masterbatch (MB), 100 mg of graphene was taken in chloroform and sonicated for 1 h using bath sonicator (Labman scientific instruments, India). The synthesized oligomer was then added into graphene-chloroform mixture followed by continuous stirring for 12 h. Chloroform was then evaporated at 60 °C under stirring condition in order to get solvent-free well-dispersed graphene in oligomer. Removal of chloroform was carried out by distillation for longer duration approximately 12 h. During polycondensation, $SnCl_2$ and PTSA were added into the graphene/oligomer dispersion in 0.4 mole % at 150 °C under vacuum condition and the reaction was continued for 30 min. Finally, it was kept under microwave heating condition for 10 min. Thus, both conventional heating and microwave heating were applied in two-step polycondensation to obtain deposited layers of PLA chain over graphene.

3.2.2.3 Coating of diluted MB on PLA pellets

Appropriate amount of MB was dispersed into methanol to make the stock solution, which was suitably used up for the fabrication of MB diluted nanocomposites with 0.05 and 0.2 wt. % of GR content. Measured amount of MB stock solution with 0.05 and 0.2 wt. % of GR was added to 20 g of PLA in order to prepare PLA-MB-0.05GR and PLA-MB-0.2GR pellets, respectively (e.g. 100 mg GR in MB was taken in 100 mL methanol to make uniform solution of GR ~1 mg/mL, and to fabricate composite PLA-MB-0.05GR, 10 mL solution was added for coating of PLA pellets). The solution of MB was taken into a beaker, which was adjusted to 50 mL by addition of methanol. It was then sonicated for 10 min in order to disperse graphene in methanol such that no residue was left at the bottom of the flask. Thereafter, PLA pellets were added into MB/methanol mixture and kept for stirring for 10 min followed by drying at 50 °C to obtain uniform coating of diluted MB onto PLA pellets (Fig. 3.1).

3.2.2.4 Fabrication of composites

The pellets thus prepared were extruded to fabricate the PLA-MB-0.05GR and PLA-MB-0.2GR strips (dimension 0.5 mm thick and 4 mm width). The procedure is already mentioned in section 2.2.2.1.

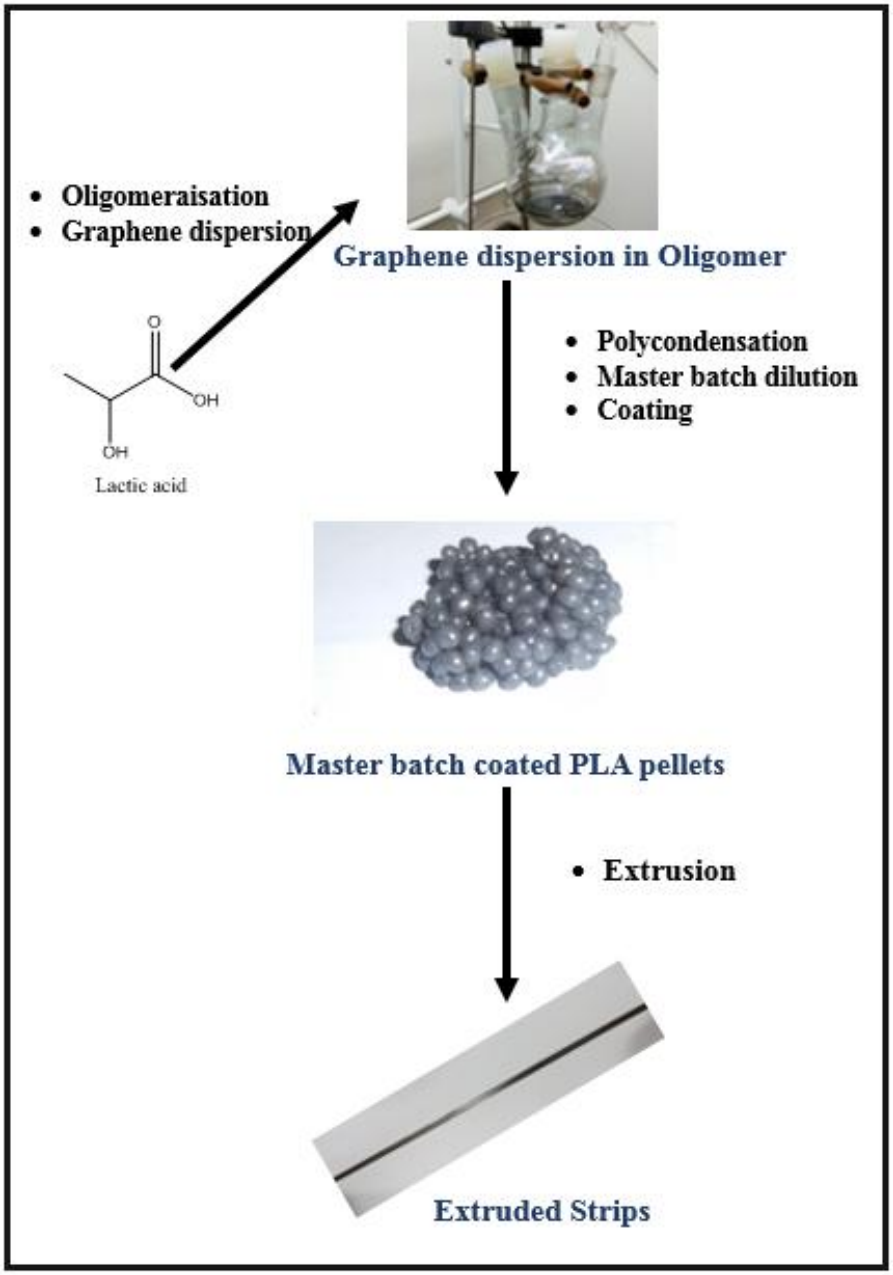

Fig. 3.1 Schematic representation of the fabrication of PLA-MB-GR nanocomposites

3.2.3 Characterization

3.2.3.1 Fourier transform infrared (FTIR) spectroscopy

The spectral analysis of GR, PLA and the nanocomposites were carried out using a FTIR spectrometer (Perkin Elmer, Model: Frontier). Details of the operating conditions are mentioned in Chapter 2.

3.2.3.2 X-ray diffraction (XRD) analysis

The diffraction patterns of GR, PLA and the nanocomposites were obtained using an advance diffractometer (Make: Bruker, Model: D8). Details of the operating procedure are mentioned in Chapter 2.

3.2.3.3 Raman spectroscopy

Raman spectra of PLA-M and its nanocomposites were carried out using a spectrometer (Make: Lab Ram HR Model: Horiba Jobin Vyon) equipped with a Nd: YAG diode-pumped laser. Details of the experimental conditions are mentioned in Chapter 2.

3.2.3.4 Morphological analysis

Details of characterization conditions are described in Chapter 2

3.2.3.5 Thermogravimetric analysis (TGA)

Thermogravimetric analyzer (Make: Perkin Elmer, Model: TGA4000) was utilized to acquire the thermal degradation pattern of PLA nanocomposites. Operating conditions are mentioned in Chapter 2 in details.

3.2.3.6 Differential scanning calorimetry (DSC)

The investigation of thermal properties of PLA and the nanocomposites was carried out using a differential scanning calorimeter (Make: NETZSCH, Model: DSC204 F1). Details of the operating conditions are mentioned in Chapter 2.

3.2.3.7 Mechanical property analysis

The mechanical properties such as tensile strength, elongation at break (%) and Young's modulus were determined using a Universal Testing Machine (Make: Kalpak instruments, Model: KIC-2-050-C, India). Details of the experimental procedure are mentioned in Chapter 2.

3.2.3.8 Dynamic mechanical analysis (DMA)

The storage modulus and tan δ values of PLA and the nanocomposites were obtained using a dynamic mechanical analyser. (Make: NETZSCH, Model: DMA 242E). Details of the operating conditions are mentioned in Chapter 2.

3.2.3.9 Contact angle analysis

The contact angle measurements of PLA-M and PLA-M-GR nanocomposites were performed using a goniometer (KRUSS goniometer) via sessile drop method. Details of experimental procedure are mentioned in Chapter 2.

3.2.3.10 Impedance analysis

The impedance analysis of PLA-M and the nanocomposites were investigated using Autolab (Metrohm). Details of the operating conditions are mentioned in Chapter 2

3.2.3.11 Melt rheology analysis

The rheological measurements of PLA and the nanocomposites were carried out by using a controlled stress rheometer (Make: Anton Parr, Model: MCR 102) having parallel plate arrangement (50 mm in diameter) in the melt state. Details of operating conditions are mentioned in Chapter 2.

3.3 Results and Discussion

3.3.1 FTIR analysis

FTIR spectra of MB in Fig. 3.2 indicates the formation of PLA chains during polycondensation reaction as the peak at 1750 cm^{-1} is corresponding to C=O stretching of PLA chains.(Li et al., 2014) Peaks corresponding to 1092, 1200 and 1450 cm^{-1} represent stretching vibration, rocking vibration, and asymmetric stretching of -C-CH_3 in PLA chains (Seligra et al., 2013). It can also be noticed that the peak at 3437 cm^{-1}, due to presence of small amount of -OH in graphene is absent in the MB. This is due to interaction of the -OH during polymerization. In case of MB diluted nanocomposites, the peaks at 1645 and 1585 cm^{-1} correspond to C=C and C-C stretching (Fig. 3.2), respectively, which is indicative of carbon backbone of GR (Exfoliated graphene) and also similar spectrum of MB is present. For MB diluted nanocomposites C=O stretching peak is observed at 1750 cm^{-1}. However, in case of normal processing for same loading, it is observed at 1746 cm^{-1} with lower intensity. It indicates better compatibility in case of MB diluted nanocomposites, as compared to normal coated composites (PLA-M-0.2GR) due to similar polymer-polymer interaction.

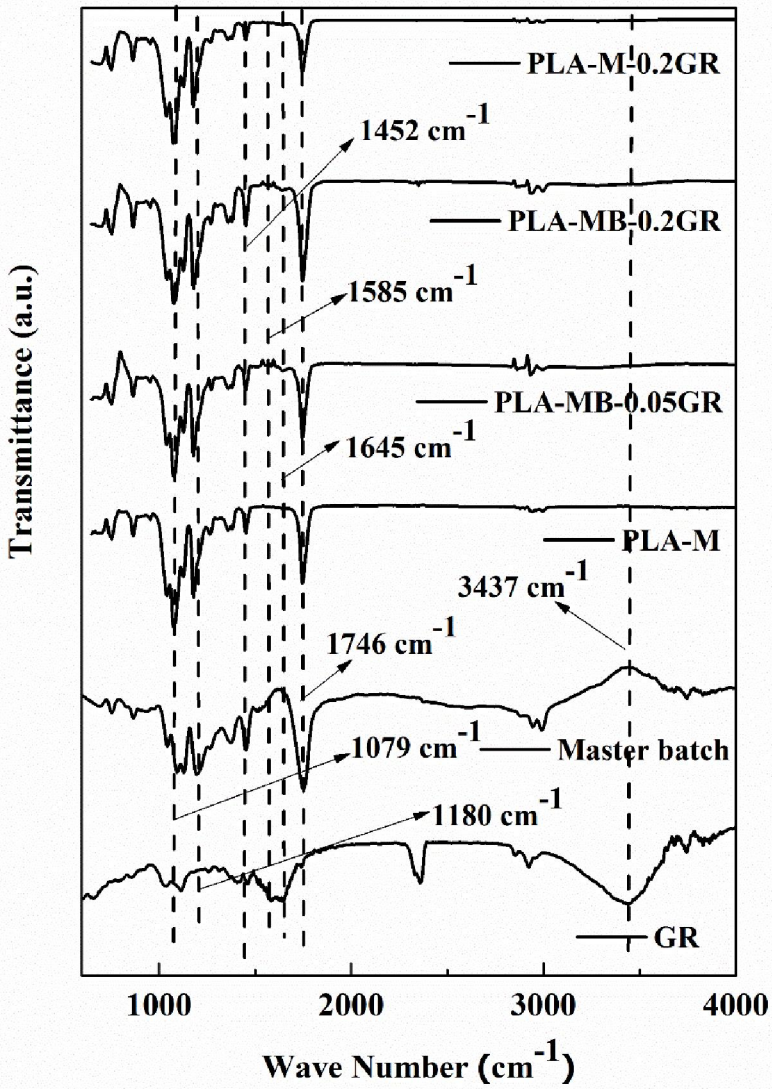

Fig. 3.2 FTIR spectra for GR, PLA-M, PLA-MB-0.05GR, PLA-MB-0.2GR and PLA-M-0.2GR nanocomposites

3.3.2 XRD analysis

XRD analysis was carried out to evaluate the exfoliation state of the graphene in the fabricated composites. A sharp diffraction peak is observed for GR at 26.52°, which corresponds to the (0 0 2) graphitic carbon structure (Murariu et al., 2010; Valapa et al., 2015a). The XRD pattern (Fig. 3.3) shows a broad spectrum at 2θ ~16.7° for PLA-M and MB diluted composites corresponding to the (1 1 0) and (2 0 0) planes of PLA (Borkotoky et al., 2017; Tripathi et al., 2016a). Crystalline regime is reduced because of the fast cooling of the extruded PLA-M and the composites from molten state to

room temperature during fabrication of the composites. In case of MB diluted composites, a broad spectrum close to 2θ ~16.7° resembles similar crystal structure for PLA even after incorporation of graphene. In case of PLA-MB nanocomposites, there is no additional peak corresponding to 2θ ~26.52°, which is indicative of GR. This observation reveals the fact that in case of MB diluted composites better dispersion is achieved. Thus, both the MB diluted nanocomposites can be said to have exfoliated nature whereas the normal coated composite (PLA-M-0.2GR) is intercalated (Al-Mulla et al., 2011).

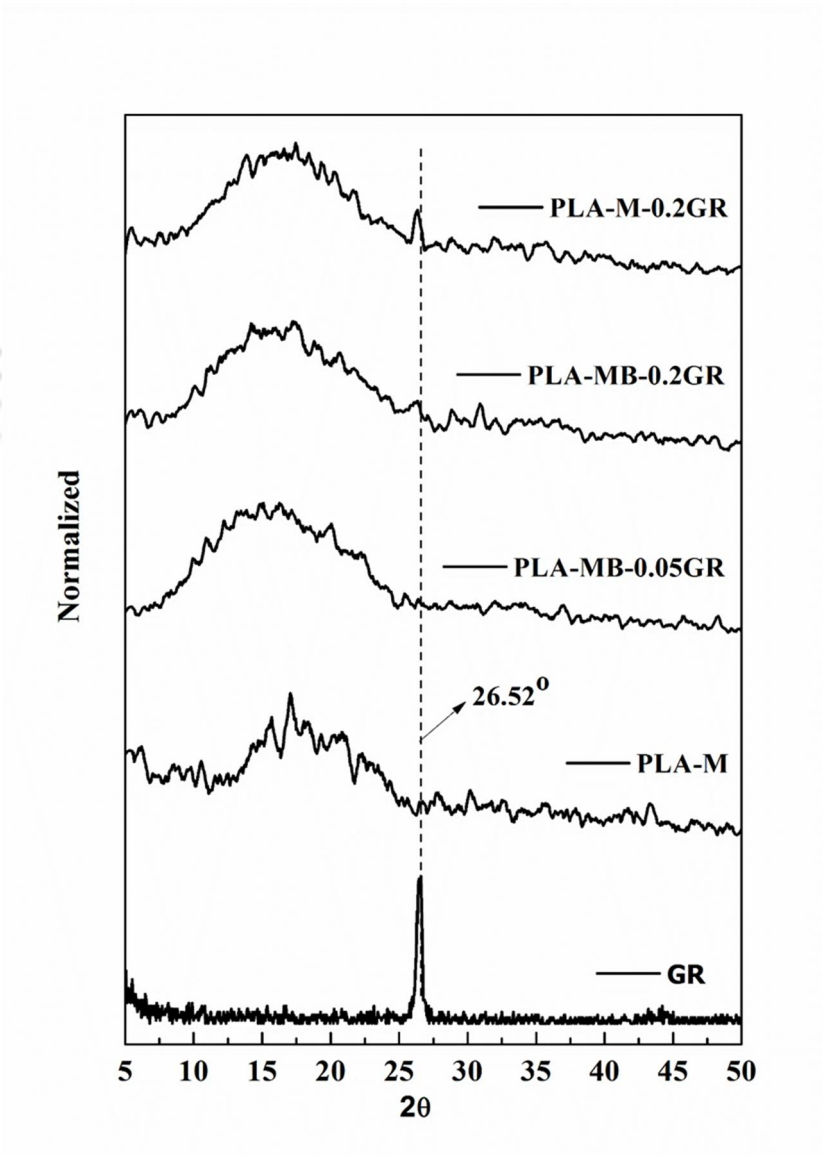

Fig. 3.3 XRD pattern for GR, PLA-M, PLA-MB-0.05GR, PLA-MB-0.2GR and PLA-M-0.2GR nanocomposites

3.3.3 Raman spectroscopy

Raman spectrum is one of the major techniques to quantify the exfoliation extent of graphene in the reinforced composites. The MB composite PLA-MB-0.2GR and normal coated composite PLA-M-0.2GR are compared through Raman spectroscopy. Appearance of I_G band corresponding to 1582.47 cm^{-1} can be noticed for GR in Fig. 3.4, which is indicative of sp^2 carbon moiety of graphene (Wall, 2011b). I_G band is shifted to 1584 cm^{-1} and 1586 cm^{-1} for PLA-M-0.2GR and PLA-MB-0.2GR, respectively. It implies reinforcement of graphene into the composites and layer gaps are further increased due to sonication and incorporation of PLA chains. During polycondensation PLA chain is incorporated into the interlayer gaps resulting an increased gap layer. The decrease of intensity of the peak indicates that number of stacks is also reduced in the composites as compared to GR. Intensity for PLA-M-0.2GR lies between GR and PLA-MB-0.2GR. Thus, it can be said that better dispersion is achieved in case of MB diluted composite considering lesser number of stacks and higher interlayer gaps of PLA-MB-0.2GR with respect to GR and PLA-M-0.2GR.

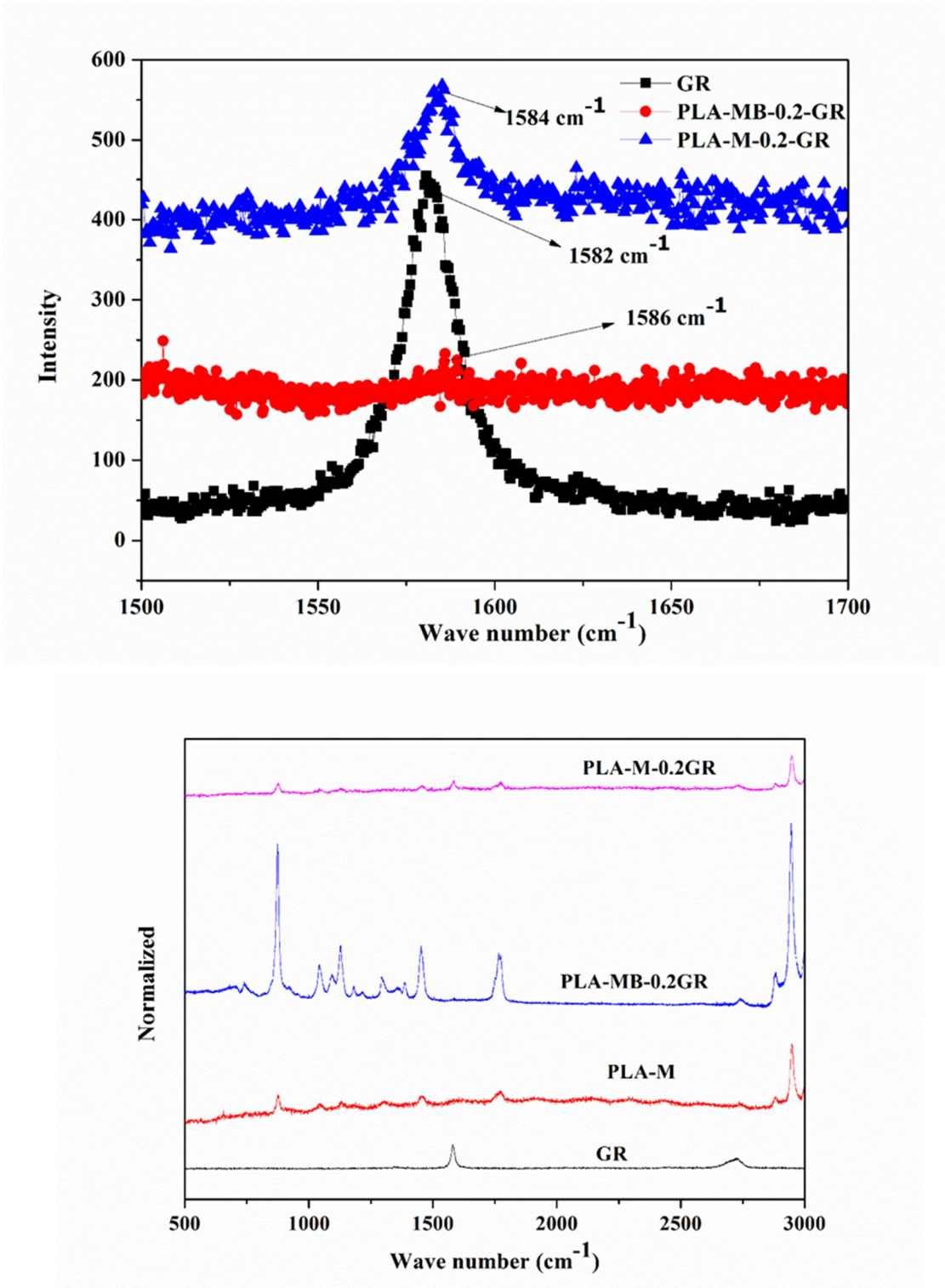

Fig. 3.4 Raman spectra for PLA-0.05-MB-GR, PLA-0.2-MB-GR and PLA-M-0.2GR nanocomposites

3.3.4 Morphological analysis

The morphological nature of the composites and dispersion of graphene can be examined from FESEM images of PLA-MB-0.2GR reported in Fig 3.5. In case of MB diluted composites, uniform dispersion can be observed (Fig. 3.5a) and layer of small chain polymer over the graphene can be seen with higher magnification (Fig. 3.5b) (Pal & Katiyar, 2016). However, agglomeration has been observed in case of PLA-M-0.2GR composite (Fig. 3.5c). In the fracture surface of PLA-MB-0.2GR, less material pull out can be noticed (Fig. 3.5d) supporting the facts of better compatibility due to similar polymer interaction and better dispersion in case of MB diluted composites.

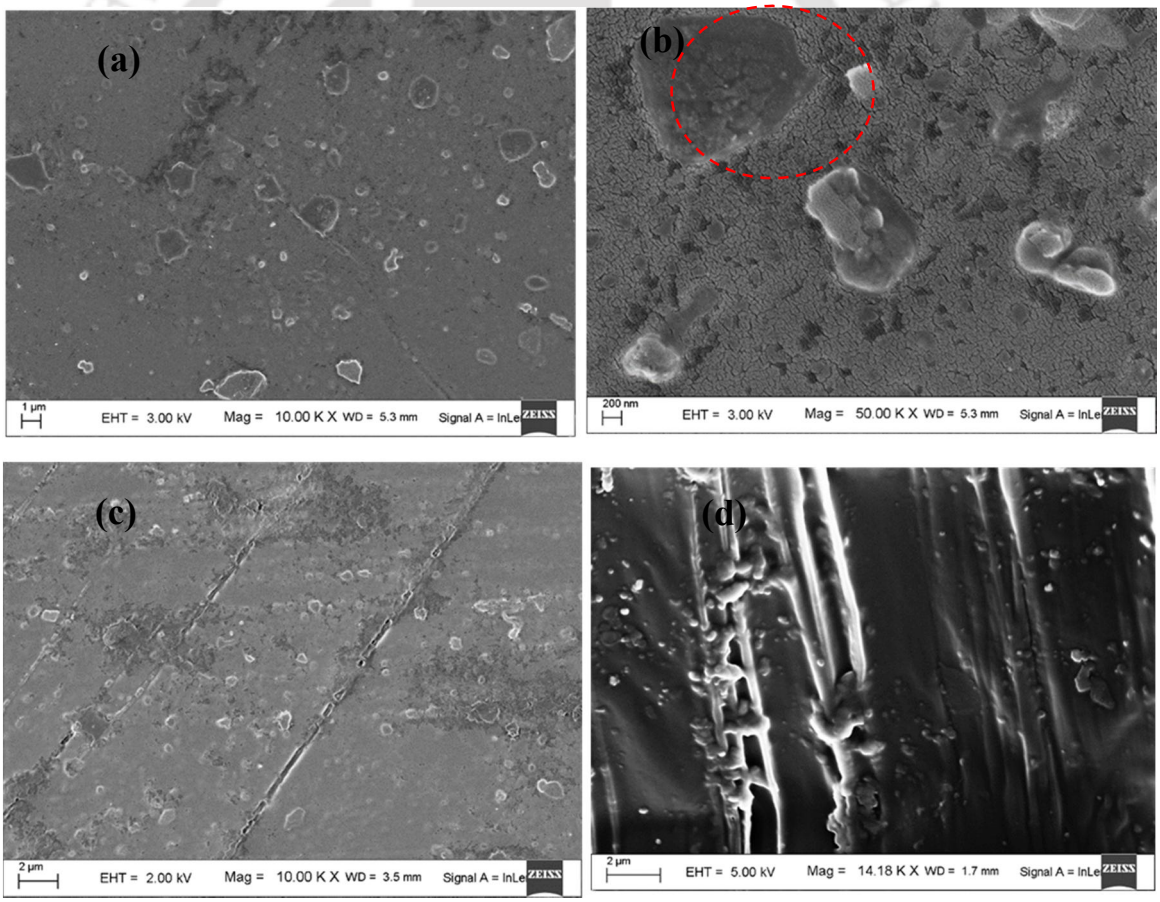

Fig. 3.5 FESEM images of (a, b) PLA-MB-0.2GR, (c) PLA-M-0.2GR and (d) fractured surface of PLA-MB-0.2GR nanocomposites

3.3.5 TGA

Presence of GR content is likely to increase the thermal stability of the composite. Again presence of short-chain PLA in the MB can affect the thermal stability of the composite. Thus, in order to examine the two contradictory effects, thermal stability of the MB diluted composites are studied using thermogravimetric analysis. It can be seen from Fig. 3.6 that the onset degradation temperature (T_{onset}) is found to be decreased for PLA-MB-0.05GR (327.3 °C) as compared to that of PLA-M (337.2 °C) indicating prominence of short-chain PLA effect over GR. However, in case of higher loading, it is increased for PLA-MB-0.2GR (341.1 °C) due to increased GR content. Further, the presence of short-chain PLA makes PLA-MB-0.2GR less stable compared to normal coated composite of same loading (PLA-M-0.2GR). A similar trend can be noticed in Table 3.1 for the temperatures where 50% weight loss takes place and where rate of degradation is maximum for the composites. Thus, choice of GR content in the MB diluted composite should be dependent on application point of view. Additionally, composite PLA-MB-0.05GR could be better degradable material in the context of waste disposal.

Table 3.1 Thermal properties of PLA-M, PLA-MB-0.05GR and PLA-MB-0.2GR and PLA-M-0.2GR

Components	T_{onset} (°C)	$T_{50\%}$ (°C)	T_{max} (°C)	X_{cc}%	T_m (°C)	T_c (°C)	T_g (°C)
PLA-M	337.2	351.4	360.2	0.29%	151.6	120.4	62
PLA-MB-0.05GR	327.3	339.6	347.7	0.36%	151.6	122.6	62
PLA-MB-0.2GR	341.1	361.9	361.8	0.24%	152.7	126	63

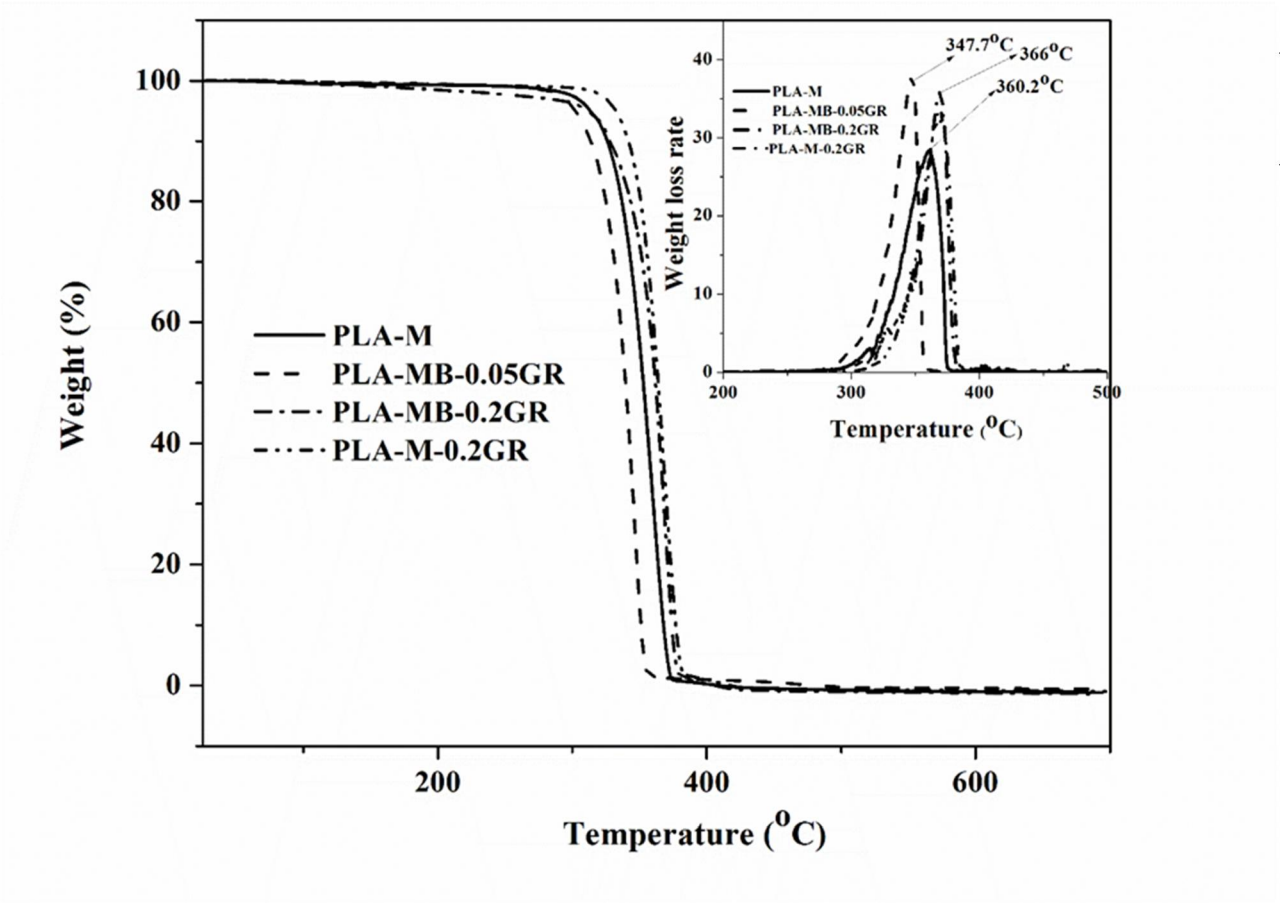

Fig. 3.6 Thermal degradation properties of master-batch diluted composites (DTG profile in the inset)

3.3.6 DSC analysis

DSC analysis was carried out to investigate the non-isothermal cold crystallization nature of PLA-M and PLA-MB-GR composites (Fig. 3.7 and Table 3.1). Glass transition temperature (T_g) of PLA-M (62 °C) is almost comparable with MB diluted composites implying similar type of chain relaxation behavior. There is no significant improvement in melting temperature (T_m), especially at lower loading. In case of higher loading of MB melting temperature is slightly improved as compared to that of PLA-M, similar to the case of normal coated composite. Crystallization temperature (T_c) is increased with loading of MB for PLA-MB-0.05GR (122.6 °C) and PLA-MB-0.2GR (126 °C) with respect to that of PLA-M (120.4 °C). The marginal improvement in crystallization temperature maybe because of the nucleating effect of the graphene (

Valapa et al., 2015a; Yuan et al., 2006). Cold crystallinity is also marginally increased in case of PLA-MB-0.05GR (0.36%) compared to that of PLA-M (0.29%). But it is again marginally decreased for PLA-MB-0.2GR (0.24%), possibly due to presence of more short-chain PLA molecules at higher loading of MB (Pal & Katiyar, 2016). Thus, the DSC analysis reveals little impact on crystallization characteristics of the composites due to addition of fillers.

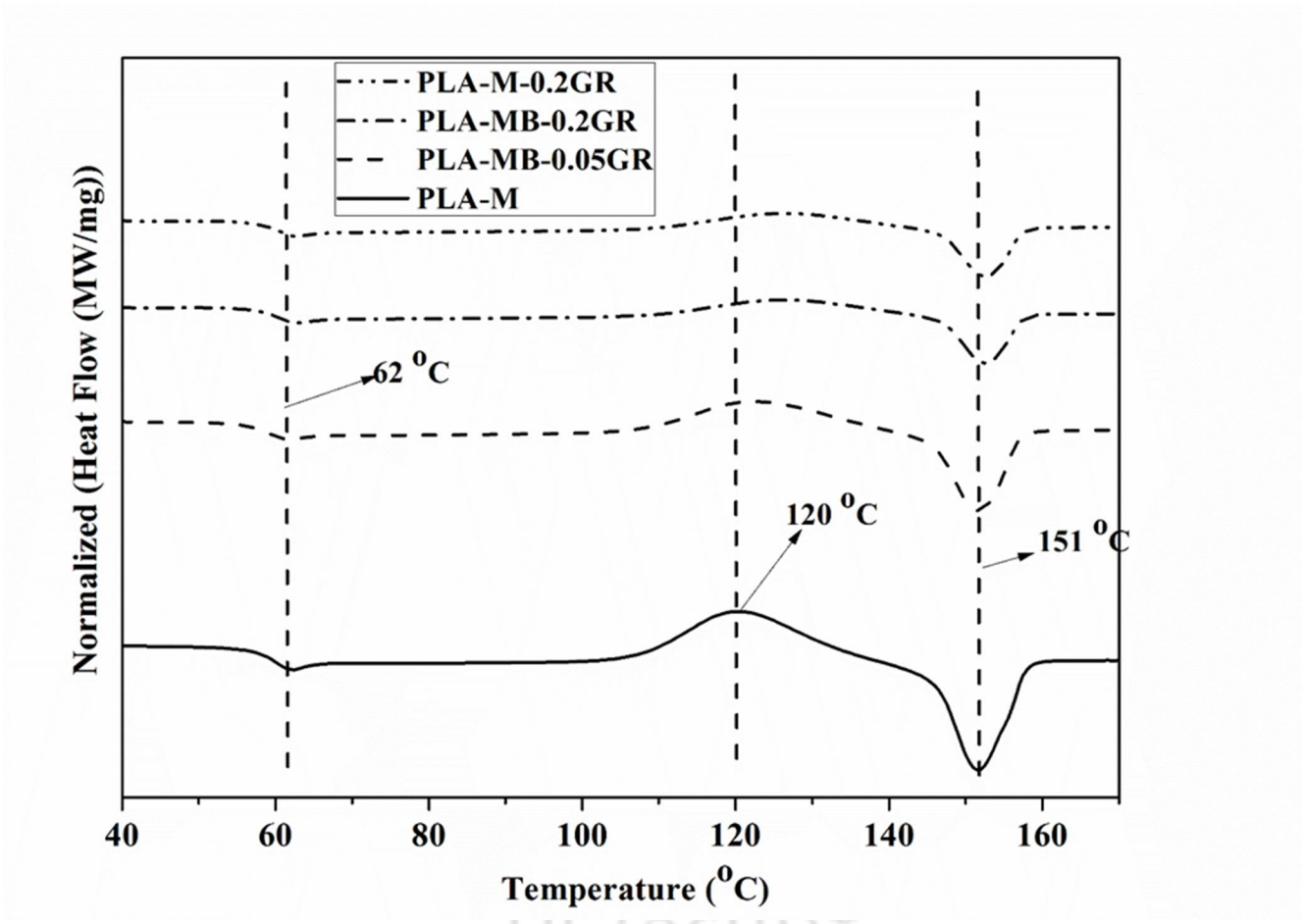

Fig. 3.7 DSC thermogram for PLA-M, PLA-M-0.05GR and PLA-M-0.2GR nanocomposites

3.3.7 Mechanical property analysis

Mechanical properties of the nanocomposites such as tensile strength, Young's modulus, and elongation at break (%) give idea about plasticity, brittleness and toughness characteristics for PLA and its composites (Table 3.2). As expected, due to

the addition of GR in the normal composite, the UTS (ultimate tensile strength) is found to increase with respect to that of PLA-M. But in case of MB composites, the UTS values are decreased below that of PLA-M because of the addition of short-chain PLA. During masterbatch (MB) preparation from oligomer, polycondensation reaction was carried out to coat GR with short PLA chains. Thereafter, the coated GR (MB) was reinforced to high molecular weight PLA (PLA 2003D). There is some degradation of PLA chains due to melt processing but majority of the short chains are incorporated along with GR to improve the compatibility and dispersion of the composites. Presence of shorter polymer chain reduces tensile strength because under tensile force shorter polymeric chains aligns faster than longer chains. The decrease is more in case of PLA-MB-0.2GR because of more short-chain PLA in the composite as GR loading increases the amount of short-chain is also increased (Pal & Katiyar, 2016). An increase in Young's modulus in the MB composites indicates better compatibility over normal composite. As GR particles are coated with short PLA chains before reinforcement in high molecular weight PLA matrix, it leads to similar molecular interaction. The latter leads to the better compatibility of GR in the MB composites (Li et al., 2014). A higher value of PLA-MB-0.05GR composite over PLA-MB-0.2GR reveals better dispersion in the former case. In case of PLA-MB-0.05GR, elongation at break (%) is improved by 17% as compared to that of PLA-M. Elongation at break improvement indicates that chain mobility of the composite is increased due to presence of short PLA chains in the MB, which acted as plasticizer for the composite (Pal & Katiyar, 2016). However, in case of PLA-MB-0.2GR, elongation at break (%) is reduced possibly due to the less strength and chain mobility of the composite, which causes faster breakage.

Table 3.2 Mechanical properties of PLA-M, PLA-MB-0.05GR, PLA-MB-0.2GR and PLA-M-0.2GR

Components	UTS (N/mm^2)	Young's modulus (N/mm^2)	Elongation at break (%)
PLA-M	29.5±3.8	4.30±0.56	12.93±3.4
PLA-MB-0.05GR	25.2±3.3	5.47±1.3	15.6±1.7
PLA-MB-0.2GR	24.0±0.3	4.87±0.35	9.3±1.9
PLA-M-0.2GR	31.3±2.8	4.58±0.61	11.7±1.7

3.3.8 DMA

The storage modulus (E) results obtained for PLA-M, PLA-M-0.2GR, PLA-MB-0.05GR, and PLA-MB-0.2GR are depicted in Fig. 3.8. At 25 °C, the storage modulus value for the composite PLA-MB-0.05GR is higher than that of PLA-M and for PLA-MB-0.2GR, it is little lower. With respect to rise in temperature, the storage modulus value for both PLA and its composites exhibited decreasing trend. After 60 °C, rate of decrement of the MB composites is found to be higher than PLA-M. Temperature corresponding to the maximum value of tan δ i.e. glass transition temperature for the PLA-MB-0.05GR (63.9 °C) is little lower than PLA-M (66 °C). But in case of PLA-MB-0.2GR, due to the presence of high amount of short-chain PLA, T_g is reduced to 58.7 °C. It implies that short-chain PLA molecules enhance the primary chain relaxation nature of the composites in the presence of thermomechanical force. In case of PLA-M-0.2GR, storage modulus is higher as compared to that of PLA-MB-0.2GR. No change in T_g is observed in case of PLA-M-0.2GR.

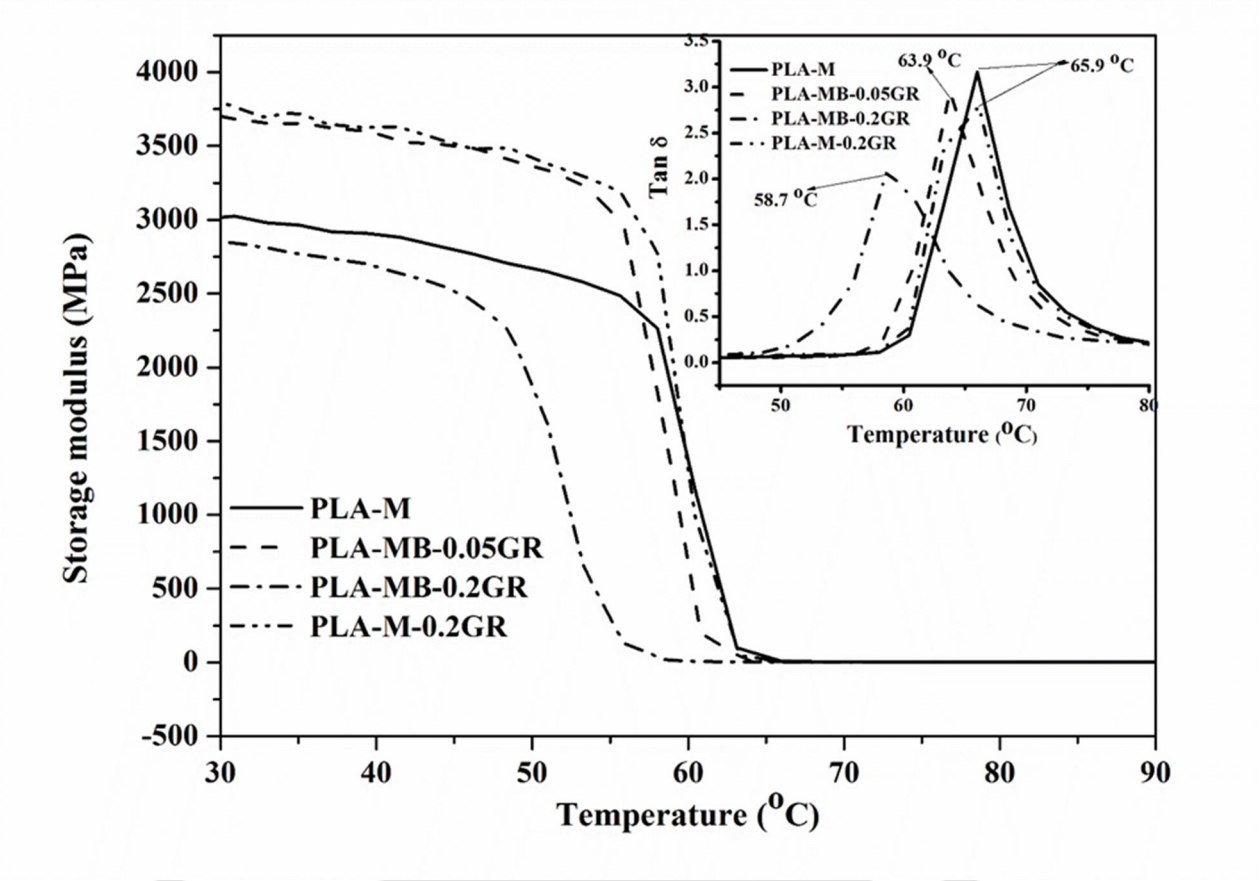

Fig. 3.8 Storage modulus and tan δ plot for master-batch diluted nanocomposites

3.3.9 Contact angle analysis

Contact angle value is slightly increased in case of PLA-MB-0.05-GR (80.5±3.5°) as compared to that of PLA-M (78.7±2.9°) due to the presence of hydrophobic graphene reinforcement. The number of open-ended chains is higher in case of MB diluted composite resulting in lower contact angle. On further increase in MB loading, contact angle is further decreased as compared to that of PLA-M. In case of PLA-MB-0.2GR, contact angle value is reduced to 69.8±2.8°, but in case of normal coated PLA-M-0.2GR, the value is 84.2±2.3º.

3.3.10 Impedance analysis

Potentiostatic frequency response analysis was carried out for the MB diluted composites. Impedance is found to be decreased with the increase of loading for the

composites. As the graphene layers are coated with nonconductive PLA chains, impedance is enhanced as compared to normally processed composite of same graphene loading (Fig. 3.9). Impedance values are found to be decreased with increase of frequency for all the samples. It may be due to discontinuity of the graphene connection within the composite causing capacitative loss. Thus, even though increase in graphene loading decreases the impedance, the value is marginal and lies in the order of 10^{11} Ω.

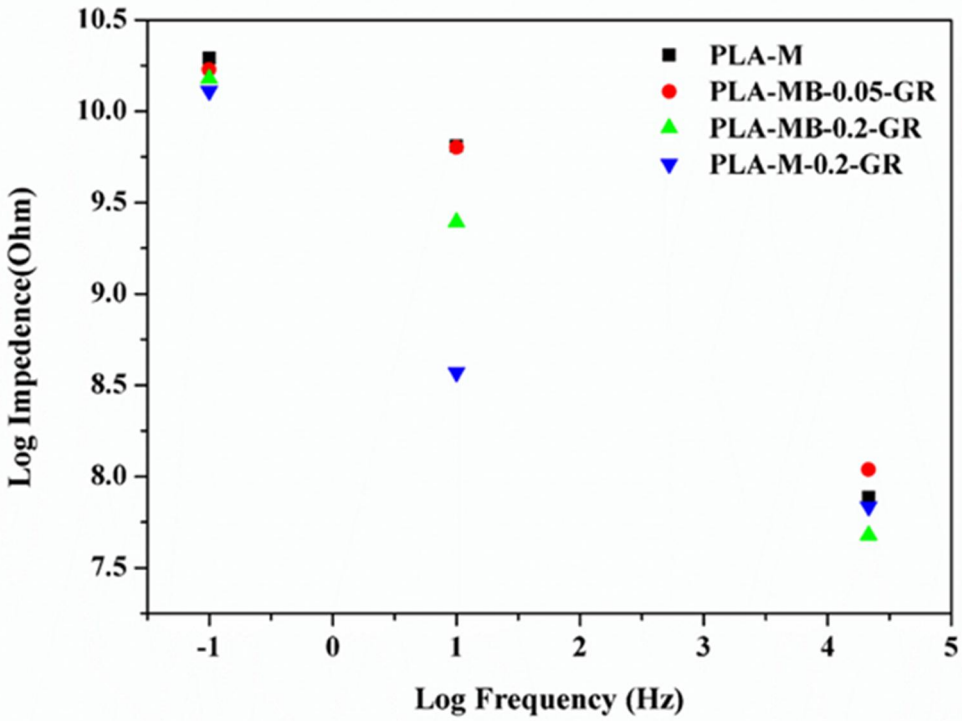

Fig. 3.9 Impedance (Ω) vs. frequency (Hz) plot at three different frequencies

3.3.11 Rheology analysis

Rheological property analysis of the melts of PLA-M, PLA-MB-0.05GR, PLA-MB-0.2GR, and PLA-M-0.2GR was carried out to study the effect of molecular structure on the flow properties of the components. In the present work, for MB coated nanocomposites, two different reinforcements were incorporated into the PLA matrix i.e. layered structured graphene and small chain PLA. Rheogram (log-log plot of elastic

modulus (G′), loss modulus (G″) and complex viscosity (η^*) with angular frequency (ω)) of PLA-M, PLA-MB-0.05GR, PLA-MB-0.2GR and PLA-M-0.2GR can be seen in Fig. 3.10. G′ for the MB diluted composite decreases with respect to that of PLA-M because of the presence of the short PLA chains in the former. In case of PLA-MB-0.2GR, storage modulus value is lower than that of PLA-MB-0.05GR because of the higher content of short-chain PLA. A similar trend also can be observed for G″ and η^*.

Slopes of ln G′ vs. ln ω and ln G″ vs. ln ω (ω values <10 rad/sec) are indicative of nature of the polymer melt (Fig. 3.11). In the case of PLA-M, PLA-MB-0.05GR and PLA-M-0.2GR, a similar trend is observed at 180 ºC and the values are 1.65, 1.81, 1.73 and 0.91, 0.98, 0.91, respectively (Table 3.3). In case of PLA-MB-0.05GR, the slopes are more close to 2 and 1, which suggests non-cross linking nature and flow behavior similar to that of homopolymers (Ahmed et al., 2010b; Al-Itry et al., 2014; Sinha Ray & Okamoto, 2003). In case of PLA-MB-0.2GR, due to the presence of large amount short PLA chains, the values are found to deviate and for both cases, slope is near to unity (0.68 & 0.98) indicating Newtonian type of fluid (Table 3.3). It can be seen in Table 3.3 that the slope values are similar for all the temperatures i.e. 180 ºC, 185 ºC, and 190 ºC.

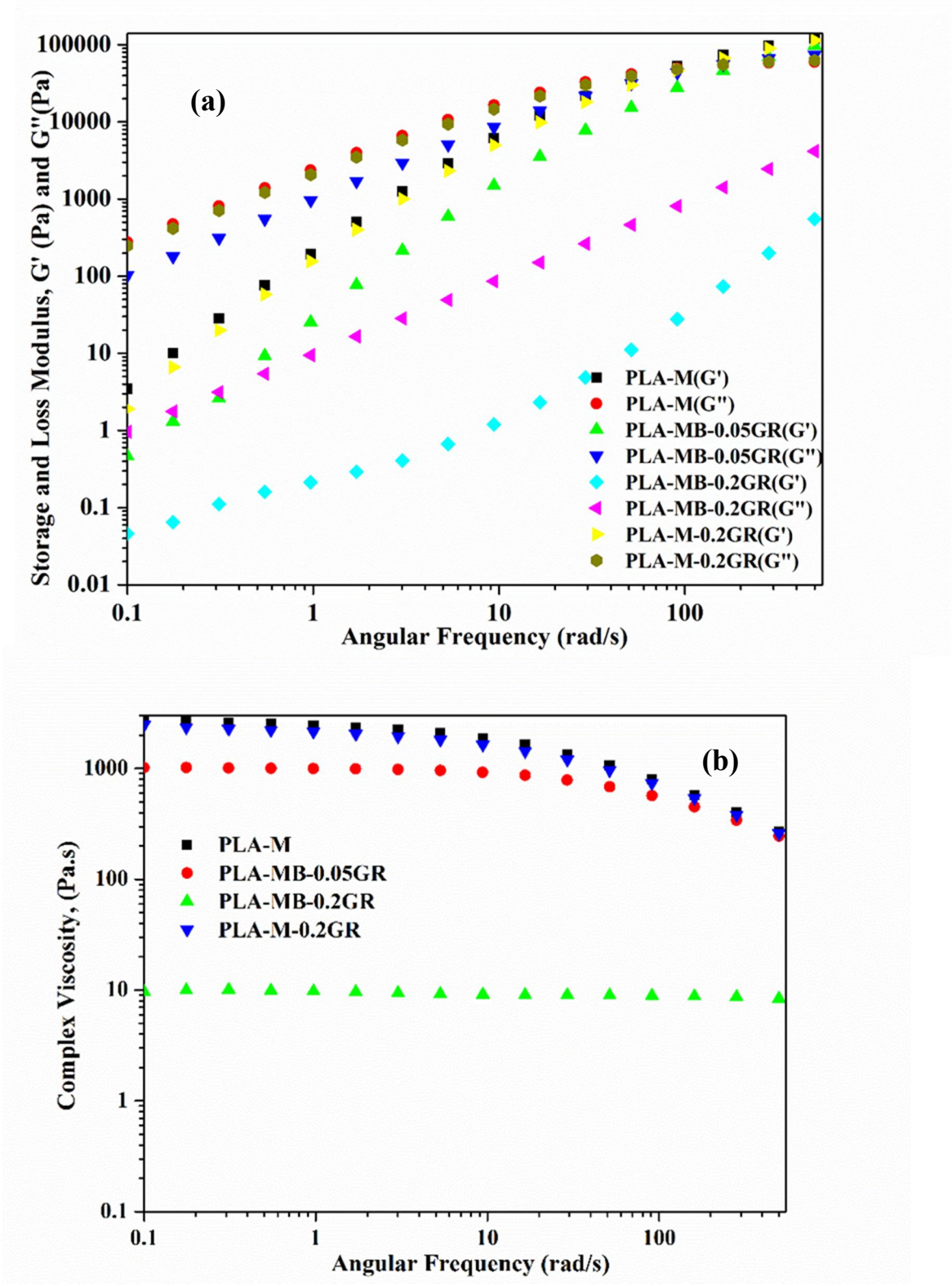

Fig. 3.10 Rheological analysis of master-batch diluted nanocomposites at 180 °C a) Storage modulus and Loss modulus and b) Complex viscosity

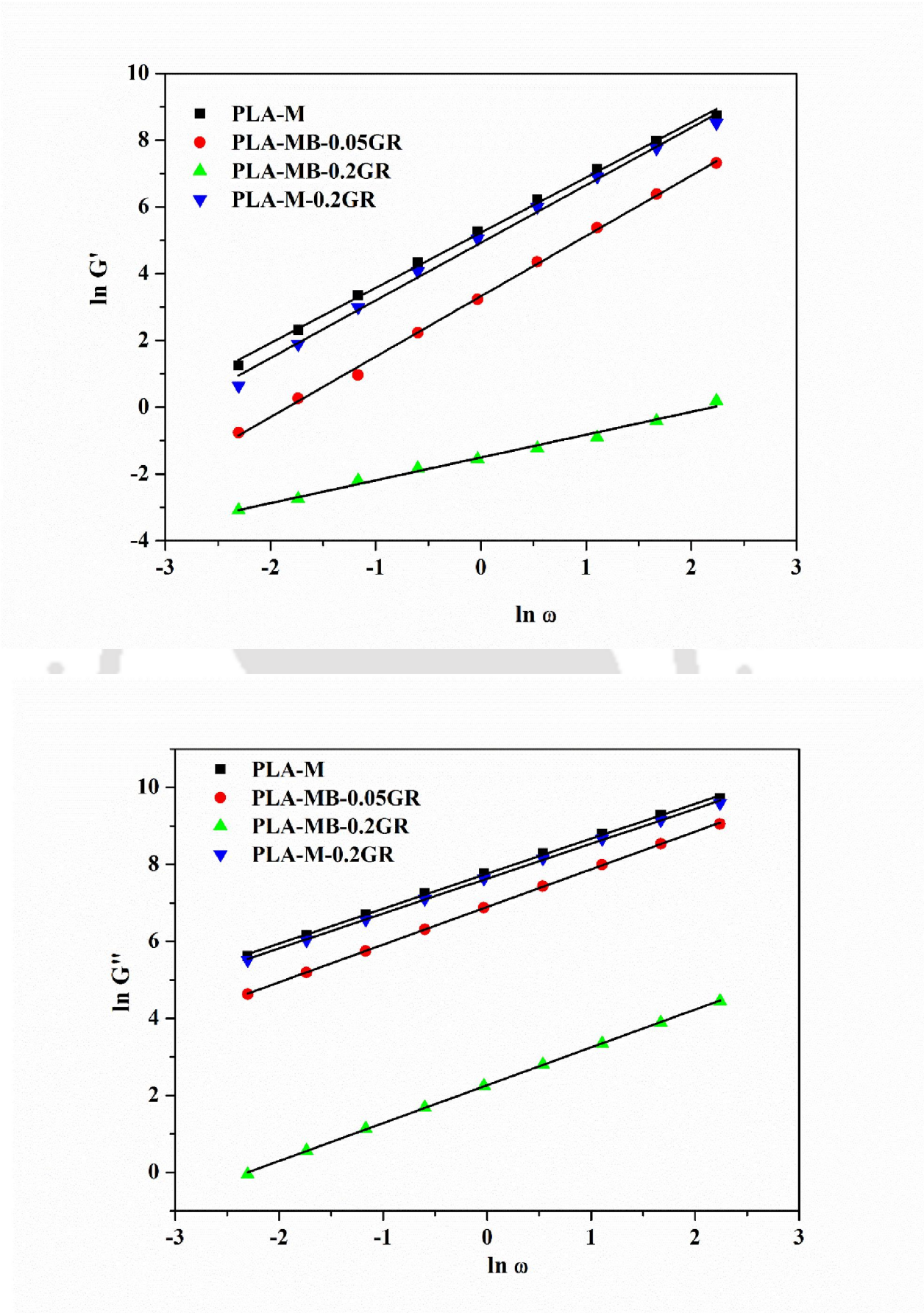

Fig. 3.11 Slopes of ln G′ vs. ln ω and ln G″ vs. ln ω (ω <10 rad/sec)

3.3.11.1 Cox-Merz approximation

Complex viscosity value decreases with an increase in temperature (Fig.3.12, PLA-MB-0.05GR as representative). Cox –Merz relation was applied ($|\eta^*(\omega)| = |\eta(\dot{\gamma})|$ $\dot{\gamma}=\omega$) to find out the slope, which is equal to (n-1) of η^* vs. ω plot in log-log scale in the power-law region (Fig. 3.13).(Cox & Merz, 1959; Sinha Ray & Okamoto, 2003) From Table 3.3, it can be seen that 'n', which is a measure of non-Newtonian nature, increases with an increase in the temperature for all the components. At 180 ºC, the values are 0.43, 0.59, 0.98 and 0.46 for PLA-M, PLA-MB-0.05GR, PLA-MB-0.2GR and PLA-M-0.2GR, respectively. It reveals that the presence of MB reduces the shear thinning nature of the composites and for PLA-MB-0.2GR, it is close to Newtonian fluid.

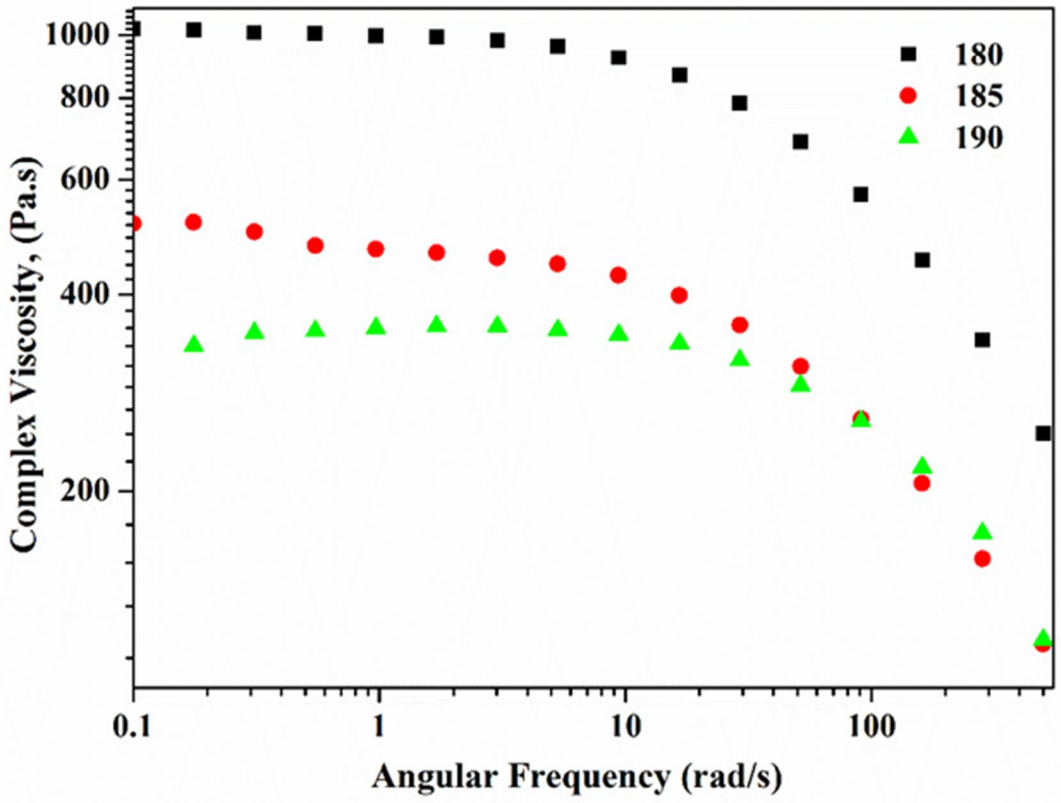

Fig. 3.12 Complex viscosity of PLA-MB-0.05GR composite at different temperatures

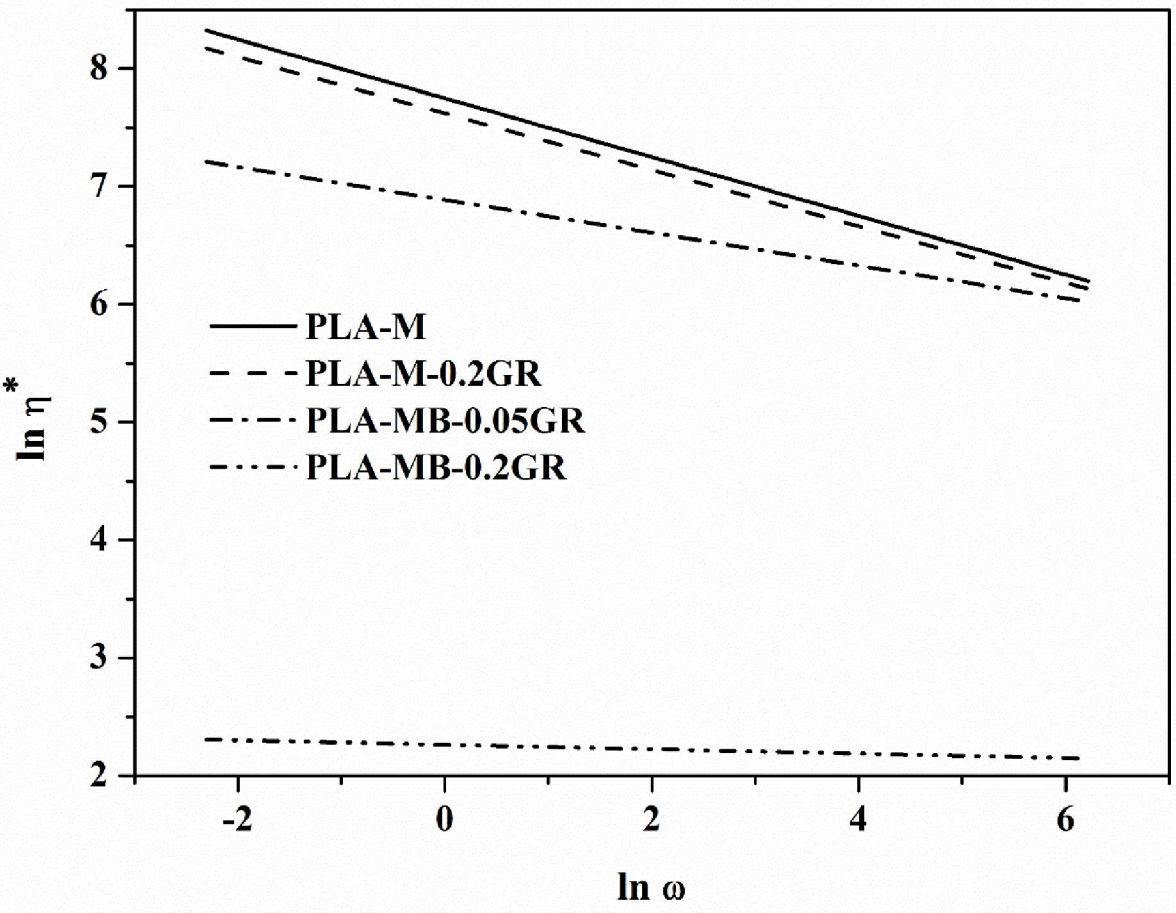

Fig. 3.13 ln η* vs. ln ω plot at 180 °C

3.3.11.2 Activation energy

Flow activation energy '*E*' (kJ/mol) was calculated from the slope of ln η^* vs. 1/T plot (Fig. 3.14) (Arrhenius equation) (Ahmed et al., 2010b; Sinha Ray & Okamoto, 2003). η^* is the dynamic viscosity modulus at 0.18 rad/s (as reference). The activation energy values are found to be 158.09 kJ/mol, 186.69 kJ/mol, 110.42 kJ/mol and 85.78 kJ/mol for PLA-M, PLA-MB-0.05GR, PLA-MB-0.2GR and PLA-M-0.2GR, respectively. Activation energy is found to be higher in case of PLA-MB-0.05GR as compared to that of other composites.

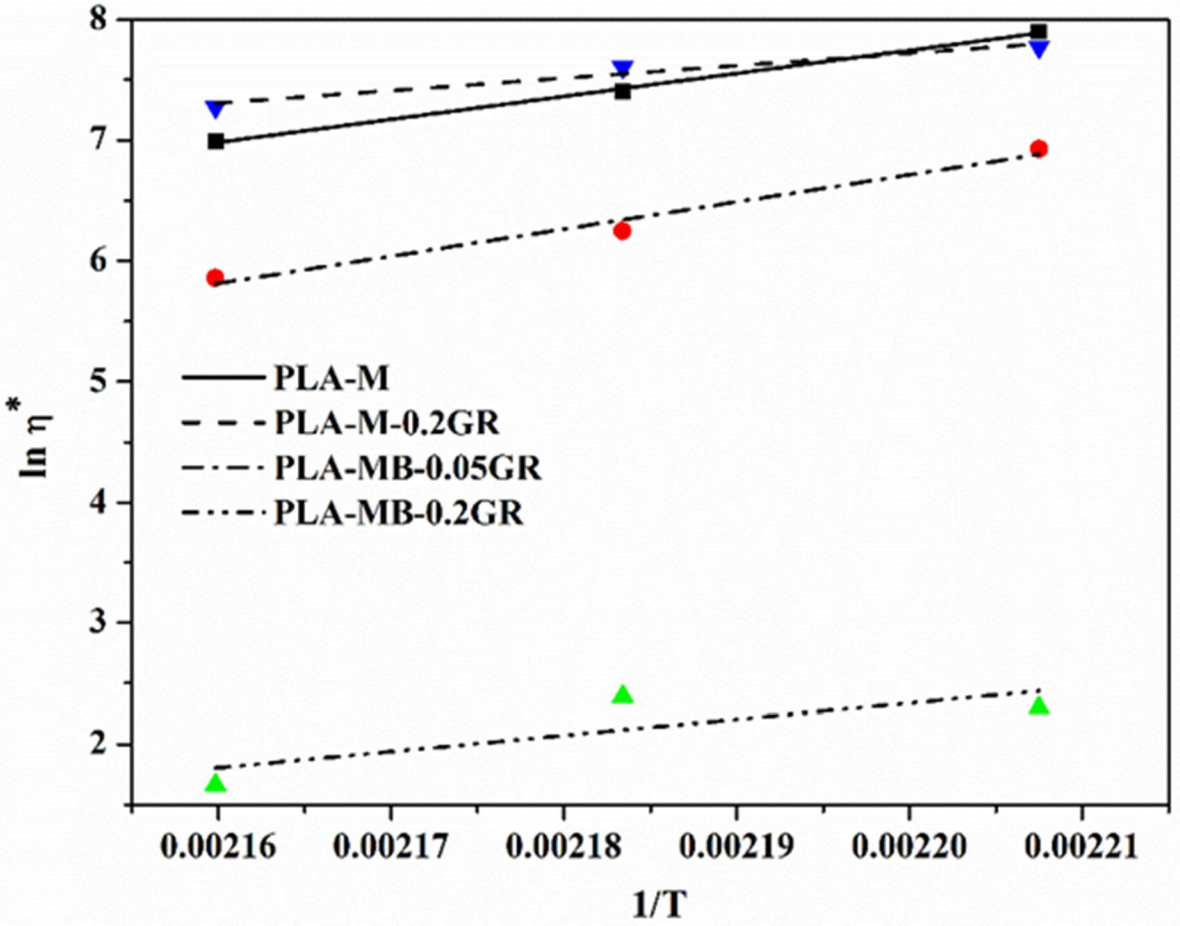

Fig. 3.14 Activation energy plot for PLA-M, PLA-MB-0.05GR, PLA-MB-0.2GR and PLA-M-0.2GR

3.3.11.3 Han plot and Phase angle

Han plot is generally used to examine the phase separation behavior within the composite. Fig. 3.15a suggests that Han plot for the PLA-M, PLA-MB-0.05GR, and PLA-M-0.2GR are linear and similar in nature. This indicates no significant phase separation. The deviation observed in case of PLA-MB-0.2GR may be because of change in the chain relaxation behavior due to the presence of higher content of short-chain PLA molecules. Phase angle change along with frequency presented in Fig. 3.15b indicates that for all the components at higher angular frequency, solid-like behavior

increases (Al-Itry et al., 2014). In case of MB diluted composites, viscous property is higher. In case of PLA-MB-0.2GR, more viscous nature can be seen even at higher frequency. With increase in temperature from 180 ºC to 190 ºC, the curve is shifted towards more viscous like characteristics. The similar nature of the slopes of the Han plot suggests that for PLA-MB-0.05GR, polydispersity of the matrix PLA is not changed due to incorporation of MB. However, for PLA-MB-0.2GR, the curve is deviated from the PLA-M in the lower values of G′ and G″, possibly because of the presence of higher amount of short PLA chains (Chen et al., 2013).

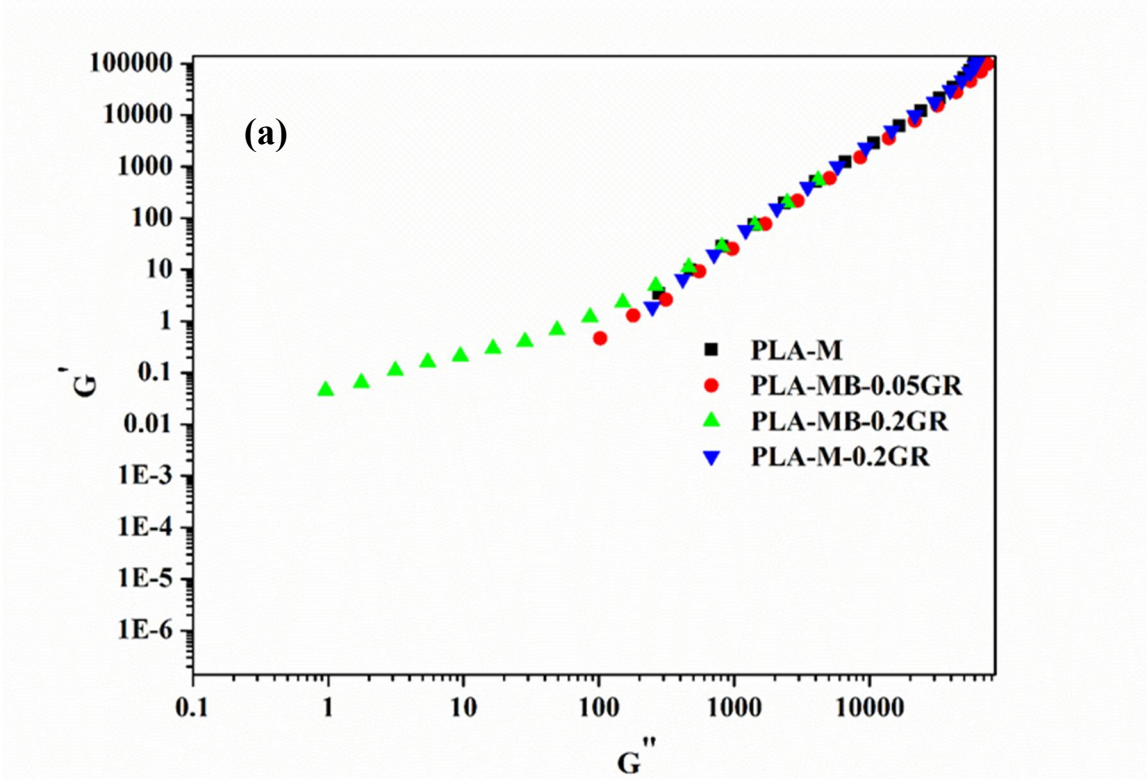

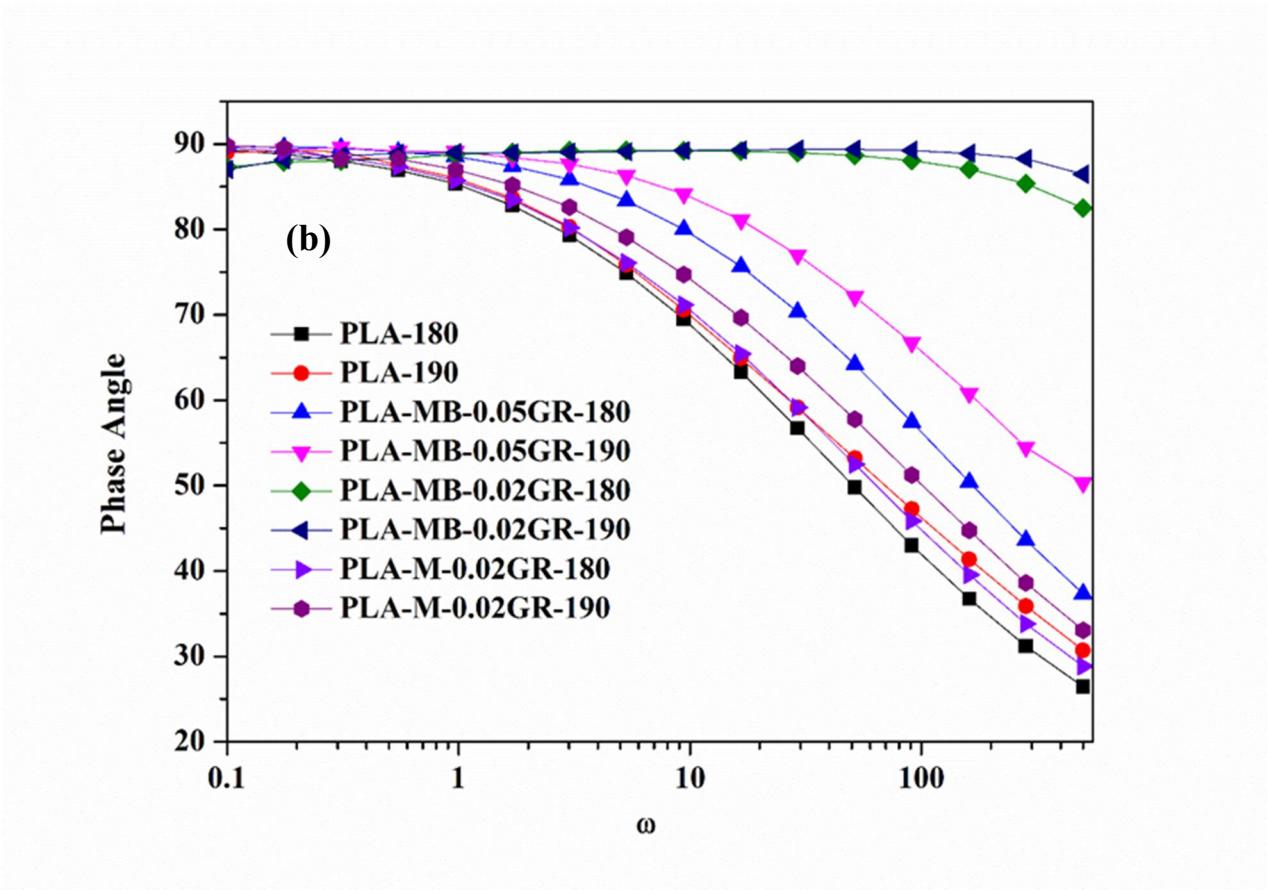

Fig. 3.15 (a) Han plot of PLA and its composites at 180°C and (b) Phase angle at different angular frequencies for the components at 180°C and 190 °C

3.3.11.4 Cole-Cole plot

Miscibility property of the nanocomposite melts was investigated using Cole-Cole plot (imaginary viscosity was plotted with respect to real viscosity) (Fig. 3.16a) (Ahmed et al., 2010b). PLA-M, PLA-MB-0.05GR, and PLA-M-0.2GR show semi-circular and smooth curves, which indicate miscible nature of the fillers in the PLA matrix. The presence of short-chain PLA enhances the loss content of the PLA-MB-0.05GR. Thus, the peak is shifted downwards. With increase in the temperature form 180 ºC to 185 ºC, the curve is again shifted to lower direction (Fig. 3.16b). This is because flowability of the sample increases with an increase in the temperature. Hence, the loss content also increases. Further increase in temperature to 190 ºC helps the composite to behave even more liquid-like with a much higher value of loss content. Hence, the plot is somewhat different from the other two temperatures.

Thus, the rheological analysis of the PLA-M and the composites (with and without MB) reveals both positive and negative aspects of all the samples studied. Overall, the composite PLA-MB-0.05GR appears to be the best of all samples considering the improved flow and processability properties like better dispersion; good miscibility and chain mobility; no phase separation; non-crosslinking nature of the chains; and higher activation energy. Increment in miscibility and dispersion would lead to better compatibility and lesser phase gap within the composite between matrix and reinforcement. Melt flow ability increment would help less power consumption during film drawing for the composites. Noncrosslinking nature indicates that thermoplasticity i.e. processing window of the composites is not changed. These impacts would be significant in case of large scale PLA film production.

Table 3.3 Analysis of rheological properties

Sample	Temperature (°C)	Slope (ln G'Vs ln ω)	Slope (ln G"Vs ln ω)	'n' of Cox–Merz model	E (kJ/mol)
PLA-M	180	1.65	0.91	0.43	
	185	1.51	0.87	0.46	158.09
	190	1.61	0.84	0.48	
PLA-MB-0.05GR	180	1.81	0.98	0.59	
	185	1.71	0.96	0.60	186.69
	190	1.42	1	0.67	
PLA-MB-0.2GR	180	0.68	0.98	0.98	
	185	0.76	1.00	0.98	110.42
	190	0.75	0.98	0.99	
PLA-M-0.2GR	180	1.73	0.91	0.46	
	185	1.73	0.94	0.51	85.78
	190	1.82	0.94	0.53	

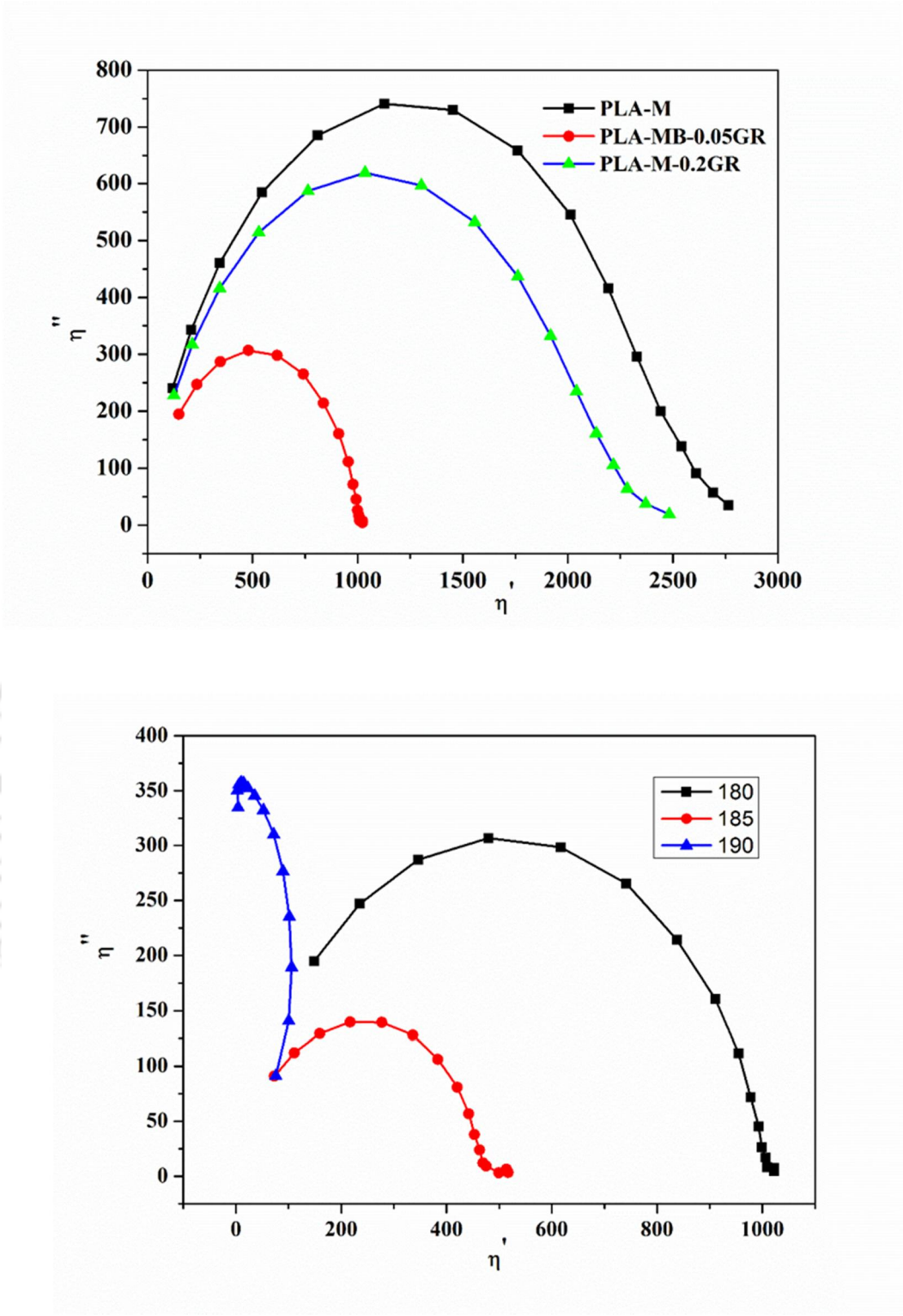

Fig. 3.16 (a) Cole-Cole plot for PLA-M, PLA-MB-0.05GR and PLA-M-0.2GR and

(b) Cole-Cole plot for PLA-MB-0.05GR at different temperatures

3.4 Summary

Successful coating of short-chain PLA on the graphene surfaces has been achieved in this work by masterbatch (MB) preparation, where the graphene layer became further less and almost to monolayer distribution. XRD, FESEM, Raman studies reveal better dispersion and interaction of reinforcement in case of the MB diluted composites (PLA-MB-0.05GR, PLA-MB-0.2GR) compared to that for normal coated composite (PLA-M-0.2GR). Thermal stability is higher for PLA-MB-0.2GR compared to that of PLA-MB-0.05GR due to the effect of graphene loading. Tensile strength is decreased for the MB diluted composites compared to that for normal coated composite. Young modulus is higher for PLA-MB-0.05GR signifying better compatibility of the reinforcement with the matrix due to similar polymer interaction. Elongation at break is increased for 0.05 wt. % loading and it is 17% higher than that for PLA-M. Contact angle is decreased with MB loading and for the same loading, it is lower than normal coated composite. DMA analysis and rheology analysis reveal that chain mobility is affected due to incorporation of short-chain PLA and is higher in case of PLA-MB-0.2GR. Thus, even though there is no major improvement in some of the mechanical properties of the GR-dispersed PLA composite compared to that of ordinary PLA-M, other properties such as dynamic mechanical, thermal and rheological properties are significantly improved for the MB dispersed GR composites. This, in turn, can help in better thermal stability, lesser power consumption and uniform film without neck formation during practical application.

Chapter 4

Exfoliated Graphene Dispersed Poly (lactic acid) based Nanocomposites Sensors for Liquid Solvent Detection

Abstract

This chapter demonstrates the utilization of exfoliated graphene (GR) for fabrication of conductive PLA/GR nanocomposites which were characterized by using XRD, FESEM and Impedance analysis. Optimum loading was found to be 1.7 wt. % GR when the impedance was drastically reduced to 10^5 Ω with respect to pure PLA (10^{11} Ω). Impedance of the composites was further gradually reduced to 10^4 Ω range for higher GR loading up to 3 wt. %. A new concept of equivalent polymer length is introduced for the impedance behaviour of the composites. Further, the composite films were exposed as sensing element for ethanol detection using state-of-the-art designed sensing platform. However, composite containing 2.5 wt. % GR loading showed the most stable conductivity and was taken as the model composite film which yielded good sensitivity and high selectivity for ethanol. In addition, the composite showed reusability of films for at least five cycles and the results from different composite batches were also found reproducible in nature. Sensitivity of PLA/GR composite towards other alcohols like methanol, isopropanol and isobutanol was investigated in this chapter. Detection behaviour of the composite towards different organic solvents having different functionality was also investigated in this chapter.

This research work has received scientific recognition as follows:

Chakraborty, G., Pugazhenthi, G., & Katiyar, V. (2019). Exfoliated graphene-dispersed poly (lactic acid)-based nanocomposite sensors for ethanol detection. ***Polymer Bulletin***, 76(5), 2367-2386.

Graphical Abstract

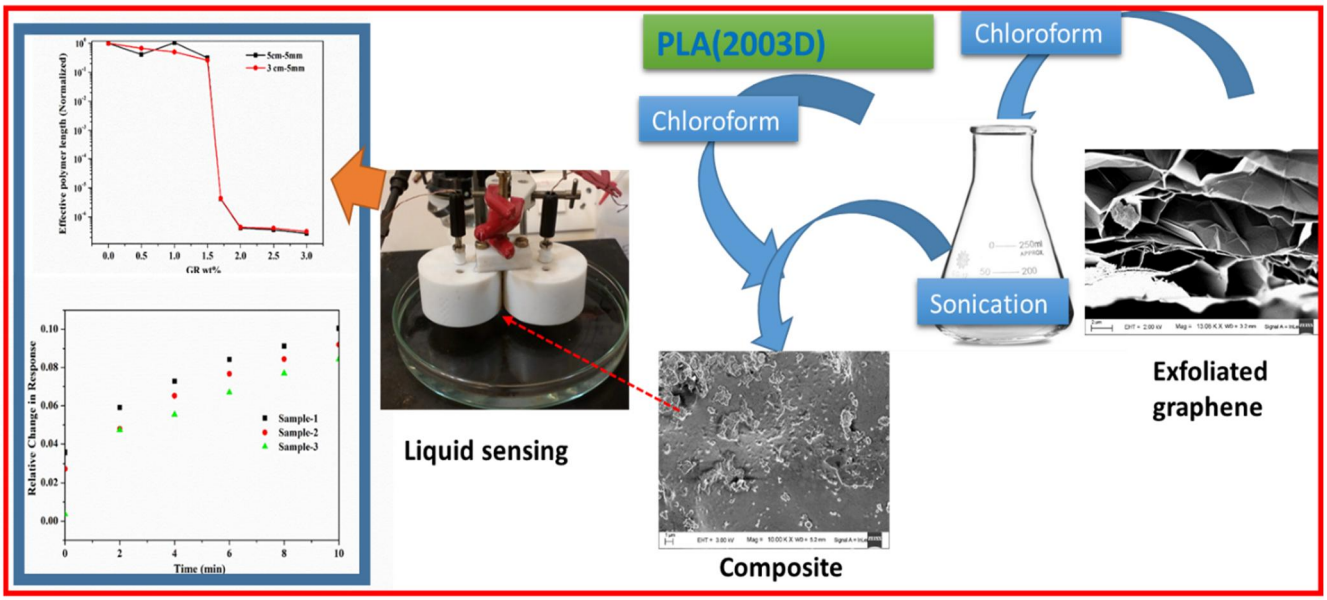

4.1 Introduction

Solid waste disposal problem of polymers and depletion of fossil resources based feedstock have become a serious threat to the sustainability of the environment. In view of this, biodegradable polymers specially polylactic acid (PLA), produced from bio-based renewable resource, has become a lucrative material for commercial applications due to its eco-friendly and biodegradable nature with comparable thermal and mechanical properties like market plastics (Lim et al., 2008). In recent years, along with packaging, applications of PLA are being extended to biomedical (Lopes et al., 2012; Reddy et al., 2013a) and conductive biomaterials (Babu et al., 2013; Han et al., 2013; Norazlina & Kamal, 2015).

Reinforcement of conductive nanoparticles such as metal-based compounds or carbon-based fillers like carbon black, carbon fiber, carbon nanotube and graphene with polymer matrices originate conductive composites (Gan & Hu, 2011; Kumar et al., 2012). PLA and other biodegradable polymer based conductive composites are used as sensing materials for various stimuli, including temperature, gases, vapours, pH and liquid (Han et al., 2013; Kobashi et al., 2008; Kumar et al., 2012; Mai et al., 2013). Potscheke et al. fabricated PLA/multiwall carbon nanotube fiber by melt spinning. Composite of 2 wt% MWCNT loading showed significant properties (Resistance 50KΩ, no fiber breakage) and was used for different solvent detection (Pötschke et al., 2010). Different reduced graphene oxide (GO) based composites were fabricated by Shen et al. (Shen et al., 2012). They reported that the highest conductivity (2.2 S/m) of the composite was achieved at 1.25 vol% of GO reduced by glucose.

Graphene is a two-dimensional layered structure of carbon having high electrical conductivity, mechanical strength and thermal stability (Potts et al., 2011; Singh et al., 2011). Incorporation of graphene-based compounds like GO and modified GO

increases the electrical conductivity of PLA remarkably and enhances the application potential (Sabzi et al., 2013; Shen et al., 2012). Sabzi et al. used graphene nanoplatelets to make PLA based nanocomposites by solution casting method and improved the electrical conductivity (Sabzi et al., 2013). In one of the earlier work of this research group (Valapa et al., 2015a), thermally exfoliated graphene (GR) reinforced nanocomposite was developed to understand the effects of GR content on the thermal, mechanical and morphological properties of the nanocomposite. The GR content used was in very low concentration ranging from 0.1-0.5 wt%. However, since GR is superior to GO in the perspective of conductive properties, the present work is undertaken with a totally different motive and objective compared to the earlier work (Valapa et al., 2015a). This work explores, possibly for the first time, the merits of GR to make a conductive film with PLA for sensor application. Wide range of wt% of GR loaded nanocomposites is developed in order to optimize the GR wt% and thereafter utilization for sensor application.

Hence, in this chapter, GR was incorporated into PLA by solution casting method to improve the electrical conductivity of the film in order to examine its application potential as a sensor. X-ray diffraction study and morphology investigation were carried out for the characterization of the composites. Impedance measurement of the composites was executed by potentiostatic frequency response analysis. A new concept of equivalent polymer length was introduced to analyze the impedance response. Graphene content was optimized for the electrically conductive composite film. Measurement setup was fabricated in order to test the sensing ability of the PLA/GR composite. As a case study, conducting PLA/GR composites were employed to detect ethanol. The applicability of the composite was examined through detection ability test for ethanol of varied concentration, reusability test, and repeatability test. In addition,

effect of ethanol on the composite was analyzed through thermogravimetric, crystallization and morphology of the composite after its use for ethanol sensing. Sensitivity of PLA/GR composite towards other alcohols like methanol, isopropanol and isobutanol were investigated in this chapter. Detection behavior of the composite towards different organic solvents having different functionality were also investigated in this chapter.

4.2 Materials and Methods

4.2.1 Materials

2003D grade of PLA purchased from NatureWorks® LLC, USA, was used for fabrication of the films. Lab synthesized exfoliated graphene (GR) was used as reinforcement substance. Chloroform and ethanol required for the present work were purchased from SISCO research laboratories (SRL Chemicals, India).

4.2.2 Experimental Section

4.2.2.1 Fabrication of PLA/GR composites by solution casting

Literature information suggests the presence of agglomeration within PLA matrix at 0.5 wt. % loading of GR when exfoliated graphene-based PLA nanocomposites were solution cast. Therefore, in this present study, wide range of wt. % of GR was loaded into PLA matrix in order to fabricate composite films of 0.5, 1, 1.5, 1.7, 2, 2.5, and 3 wt. % GR in PLA, while chloroform was used as solvent. Accordingly, pure PLA and the composites are termed as PLA-S, PLA-S-0.05GR, PLA-S-1GR, PLA-S-1.5GR, PLA-S-1.7GR, PLA-S-2GR, PLA-S-2.5GR AND PLA-S-3GR.In order to cast the composites, 0.5 gm of PLA was taken in 20 mL chloroform and was stirred till the dissolution. GR was taken in 15 mL chloroform and sonicated for 1 h. till the solution becomes uniform with no residue left at the bottom. The two solutions were mixed and

stirred using magnetic stirrer for 10 h. Finally, the solution was cast into film on a glass petri dish (Fig. 4.1)

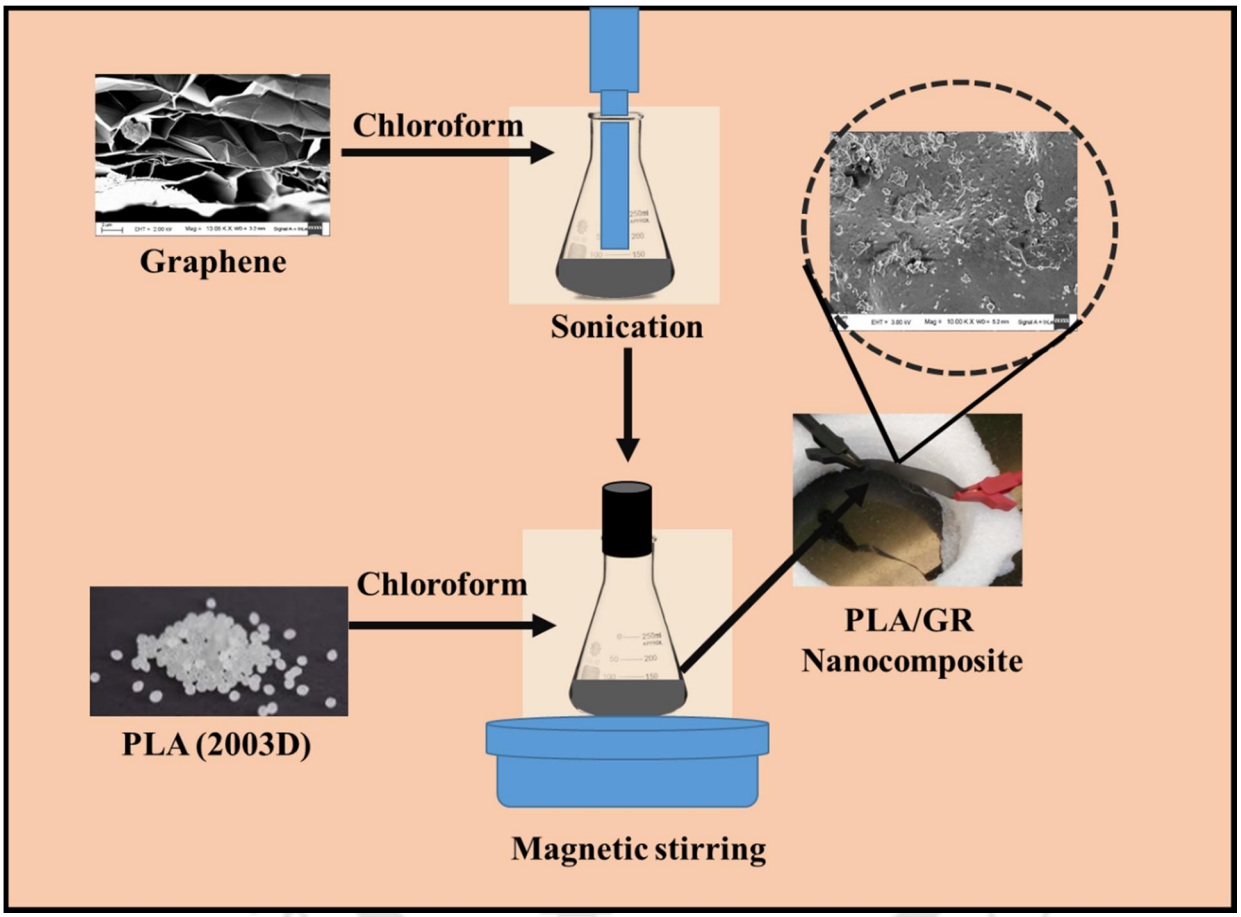

Fig. 4.1 Schematic representation of solution casting of PLA-S-GR composites

4.2.3 Characterization

4.2.3.1 XRD analysis

Details of the characterization conditions are mentioned in Chapter 2

4.2.3.2 FESEM analysis

Details of the characterization conditions are mentioned in Chapter 2

4.2.3.3 Impedance analysis

Details of the characterization conditions are mentioned in Chapter 2

4.2.3.4 Sensing of liquid solvents

PLA/GR composites of 2.5 wt. % GR was taken for the ethanol sensing study. Film of 5 mm width, 0.1 mm thickness and 85 mm length was taken for the investigation. The sensing platform was fabricated by compiling two Teflon cups and electrically conductive elements so that 11 mm length of the films was in direct contact with ethanol and the rest of the part was in the air. The film was dipped into the ethanol (or other liquids) for 10 min and values of impedance were recorded in 2 min interval. During the drying cycle, the wet film was taken upward and detached from the liquid and dried for 10 min in air. In drying cycles also, impedance measurement was carried out in every 2 min interval. In each case relative change in impedance (R_{rel}) was measured, which is defined by equation (4.1) below.

$$R_{rel} = (Z_t - Z_d) / Z_d \quad \text{..... (4.1)}$$

Where, 'Z_t' is the impedance of the film measured at time't' and 'Z_d' is the impedance of the dry film. Three consecutive 'Dipping-Drying' cycles were investigated to evaluate the effect of GR content in sensing ethanol (Fig. 4.2).

Reproducibility of the result was investigated by taking different films of same batch and from different batches. Usability test ('R_{rel}' value after 2 min dipping for multiple times using one drying condition 5 min at 50 ºC followed by 5 min at 24 ºC) was performed using ethanol. Different vol % of ethanol with respect to water were tested using 2.5 wt. % composite.

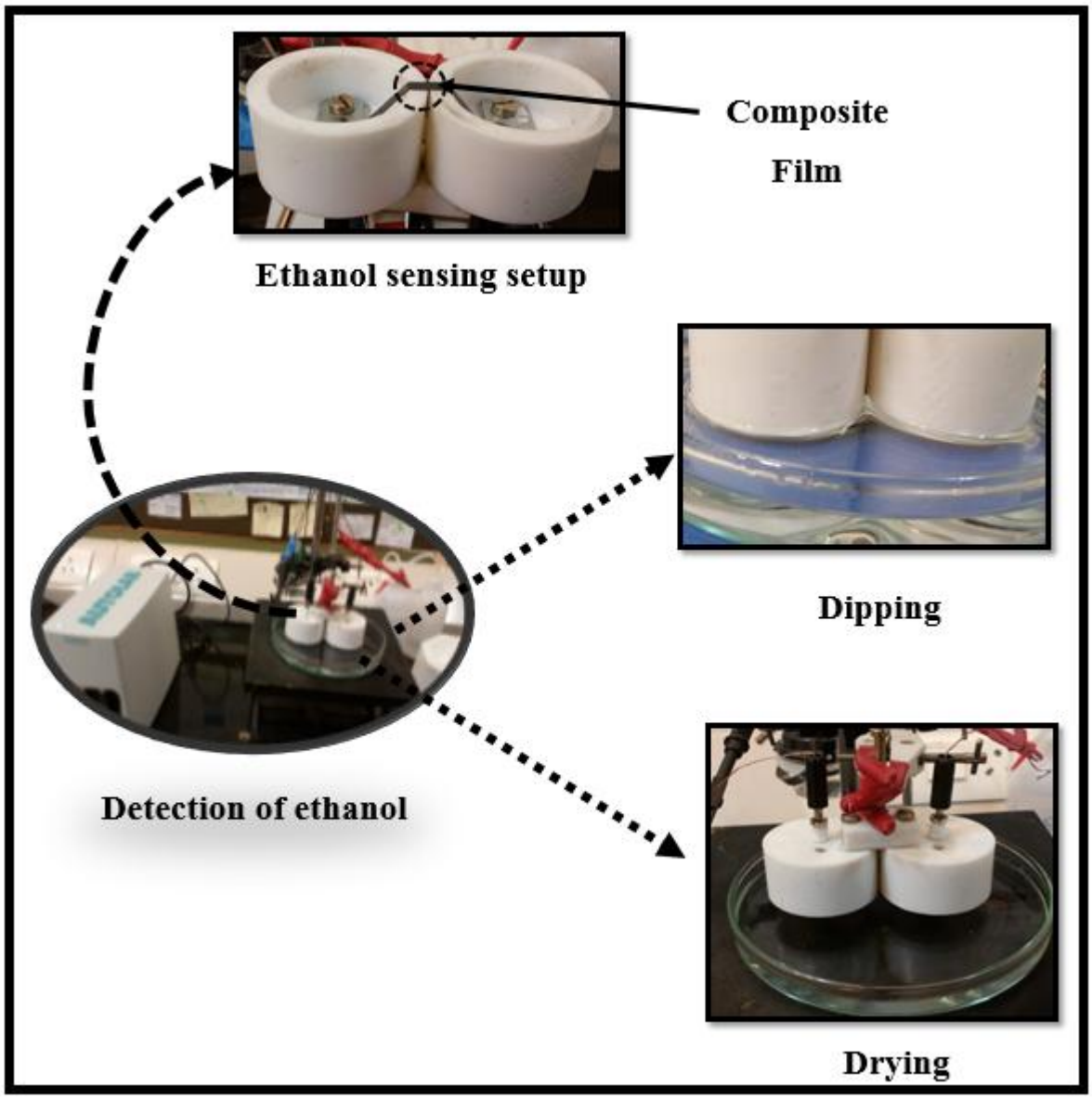

Fig. 4.2 Lab made ethanol sensing setup

4.2.3.5 TGA

Thermal degradation behaviour of PLA/GR nanocomposites was analyzed using TGA4000 of PerkinElmer. The analysis of samples was carried out by taking 3±0.3 mg of each component and heated in the range of 25 to 700 °C at a heating rate of 10 °C/min under nitrogen flow of 20mL/min.

4.2.3.6 DSC analysis

DSC analysis of the samples was carried out using METTLER TOLEDO (Model-DSC1, Star System (USA)) under nitrogen atmosphere. The samples were subjected to DSC analysis in the temperature ranging from 25 to 180 °C at a heating rate of 10 °C/min. After the first heating cycle, an isothermal condition was maintained at 180 °C for 5 min in order to remove the thermal history. Thereafter, the samples were cooled down to 25 °C at a cooling rate of 10 °C/min which was then followed by a second heating cycle of 10°C/min upto 180 °C. Second heating cycle data was analysed to get the glass-transition temperature, crystallisation temperature, melting temperature, and crystallinity.

4.3 Results and Discussion

Optimization of GR loading

This section establishes the optimum GR loading for the film through analysis of XRD, FESEM, and Impedance data for various composites fabricated.

4.3.1 XRD analysis

XRD pattern depicts the nature of the reinforced composite in terms of filler dispersion. Exfoliation of GR and lattice plane dimensions of the PLA film (termed as PLA-S), and PLA/GR composites (termed as PLA-S-0.5GR, PLA-S-1.5GR, PLA-S-1.7GR, PLA-S-2GR PLA-S-2.5GR and PLA-S-3GR based on 0.5, 1.5, 1.7, 2, 2.5 and 3 wt. % GR loading) also can be investigated from Fig. 4.3. For GR, a sharp diffraction peak is observed at 26.52º which resembles (0 0 2) graphitic carbon structure (Murariu et al., 2010; Valapa et al., 2015a). It can be noticed that in case of lower loading (0.5 wt. %) of PLA/GR composites, only 2θ ~16.5° peak is present which is indicating (1 1 0) and (2 0 0) planner structure of PLA (Krikorian & Pochan, 2003; Tripathi & Katiyar,

2016a). In case of higher loading of GR, starting from 1.5 wt. %, presence of peak at 2θ ~26.5º, which is the characteristics of GR can be seen along with the peak at 2θ ~16.5º. These results reveal that in case of lower loading (0.5 wt. %), the composites are fully exfoliated in nature but with further incorporation of GR with the same sonication time, layers of GR are not separated completely as indicated by presence of 2θ~ 26.52° peak. The PLA chains are diffused in the interlayers of the graphene sheets. Thus, the intercalated nature of the composites is observed in higher loading (more than 0.5 wt. %)

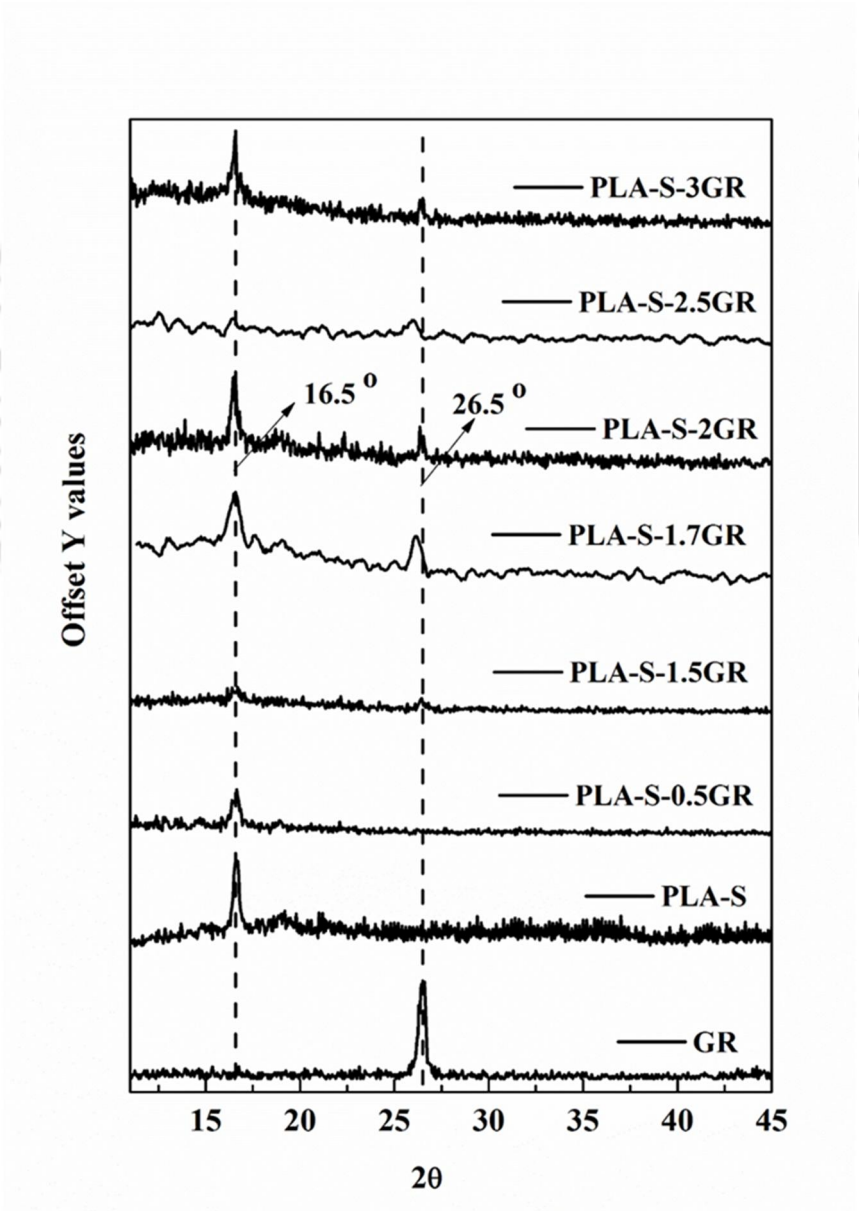

Fig. 4.3 X-ray diffraction pattern of the samples

4.3.2 FESEM analysis

Morphological changes due to incorporation of GR at low loading (0.5 wt. %), high loading (2.5 wt. %) and medium loading (1.7 wt. %) conditions were observed through the FESEM analysis of the composites PLA-S-0.5GR, PLA-S-2.5GR and PLA-S-1.7GR, respectively (Fig. 4.4). In the case of PLA-S-0.5GR, less amount of particle agglomerations is present (Fig. 4.4a). However, in case of higher loading (PLA-S-1.7GR and PLA-S-2.5GR), interconnected agglomerates can be noticed in Fig. 4.4b and Fig. 4.4c, which are indicated by arrow. The number of interconnections are increasing with the loading of GR. The interconnected networks are the prime reasons for the electrical conductivity of the composites (Pötschke et al., 2010)

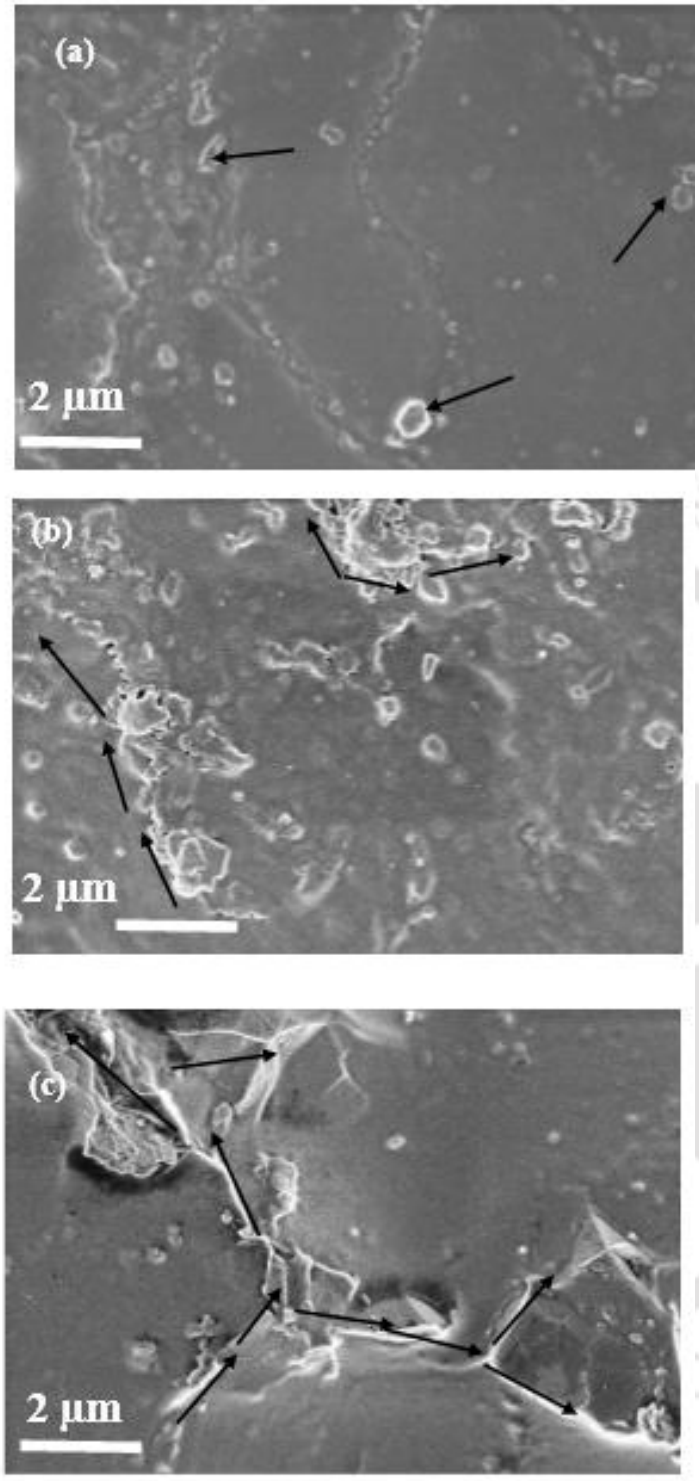

Fig. 4.4 FESEM images of (a) PLA-S-0.5GR, (b) PLA-S-1.7GR and (c) PLA-S-2.5GR

4.3.3 Impedance analysis

Since the number of interconnected networks controls the conductivity of PLA/GR composites, it is necessary to understand the optimum loading of GR for a meaningful and low-cost composite to be used as sensor exploiting the conductivity characteristics of the composite. Therefore, potentiostatic frequency response analysis of the composites with a wide range of GR loading was carried out to investigate the effect of GR loading on the electrical impedance of the composites. For PLA-S and composites PLA-S-0.5GR, PLA-S-1GR and PLA-S-1.5 GR, similar type of impedance-frequency dependency can be observed from Fig. 4.5. The value of impedance is as high as $10^8\,\Omega$ or above in case of GR loading up to 1.5 wt. %. Even though existence of GR structure is found in XRD but it is not enough to construct effective conductive network. In case of PLA-S-1.7GR, impedance value is drastically decreased to $10^5\,\Omega$ range from $10^{11}\,\Omega$ for PLA-S. Thereafter, with further increase in GR loading i.e. for PLA-S-2GR, PLA-S-2.5GR and PLA-S-3GR, the decrease of impedance value is gradual and reaches to $10^4\,\Omega$ range. This suggests that due to incorporation of further GR above 1.5 wt.% better conductive network is formed, which is responsible for easier electrical mobility through the composites (Pötschke et al., 2010). Increase of networks or interlinks with loading is also observed in the FESEM images (Fig. 4.4b and 4.4c) as discussed earlier. Incidentally, no significant change in impedance value is noticed while changing the GR loading from 2.5 wt. % to 3 wt. %. This is due to formation of almost adequate and continuous networks/interlinks with 2.5 wt. % loading of GR.

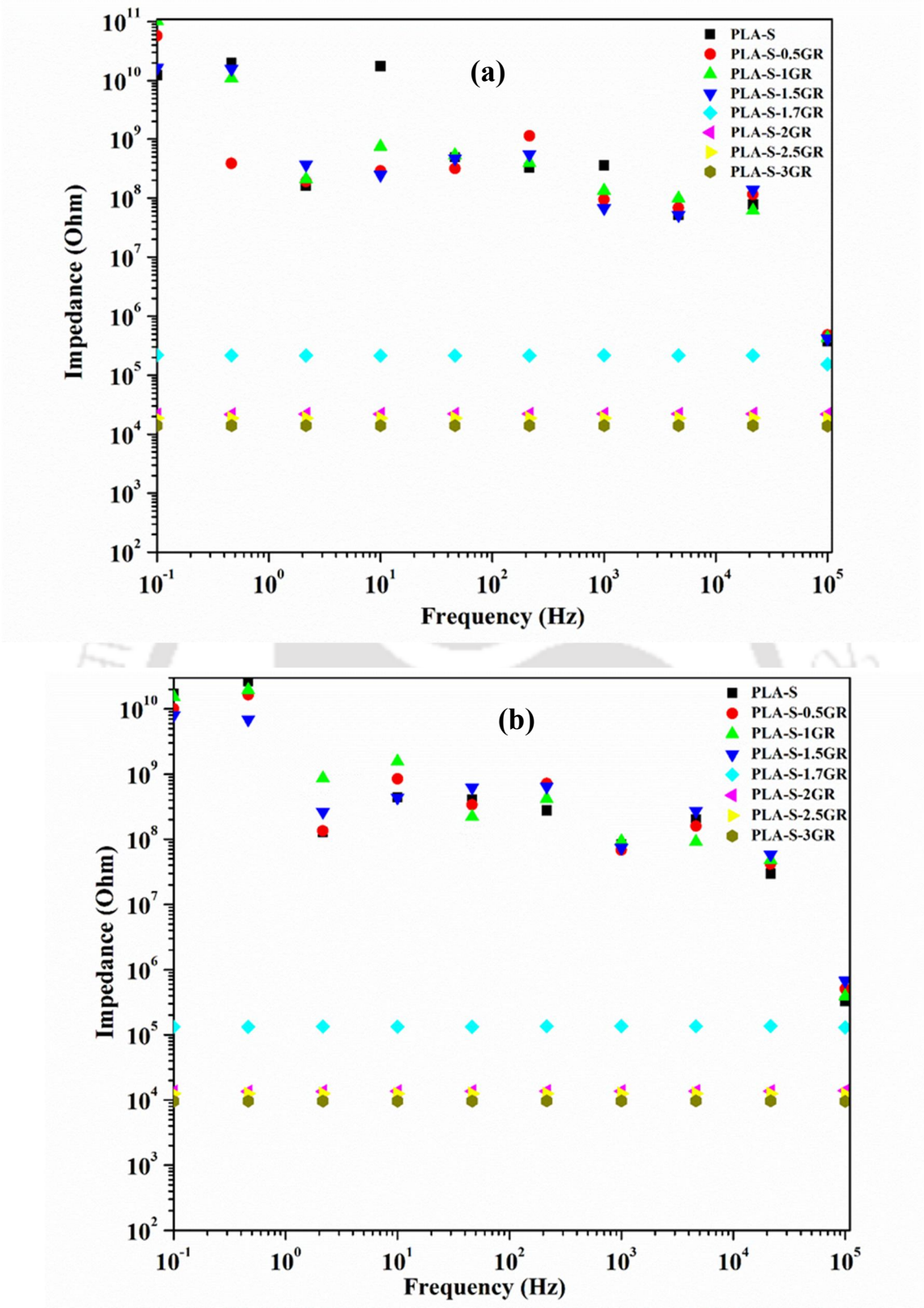

Fig. 4.5 Impedance analysis of the films of (a) length 5cm and width 5mm and (b) length 3cm and width 5mm

The nonlinear nature of the frequency response pattern of the impedance (Fig. 4.5) for lower loading (up to 1.5 wt. %) indicates that the conductive pathway consists of capacitative loss along the path. This is due to the discontinuity of the GR network /interlinks in the composite matrix corroborating the findings of FESEM (Fig. 4.4a). However, in case of higher GR loading (1.7 wt. % and above), the frequency response pattern is almost linear in all the frequency range, which is indicative of resistive response.

Since GR loading 2.5 wt% and 3 wt% showed similar but the lowest impedance and the best conductivity in the range of the composites studied, in order to study the effect of length and area of the composites, resistivity was further checked by varying the dimensions of the strips for PLA-S-2.5GR and PLA-S-3GR composites. Composites of two different lengths of 5 cm and 3 cm with width of 5 mm were used to see the effect of length (L). Composites of two different widths 5 mm and 10 mm with length 5 cm were also used to observe the effect of area (A). The thickness of the sample was 0.1 mm in all the cases. The results are depicted in Fig. 4.6. It can be seen in Fig. 4.6 that with an increase in length, impedance value increases while an increase in width i.e area, impedance value decreases. This indicates that the composites follow Ohm's law of electrical resistance in an electrical circuit (Eq. 4.2).

$$R = \rho \frac{L}{A} \quad \text{(4.2)}$$

Where 'R' is resistance, 'L' is length, 'A' is area and 'ρ' is electrical resistivity. Typical values of 'ρ' for the composites are calculated employing Eq. 4.2 and the values are reported in Table 4.1. For the same GR loading 'ρ' values are almost same as expected and independent of the frequency. In case of higher loading of GR (3 wt. %), 'ρ' value

(14-16.5 Ω-cm) is lower than 2.5 wt. % (19-21 Ω-cm). This further indicates the change in composite morphology due to the addition of extra GR. As a result, marginal decrease in 'ρ' is noticed and thereby marginal increase in conductivity is observed for change of GR loading from 2.5 wt.% to 3 wt.%.

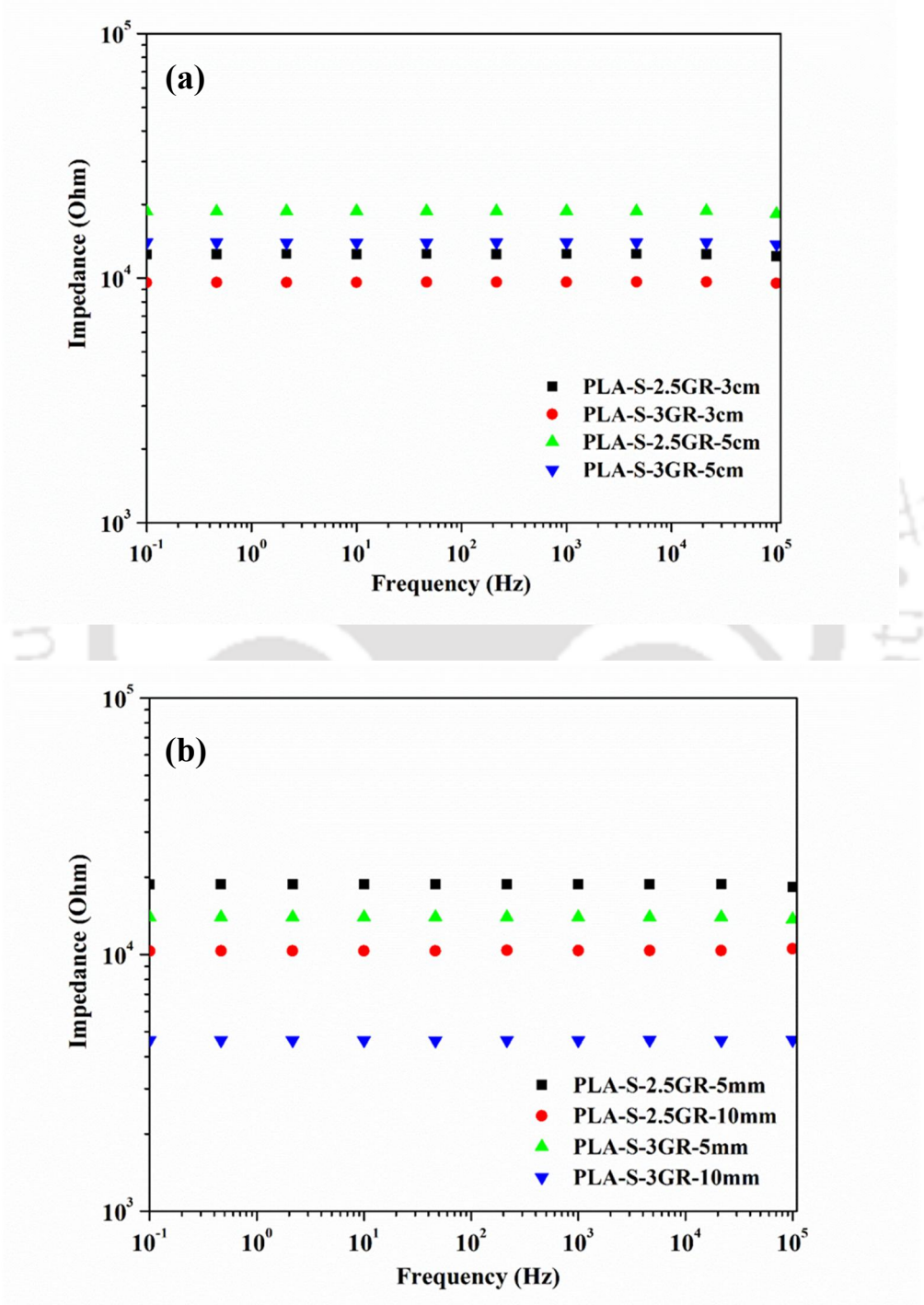

Fig. 4.6 Impedance analysis of the films of PLA-S-2.5GR and PLA-S-3GR (a) variation in length and (b) variation in width

Now, it is needless to mention that GR has very high electrical conductivity. So, the resistance offered by a PLA/GR composite is mainly by its PLA counterpart. As the area of the samples is kept constant, the resistance is due to the length of the PLA matrix in the composite. However, the 'ρ' value of the composites is drastically reduced compared to the pure PLA film even though the length is maintained the same in all the cases. This indicates a drastic reduction in the effective length of the PLA matrix alone that offers the resistance even though the overall length is maintained at a constant value. This can be understood by considering a hypothetical composite of two sections in series (Fig. 4.7). The first section (Section 1) is the major length of the composite in which the total length is covered by GR network/interconnection through the PLA matrix without any discontinuity. All the small continuous GR networks/interconnections in PLA matrix in the real composite is lumped into this section. This section has conductivity similar to GR. The other section (Section 2) is devoid of any GR content and has the pure PLA matrix only. Though small in length (hereafter termed as effective polymer length), this section mainly offers the electrical resistance. All the small sections of the real composite having only PLA matrix and no GR is lumped into this section. Hence it would be interesting to note the variation of effective polymer length along with variation of GR loading, which is discussed subsequently.

For the two sections as discussed in Fig. 4.7, Eq. 4.2 can be written in the form of Eq. 4.3 for any composite of constant area.

$$\varrho_c L_c = \varrho_p L_{p1} + \varrho_g L_{g1} \quad \text{(4.3)}$$

Where,'ϱ_c' and 'L_c' are the resistivity and overall length of the composite, 'ϱ_p' is the resistivity of section 2 i.e. of polymer, 'L_{p1}' is the effective polymer length of PLA,

which is mainly responsible for the resistance in the composite, 'ϱ_g' is resistivity of section 1 and 'L_{g1}' is the length of section 1. As said earlier, section 1 has properties of GR and it consists of continuous GR networks/connectivity responsible for resistance. Since, resistivity of GR is negligible as compared to PLA, the Eq. 4.3 can be rewritten as Eq. 4.4

$$\varrho_c L_c = \varrho_p L_{p1} \Rightarrow L_{p1} = \varrho_c L_c / \varrho_p \quad \text{..... (4.4)}$$

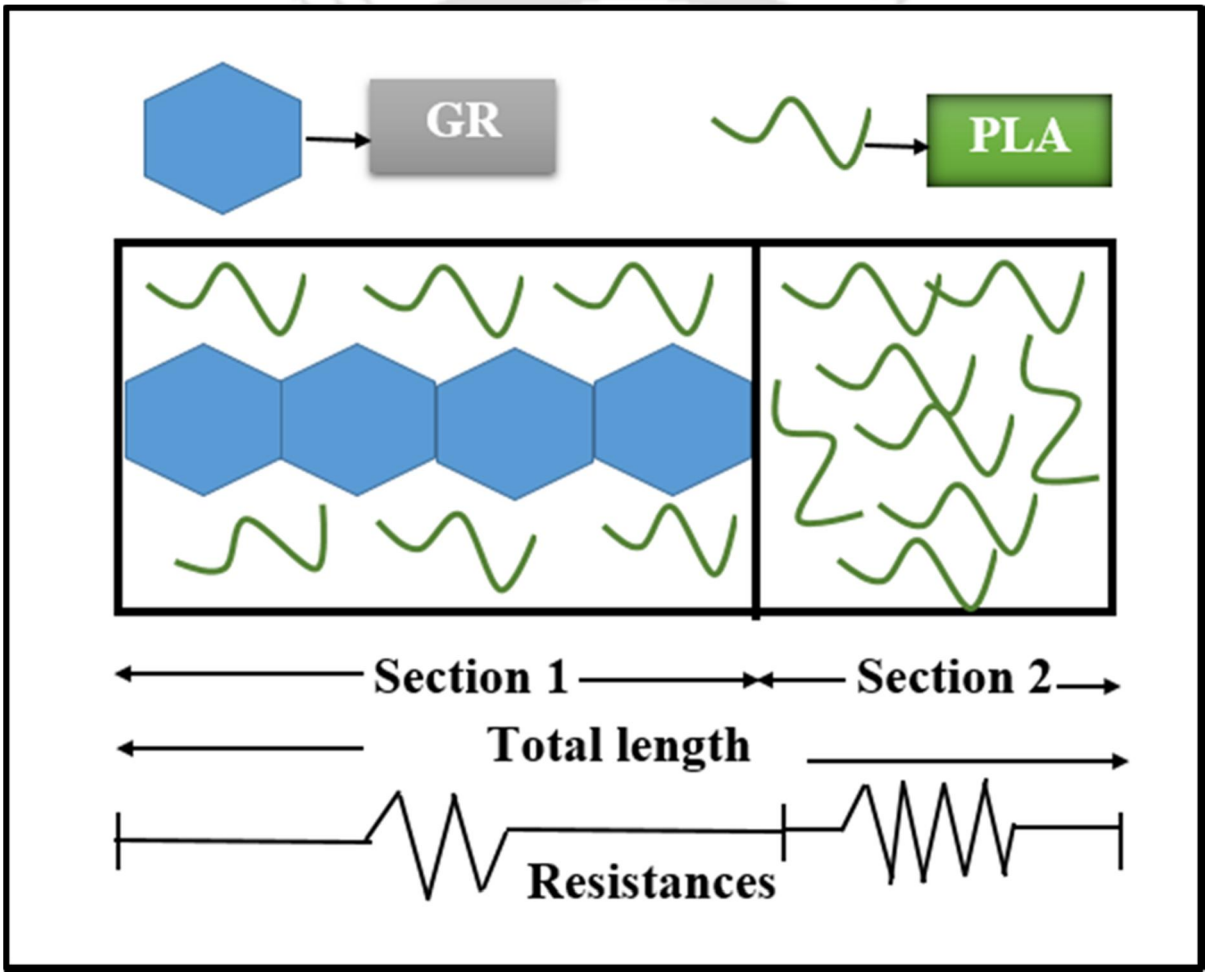

Fig. 4.7 Two section model (Scale is not in proportion)

Table 4.1 Electrical resistivity data

Sample name	Weight %	Sample dimension (Length-Width)	Frequency (Hz)	Resistivity (Ohm-cm)
PLA-S-2.5GR	2.5	5cm-5mm	0.1	18.75
			10	18.81
			21544	18.86
	2.5	3cm-5mm	0.1	20.83
			10	20.88
			21544	20.89
	2.5	5cm-10mm	0.1	20.61
			10	20.69
			21544	20.72
PLA-S-3GR	3	3cm-5mm	0.1	15.96
			10	16.03
			21544	16.08
	3	5cm-5mm	0.1	14.00
			10	13.99
			21544	14.00
	3	5cm-10mm	0.1	16.04
			10	16.02
			21544	16.50

The variation in effective PLA length (normalized as L_{p1}/L_c) responsible for composite resistance due to variation in GR loading is calculated using Eq. 4.4 and the results are shown in Fig. 4.8. It can be observed from the figure that for both the cases, where 'L_c' is 3 cm and 5cm, there is a drastic fall of effective polymer length to the change of GR loading from 1.5 wt.% to 1.7 wt.%. In the case of 1.7 wt. % loading, the effective polymer length is decreased to 10^{-5} from ~ 5×10^{-1} range. Then it is gradually reduced to 10^{-6} range due to further increase of GR loading up to 3 wt %. This also reflects the findings of the FESEM, and XRD of network formation. Thus, in this work, there exists an optimum GR loading of about 1.7 wt. % at which considerable conductivity of the composite is observed. Further increase in GR loading will increase the cost of the composite unnecessarily without much change in conductivity.

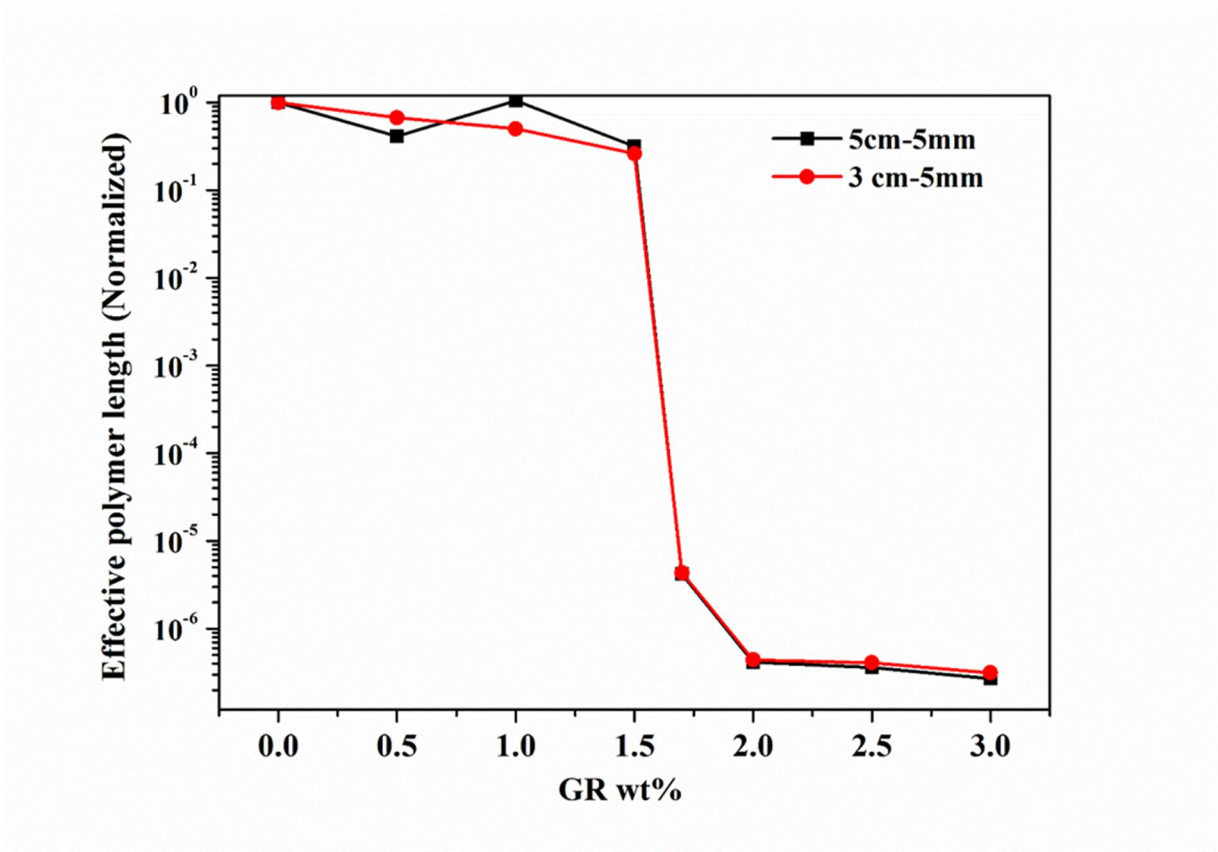

Fig. 4.8 Change of effective length of PLA responsible for resistance of composite with respect to GR loading

Case study for applicability as sensor

In order to understand the applicability of the composite as a sensor, ethanol was chosen as solvent. This study was carried out by analyzing the performance of a composite sample in sensing ethanol of varied concentration, the reusability of the samples for five consecutive cycles and by analysing the repeatability of the samples fabricated in three different batches.

4.3.4 Ethanol sensing analysis

In view of the stable performance observed during impedance analysis, PLA-S-2.5GR composite was used for the detection of ethanol solvent by direct immersion technique using lab-made sensing platform (Fig. 4.2). Relative change in impedance was recorded as a measure of response. For comparison, 0.1 Hz frequency data was analyzed. It can be seen from Fig. 4.9a that for PLA-S-2.5GR, relative change in response (R_{rel}) increases slowly with immersion time within ethanol during 10 min dipping cycle. During the drying cycle (Fig 4.9b), R_{rel} decreases slowly with exposure time in open air. An increase in R_{rel} occurs due to solvent diffusion within the PLA matrix (Kobashi et al., 2008; Pötschke et al., 2010). Because of the diffusion, existing conductive networks get disturbed and impedance increases. However during drying, even though some ethanol is removed, still all the previous networks are not able to come back to the original condition. As a result of this, an increase of impedance during dipping and little decrease of the same during drying cycle were observed (Kobashi et al., 2008). The composite was subjected to three consecutive 10 min dipping followed by 10 min drying cycles. It can be noticed that R_{rel} is quite close for PLA-S-2.5GR for first, second and third (C1, C2, C3) cycles.

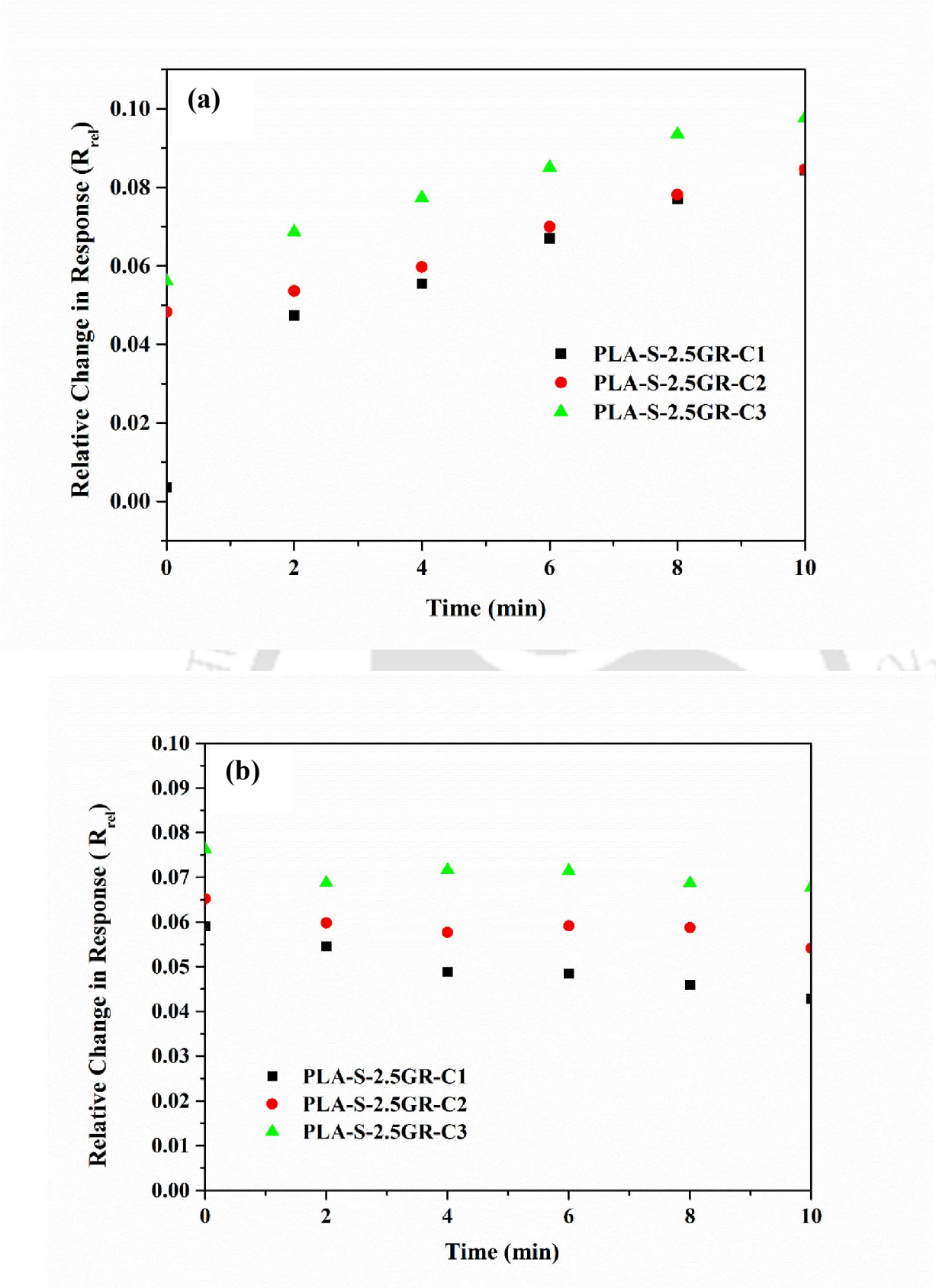

Fig. 4.9 Relative change in response (R_{rel}) analysis for (a) dipping and (b) drying cycle in ethanol of 2.5 wt. % composite

Different vol% of ethanol with respect to millipore water were used to observe the effect of concentration of ethanol on the response of PLA-S-2.5GR. It can be noticed from the Fig. 4.10 that the R_{rel} decreases with decrease of ethanol concentration. R_{rel} is the highest in the case of 100% ethanol and the lowest in case of 25%. Thus, this property of response as a function of ethanol concentration is extremely useful to sense the presence of ethanol concentration in an unknown sample.

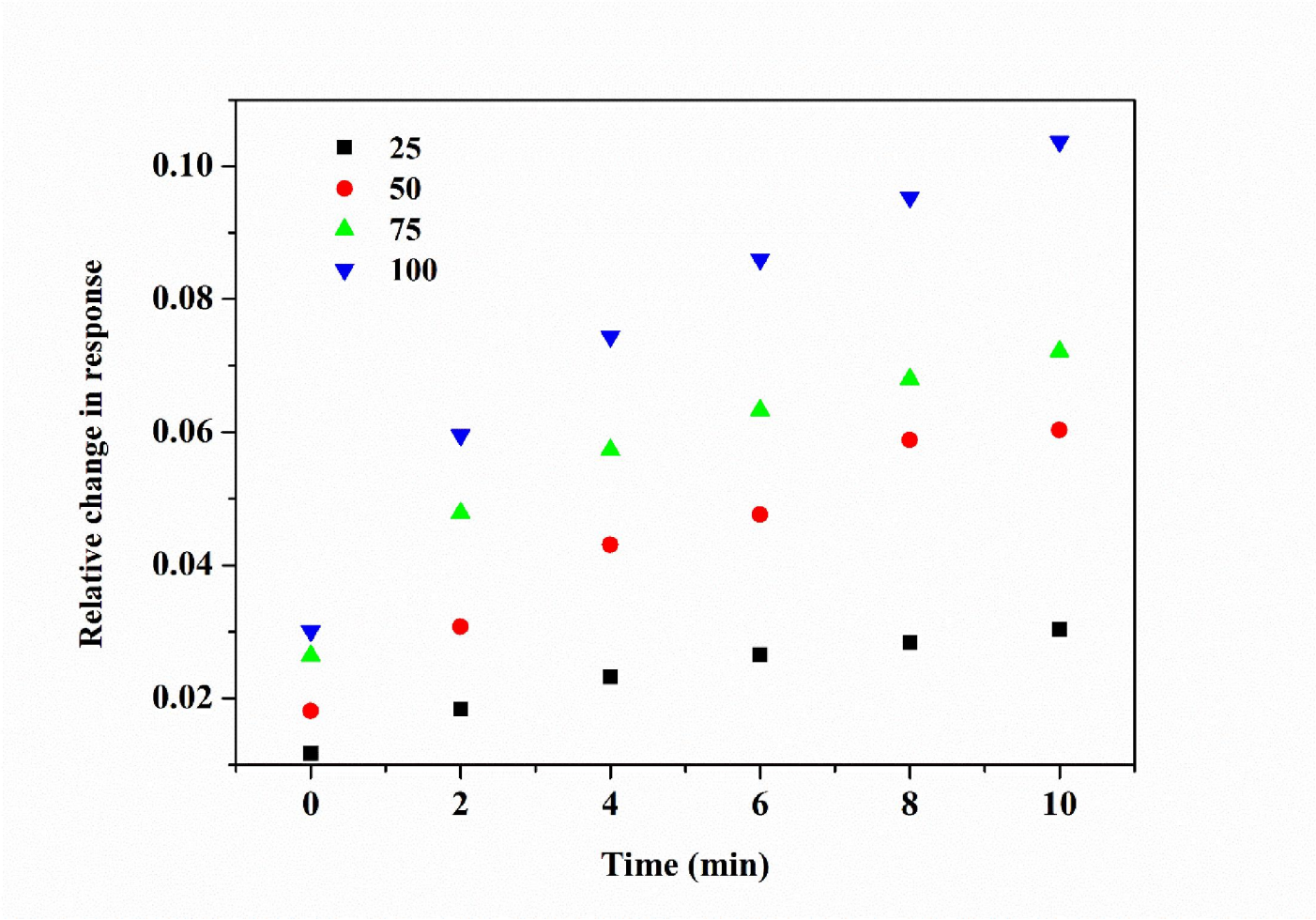

Fig. 4.10 Relative change in response (R_{rel}) analysis for dipping cycle in different volume% of ethanol of 2.5 wt. % composite

Reusability study

Reusability test was performed to check the effectiveness of PLA-S-2.5GR sample for multiple time use. Fig. 4.11a depicts the change in R_{rel} for two different vol% of ethanol, 15% and 25% taken for this study. The PLA-S-2.5GR strip was dipped for 2 min and the R_{rel} was recorded. The same strip was used 5 times in the same ethanol concentration before drying it at 50 °C for 5 min followed by drying at 24 °C for 5 min. The results suggest that the sample could be reused successfully for two different concentrations without appreciable change in the response even for the wide range of frequencies.

Repeatability study

The repeatability test was carried out by taking three different samples of the composite PLA-S-2.5GR fabricated in three different batches using 100 vol% ethanol. Fig. 4.11b represents the test data of three different samples taken for measurement and the results are quite close. The existing difference could be due to structural variation of the samples that might have been generated for the different batch samples. However, a better-controlled process for fabrication i.e. maintenance of the same level of crystallinity of the composite might substantially reduce the observed variation.

Thus, the fabricated conductive nanocomposite films successfully and selectively detect ethanol from water in the range of the concentration of the former 15 to 100 vol% studied in the present work. The films are found to be reusable and repeatable. The steady response is achieved within 30 s of exposure. However, about 2 mins of exposure time was given in each case in this study to ascertain a stable response. For GR loading of 1.7 wt% and above the frequency (0.1 Hz to 1000 Hz) response is almost linear due to resistive response.

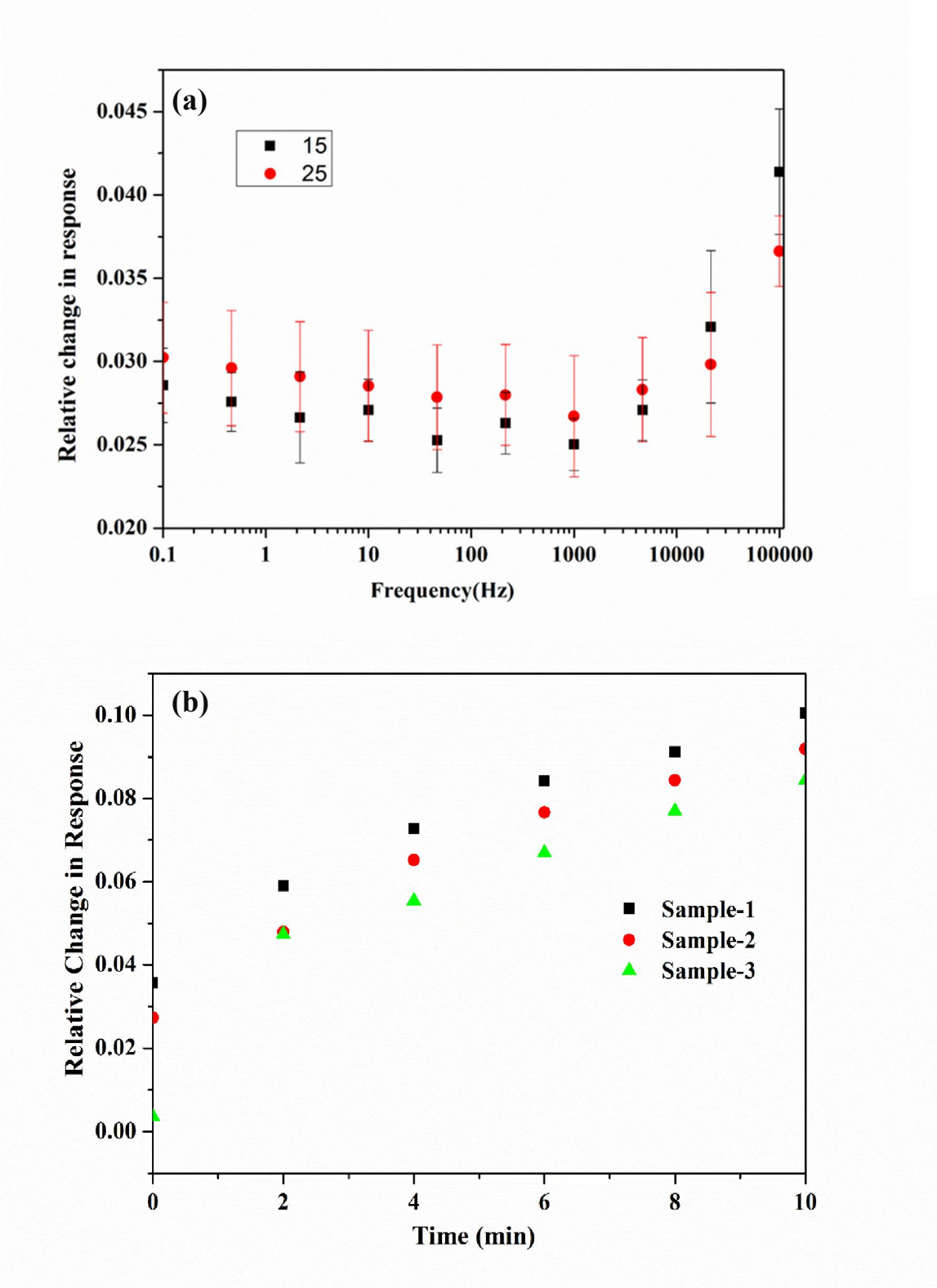

Fig. 4.11 Relative change in response (R_{rel}) analysis for dipping cycle in ethanol of 2.5 wt. % composite for (a) Reusability test and (b) Repeatability test

Characterization after use

Thermogravimetric, crystallization and morphological analyses were carried out with the composite PLA-S-2.5GR before and after use for ethanol sensing in order to examine the relevant changes in the characteristics, if any.

TGA

Even though polymer swelling due to ethanol diffusion into the composites determines the response, still changes in response with time also depend on the interactions and distributions of GR in the PLA matrix. Thermal stability profiles showing the degradation of PLA-S-2.5GR, PLA-S-2.5GR-C1 (after one dipping cycle) and PLA-S-2.5GR-C3 (after three dipping cycle) are presented through Fig. 4.12. TGA analysis data for the composites are reported in Table 4.2. It can be seen from the table that after one cycle, T_{onset}, T_{50}, T_{max} are increased to 356.7 ºC, 370.6 ºC and 375.9 ºC, respectively as compared to 350.4 ºC, 368.4 ºC and 372.8 ºC for the composite PLA-S-2.5GR. The effect on onset temperature is little higher when compared to the other two temperatures. This may be due to dipping of the composite being associated with removal of some amorphous PLA. However, in case of PLA-S-2.5GR-C3, the above temperatures are comparable with PLA-S-2.5GR (Table 4.2). This may be due to removal of some GR from the composite along with the amorphous PLA because of multiple time dipping and drying operation. Thus, the two opposing effects in thermal stability due to loss of amorphous PLA and GR are responsible for the reduction in temperatures of PLA-S-2.5GR-C3.

Table 4.2 TGA analysis data for PLA-S-2.5GR, PLA-S-2.5GR-C1 and PLA-S-2.5GR-C3

Sample	T_{onset} (°C)	T_{50}(°C)	T_{max}(°C)
PLA-S-2.5GR	**350.4**	**368.4**	**372.8**
PLA-S-2.5GR_C1	**356.7**	**370.6**	**375.9**
PLA-2.5GR_C3	**351.8**	**365**	**371.0**

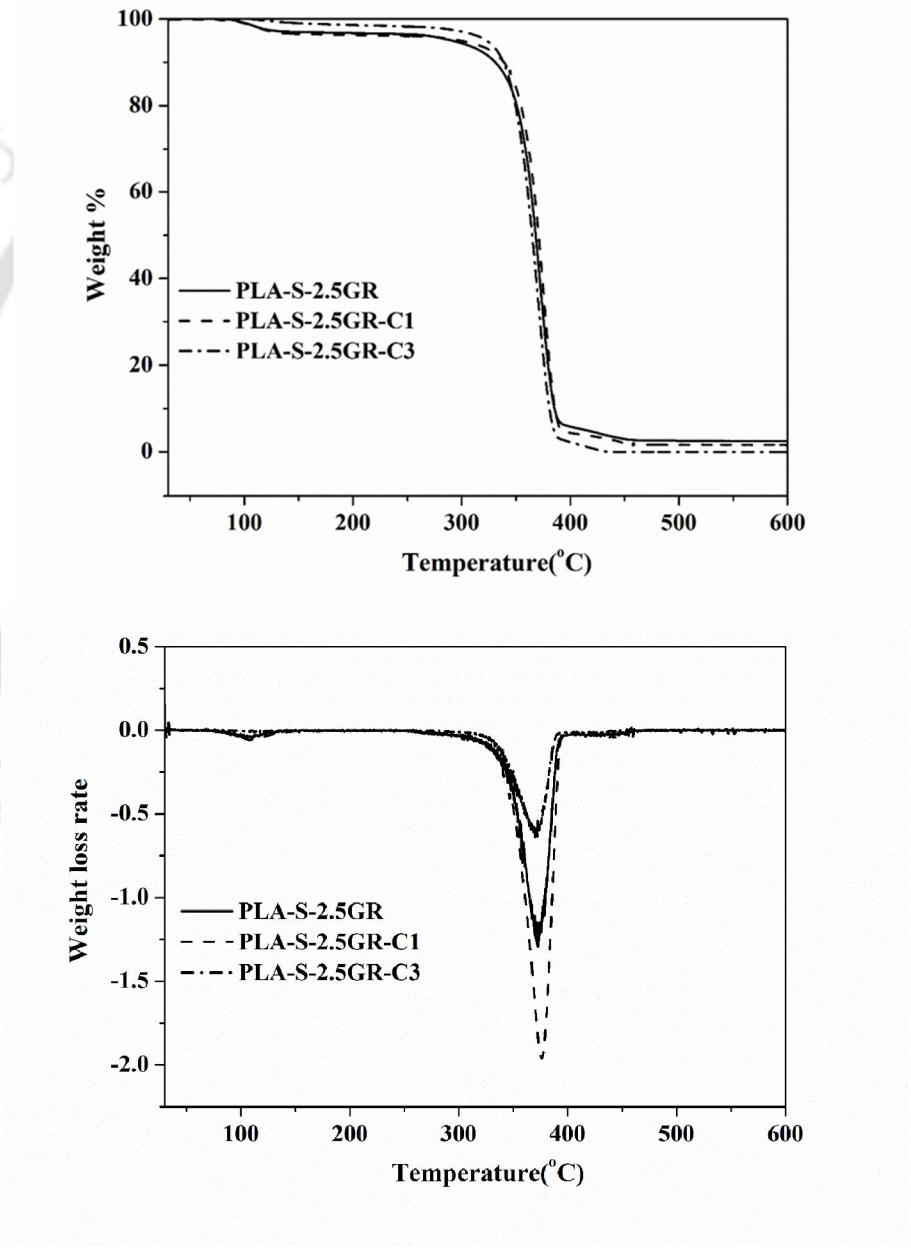

Fig. 4.12 Thermal degradation stability analysis of PLA-S-2.5GR, PLA-S-2.5GR-C1 and PLA-S-2.5GR-C3

Crystallization analysis

The differential scanning calorimetry (DSC) analysis data for the composite PLA-S-2.5GR before and after use for ethanol sensing are reported through Fig. 4.13 and Table 4.3. The results indicate that the crystallization properties are also affected by ethanol diffusion in the PLA-S-2.5GR composite. It can be seen from Table 4.3 that the glass transition temperature (T_g), the cold crystallization temperature (T_{cc}) and the melting temperature (T_m) are decreased after first cycle of study corroborating the fact of removal of some amorphous PLA moiety as discussed in case of TGA studies. However after third cycle, it shows similar characteristics of PLA-S-2.5GR. This again corroborates the reasons stated in TGA analysis where role of removal of both the amorphous PLA and GR is important.

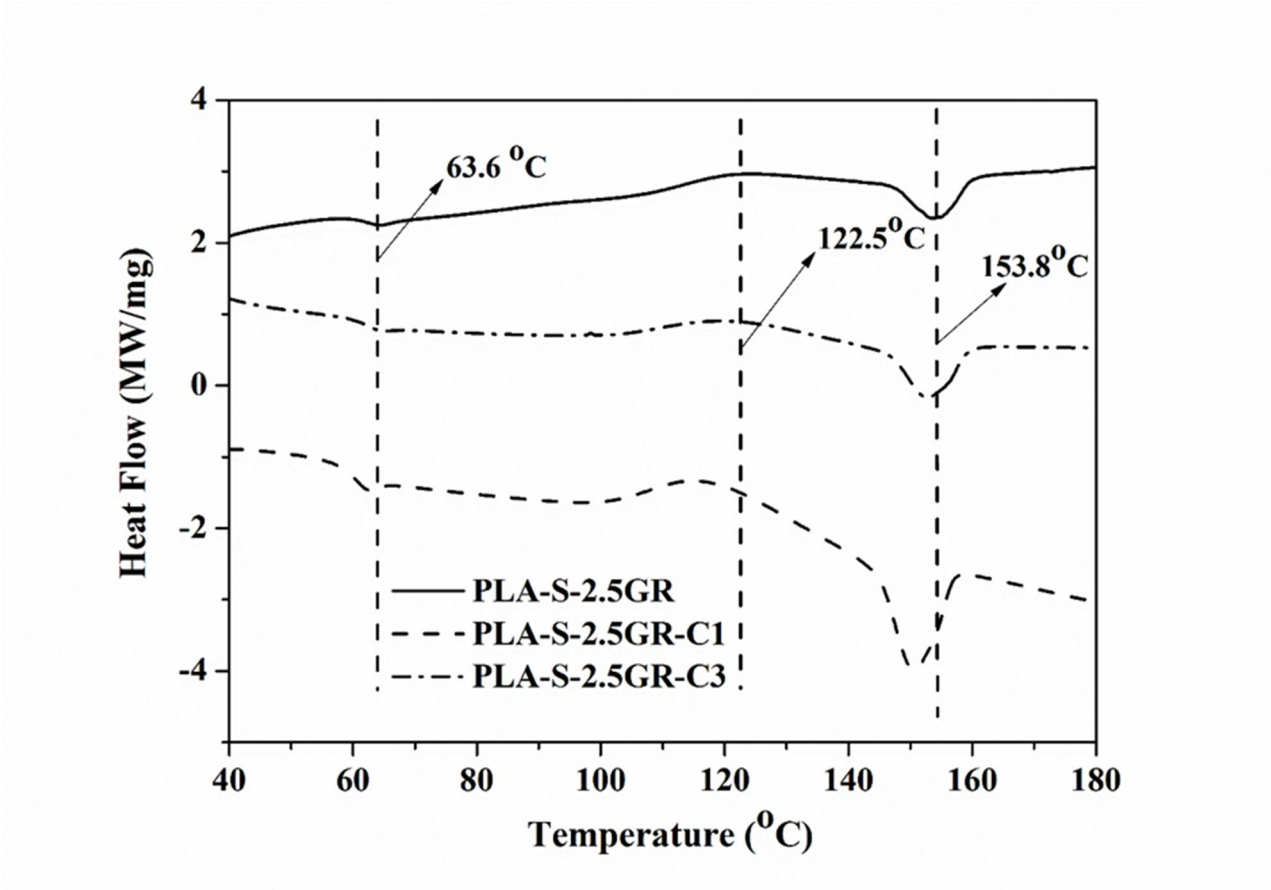

Fig. 4.13 DSC analysis of PLA-S-2.5GR, PLA-S-2.5GR-C1 and PLA-S-2.5GR-C3

Table 4.3 DSC data for PLA-S-2.5GR, PLA-S-2.5GR-C1, and PLA-S-2.5GR-C3

Samples	T_g(°C)	T_{cc} (°C)	T_m (°C)	%X_c
PLA-S-2.5GR	63.6	122.4	153.8	0.58
PLA-S-2.5GR-C1	62.8	115.9	150.5	0.73
PLA-S-2.5GR-C3	63.6	120.5	152.8	0.28

Morphological analysis

FESEM images of the composite PLA-S-2.5GR before and after use for ethanol sensing are reported through Fig. 4.14. The FESEM image of PLA-S-2.5GR-C1 shows the presence of circular patches on the composite after dipping. Those patches are formed due to PLA chain washing from the weak amorphous sites, which is responsible for distortion in conductive network and increment in impedance i.e R_{rel}. Also, changes in thermal and crystallization characteristics as discussed in the earlier sections are also observed due to this change in morphology.

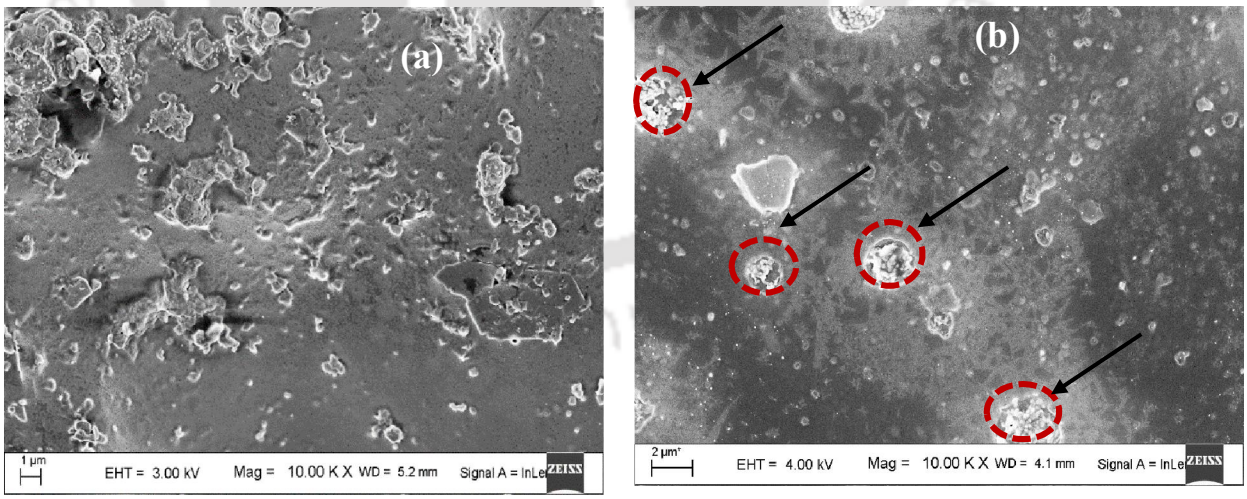

Fig. 4.14 FESEM images of (a) PLA-S-2.5GR and (b) PLA-S-2.5GR-C1

4.3.5 Different alcohol detection

Liquid sensing behavior of PLA-S-2.5GR was also tested using different alcohols of various molecular weights. It can be seen from Fig. 4.15 that response is increasing for all the alcohols with time 0 to 10 min. R_{rel} is high for methanol and sharpe increment can be seen with time. In case of ethanol increment is less compared to methanol but higher compared to iso-propanol and iso-butanol. In case of iso-butanol change in response is very less. R_{rel} is dependent on the diffusion of liquid molecules into the matrix of PLA. So, with increase in molecular weight for the alcohol in analogous series

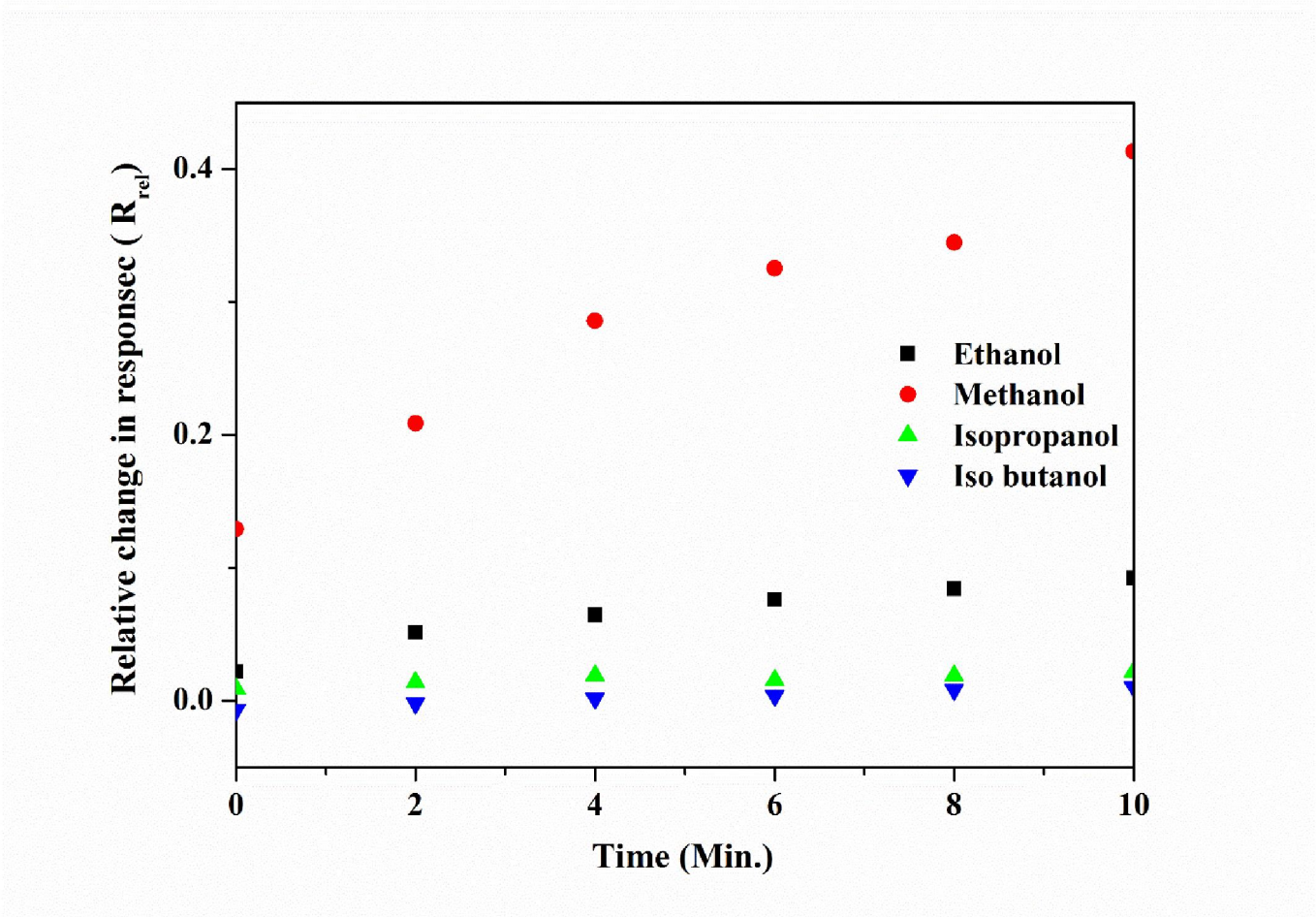

Fig. 4.15 Relative change in response of composite PLA-S-2.5GR in different alcohols

4.3.6 Different organic solvent detection (Different functional group)

Different organic solvents of various categories like acetone and formic acid were also subjected to sensing using PLA-S-2.5GR composite in a similar way as described in 4.2.3.4. It can be seen that the R_{rel} is very high for acetone and formic acid compared to alcohols (Fig. 4.16). This may be because of higher reactivity of the functional group –C=O and –COOH present in acetone and formic acid with polyester PLA compared to alcohols.

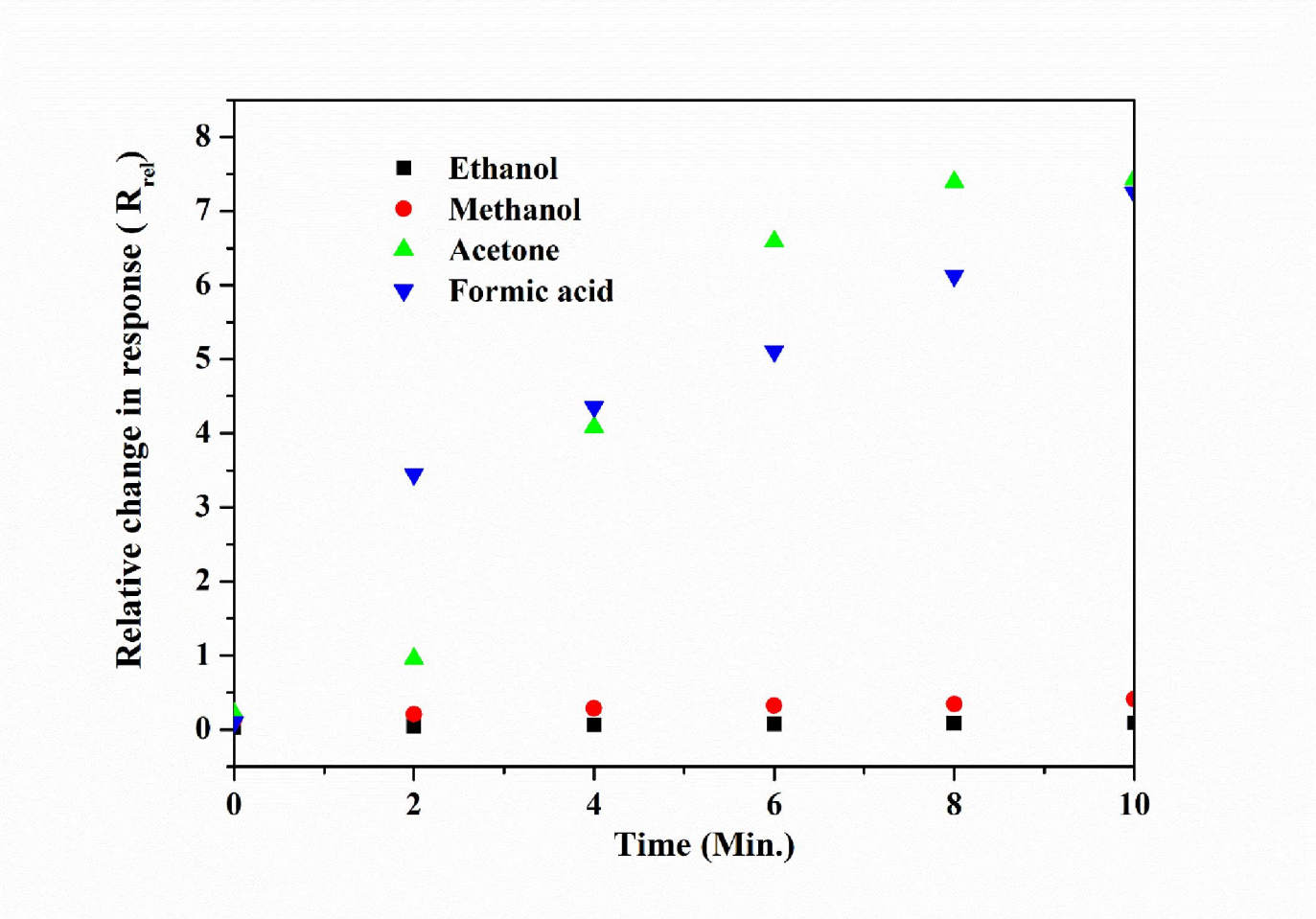

Fig. 4.16 Relative change in response of composite PLA-S-2.5GR in different organic solvents

4.3.7 Mechanistic investigation

Incorporation of conductive filler constructs conductive networks in the polymer matrix (Kumar et al., 2012). As discussed in the 4.3.3 section, graphene reduces effective polymer length with loading. This is probably because of conductive networks inside the composite enhances electron mobility (Fig. 4.17a). During the sensing study of PLA-S-2.5GR, relative change in response increases for the dipping cycle. This is due to diffusion of liquid molecule inside matrix, altering some of the networks, which increases the impedance as shown in Fig. 4.17b. Liquid molecule diffusion increases with immersion time and increases the response (Fig. 4.17c). Now, in case of drying cycle, liquid molecule comes out of the composite and some of the networks are restored to previous form and with increasing drying time extent of such restoration can increase till reaching nearly to original situation before dipping. It causes decrement of the disorder networks. However, impedance does not come back to original as all the networks do not get back to previous form (Fig 4.17 d-e).

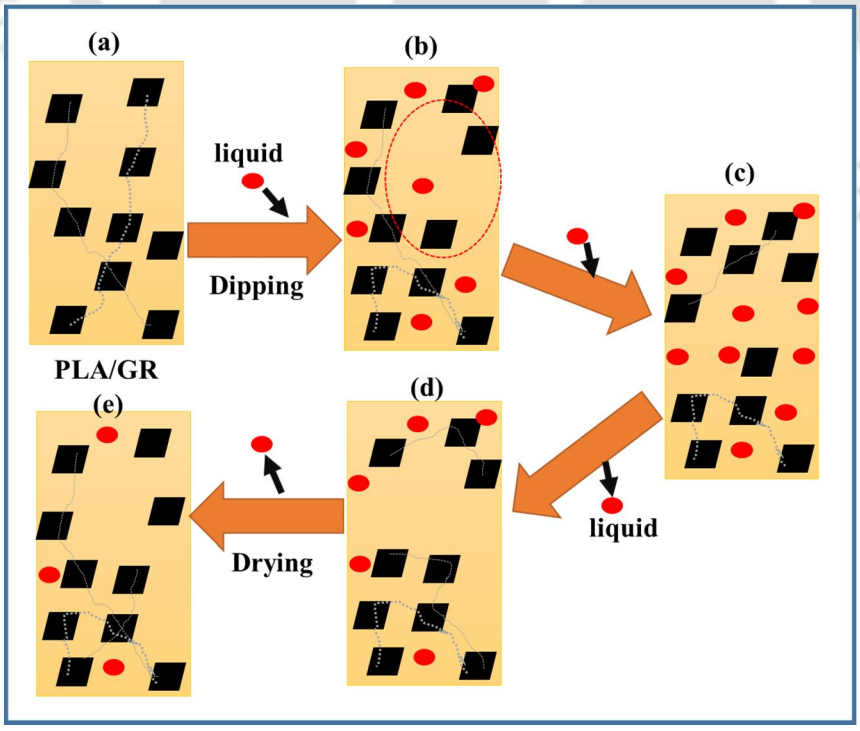

Fig. 4.17 Schematic of probable interaction of liquids with PLA-S-2.5GR nanocomposite

The response of composite depends on the diffusion of liquid molecules. It depends on both the concentration present in the environment as well as interaction parameter with PLA matrix. Solubility parameter controls the interaction parameter (χ). So solvents which are having more close solubility parameter with PLA give lesser value of interaction. For instance, chloroform solubility parameter is 19.0 $(J/cm^3)^{1/2}$, which is close to PLA (19-21$(J/cm^3)^{1/2}$). Interaction parameters for some common solvents are listed below.

PLA-Solvent	Chloroform	Methanol	Toluene	Water
χ_{12}	0.62	0.65	1.16	4.38

In the case of alcohol sensing, it has been seen in section 4.3.5 that with an increase in molecular weight, R_{rel} decreases. Diffusion coefficient (D) decreases with an increase in molecular weight, which is similar to diffusion of component A into non-diffusing B. Thus, the amount of solvent incorporation decreases with increasing alcohol molecular weight.

In the case of functional compound, reactivity of the functional groups also causes in response change along with diffusion. Like alcohols are not reacting compared to ketone(C=O) and acid (COOH). In case of formic acid, reactivity–COOH is higher, hence change in response is higher as compared to ketone or alcohols.

4.4 Summary

This work utilized the conductivity of exfoliated graphene (GR) to be used for sensor application after dispersing suitably in a PLA matrix. Ethanol of varied concentration was used for detection test by the fabricated composite.

Initially, the GR content was optimized to get suitable conductivity for the PLA/GR composites. The formation of conductive networks of GR within PLA matrix was noticed from impedance values and FESEM analysis. In case of 1.7 wt% GR loading, a sudden fall in impedance was observed because of conductive network formation. The conductivity was further increased gradually in case of 2, 2.5 and 3 wt. % GR loaded composites. Impedance of the PLA/GR composites was reduced from $10^{11}\Omega$ for PLA to $10^{4}\Omega$ range due to incorporation of GR. The normalized effective polymer length of the composite responsible for resistive response is reduced to a very low value of 10^{-6}.

The composite with 2.5 wt. % GR loading (PL-S-2.5GR) was successfully applied for the detection of ethanol of varied concentration. The composite film could be reused at least five times without any significant change in response. Repeatability study of the composites from different batches suggests that controlled fabrication of the composite in terms of crystallinity and uniform thickness is necessary to make it an application ready material. Solvent diffusion is the main governing phenomena and the composites demonstrated desired ethanol selectivity and sensitivity. It also observed to have selectivity towards various alcohols depending on molecular weight and towards organic liquids based on both interaction parameter and chemical reactivity. Overall, the PLA/GR composite with suitable GR loading proved itself as a potential material for sensor application. The information revealed from the above work along with application-oriented initiative for utilization of biopolymers would open up a new arena for development of sustainable material for sensor application.

Chapter 5

Applicability of Fe-CNC/GR/PLA Composite as Potential Sensor for Biomolecules

Abstract

Iron oxide decorated cellulose nanocrystal (Fe-CNC) was incorporated into poly lactic acid (PLA) and exfoliated graphene (GR) system (PLA-S-2.5GR) to investigate the impact of Fe-CNC inclusion on the various properties of PLA/GR composite system and to optimise the Fe-CNC loading. Thermal, mechanical, morphological and impedance analyses of different iron loaded composites were conducted. Fe-CNC loading of 0.5 wt. % (PLA-S-2.5GR-0.5Fe) was found to have comparable thermal stability, better dispersion, better mechanical strength and unaltered GR networks inside composite. Then, PLA-S-2.5GR-0.5Fe was utilized as ethanol sensor. Recycle study, reusability study and repeatability study followed by stability analysis of the composite after use were conducted. The results clearly demonstrated that PLA-S-2.5GR-0.5Fe is a suitable candidate for ethanol detection study. In addition, the PLA based composite film possibly the first time, was successfully used as an electrode for detection of biomolecules such as D-glucose and glycine. This investigation indicated that the composites has potential to generate distinct current voltage response pattern in presence of different stimuli of various concentrations that can be utilized to detect and measure different biomolecules and their concentrations.

This research work has received scientific recognition as follows:

Chakraborty, G., Dhar, P., Pugazhenthi, G., & Katiyar, V. (2019). Applicability of Fe-CNC/GR/PLA Composite as Potential Sensor for Biomolecules. ***Journal of Materials Science: Materials in Electronics*** (Under Review)

Graphical abstract

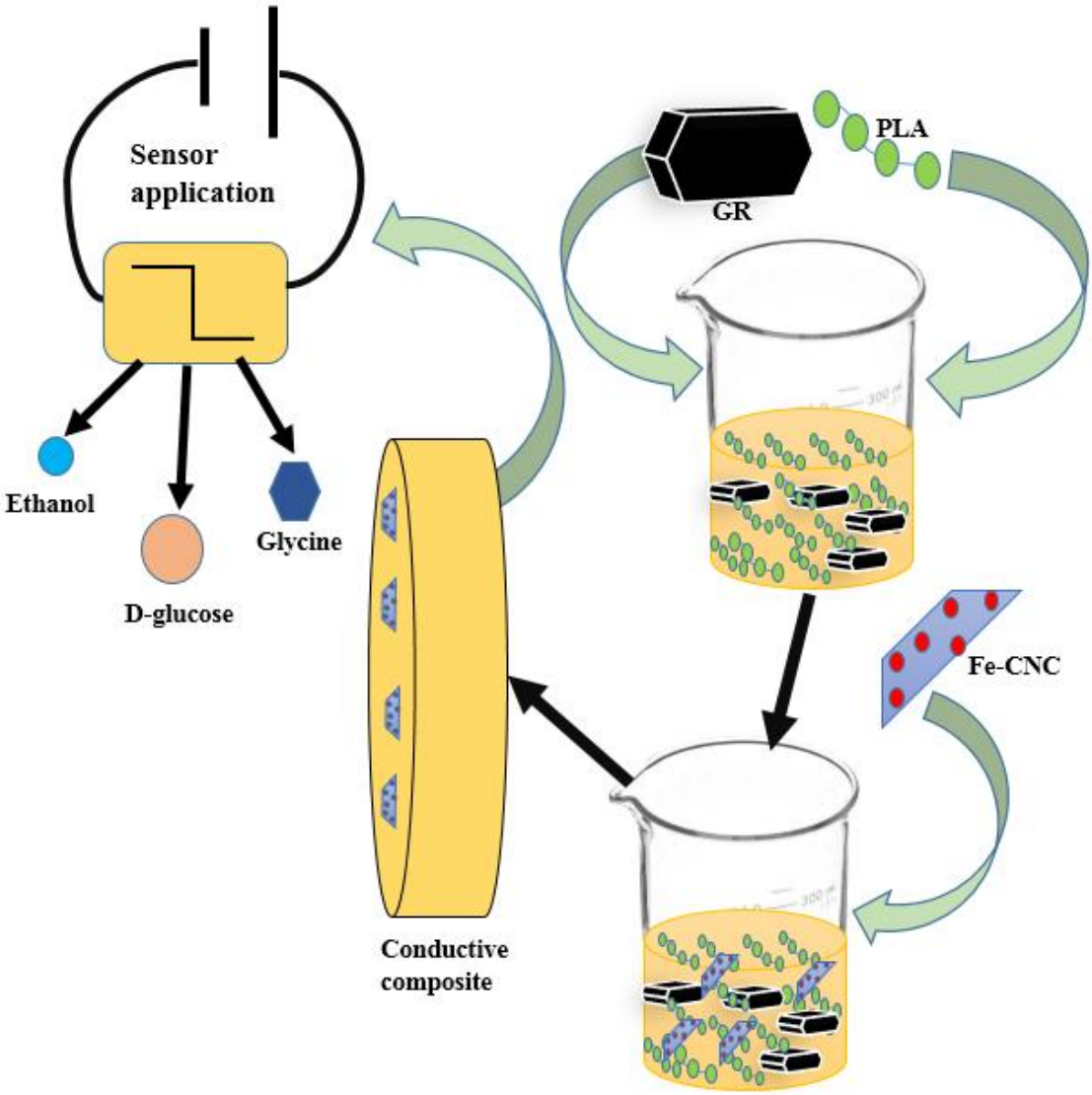

5.1 Introduction

Polymer based conductive composites are now a days used for several applications like electrochemical sensor (Qi et al., 2013; Tamm et al., 1997), biosensor (Gerard et al., 2002; Lei et al., 2014), capacitor (Girija & Sangaranarayanan, 2006; Xiao & Zhou, 2003), semiconducting material (Kolb et al., 1996), etc. because of their lightweight, easy processability, easiness in handling for casting and uses like mobile kit. However, dumping of waste polymeric electronic devices is a prime source of electronic hazards. Biodegradable, thermoplastic and abundantly available polymer like polylactic acid (PLA) has come up as noticeable alternative for the petroleum based polymers (Auras et al., 2004; Lim et al., 2008; Reddy et al., 2013a). Usability of PLA in the field of electrical or electronics requires suitable modification for customization. Different conductive fillers like multi-wall carbon nanotube (MWCNT), graphene, graphite are thus, utilized to fabricate conductive PLA composite for various applications (Kobashi et al., 2008; Kumar et al., 2012; Mai et al., 2013).

With regard to the sensor application of any composite irrespective of electrochemical sensor or biosensor, the primary requirement of it is to have conductive nature in order to generate response in the presence of the corresponding stimuli (Pumera et al., 2010; Tamm et al., 1997). Similar to several polymeric composites being investigated by different groups of researchers, PLA based conductive composites are also being utilized in some of the cases. Kumar et al., 2012 developed MWCNT reinforced conductive PLA nanocomposites by solution processing, where 2 wt. % MWCNT showed the percolation point for electrical conductivity. Sensor selectivity was found to be the highest for chloroform and the lowest for water (Kumar et al., 2012). Pötschke et al., (2010) developed PLA/MWCNT composite fibers from melt state by spinning at different loading and take up velocity. Resistance of the composite fibres was reduced

to 50 kΩ at 2 wt. % loading. Liquid sensing property of the composite was observed to be dependent on the interaction parameters between liquid stimuli and the sensor matrix. Additionally, while testing for sensing of ethanol, the response was reported to be dependent on ethanol concentration and loading of the MWCNT (Pötschke et al., 2010). Han et al., (2013) fabricated platinum (Pt) loaded graphene oxide (GO)/PLA composite by grafting technique. The synthesized composite was used to sense serotonin. The sensing behavior of the composite was observed to be electrochemical in nature and the cyclic voltammetry response was influenced by the presence of other materials like uric acid, ascorbic acid, etc. (Han et al., 2013).

The previous chapter discussed about PLA based exfoliated graphene (GR) reinforced conductive nanocomposite, which was also applied as sensor for ethanol. Even though it is showing sensitivity and selectivity towards ethanol, the performance of the sensor needs to be enhanced in order to achieve more precise detection. Several strategies that are required to be adopted to improve the sensor performance include reduction of film thickness, increase of contact area, and addition of suitable active components that add to the driving force. It was reported in the literature that metal oxides have affinity towards bio-molecules like glucose, uric acid, etc. (Liu et al., 2013; Rahman et al., 2010). This metal oxide based detection can reduce the cost of enzymatic pathway of sensing. Zhang et al., (2014) prepared calcinated copper oxide nanowire for the detection of glucose present in human serum. Glassy carbon electrode was used as a support and 50 mM NaOH solution was added before analysis. The sensor showed good sensitivity in the current density range of 648.2 $\mu A\ cm^{-2}\ mM^{-1}$ to 119.9 $\mu A\ cm^{-2}\ mM^{-1}$ and fast response time of less than 5s. The sensor also showed good selectivity towards ascorbic acid, uric acid, and acetaminophen (Zhang et al., 2014). Liu et al., (2013) reported graphene sheet wrapped with Cu_2O having good electrochemical selectivity

towards glucose in the concentration range of 0.3 to 3.3 mM and high selectivity and less response time. Ibupoto et al., (2013) fabricated flower-like NiO to sense glucose. Sensitivity range reported to be 0.001 mM to 8 mM with high selectivity.

Therefore, considering the high electropositivity of Fe, Fe_3O_4 decorated CNC based PLA/GR nanocomposite was attempted in this work for detection of biomolecules like D-glucose and glycine. Good mechanical strength, thermal stability, and lightweight of the strips can facilitate the application in the form of a mobile kit.

In view of the above, the present study is undertaken where composite PLA/GR with previously optimized GR loading was first fabricated, followed by addition of iron-loaded cellulose nanocrystal (Fe-CNC) with a view to improve the sensitivity and detection ability of the composite. This is because Fe-CNC is the Fe_3O_4 decorated cellulose nanocrystal having high magnetic moment, iron like chemical property and ability to upgrade the mechanical strength and crystallinity of the composite (Dhar et al., 2016). The properties of the synthesized composites after incorporation of Fe-CNC were optimized through morphological, thermal and mechanical analysis. Then performance of the synthesized composites with most suitable composition was used again to sense and detect ethanol of different concentrations. Recycle test, reusability test, and repeatability test were carried out during the detection of ethanol. In addition to successful and precise detection, mobility and easy handling of a sensor is highly desirable for its end-use. Therefore, in order to explore the practical applicability of the fabricated PLA based composite, the latter was used as an electrode and applied to detection of two different categories of organic compounds viz. D-glucose and glycine. To the best of our knowledge, no such study that used PLA based composite as electrode material for sensing various stimuli is reported yet in the literature. For such detection of glucose and glycine, current-voltage response analysis was performed with

different diluted samples. Finally, stability of the film after use for each application was checked with the help of TGA, DSC and morphological analysis.

5.2 Materials and Methods

5.2.1 Materials

NatureWorks® LLC, USA, supplied 2003D grade of PLA which was utilised for fabrication of nanocomposite films. As a reinforcement substance exfoliated graphene EXG 750 (GR) was synthesized in laboratory (Valapa et al. 2015a). Chloroform, ethanol and D-glucose, were procured from SISCO research laboratories (SRL Chemicals, India). Glycine was supplied by Merck Specialities Pvt. Ltd. (MERCK).

5.2.2 Experimental Section

5.2.2.1 Preparation of Fe-CNC

Co-precipitation method was adopted to decorate iron oxide nanoparticles (Fe_3O_4) over the surface of CNC. In the sonicated alkaline solution of CNC, $FeCl_3$ and $FeCl_2$ salts were added in a 2:1 molar ratio and the solution was subjected for stirring vigorously (~1000 rpm) at 90°C for the duration of 4 hr. to make it uniform. Then, ammonium hydroxide solution (10 vol %) (7.5 mL) was added to it. The reaction was continued for 4 hr. at 85°C. The black precipitate was then separated using a permanent magnet. Finally, the precipitate was washed repeatedly using ethanol and stored after drying at 50°C (Dhar et al., 2016).

5.2.2.2 Fabrication of nanocomposites

While working with PLA-GR nanocomposites, 2.5 wt. % of GR was found to be optimum showing steady impedance value. Therefore, in this case, 2.5 wt. % of GR was added to 15 mL of chloroform and sonicated for 1.5 h till no black leftover at the bottom. The sonicated GR mixture was then added to the mixture of PLA (0.5 g)

dissolved in chloroform (20 mL). Two different loadings i.e. 0.5 wt. % and 1 wt. % of Fe-CNC was considered for the preparation of Fe-CNC reinforced film. Weighted amount of Fe-CNC was added to 15 mL of chloroform and subjected to sonication for 30 min before it was mixed to the above-mentioned composition. Then, the mixture was stirred for about 10 h using magnetic stirrer before cast into thin film. The films are designated as PLA-S-2.5GR, PLA-S-2.5GR-0.5Fe and PLA-S-2.5GR-1Fe corresponding to 0.0 wt. %, 0.5 wt. % and 1.0 wt. % Fe-CNC loading, respectively.

5.2.3 Characterization

5.2.3.1 Morpholoical analysis

The topography nature of the films and fractured samples was examined using scanning electron microscopy with field electron emission facility (FESEM). Gold coating was carried out for 270 s prior to place for study in FESEM (Sigma, Zeiss) at accelerating voltage of 2-3 kV. Energy dispersive X-ray (EDX) analysis of fractured sample of PLA-S-2.5GR-0.5Fe was carried out at 20 kV with a working distance of 8.5 mm in secondary electron detection mode to examine distribution of iron in the bulk of the composite.

5.2.3.2 TGA

Instrument details and operating conditions are mentioned in Chapter 4.

5.2.3.3 DSC analysis

Instrument details and operating conditions are mentioned in Chapter 4.

5.2.3.4 DMA

Instrument details and operating conditions are mentioned in Chapter 2

5.2.3.5 Impedance analysis

Instrument details and operating conditions are mentioned in Chapter 4.

5.2.3.6 Electrochemical sensing of ethanol

Instrument details and operating conditions are mentioned in Chapter 4.

5.2.3.7 Bio-sensor for D-glucose and glycine

Current-Voltage (I-V) response of the composite films was obtained by keeping start potential at -1.00 V and stop potential at -1.00 V (upper vertex potential 1.00 V, lower vertex potential -1.005 V, step potential 0.00200 and scan rate 0.1000 V/s)(Fig. 2.5). D-glucose and glycine of 20 ppm concentration were taken for the study. Effects of multiple cycles, step potential and concentration were examined.

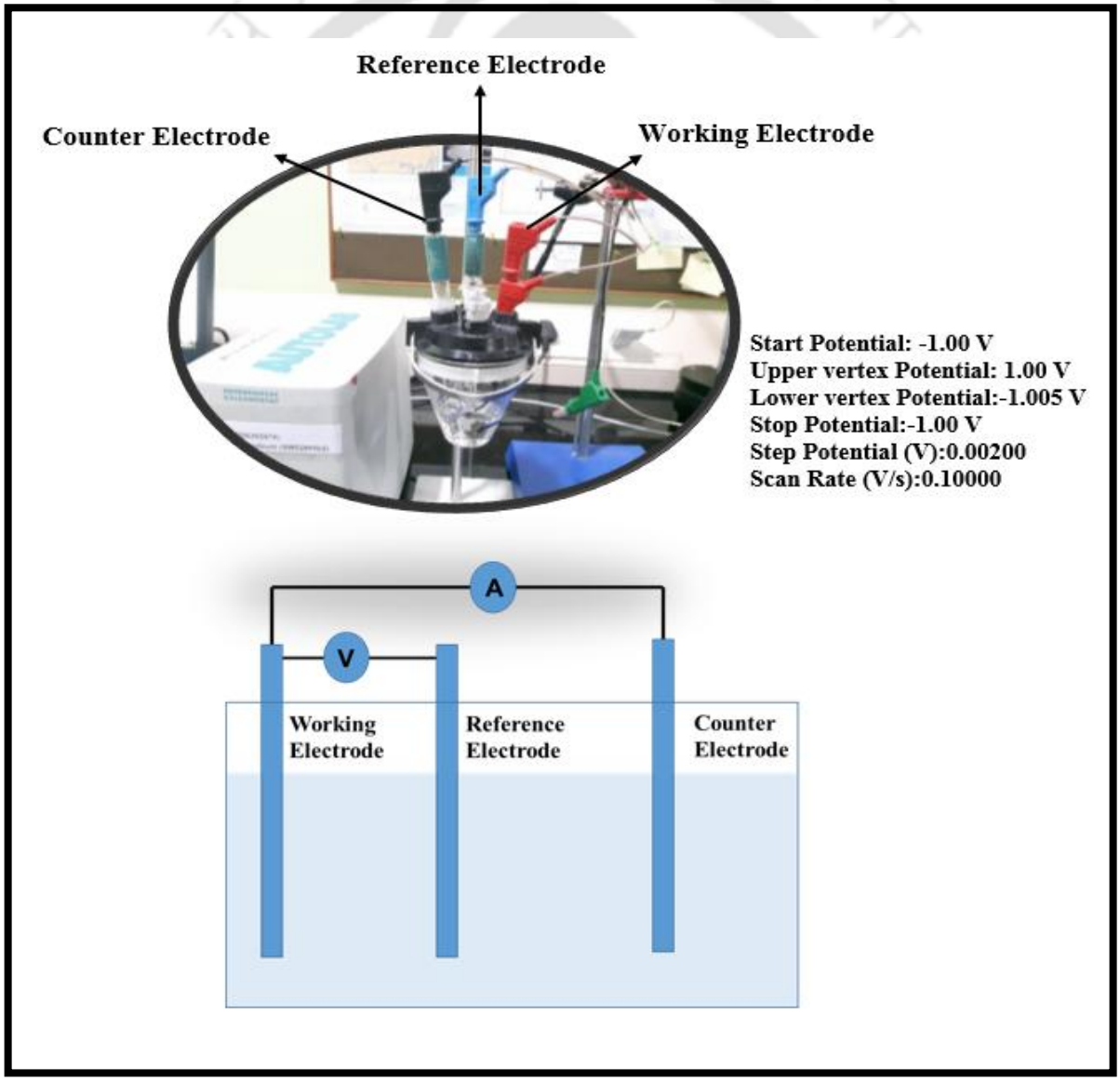

Fig. 5.1 Three electrode experimental setup for D-glucose and glycine sensing

5.3 Results and Discussion

Fe-CNC loading optimization

Effects of incorporation of Fe-CNC in PLA/GR system on different properties such as dispersion, thermal stability, crystallization nature, morphological evenness, mechanical strength, and impedance were evaluated to optimize the Fe-CNC loading.

5.3.1 Morphology analysis

Effect of incorporation of Fe-CNC on the morphology of the composites PLA-S-2.5GR-0.5Fe (PLA with 2.5 wt. % GR and 0.5 wt. % Fe-CNC) and PLA-S-2.5GR-1Fe (PLA with 2.5 wt. % GR and 1wt. % Fe-CNC) was investigated by FESEM image analysis and EDX analysis. Spherical shaped Fe_3O_4 nanoparticles (size distribution ~18-30 nm) decorated CNC can be seen from Fig. 5.2a (Dhar et al., 2016). Fig. 5.2 (b-c) suggests that for 0.5 wt. % loading of Fe-CNC, the dispersion of Fe-CNC in the composite is uniform. However, in the PLA-S-2.5GR-1Fe (Fig. 5.2d) with higher loading of Fe-CNC (1wt %), both agglomerates and dispersed nature of the composite can be seen, which is an indication for developing non-uniformity at higher loading. FESEM images and EDX mapping of the fracture surface of PLA-S-2.5GR-0.5Fe (Fig. 5.2e and Fig. 5.3) reveal the incorporation of Fe-CNC within PLA matrix. EDX mapping of fractured surface of PLA-S-2.5GR-0.5Fe can be seen in Fig. 5.3 showing presence of Fe (marked with arrow) i.e. Fe_3O_4 decorated CNC all over in the bulk of the composite. Thus, morphological analysis suggests better and uniform distribution of Fe-CNC in case of PLA-S-2.5GR-0.5Fe with respect to PLA-S-2.5GR-1Fe.

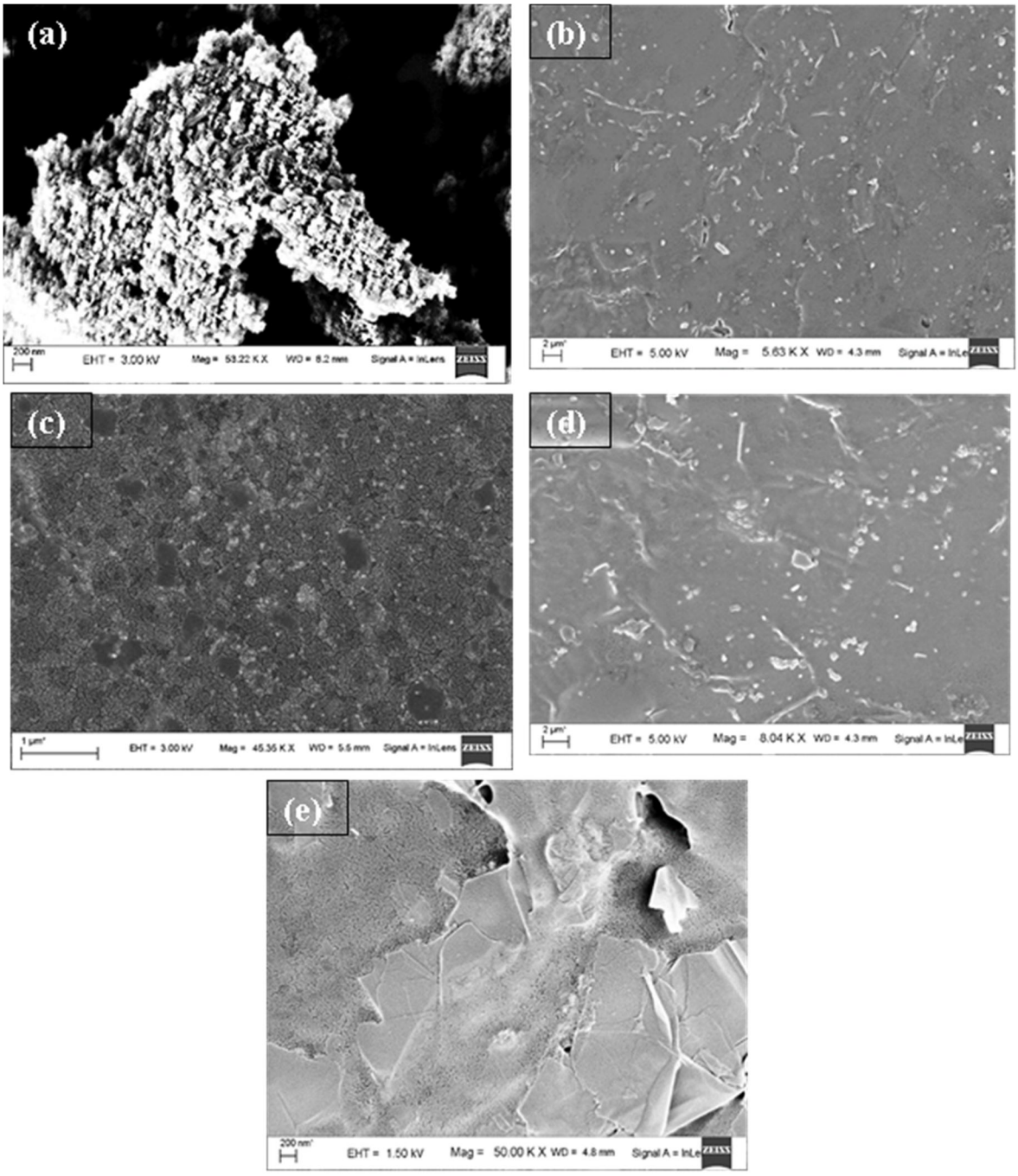

Fig. 5.2 FESEM image of (a) Fe-CNC, (b-c) PLA-S-2.5GR-0.5Fe, (d) PLA-S-2.5GR-1Fe and (e) fracture surface of PLA-S-2.5GR-0.5Fe

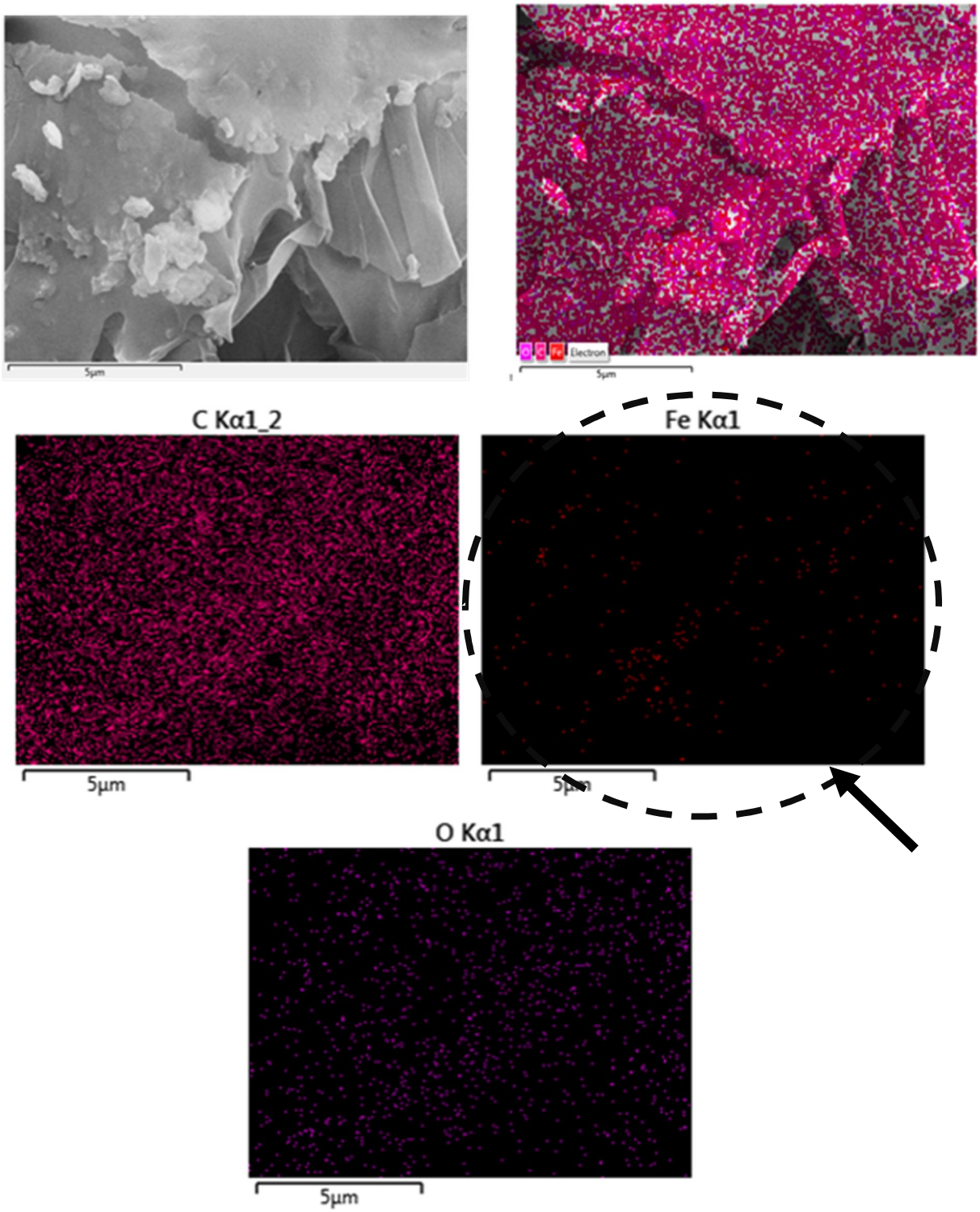

Fig. 5.3 EDX mapping of fractured surface of PLA-S-2.5GR-0.5Fe

5.3.2 TGA

The thermal stability of the nanocomposites was studied using thermogravimetric analyzer. Since GR possesses layered morphology, it acts as a barrier towards the gaseous and volatile product after degradation (Valapa et al., 2015a). Effect of incorporation of Fe-CNC on the thermal stability of PLA-S-2.5GR can be seen from Fig. 5.4. Onset degradation temperature (T_{onset}) of the composites is recorded to be 348.5 °C, 347 °C, 334.7 °C for PLA-S-2.5GR, PLA-S-2.5GR-0.5Fe and PLA-S-2.5GR-1Fe, respectively (Table 5.1). Improvement of thermal stability due to incorporation of 2.5 wt. % of GR in PLA matrix is significant as compared to that of PLA (311°C) (Valapa et al., 2015a). A similar trend can also be seen in case of 50 wt. % degradation ($T_{50\%}$) and maximum degradation temperature (T_{max}). The barrier effect of graphene enhances the T_{onset} by ~37 °C, $T_{50\%}$ by ~33 °C and T_{max} by ~22 °C for PLA-S-2.5GR as compared to that of PLA. Fe-CNC loading of 0.5 wt. % shows insignificant impact on the thermal stability of PLA-S-2.5GR, which is obvious from the almost similar values of T_{onset}, $T_{50\%}$ and T_{max} for PLA-S-2.5GR-0.5Fe and PLA-S-2.5GR composites. However, at 1 wt. % loading of Fe-CNC, thermal stability of the composite is considerably decreased. T_{onset}, $T_{50\%}$ and T_{max} of PLA-S-2.5GR-1Fe are reduced by 14 ^{o}C, 11 ^{o}C and 8 ^{o}C, respectively while compared with that of PLA-S-2.5GR. This can be attributed to the formation of agglomerates that allows local thermal stress generation and thereby making the composite more susceptible to thermal degradation. Liu et al. (2015) fabricated different metal oxide (Bi_2O_3, Fe_2O_3, and CuO) based PLA composite by solvent casting method to investigate the impact of metal oxides on the thermal degradation of PLA. It was observed that onset degradation temperature and maximum degradation temperature were decreased by 30 K and 62 K on incorporation of 1 wt. % Fe_2O_3 into PLA matrix as compared to neat PLA. Dong et al. (2011) studied

different metal oxide catalyzed depolymerization of PLA and observed that incorporation of metal oxides significantly reduced the depolymerization temperature of PLA. In addition, higher concentration of iron in the matrix might also cause catalytic effect on the PLA chains that leads to degradation of the chains as well as the matrix at a relatively lower temperature (Dong et al., 2011; Liu et al., 2015). Thus, though the presence of metal compounds significantly reduces the thermal stability of the composite, 0.5 wt. % loading of Fe-CNC in PLA-S-2.5GR in the present work does not show any such adverse impact.

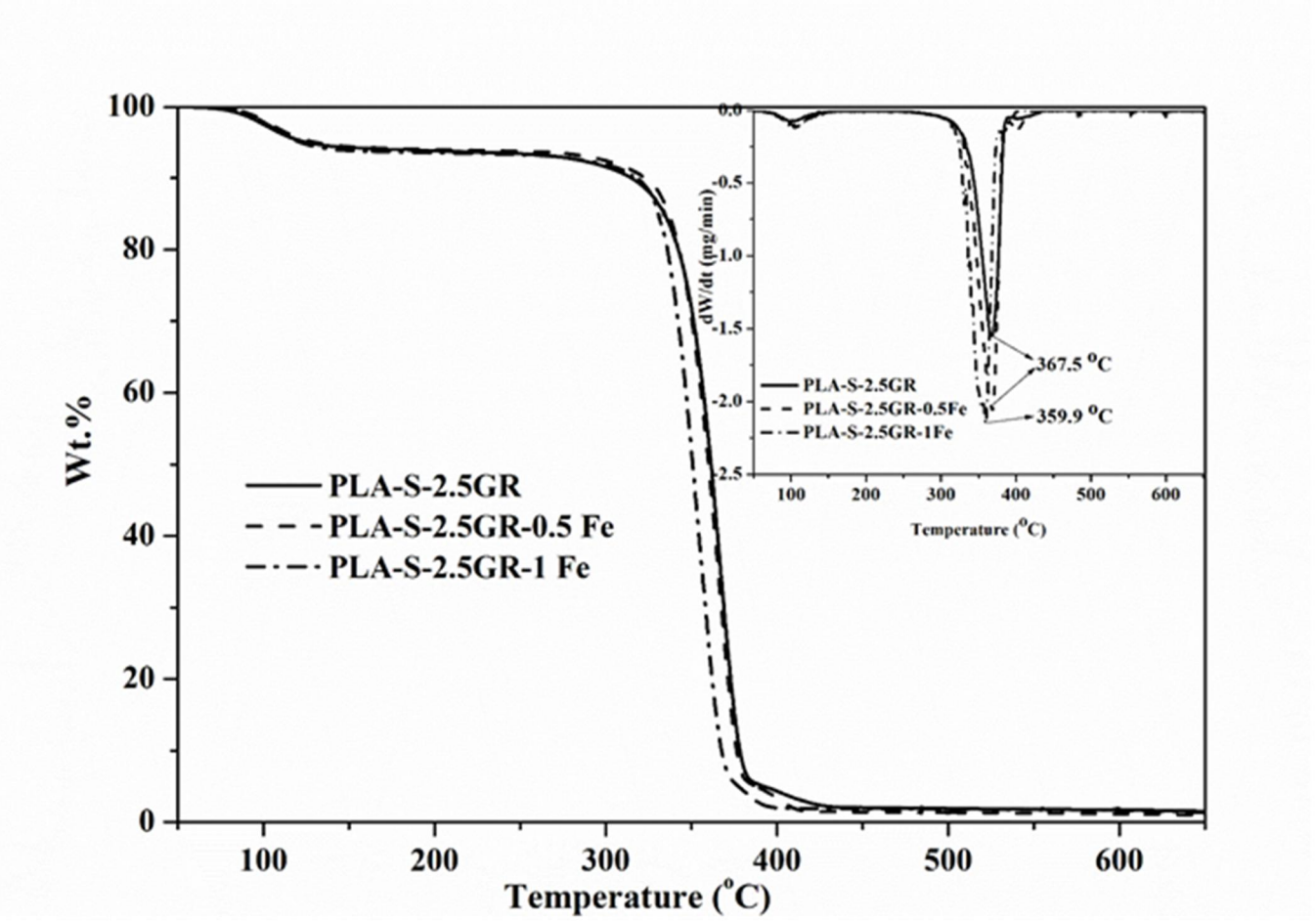

Fig. 5.4 TGA plot of PLA-S-2.5GR, PLA-S-2.5GR-0.5Fe and PLA-S-2.5GR-1Fe, DTG profile of PLA-S-2.5GR, PLA-S-2.5GR-0.5Fe and PLA-S-2.5GR-1Fe (Inset)

Table 5.1 Thermal analysis data for PLA-S-2.5GR, PLA-S-2.5GR-0.5Fe and PLA-2.5GR-1Fe

Component	T_{Onset} (°C)	$T_{50\%}$ (°C)	T_{max} (°C)	T_g (°C)	T_{cc} (°C)	T_m (°C)
PLA-S-2.5GR	348.5	361.9	367.5	63.8	123	153.8
PLA-S-2.5GR-0.5 Fe	347	359.8	367.5	62	111	149.7,153.8
PLA-S-2.5GR-1 Fe	334.7	350.8	359.9	59	111	148.2,152.5
PLA	311	329	345	62	110	148

5.3.3 DSC analysis

Differential scanning calorimetric (DSC) analysis of the PLA-S-2.5GR, PLA-S-2.5GR-0.5Fe and PLA-S-2.5GR-1Fe composites was carried out to examine the behavior of the composites in presence of thermal scanning. Cold crystallization behavior of the composites can be seen from Fig. 5.5. In case of PLA-S-2.5GR, glass transition (T_g), cold-crystallization (T_{cc}) and melting (T_m) temperatures are 63.8 °C, 123 °C and 153.8 °C, respectively, whereas for PLA, the values are 62, 110 and 148 °C (Table 5.1), respectively. Insignificant change in T_g of PLA-S-2.5GR, PLA-S-2.5GR-0.5Fe and also PLA-S-2.5GR-1Fe implies the fact that the primary chain relaxation behavior remained similar and no structural changes had happened in the composites with respect to PLA (Miyata & Masuko, 1998; Yuan et al., 2006). A significant increase in T_m and T_{cc} values of PLA-S-2.5GR compared to PLA is due to possible nucleation effect of the almost homogeneously mixed graphene surface into PLA matrix. The two T_m values for the Fe-CNC loaded composites resembling with PLA and with PLA-S-2.5GR indicate non-homogeneity of the composite matrix and reduction in crystallinity due to incorporation of Fe-CNC into matrix of PLA-S-2.5GR. However, the little reduction in T_g values can be attributed to inability of the polymer chains to be incorporated in growing crystalline

lamella. Another possible reason may be prevention of large crystalline domain formation due to restriction of space owing to the presence of filler. However, for PLA-S-2.5GR-0.5Fe and PLA-S-2.5GR-1Fe, T_{cc} values are significantly decreased nearly to PLA. This can again be, as discussed earlier, due to the facts of non-homogeneity of the composite matrix and reduction of crystallinity due to presence of Fe-CNC (Chu et al., 2017; Dong et al., 2011). Thus, presence of Fe-CNC into PLA-S-2.5GR though changes the crystallinity and homogeneity to some extent, doesn't alter the glass transition temperature. Again PLA-S-2.5GR-0.5Fe is found to be marginally better than PLA-S-2.5GR-1Fe in these aspects.

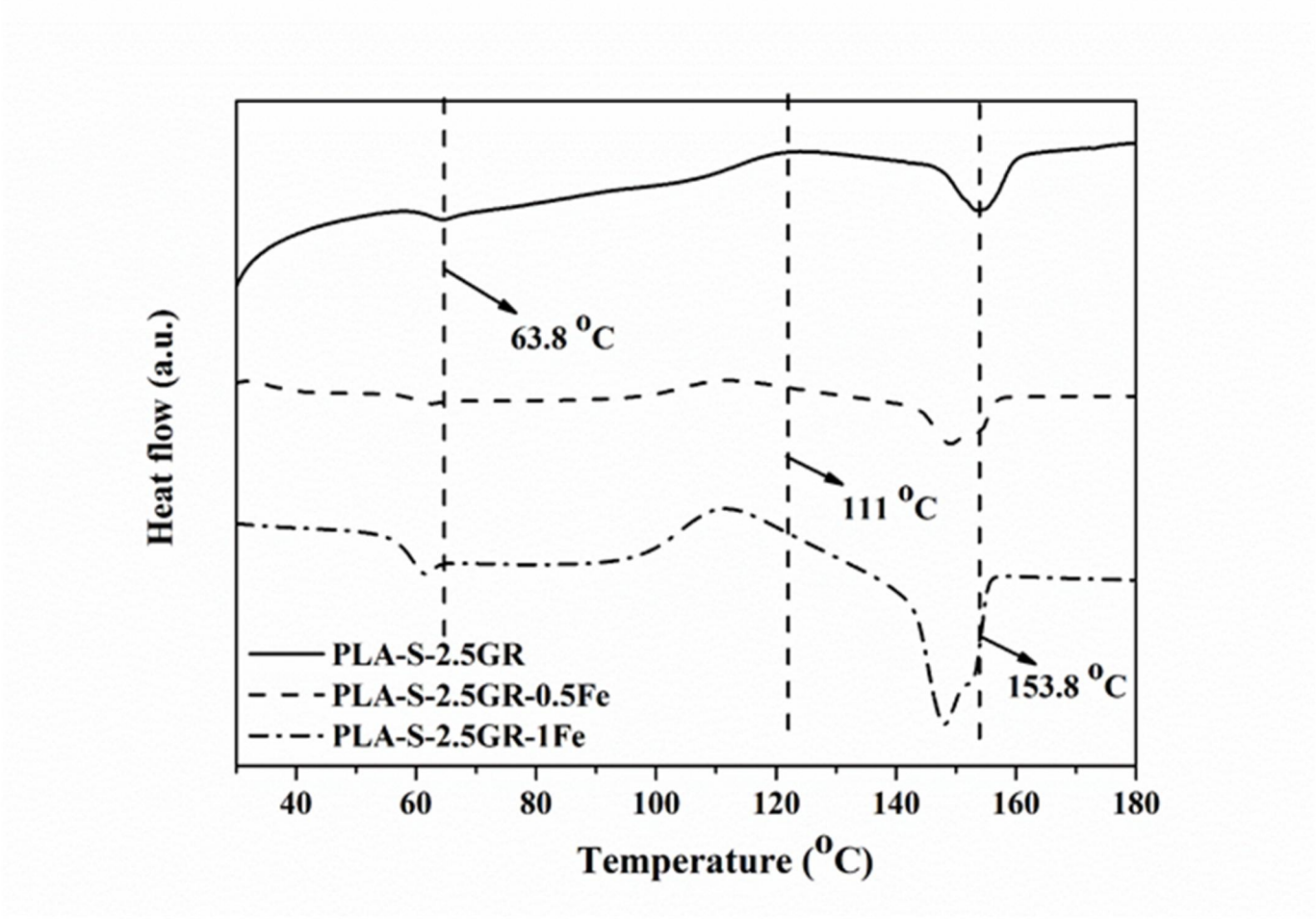

Fig. 5.5 DSC profile of PLA-S-2.5GR, PLA-S-2.5GR-0.5Fe and PLA-S-2.5GR-1Fe

5.3.4 DMA

The dynamic mechanical property of the Fe-CNC loaded composites is examined and compared with respect to PLA-S-2.5GR (Fig. 5.6). With incorporation of Fe_3O_4 decorated CNC, the storage modulus is increased for the composites (PLA-S-2.5GR-0.5Fe and PLA-S-2.5GR-1Fe). Dynamic storage modulus (E') is increased significantly to 2859 MPa for PLA-S-2.5GR-0.5Fe as compared to that for PLA-S-2.5GR (1477 MPa) at 35°C. This implies that presence of Fe-CNC increases the elastic property of the composite as Fe-CNC restricts the chain deformation of PLA at lower temperature. However, in case of PLA-S-2.5GR-1Fe, the improvement is less (2357 MPa) as compared to that for PLA-S-2.5GR-0.5Fe. This is again attributed to the formation of agglomerates, which led to non-uniformity in the distribution and disproportionate elastic property of the composite as compared to the uniformly dispersed Fe-CNC composite, PLA-S-2.5GR-0.5Fe. At higher temperature, the rate of decrement of E′ is higher for the Fe-CNC loaded composites compared to PLA-S-2.5GR. At 55°C, storage modulus of PLA-S-2.5GR, PLA-S-2.5GR-0.5Fe and PLA-S-2.5GR-1Fe are 677, 624 and 287 MPa, respectively. Though presence of Fe increased elasticity and rigidity, with an increase in the temperature, those properties are reduced because of higher thermal energy imparted on the molecules. Therefore, beyond ~55°C, PLA-S-2.5GR and PLA-S-2.5GR-0.5Fe show overlapping profile of E′. Further rise in the temperature above glass transition temperature, E′ profile of the components are similar. Tan δ for PLA-S-2.5GR-0.5Fe is slightly shifted towards right as compared to that for PLA-S-2.5GR due to better dispersion and compatibility. It can be seen that the chain relaxation behavior is identical for all the components even after incorporation of Fe_3O_4 decorated CNC. Thus, the composite PLA-S-2.5GR-0.5Fe is found to show better mechanical

strength than PLA-S-2.5GR up to temperature of about 50 ºC and always better than PLA-S-2.5GR-1Fe.

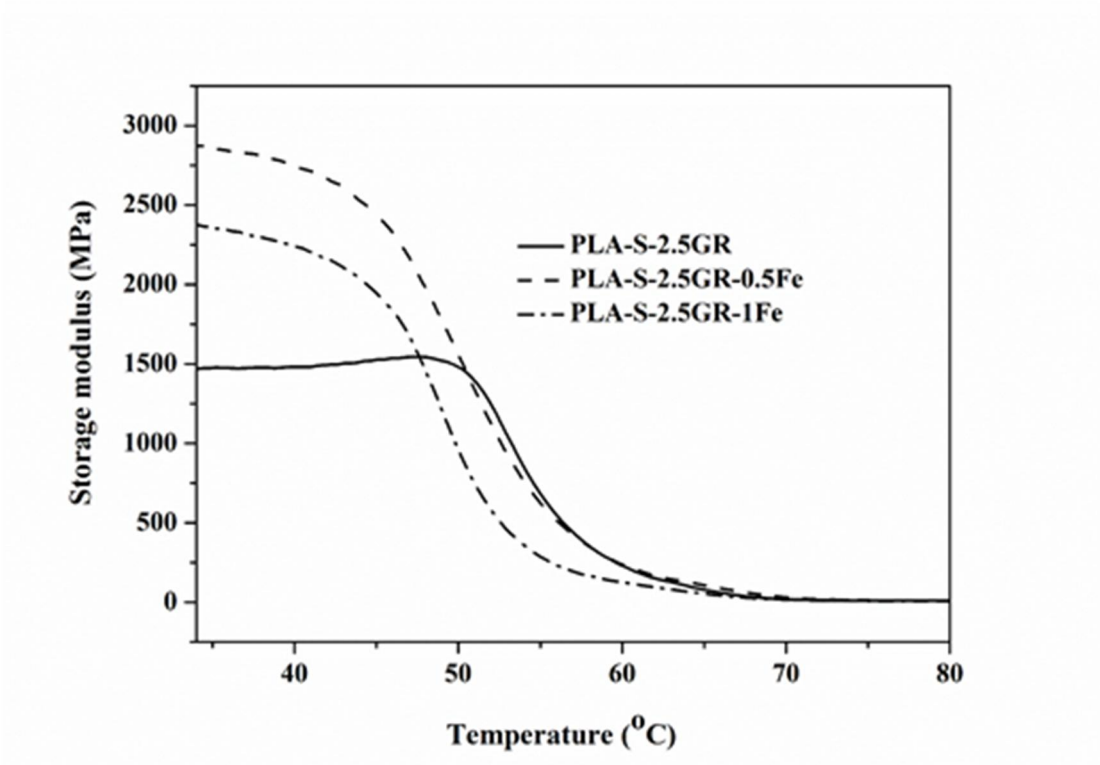

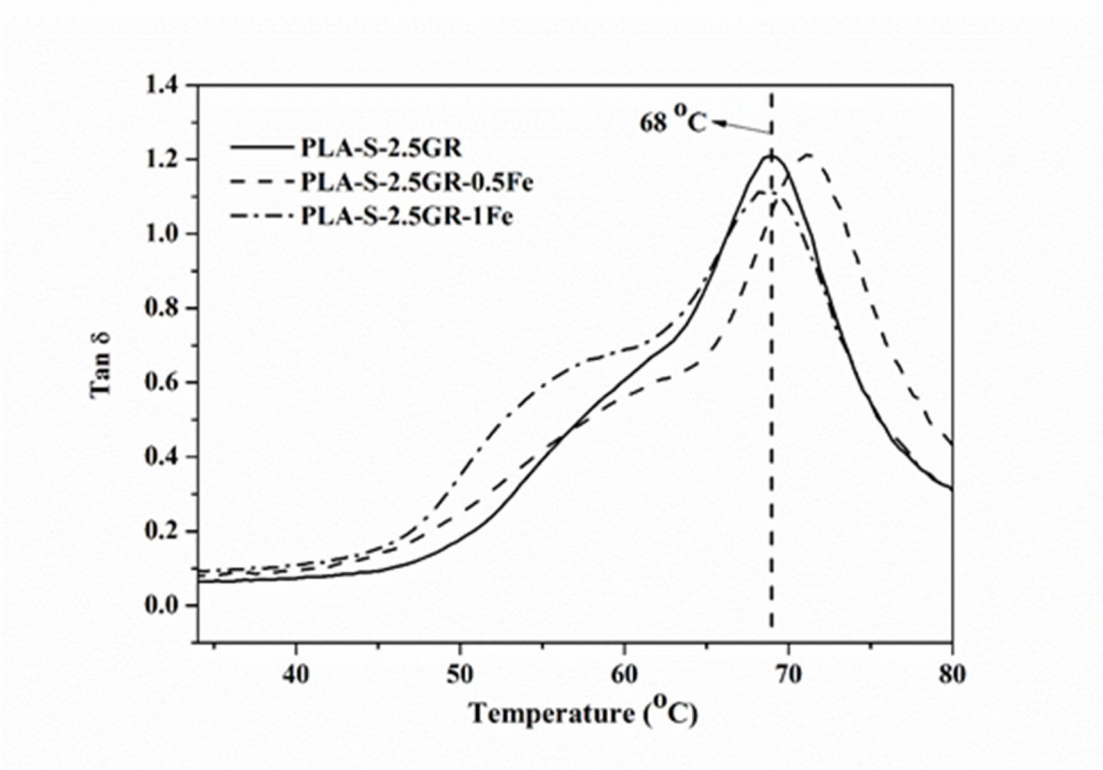

Fig. 5.6 DMA plot for PLA-S-2.5GR, PLA-S-2.5GR-0.5Fe and PLA-2.5GR-1Fe

5.3.5 Impedance analysis

Impedance of material dictates the conductive nature as it is the barrier against the flow of electron. In this chapter, the effect of Fe-CNC towards the conductivity of PLA-S-2.5GR is examined. Fig. 5.7 implies that the incorporation of Fe-CNC doesn't significantly alter the impedance of PLA-S-2.5GR (~ $10^4\,\Omega$), which is much lower than the value of solution cast PLA (PLA-S in Fig. 5.7). It implies that Fe-CNC introduction into PLA-S-2.5GR doesn't disturb the connective networks of graphene sheets inside the PLA matrix.

Thus, from morphology, TGA, DSC, DMA and impedance analysis, the composite, PLA-S-2.5GR-0.5Fe appears to be better over PLA-S-2.5GR-1Fe composite. PLA-S-2.5GR-0.5Fe also showed higher elasticity and rigidity over PLA-S-2.5GR up to 50°C. In the case of PLA-S-2.5GR-0.5Fe, uniform distribution of Fe (Fe-CNC) within the composite bulk as well as in the surface is observed. PLA-S-2.5GR-0.5Fe also demonstrates similar thermal stability and crystallization behavior to those of PLA-S-2.5GR. Incorporation of Fe-CNC doesn't disturb the conductive network of GR within the PLA matrix. Therefore, PLA-S-2.5GR-0.5Fe is chosen for further experimentation to determine the sensitivity and selectivity towards stimuli like ethanol, D-glucose and glycine.

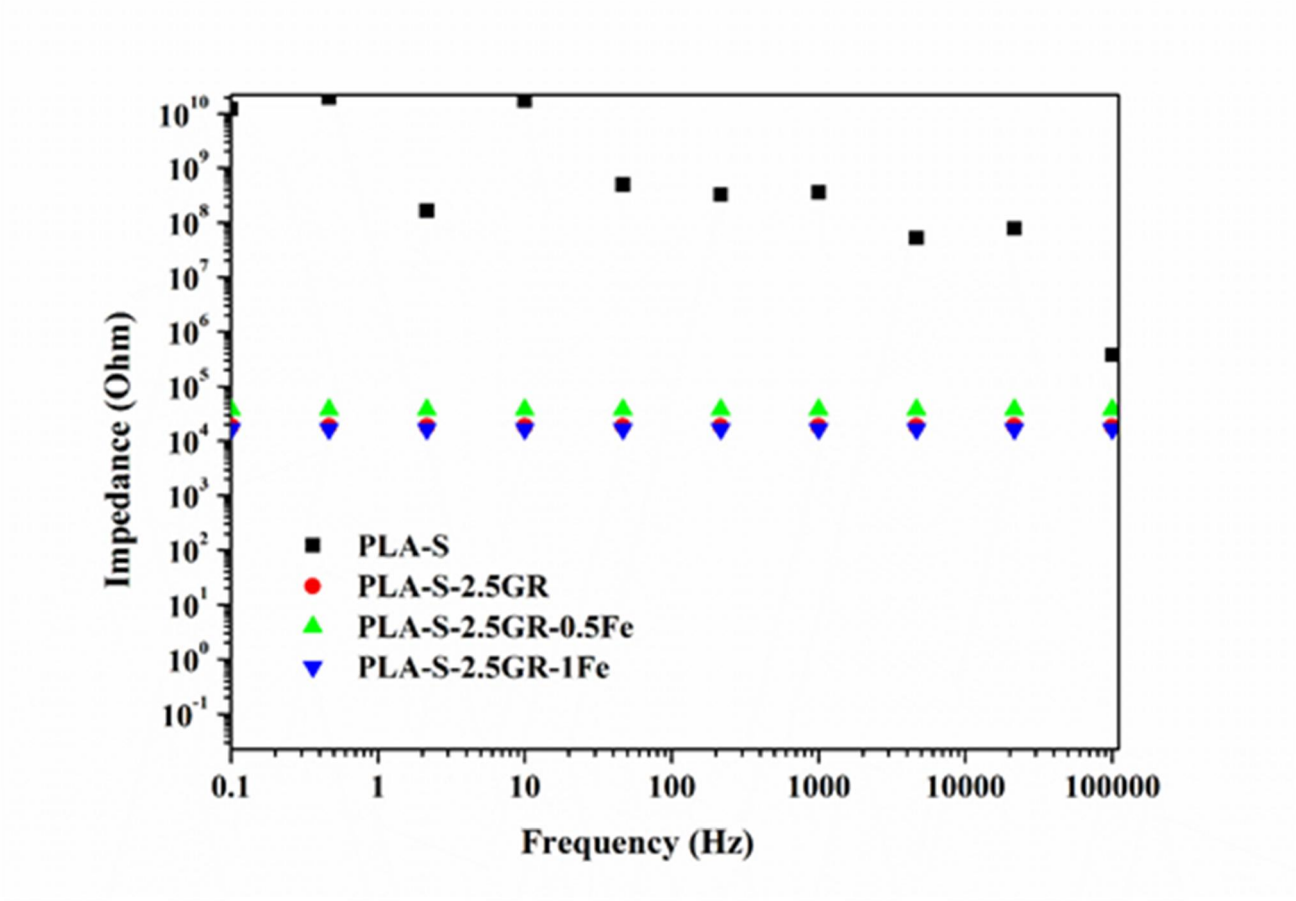

Fig. 5.7 Impedance plot for PLA-S-2.5GR, PLA-S-2.5GR-0.5Fe and PLA-2.5GR-1Fe in comparison with solution cast PLA (PLA-S)

Sensing study

Applicability of Fe-CNC loaded PLA/GR nanocomposite films is studied as a conductive material for electrochemical sensor application. Sensor application was carried out in two ways. The first case is electrochemical sensing for detection towards ethanol. In this case, the thin film is dipped into the solvent followed by measurement of impedance as discussed in chapter 4 in order to sense and detect the stimuli, which is ethanol in the present case. The composite PLA-S-2.5GR-0.5Fe is used for this study. The second case is to study the applicability of the composite as a thin film electrode where two different categories of biomolecules such as D-glucose and glycine are used for their detection study. In this case, the thin film of the composite is used as electrode along with a reference electrode immersed into the solution containing the stimuli.

Difference in the current between the two circuits enables to estimate the working electrode current flow. In this case, the composite PLA-S-2.5GR and PLA-S-2.5GR-1Fe are also used along with PLA-S-2.5GR-0.5Fe in order to gather more and extensive information as there has been no such study reported so far that used PLA based composite as electrode.

5.3.6 Electrochemical sensor

Ethanol

In view of uniformity of dispersion, comparable thermal stability, electrical conductivity and improved mechanical strength of PLA-S-2.5GR-0.5Fe compared to PLA-S-2.5GR and PLA-S-2.5GR-1Fe, it was taken for sensing of ethanol. As lower concentration of ethanol detection is important for chemical and beverage industries, 25 vol% of ethanol was taken as solvent for this study. In order to accomplish this investigation, recycle test, repeatability test, and reusability test were also performed.

Recycle test

Recycle test was conducted to investigate the applicability of the PLA-S-2.5GR-0.5Fe film for consecutive three cycles. It can be seen that during dipping of each cycle (C1, C2, and C3), the relative change in response (R_{rel}) increases with dipping duration and decreases during drying time (Fig. 5.8). Diffusion of ethanol into PLA matrix is responsible for the increase in impedance, which causes additional resistance to the existing conductive networks of graphene within the matrix. During drying cycle when the solvent is going out of the matrix, this additional resistance is dropped again leading to decrement in impedance. It can be seen from Fig. 5.8 that for all the three consecutive cycles the responses are quite similar showing constant pattern for both dipping and drying, which establishes the consistency of the result for a single strip. The minor

differences in the R_{rel} values for different cycles could possibly be attributed to ethanol/water left over within the matrix.

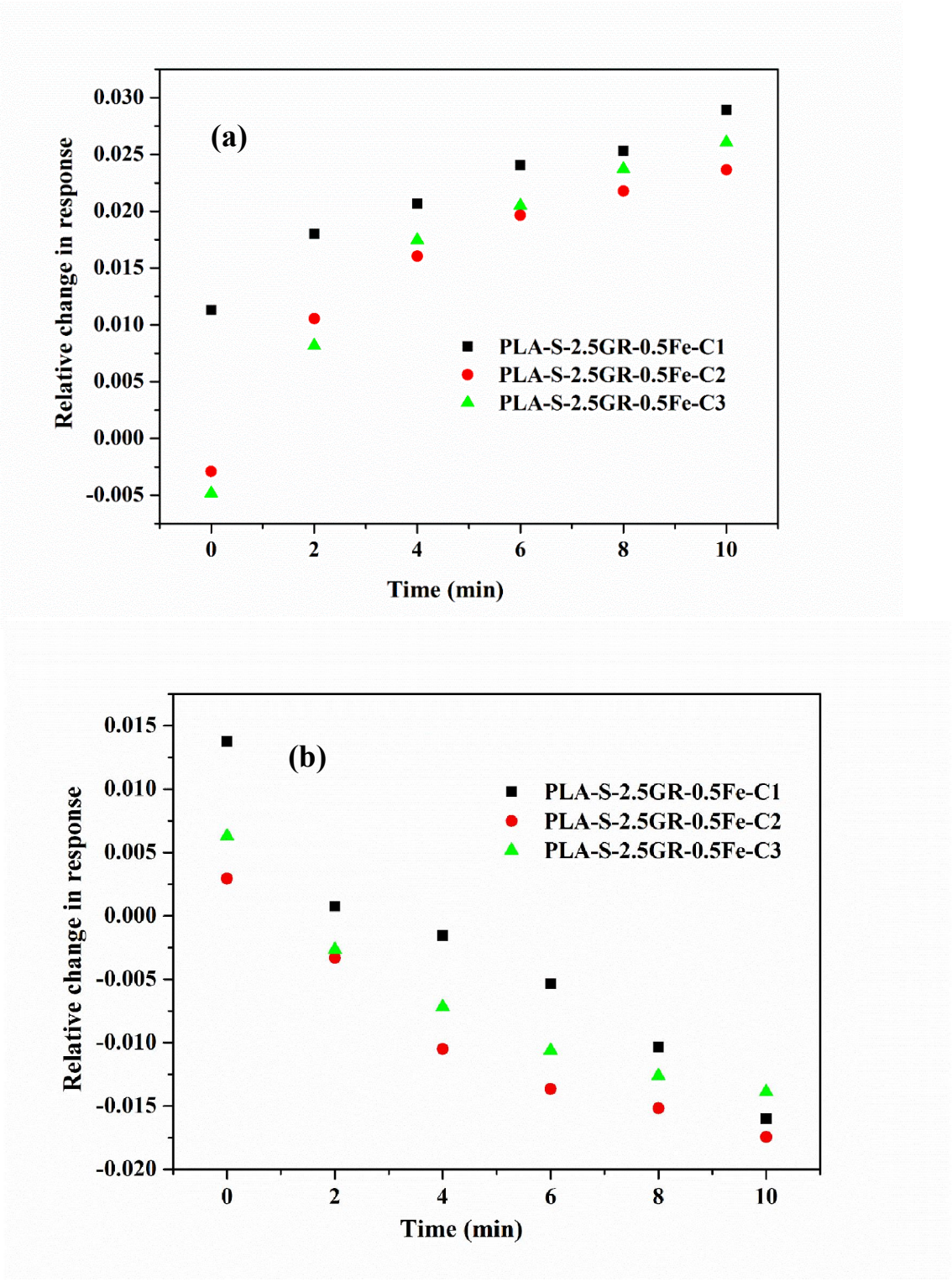

Fig. 5.8 Recycle test for PLA-S-2.5GR-0.5Fe (a) dipping and (b) drying

Repeatability test

In order to see the repeatability of the response of PLA-S-2.5GR-0.5Fe, two samples (S_1, S_2) from the same batch of synthesis and two samples (S_1/S_2, S_3) from different batches of synthesis were taken for 25% ethanol detection. The dipping cycle data can be seen from Fig. 5.9. It indicates that the 'R_{rel}' values are overlapping for both the samples taken from the same batch. The variations in response between different batch samples could be due to variations in homogeneity and experimental limitations. More sophisticated experimental set up for fabrication as well as detection can possibly bring down the observed variations between the samples of different batches. However, a typical set of values of response of PLA-S-2.5GR-0.5Fe is compared with that of PLA-S-2.5GR in Fig. 5.10. Though the result shows similar trend, the incorporation of Fe-CNC increases the response value possibly due to affinity of Fe_3O_4 towards ethanol as well as additional resistance offered by Fe_3O_4. Thus, Fe-CNC reinforced PLA/GR composite shows similar performance like PLA/GR composite in detecting ethanol. However, PLA/GR/Fe-CNC composite has the advantage over PLA/GR composite from the perspective of better mechanical strength and higher affinity of Fe_3O_4 towards ethanol.

`

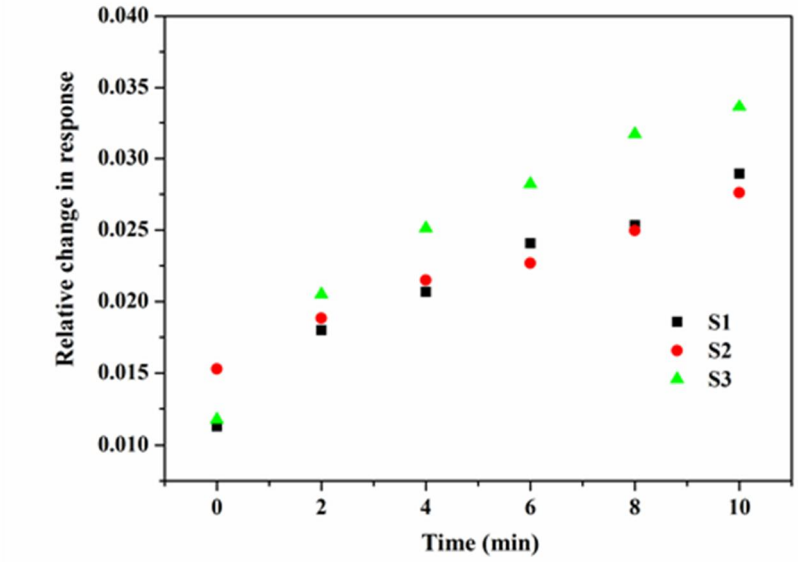

Fig. 5.9 Repeatability test for PLA-S-2.5GR-0.5Fe in 25% ethanol

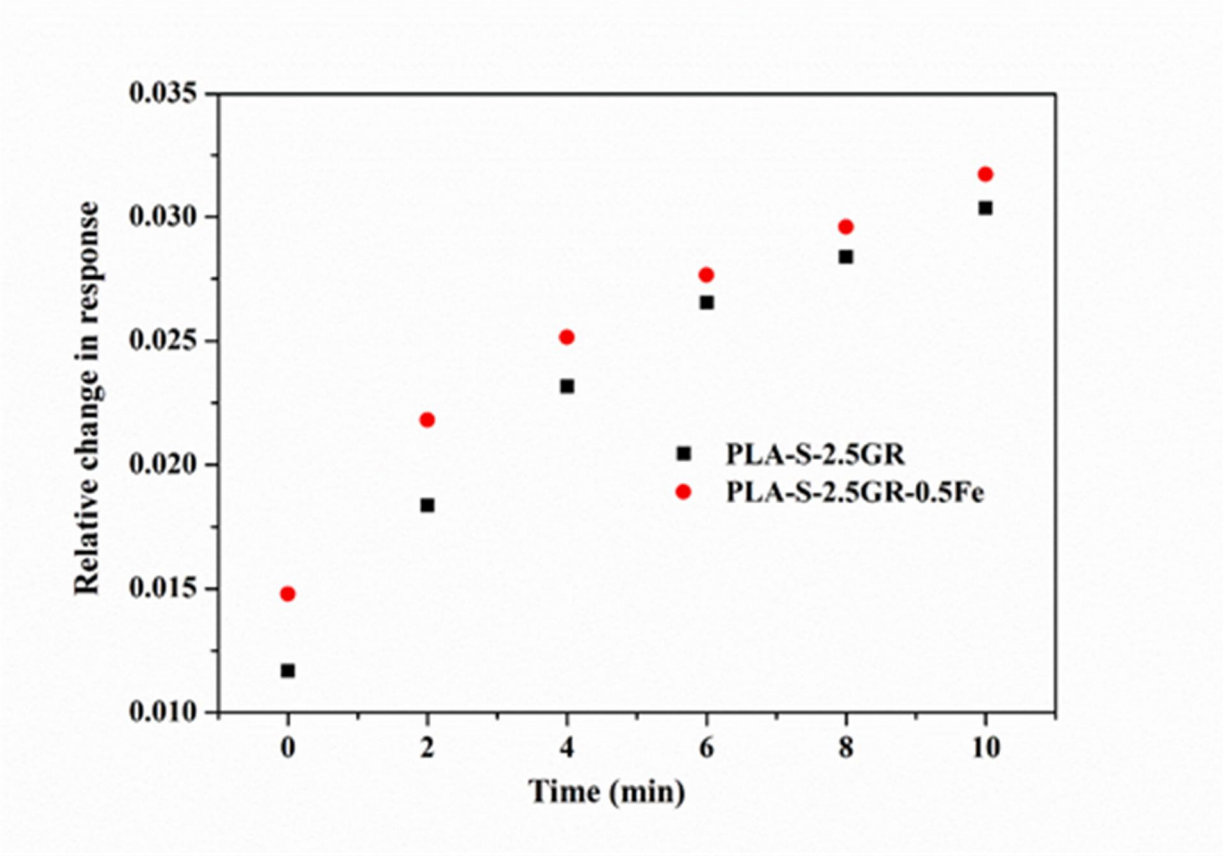

Fig. 5.10 Comparison of response between PLA-S-2.5GR and PLA-S-2.5GR-0.5Fe in 25% ethanol

Reusability test

Reusability of PLA-S-2.5GR-0.5Fe thin film was tested for consecutive 5 times. During each case, the impedance was recorded after 2 min dipping and between the two dipping cycles, one drying condition was maintained i.e. heated at 50 °C for 5 min followed by 5 min at 24°C. The findings are recorded with the variance in the Fig.5.11. It can be seen from Fig. 5.11 that response is lower in case of 15 vol% ethanol compared to 25 vol%. This implies concentration sensitivity of the film and proves its ability to distinguish and detect the presence of ethanol in various concentrations. Thus, calibration of the film for various concentrations of ethanol can help in estimation of concentration of ethanol of an unknown sample with a fair degree of accuracy and within experimental error.

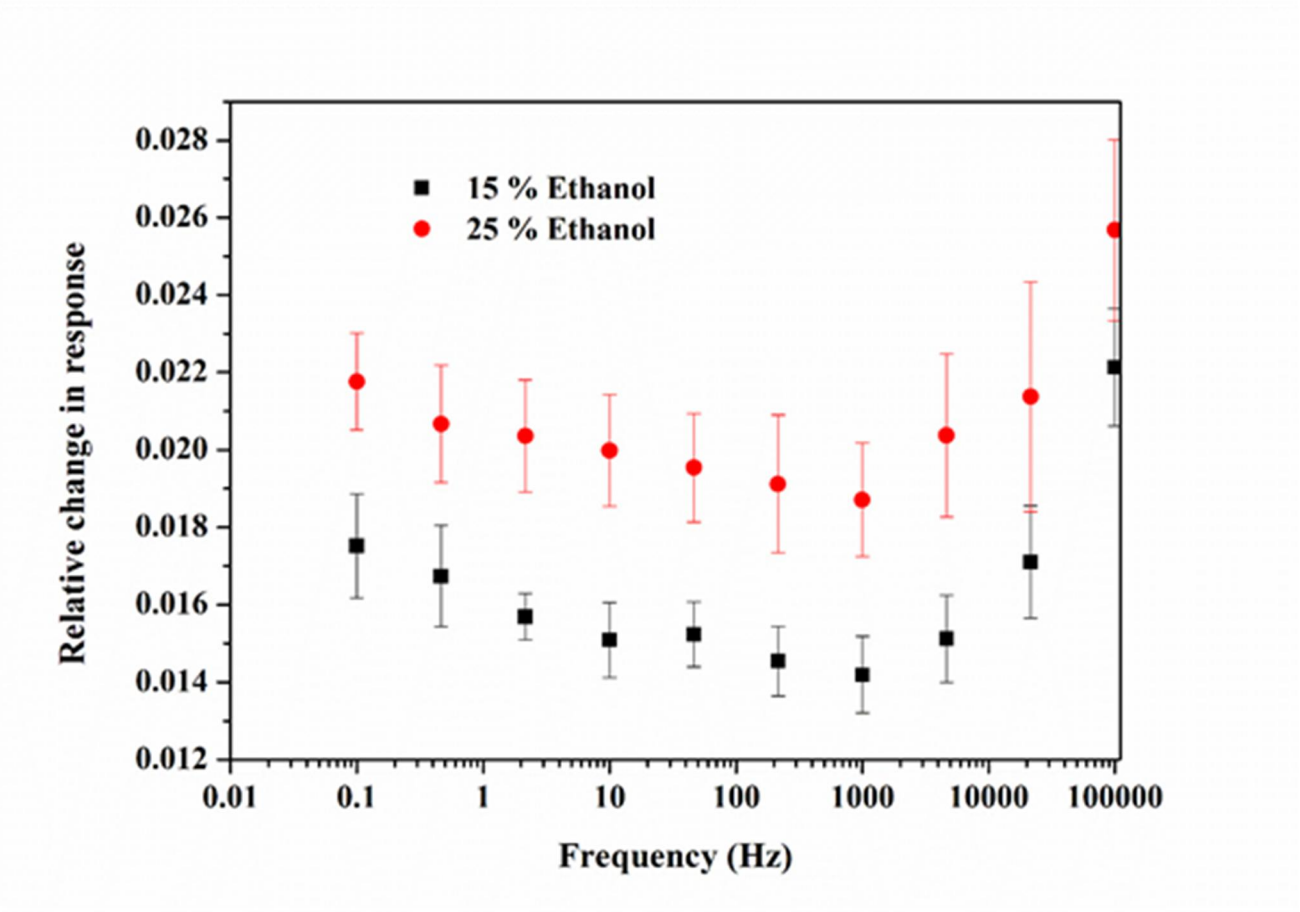

Fig. 5.11 Reusability test for PLA-S-2.5GR-0.5Fe in 25% and 15% ethanol

Stability analysis

The stability of thin-film in alcohol is very much important to be used as a sensing material especially for multiple times. Therefore, film stability of the PLA-S-2.5GR-0.5Fe after application in 25 vol% ethanol was examined by means of morphology analysis, thermogravimetric analysis, and crystallization property analysis.

Morphology change due to dipping in ethanol was checked using FESEM. Fig. 5.12 suggests that in case the composite dipped for less time i.e. PLA-S-2.5GR-0.5Fe-C1, small patches appeared over the composite surface possibly due to removal of amorphous PLA. The presence of iron oxide can be seen in the magnified images (Fig. 5.12e) of the patches (white dots). The surface of PLA-S-2.5GR-0.5Fe-C3 (Fig. 5.12f) faces more leaching of PLA chains, as the immersion time is more for C3 than C1.

However, the results obtained for R_{rel} as discussed earlier section confirm its ability to detect efficiently till the third cycle.

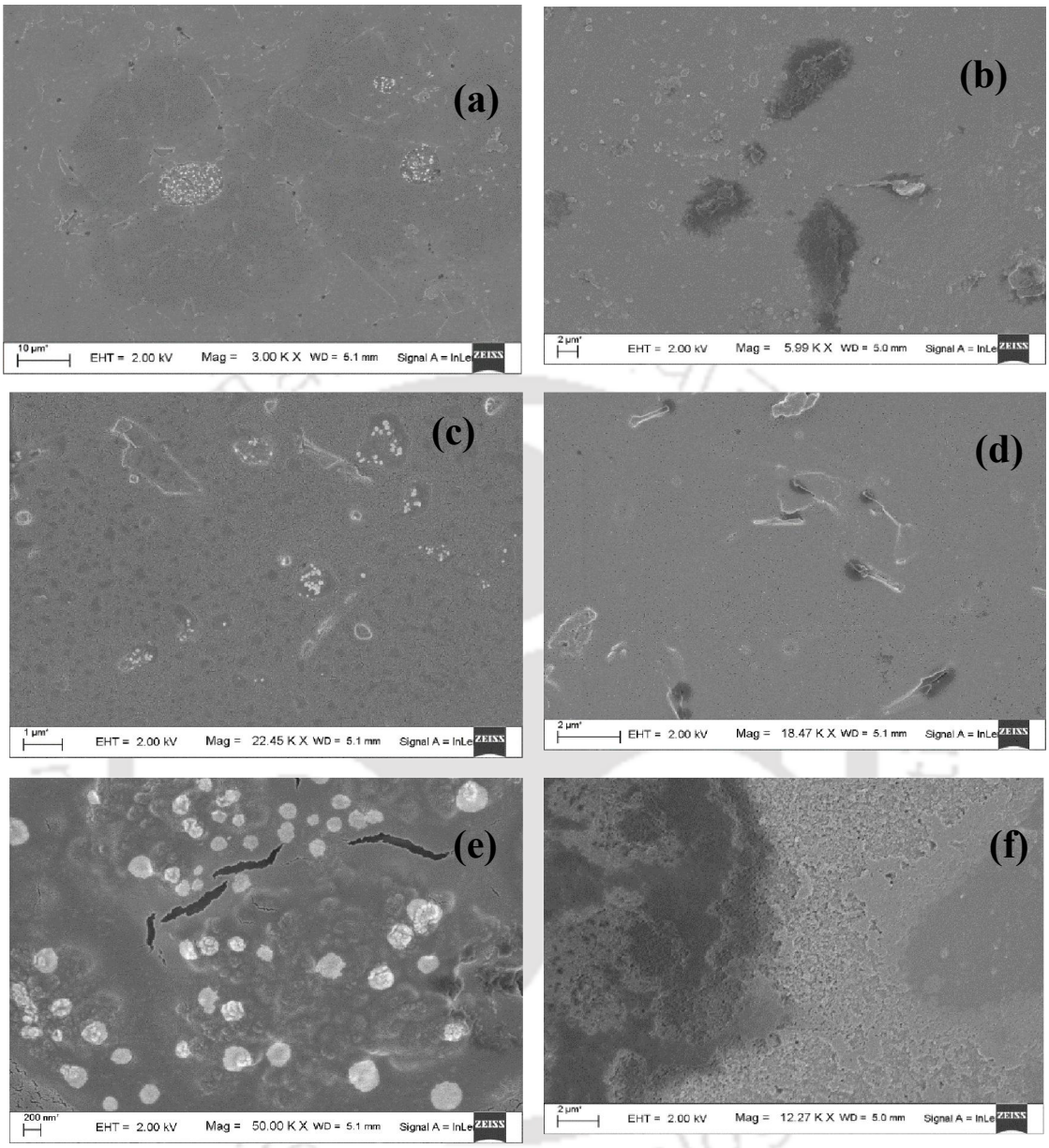

Fig. 5.12 FESEM images of (a-e) PLA-S-2.5GR-0.5Fe-C1 and (f) PLA-S-2.5GR-0.5Fe-C3

TGA analysis was carried out to observe the change in thermal stability of the film after application in 25 vol% ethanol. The thermal stability of the composite film is found to be increasing slightly after first dipping cycle (PLA-S-2.5GR-0.5Fe-C1) and it is not further changed even after third dipping cycle (PLA-S-2.5GR-0.5Fe-C3) (Fig. 5.13).

T_{onset}, $T_{50\%}$, and T_{max} for PLA-S-2.5GR-0.5Fe-C1 are 354, 369 and 376 °C, respectively and that for PLA-S-2.5GR-0.5Fe are 347, 359.8 and 367.5 °C, respectively. This change in thermal stability is due to the removal of short PLA chains because of dipping in ethanol, which further corroborates the morphological changes as discussed in the previous paragraph. However, no change after third cycle suggests stable structure obtained for the Fe-CNC based composites after dipping in ethanol.

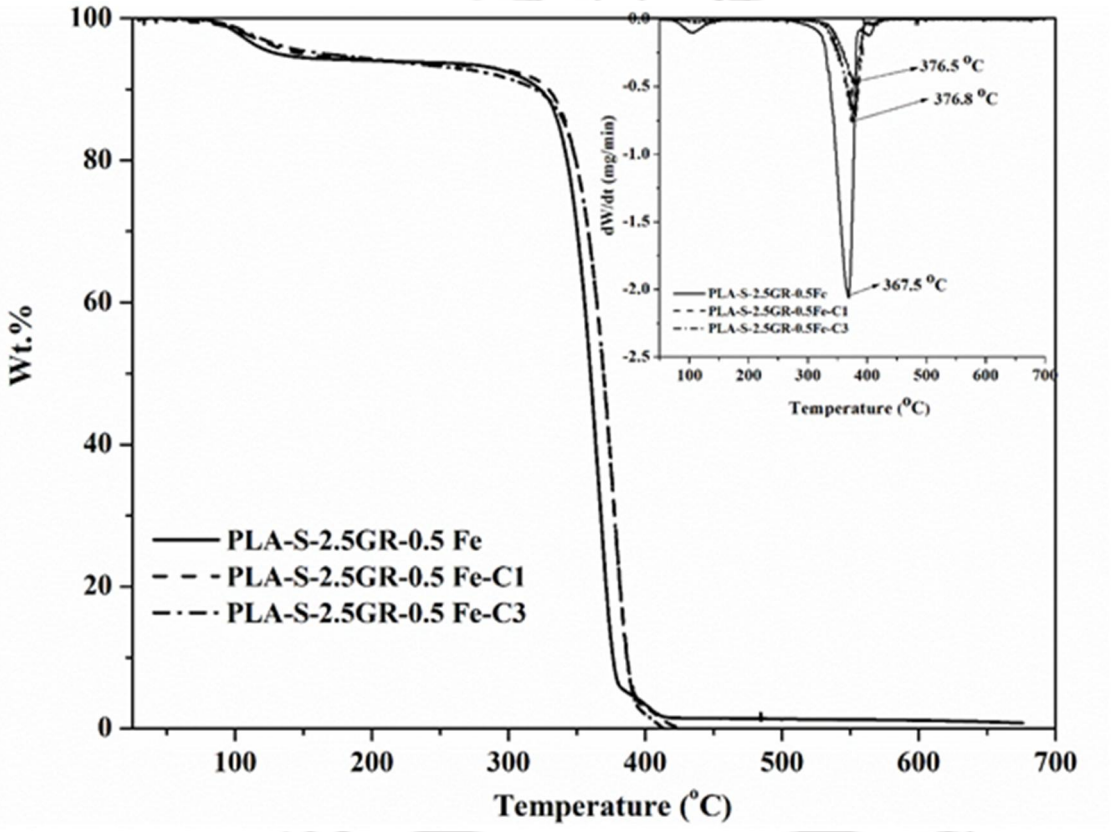

Fig. 5.13 Thermal degradation profile of PLA-S-2.5GR-0.5Fe, PLA-S-2.5GR-0.5Fe-C1 and PLA-S-2.5GR-0.5Fe-C3, DTG profile of PLA-S-2.5GR-0.5Fe, PLA-S-2.5GR-0.5Fe-C1 and PLA-S-2.5GR-0.5Fe-C3 (Inset)

DSC analysis results of the PLA-S-2.5GR-0.5Fe after dipping in ethanol is reported in Fig. 5.14 and Table 5.2. It can be seen that T_g is slightly reduced and T_{cc} values are slightly increased for the PLA-S-2.5GR-0.5Fe-C1 and PLA-S-2.5GR-0.5Fe-C3 as compared to PLA-S-2.5GR-0.5Fe. These changes are again attributed to the removal of

short PLA chains from the matrix after dipping in ethanol. Unchanged T_m values of the composites indicate no impact on the crystalline characteristics of the composites even after dipping in ethanol. The above properties remain unchanged after exposure for third cycle.

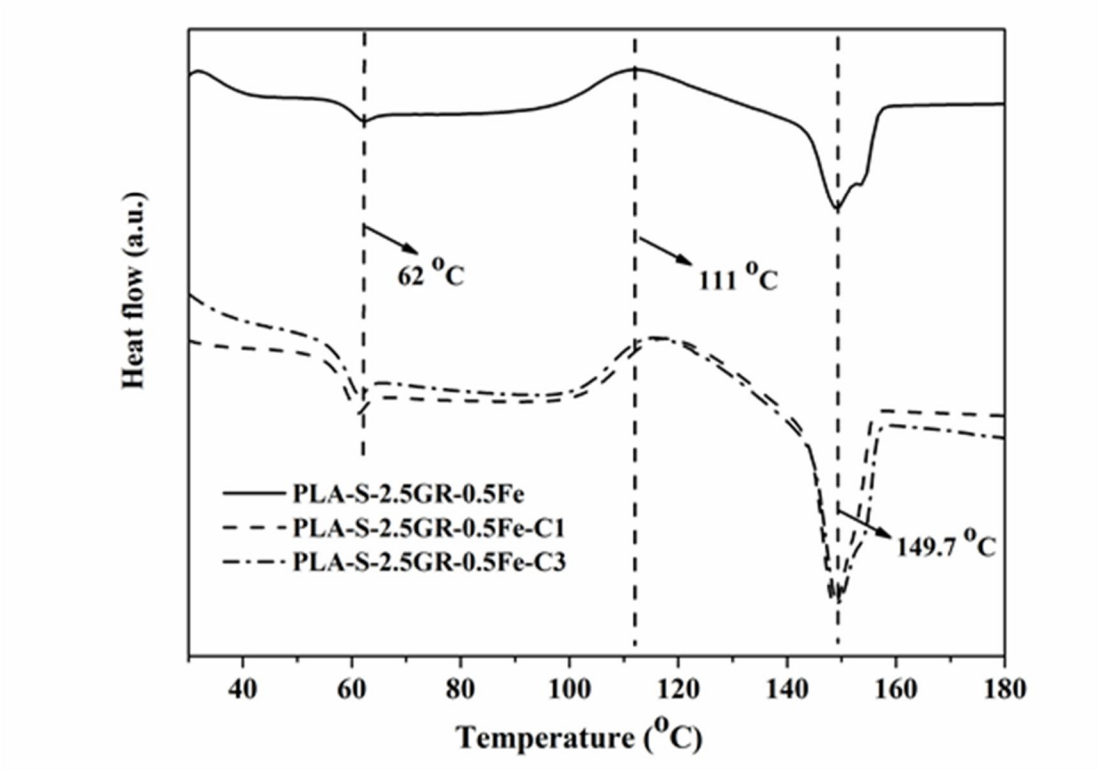

Fig. 5.14 DSC profile of PLA-S-2.5GR-0.5Fe, PLA-S-2.5GR-0.5Fe-C1 and PLA-S-2.5GR-0.5Fe-C3

Table 5.2 Thermal analysis data for PLA-S-2.5GR-0.5Fe, PLA-S-2.5GR-0.5Fe-C1 and PLA-2.5GR-0.5Fe-C3

Component	T_{onset} (°C)	$T_{50\%}$ (°C)	T_{max} (°C)	T_g (°C)	T_{cc} (°C)	T_m (°C)
PLA-S-2.5GR-0.5 Fe	347	359.8	367.5	62	111	149.7,153.5
PLA-S-2.5GR-0.5 Fe-C1	354	369	376	59	117.5	148.8, 153.8
PLA-S-2.5GR-1 Fe-C3	354	369	376	59	115	149, 153.8

5.3.7 Bio-sensor electrode

In view of better performances as seen in the previous sections, PLA-S-2.5GR-0.5Fe was further used in this work to examine the detection of D-glucose and Glycine. Response, selectivity and multiple cycle usage were also studied. However, cyclic voltammetry analysis was performed using thin films of the fabricated composites, PLA-S-2.5GR, PLA-S-2.5GR-0.5Fe and PLA-S-2.5GR-1Fe as working electrode. A Pt-electrode was used as a reference electrode and KCl- electrode as counter electrode. Results are presented in the form of current-voltage diagram.

D-glucose

Cyclic voltammetry analysis of D-glucose is showing one quasi-reversible I-V plot (Fig. 5.15 (a-d)). In applied voltage range of -1 to +1V in the working electrode, forward current (+1V applied to working electrode) through the circuit is always higher than the backward current (-1V applied to the working electrode). In both the forward and backward paths, current is proportional to the applied voltage when the working electrode potential is negative i.e. used as cathode. A non-linear but increasing relationship is observed when the working electrode potential is positive i.e. used as anode. The hysteresis observed between the forward and backward paths indicates voltage loss during the backward path i.e. applied working voltage from +1 to -1V. When the composite film electrode is converted as anode, in addition to the movement of electron, movement of the glucose molecules towards the anode also takes place because of the electronegative carboxyl oxygen getting attracted to the electropositive Fe present in the electrode. This, in turn, reduces the rate of electron movement resulting in lower current as compared to the case when the working electrode is used as cathode where only the movement of electron is present. Lower current during the backward path in the loop like position that is due to the hindrance offered by the

glucose molecules being concentrated near the working electrode during the forward path

In this case, glucose solution was used to study the repeatability of PLA-S-2.5GR-0.5Fe (Fig. 5.15a), the effect of scan rate variation (Fig. 5.15b), concentration variation (Fig. 5.15c), and use for multiple cycles (Fig. 5.15d). The films show repeatability in response while applied for same concentration of glucose. An increase in scan rate leads to increase in response current as the later is proportional to the scan rate square root. Change in concentration slightly changes the path that may help distinguishing samples of different concentrations. Multiple cycle applications follow the same path even after 10 cycles. For the same concentration of D-glucose (20 ppm), the response current is marginally higher for PLA-S-2.5GR-0.5Fe (Fig. 5.16). Thus, the study reveals that the fabricated composite can be used as electrode to detect the presence of D-glucose as well as distinguish the difference in concentration of glucose.

Glycine

Glycine was taken as a representative amino acid for the sensing analysis using PLA-S-2.5GR-0.5Fe composite. The scan rate for the analysis was kept at 0.0300 V/s since higher scan rate increases the noise. It can be seen from Fig. 5.17(a) that with increasing the concentration from 20 ppm to 80 ppm, the response of the composite film also changes especially in the voltage range of -1.00 V to -0.75 V. In case of consecutive 20 cross in the 20 ppm glycine solution, the film is stable similar to the case of D-glucose (Fig. 5.17(b)). The response of the composite is dependent on the stimuli subjected for analysis. Distinct I-V loop for D-glucose and Glycine can be seen from Fig. 5.17(c). It can be seen that the response current in case of glycine is much lower than that of glucose almost throughout the cyclic path. This can be attributed to the fact that amino acid can exhibit zwitterionic form where the carboxyl oxygen remains deprotonated

and amine group remains protonated. This deprotonated carboxyl oxygen has good affinity for metal ions such as Fe in the present case where there is a possibility of complexation between them (Djurdjevic et al., 1990). As a result, glycine molecules accumulate near the composite electrode surface resulting in hindrance to the free electron flow. This phenomenon becomes stronger when the composite film acts like an anode (+1V) that results in more suppression of current.

So, from the above studies, it can be concluded that PLA/GR/Fe-CNC composite based thin film electrode has the potential to apply for the detection of various biomolecules as well as measurement of different concentrations. During the application process, it generates current of different magnitude and also follows different paths for different cases. Development of a database of the patterns of the I-V curves can help to identify and sense various biomolecules and their concentrations by such composite. However, further sophistication with respect to casting of film and film uniformity are required for more precise and quantitative measurements as necessary for real-life application. In addition, depending upon literature established interactions between a biomolecule and metal ion, specific films of such biomolecules through such electrode sensor application studies are highly essential. The high thermal stability of the composite can be exploited to maintain proper thermophysical condition for the interaction desired.

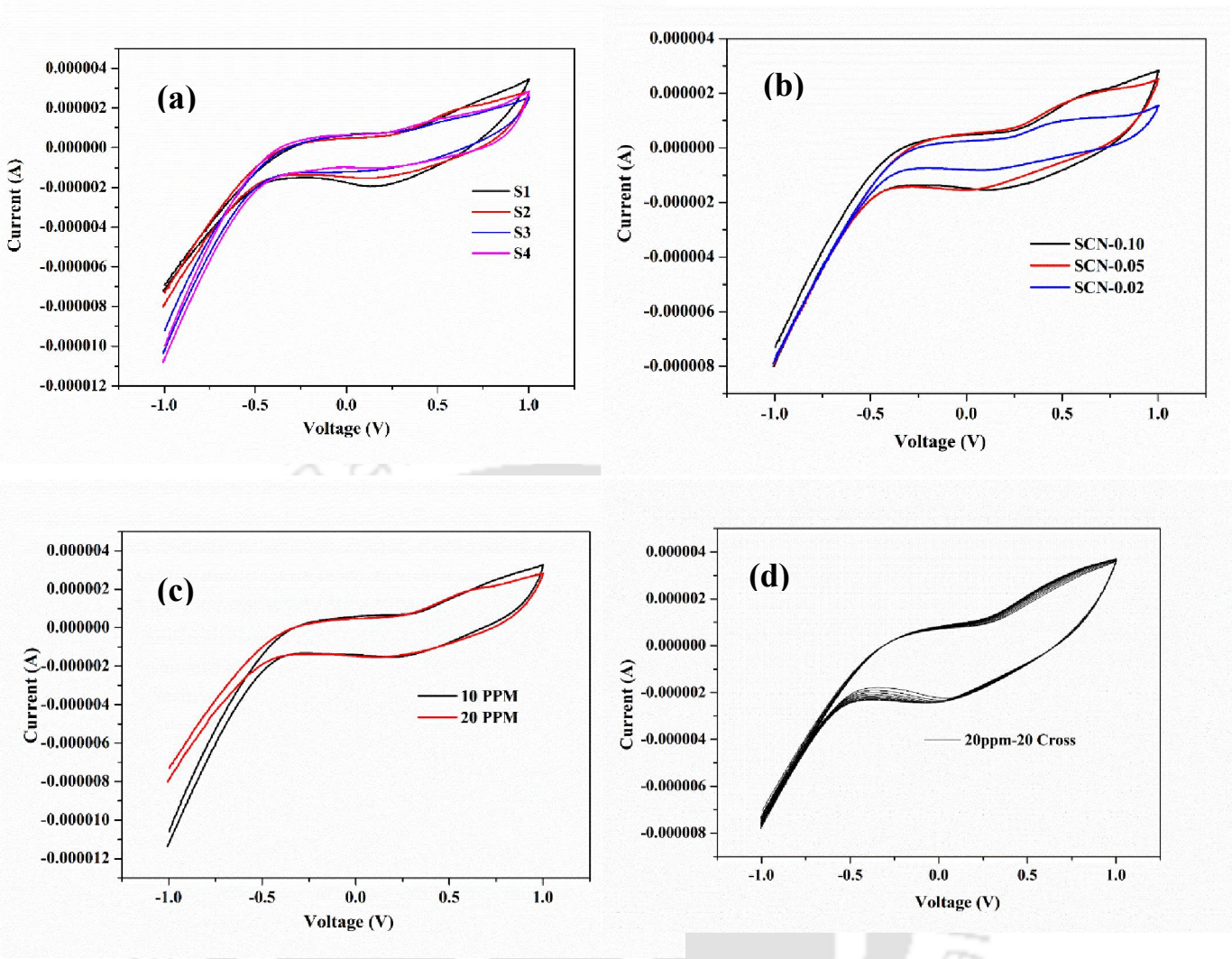

Fig. 5.15 (a) I-V response curve of PLA-S-2.5GR-0.5Fe in 20 ppm D-glucose for repeatability study, (b) I-V response curve of PLA-S-2.5GR-0.5Fe in 20 ppm D-glucose in different scan rate, (c) I-V response curve of PLA-S-2.5GR-0.5Fe in 20 ppm D-glucose in different concentration and (d) I-V response curve of PLA-S-2.5GR-0.5Fe in 20 ppm D-glucose for consecutive 10 cycle

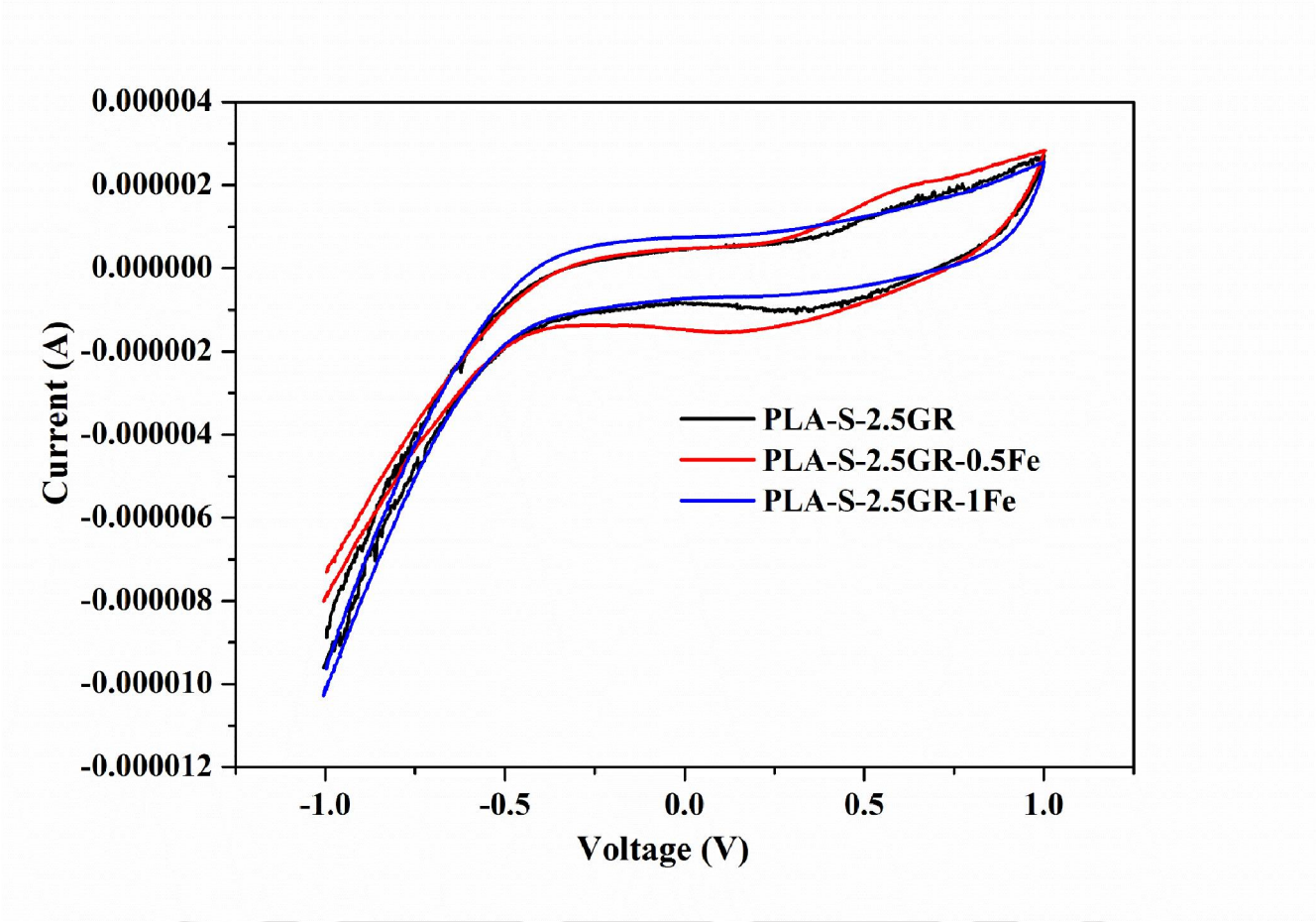

Fig. 5.16 I-V response curve of PLA-S-2.5GR, PLA-S-2.5GR-0.5Fe and PLA-S-2.5GR-1Fe in 20 ppm D-glucose

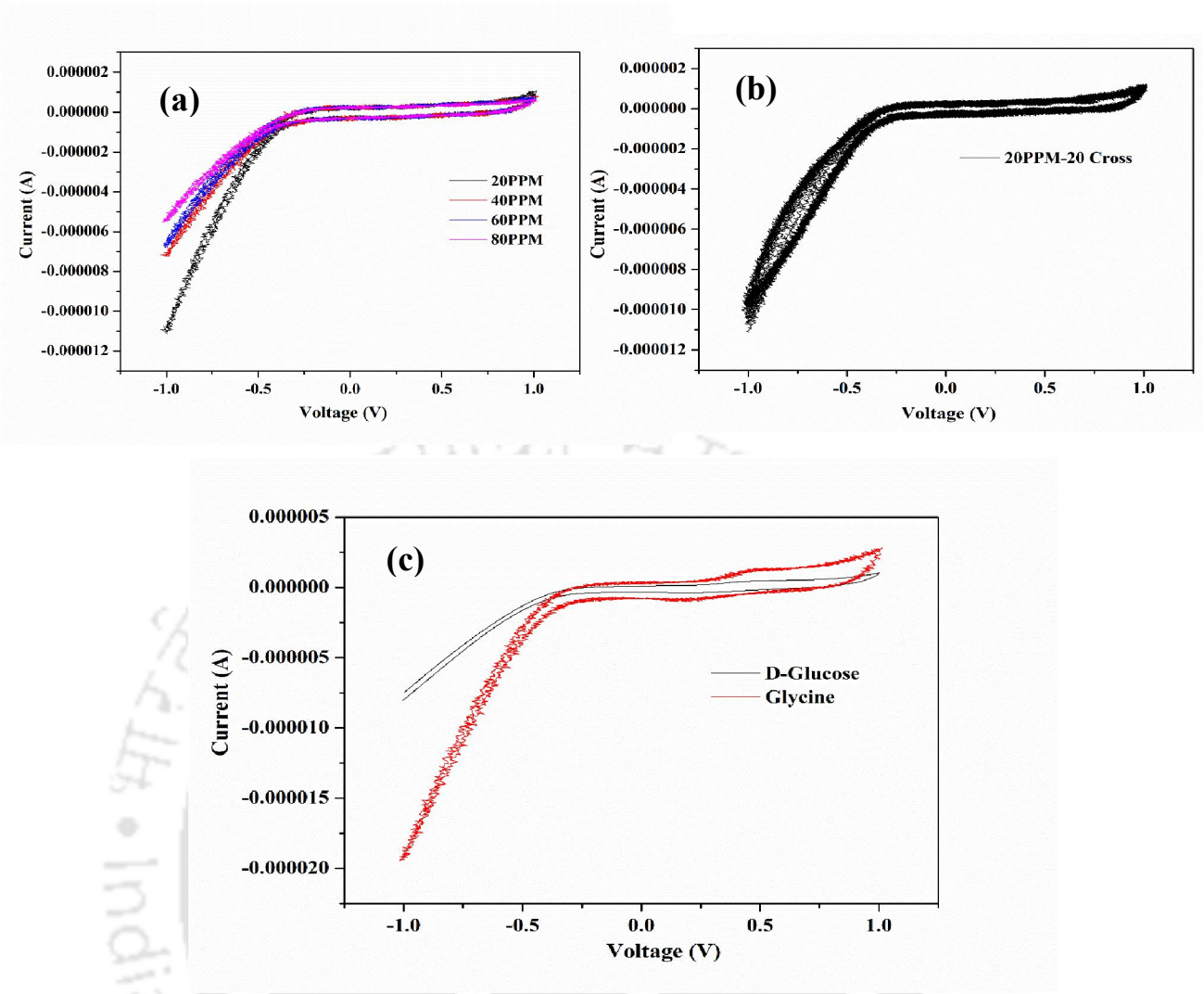

Fig. 5.17 I-V response curve of PLA-S-2.5GR-0.5Fe in different concentration of (a) glycine, (b) multiple cycle in 20 ppm glycine and (c) comparison between 20 ppm D-glucose and glycine

5.4 Summary

In this present study, PLA, GR, and Fe-CNC were utilized to fabricate composite by solution casting approach. Fe-CNC was added to the optimized PLA-S-2.5GR composite to improve the sensing capability of PLA/GR composite for ethanol as well as biomolecules like D-glucose and glycine.

Firstly, the optimization of Fe-CNC loading was done by taking two different loading of Fe-CNC i.e. 0.5 wt. % of Fe-CNC (PLA-S-2.5GR-0.5Fe) and 1 wt. % Fe-CNC (PLA-S-2.5GR-1Fe). FESEM and mapping analysis showed better dispersion and less agglomeration in case of PLA-S-2.5GR-0.5Fe. The results of DMA and TGA analysis indicated that PLA-S-2.5GR-0.5Fe has better mechanical strength and comparable thermal stability. Impedance analysis of all the samples reveals that by incorporation of Fe-CNC, conductive network is not altered. Thus, considering above findings, PLA-S-2.5GR-0.5Fe turns out to be the better composite.

Finally, thin polymeric films of PLA-S-2.5GR-0.5Fe were used for electrochemical sensing of ethanol, D-glucose and glycine. In the case of ethanol sensing, the films were used as sensing element between two probes. D-glucose and glycine detection studies were carried out imparting the film possibly the first time as a working electrode of a three-electrode system. PLA-S-2.5GR-0.5Fe showed better response towards 25% ethanol detection. It reflects that incorporation of Fe-CNC increased the driving force of ethanol diffusion and thus change in response is higher. Stability analysis of the composite film after use also confirmed the ethanol diffusion through composite film and also indicated that the films are stable even after used for third cycles. The performance of the composites was also found to be repeatable, reusable and consistent. D-glucose and Glycine sensing studies showed that the PLA-S-2.5GR-0.5 Fe film has selectivity and sensitivity toward these components. Difference in the I-V response during cyclic voltammetry analysis could be explained from the aspect of interaction between electrode material and biomolecule. Thus, appropriate selection of metallic filler followed by fabrication of the composite and sensing study with proper thermo-physical condition can effectively and efficiently be applied for various types of biomolecules.

Chapter 6

Enrichment of PLA/GR Nanocomposites by Suitable Additives for the Detection of Metal Ions

Abstract

This chapter attempts the fabrication of thin-film based metal ion sensor, where bio-based thermoplastic polymer, PLA is used as matrix because of its mechanical strength and casting ease. Detection of copper ion as representative metal ion is aimed in this work. Graphene (GR) was used as reinforcement material to impart high conductivity in the PLA composite due to its high mechanical strength, thermal stability and electrical conductivity. A comparison of concentration detection with commercial conductivity meter was also carried out. Dependency of current in different metal ions and different anionic environment was also studied. Different materials such as EDTA, albumin and silk nanocrystal (SNC) having bonding property with metal ions were also incorporated into the PLA/GR system in order to improve the sensitivity and selectivity towards copper ion chosen for this work. Basic characteristics like morphology, thermal stability, crystallization property and dynamic mechanical strength of the composite films were investigated before use as sensor. I-V characteristics indicate the presence of peak current for different cases based on the binder. Peak current is found to be increased with concentration of copper.

Graphical abstract

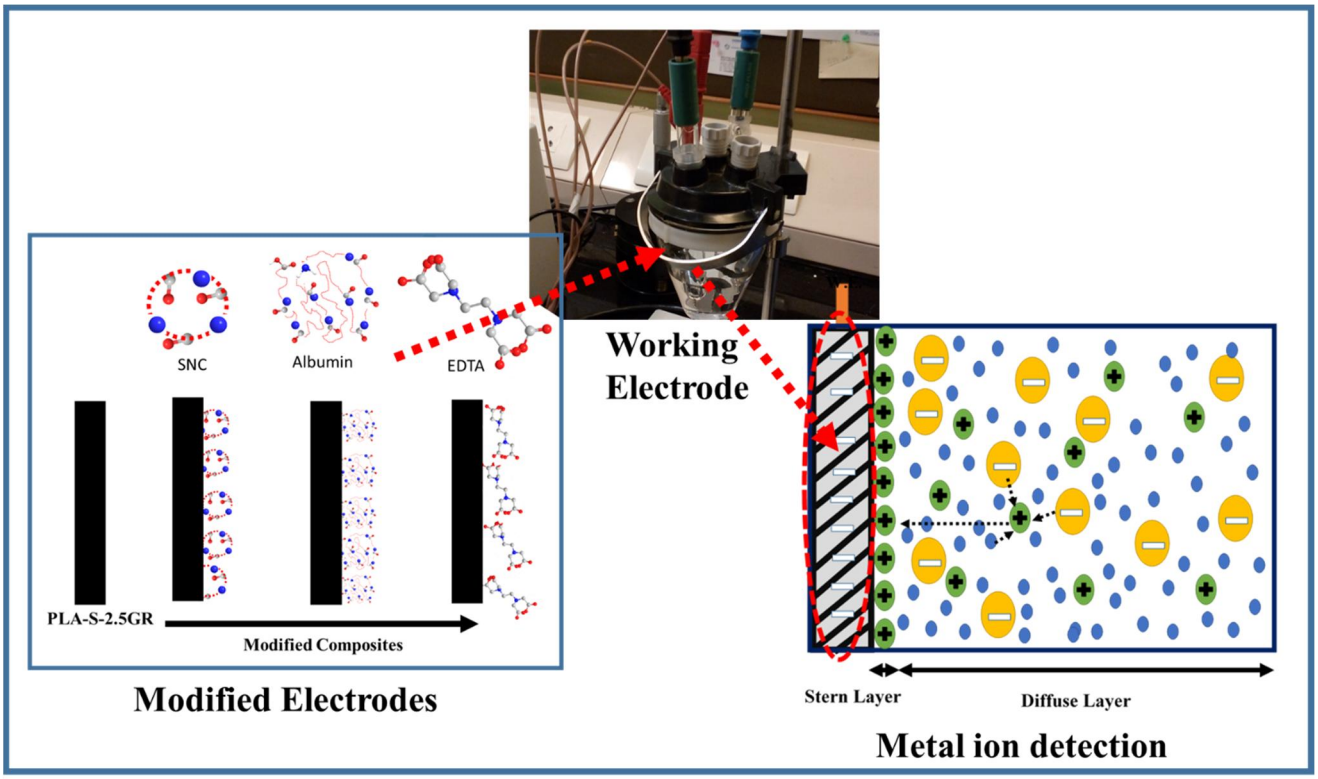

6.1 Introduction

Waterbody pollution by micropollutants like metal ions is increasing with increase of effluents from different industries such as fertilizer, cosmetics, and other chemical plants. Metal ions do not decompose and have tendency to accumulate inside living organisms, which causes various diseases and disorders (Bansod et al., 2017). Thus, regular detection and monitoring of concentration of these metal ions in the water body is absolutely necessary. Hence, development of highly sensitive and selective materials for accurate detection of metal ions is required for different aqueous samples like natural water, drinking water, biological samples, etc. (Gao et al., 2016; Jing et al., 2016; Long et al., 2013).

Electrochemical analysis is recognized as one of the sensitive methods for detection of metal ions. Surface treatment of solid electrodes followed by selective metal ion sensing are being investigated by several groups. Conductive polymers like polypyrrole and polyaniline were also utilized as electrode material (Tamm et al., 1998). Heitzmann et al. (2007) used oxidative electropolymerization technique to prepare polymer coated electrodes for electrochemical detection of Cu (II), Pd (II) and Cd (II) ions. Ethylenediaminetetraacetic (EDTA) based derivatives, which possess excellent metal binding property was incorporated in the polymerization stage. Pre-structured poly (EDTA-like) electrode material was reported to have good affinity towards Cu (II) ions (Heitzmann et al., 2007). Tamm et al., (1998) used polypyrrole film separately doped with sulfate, naphthalene-2-sulphonate and naphthalene-1, 5-disulphonate to detect various cations by potentiometric measurement. Cyclic voltammetry response was found to be dependent on the nature of the dopant as well as the cation (Tamm et al., 1998).

Though bio-based polymers like polylactic acid (PLA), cellulose, chitosan are nowadays lucrative for conductivity driven applications because of their comparable strength, casting ease, bio-compatibility and biodegradability (Feig et al., 2018; Khalid et al., 2018; McKeon et al., 2010), most of them are not conductive in nature to be used as sensor. Therefore, necessary modification of this polymers are required either by blending with conductive polymers like polyaniline, polypyrrole (Huang et al., 2008; Rajeswari et al., 2013) or by reinforcing different conductive fillers like graphene, graphene oxide, carbon nanotube (Pötschke et al., 2010; Sabzi et al., 2013; Shen et al., 2012). Biodegradable conductive composites are utilized in variety of applications like capacitor, biomedical application, and sensor applications. Electrochemical sensing and biosensing are the emerging areas of applications of these types of materials. Kumar et al., (2012) fabricated PLA/CNT based conductive polymeric sensor for organic vapours. Relative change in response was found to be dependent on the interaction parameters between PLA and the organic molecules (Kumar et al., 2012). Han et al., (2013) utilized PLA based conductive composites for ethanol sensing and in chapter 5 of the thesis PLA based conductive composites were used as biosensor. In particular to the metal ion detection study both the conductive nature and selectivity towards ions are essential requirements for a sensor (Han et al., 2013). The organic molecules such as EDTA, albumin and silk nanocrystal (SNC)(Tesfaye et al., 2016) have metal-binding capability, which can be explored to impart selectivity in a sensor for detection of metal ions (Heitzmann et al., 2007). Labanowski et al., (2008) studied metal ion extraction using EDTA and observed good binding capability of EDTA towards Cu (Labanowski et al., 2008). Sundberg et al., (1974) utilized functionalized EDTA for specific binding of metal ions. Sokolowska et al., (2002) used human and bovine serum albumin terminal binding sites for Cu (II) and observed indication for binding of metal

ion with the N-terminal sites of the albumins. Kruck et al., (1976) designed serum albumin for binding of Cu and reported increment of binding capacity by 3 times as compared to albumin.

The work of this chapter attempts the fabrication of thin-film based metal ion sensor, where bio-based thermoplastic polymer, PLA is used as matrix because of its mechanical strength and casting ease. Detection of copper ion as representative metal ion is aimed in this work. Exfoliated graphene (GR), which is having high mechanical strength, thermal stability, and electrical conductivity is used as reinforcement material to impart high conductivity in the PLA/GR composite. Previously optimized GR loading of 2.5 wt. % as discussed in chapter 5 is used for the current study. The fabricated nanocomposite is first used as an electrode to examine its potential to detect various metal ions namely, Cu^{2+}, Mg^{2+}, Fe^{3+}, Zn^{2+} and Co^{2+}. Thereafter, in order to improve the selectivity and sensitivity towards such metal ions, the PLA/GR nanocomposite was modified with different materials such as EDTA, albumin and silk nanocrystal (SNC) having bonding property with metal ions. Copper (II) ion is chosen as representative metal ion for this extended study. Finally, the detection performance of the thus improvised nanocomposite is explained through mechanistic analysis. Prior to application of the composite films as sensor material the basic characteristics like morphology, thermal properties and mechanical strength were examined.

6.2 Materials and Methods

6.2.1 Materials

PLA of density 1.24 g/cm^3 and M_n 150000 (2003D) supplied by Nature Works LLC, USA was exploited for fabrication of films. Considering conducting behaviour of graphene exfoliated graphene EXG 750 (GR) (Valapa et al., 2015a) was reinforced into

the PLA matrix to impart conductive nature. SISCO research laboratories was supplied other required chemicals such as copper chloride, ferric chloride, zinc chloride, magnesium chloride, copper sulphate, albumin, EDTA for this study. Silk nanocrystal (SNC) used for this work was lab synthesized from muga silk (Tesfaye et al., 2016).

6.2.2 Experimental Section

6.2.2.1 Modification of PLA/GR nanocomposites for metal ion detection

In order to fabricate modified PLA/GR composite with additives for metal ion detection, 2.5 mg. of Albumin, EDTA and SNC was added separately to the mixture of the solutions mentioned in Chapter 4 (4.2.2) for preparation of PLA/GR composite by solution casting. Then the solution was casted for the respective film preparation, namely PLA-S-2.5GR-0.5Alb (0.5 wt. % albumin), PLA-S-2.5GR-0.5EDTA (0.5 wt. % EDTA) and PLA-S-2.5GR-0.5SNC (0.5 wt. % SNC).

6.2.3 Characterization

6.2.3.1 XRD analysis

Instrument details and operating conditions are mentioned in Chapter 2.

6.2.3.2 Morphological analysis

Instrument details and operating conditions are mentioned in Chapter 4.

6.2.3.3 FTIR analysis

Instrument details and operating conditions are mentioned in Chapter 2.

6.2.3.4 Thermal stability analysis

Instrument details and operating conditions are mentioned in Chapter 4.

6.2.3.5 DSC analysis

Instrument details and operating conditions are mentioned in Chapter 4.

6.2.3.6 DMA

Instrument details and operating conditions are mentioned in Chapter 2.

6.2.3.7 Impedance analysis

Instrument details and operating conditions are mentioned in Chapter 4.

6.2.3.8 Metal ion sensing study

In order to investigate the detection of metal ions by using the composites three-electrode system was used (Fig. 6.1). The composite strip of dimension 5cm×5mm×0.1mm was taken as working electrode for the present study. Pt-electrode and saturated 3(M) KCl solution were utilized as reference and counter electrodes, respectively. Current-Voltage (I-V) response of the films were carried out by setting start potential at -1.00 V and stop potential at -1.00 V (upper vertex potential was 1.00 V, lower vertex potential was -1.005 V, step potential was 0.00200 and scan rate was 0.1000 V/s). Effect of concentration of the ions in the I-V response was examined in the concentration range of 100-5 ppm of the ions. Effect of scan rate, effect of multiple cycle was examined for 20 ppm solution. Selectivity of the organic metal binders was compared using 20 ppm Cu solution as reference at 0.1000 V/s scan rate.

For PLA-S-2.5GR composite one comparison of performance between the results of Autolab and commercial conductivity meter (VSI Electronics PVT.Ltd.) was studied by taking 25ppm, 50ppm, and 70ppm Cu solution as unknown samples. Before such comparison study calibration curves were drawn for both the cases with the help of known ion concentrations.

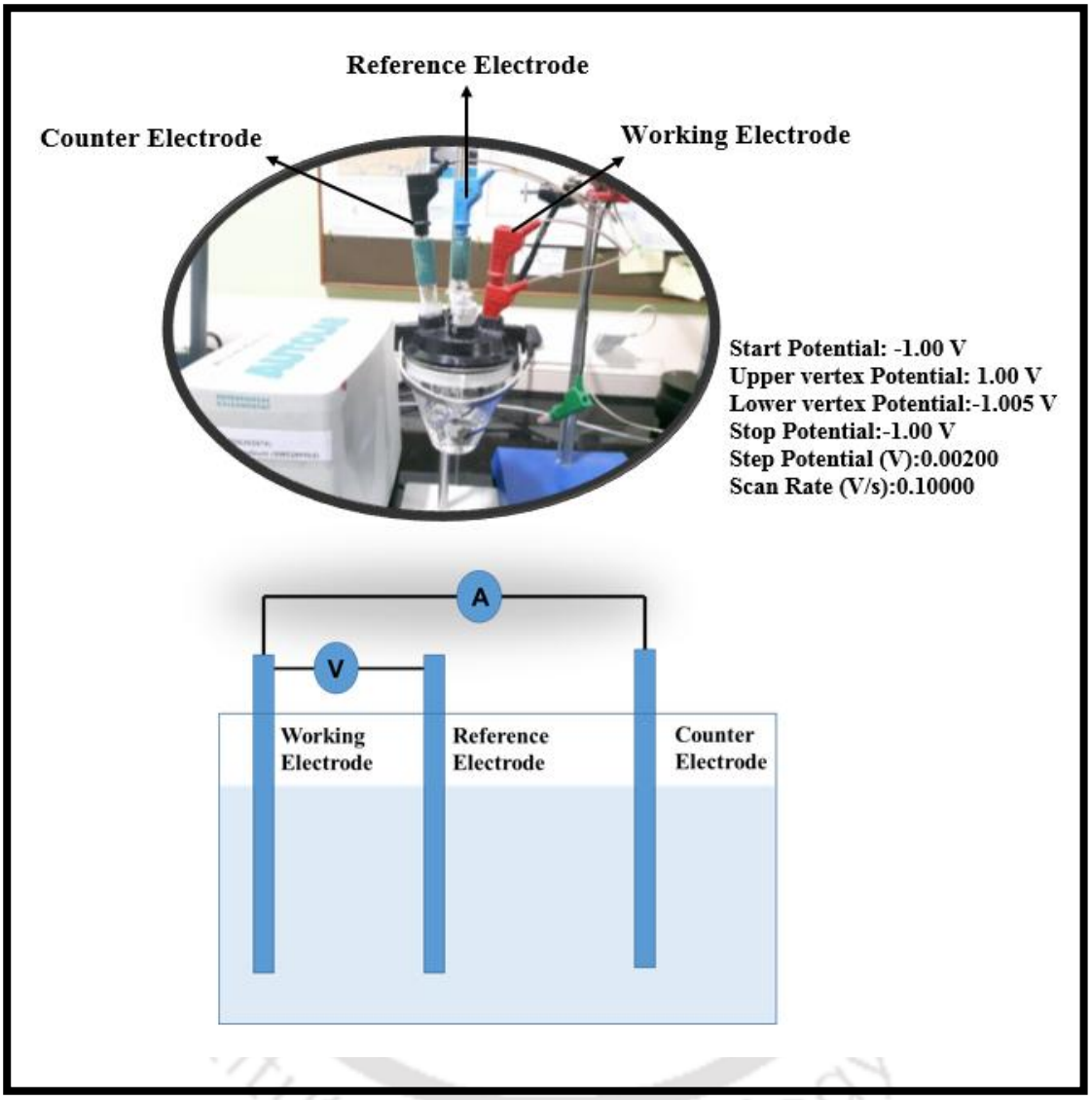

Fig. 6.1 Three electrode experimental setup for metal ion sensing

6.3 Results and Discussion

6.3.1 XRD analysis

The crystallographic nature of the composites before and after protein modification was investigated from X-ray diffraction pattern analysis. Fig. 6.2 reveals the presence of 2θ=26.6º in all the composites PLA-S-2.5GR, PLA-S-2.5GR-0.5Alb, PLA-S-2.5GR-0.5SNC, and PLA-S-2.5GR-0.5EDTA, indicating the presence of graphitic plane (002) corresponding to GR (Valapa et al., 2015a). The peaks corresponding to 16.5º and 19º are indicative of (110)/ (200) and (203) planes of PLA. The major peak at ~16º is due to α-crystal form of PLA (Tripathi & Katiyar, 2016a). The uniformity of diffraction pattern for all the composites reveals that after the incorporation of EDTA, SNC and albumin the crystal nature of PLA/GR system remains unaltered.

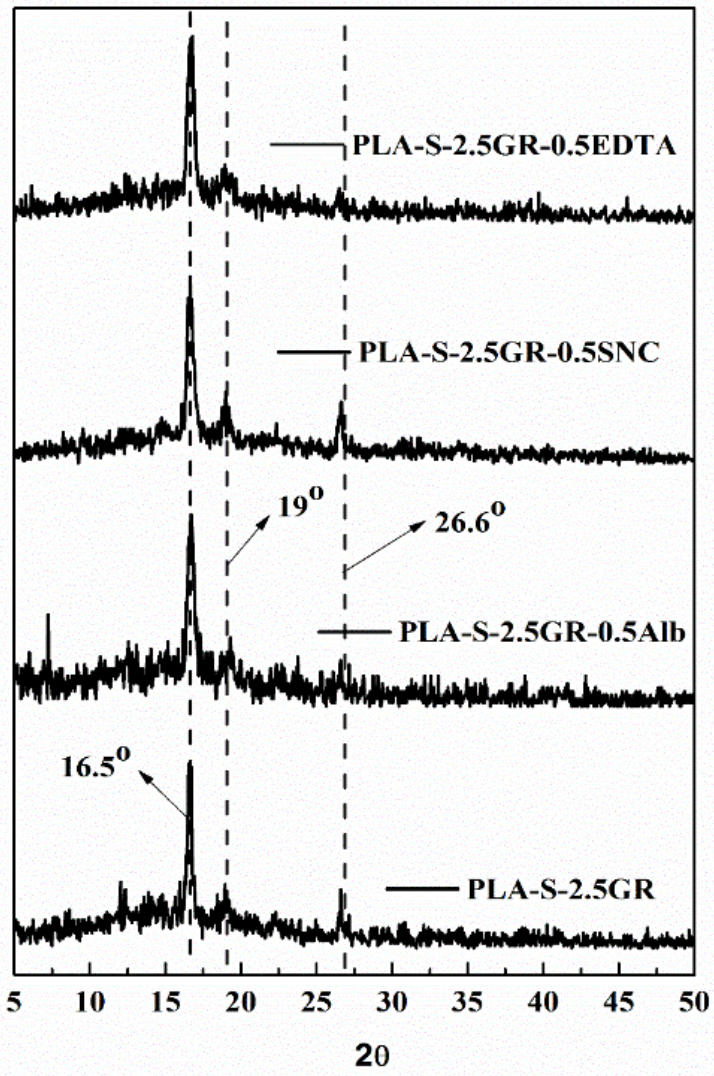

Fig. 6.2 XRD profile of PLA-S-2.5GR, PLA-S-2.5GR-Alb, PLA-S-2.5GR-EDTA and PLA-S-2.5GR-SNC nanocomposites

6.3.2 Morphological analysis

The distribution of graphene and additives (EDTA, SNC, and albumin) inside the PLA matrix for PLA-S-2.5GR, PLA-S-2.5GR-0.5Alb, PLA-S-2.5GR-0.5EDTA, and PLA-S-2.5GR-0.5SNC can be seen from FESEM images displayed in Fig. 6.3 (a-d), respectively. The presence of the additive molecules are shown by red circle and arrow in the respective images. The layer like morphology of GR is present in the composites. The distribution of EDTA (Fig. 6.3b) and SNC (Fig. 6.3c) is more uniform as compared to albumin (Fig. 6.3d). The hydrophobic nature of SNC possibly facilitates its

dispersion inside PLA matrix. Smaller size of EDTA and the possible ionic interaction between EDTA and PLA unit might have promoted the distribution of EDTA inside PLA matrix (Baran et al., 2002). However in case of albumin, the inherent protein character restricted the uniform mixing, which creates agglomerate cites inside the matrix (Furlan et al., 2007).

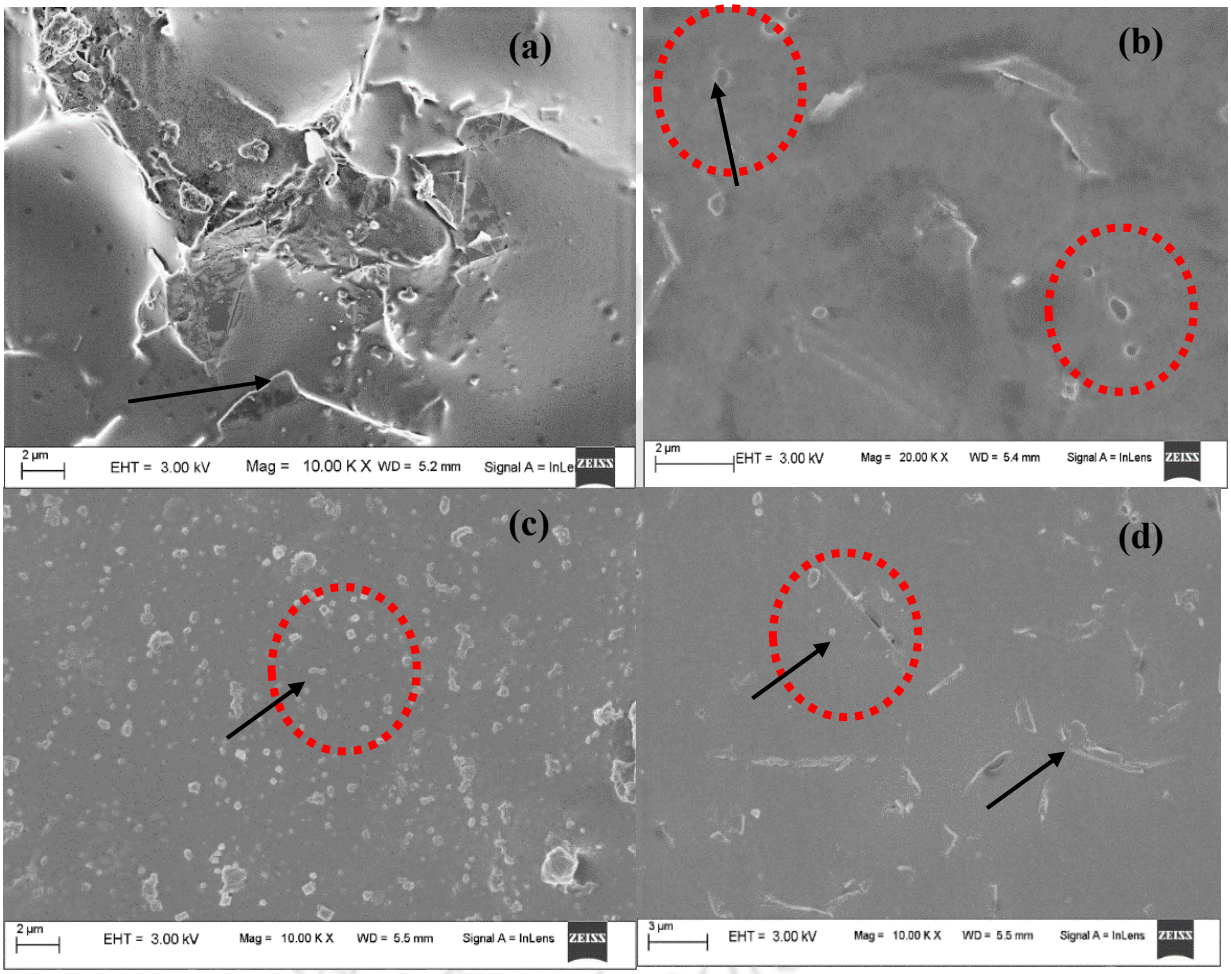

Fig. 6.3 FESEM images for (a) PLA-S-2.5GR, (b) PLA-S-2.5GR-Alb, (c) PLA-S-2.5GR-EDTA and (d) PLA-S-2.5GR-SNC nanocomposites

6.3.3 FTIR analysis

The structural vibration nature of the composites PLA-S-2.5GR, PLA-S-2.5GR-0.5Alb, PLA-S-2.5GR-0.5EDTA, and PLA-S-2.5GR-0.5SNC were examined by FTIR analysis (Fig. 6.4). Peaks corresponding to 1749 cm^{-1}, 1355 cm^{-1} and 1455 cm^{-1} and 1080 cm^{-1}

and 1183 cm^{-1} indicate stretching of C=O,C-CH_3 and C-O bonds, respectively which is similar to the structural vibration of PLA (Tripathi & Katiyar, 2016a). The presence of these peaks for all the composites reveals structural similarity among the composites (Fig. 6.4). In case of PLA-S-2.5GR-0.5EDTA, structural vibration of EDTA molecule consists of vibrations of -OH, -NH and C=O. The vibrations of -OH and -C=O bonds are superimposed with the similar vibrations of the bonds present in PLA. The observed higher intensity of the –C=O peak at 1752 cm^{-1} for PLA-S-2.5GR -0.5EDTA with respect to PLA-S-2.5GR is the result of the same. This indicates the presence of more free –COO sites in the component (Tripathi & Katiyar, 2016a). Peaks corresponding to 1515 cm^{-1}, 1533 $cm^{-1,}$ and 1653 cm^{-1} are indicative of –N-H vibration, C-N vibration and amide C=O vibration for albumin (Abrosimova et al., 2016; Mahobia et al., 2016). For the composite PLA-S-2.5GR-0.5Alb the above-mentioned peaks correspond to PLA and albumin are present, representing the reinforcement of albumin into PLA matrix.

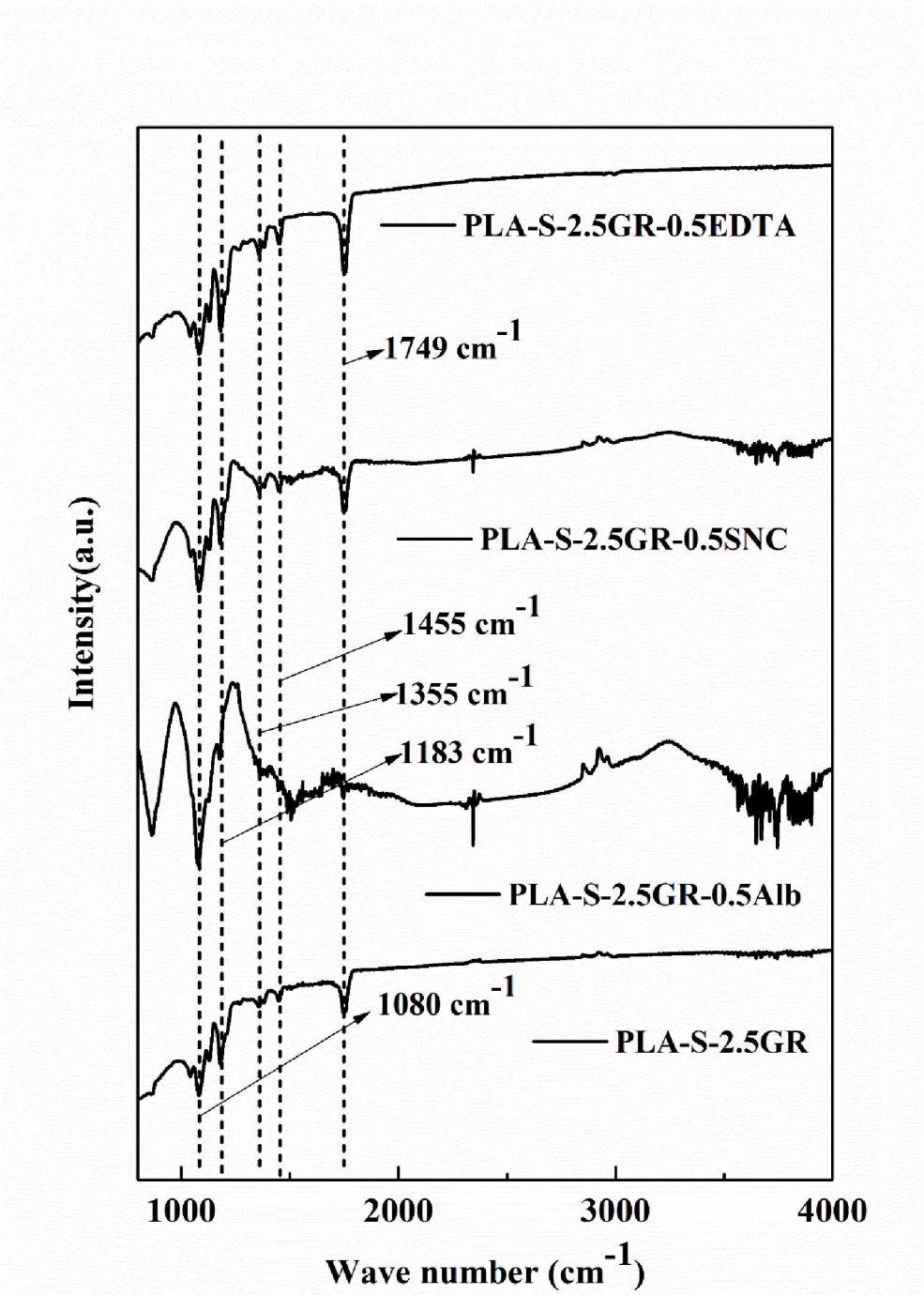

Fig. 6.4 FTIR images for PLA-S-2.5GR, PLA-S-2.5GR-Alb, PLA-S-2.5GR-EDTA and PLA-S-2.5GR-SNC nanocomposites

6.3.4 TGA

The thermal stability of the composites was investigated from the data of weight loss and derivative weight loss (DTG) obtained using thermogravimetric analyzer (TGA) for PLA-S-2.5GR, PLA-S-2.5GR-0.5Alb, PLA-S-2.5GR-0.5EDTA, and PLA-S-2.5GR-0.5SNC samples. Fig. 6.5 depicts the degradation behaviour of the prepared

nanocomposites. It can be seen from Table 6.1 that upon incorporation of additives, the thermal stability of the composites decreases. Decrement in onset degradation temperature is higher for PLA-S-2.5GR-0.5Alb (345.6 ºC) as compared to PLA-S-2.5GR (360 ºC) system. Temperature of 50% degradation (T_{50}) and maximum degradation temperature (T_{max}) are also found to be decreasing with the incorporation of EDTA, SNC, and albumin in the PLA/GR system. Stability of the SNC incorporated composite is relatively better as compared to that of the other two modified composites. Amongst the three composites with additives studied in this work, thermal stability of PLA-S-2.5GR-0.5SNC is though less but closer to PLA-S-2.5GR when these are subjected to high temperature. This could be as discussed elsewhere (section 6.3.2) because of good dispersion of SNC and better compatibility between PLA and SNC due to hydrophobic characteristics of SNC. The decrease in thermal degradation is the maximum in case of PLA-S-2.5GR-0.5Alb corroborating the fact of non-compatibility and agglomeration as mentioned earlier. However, stability of the composites is much higher as compared to that of PLA (Valapa et al., 2015a). This is due to barrier effect of GR (layer like morphology) towards gaseous products after degradation (Valapa et al., 2015a).

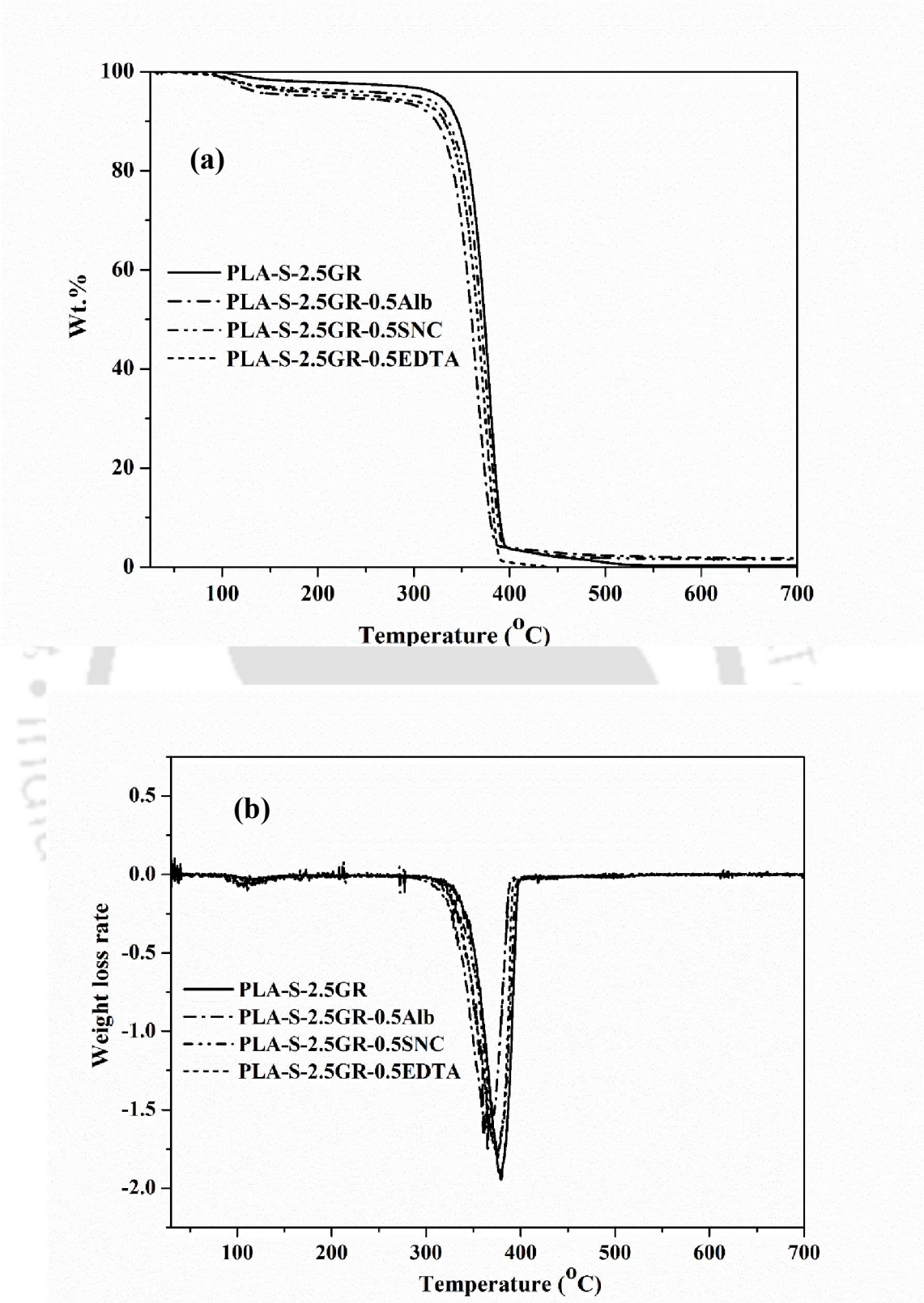

Fig. 6.5 (a) TGA and (b) DTG plot for PLA-S-2.5GR, PLA-S-2.5GR-Alb, PLA-S-2.5GR-EDTA and PLA-S-2.5GR-SNC nanocomposites

Table 6.1 Thermal analysis data of PLA-S-2.5GR, PLA-S-2.5GR-0.5Alb, PLA-S-2.5GR-0.5EDTA, PLA-S-2.5GR-0.5SNC nanocomposites

Components	T_{onset} (ºC)	T_{50} (ºC)	T_{max} (ºC)	T_g (ºC)	T_{cc} (ºC)	T_m (ºC)
PLA-S-2.5GR	360	373.9	378.9	63	119	151
PLA-S-2.5GR-0.5EDTA	354.8	366.7	374.9	61	121	151
PLA-S-2.5GR-0.5SNC	356.5	370.6	376.5	62	116	151,155
PLA-S-2.5GR-0.5Alb	345.6	360.2	365.3	62	115	151,155

6.3.5 DSC analysis

Differential scanning calorimetric investigation of the composites was carried out to investigate the chain folding behavior of PLA in the PLA/GR system in the presence of the additives, EDTA, SNC and albumin for PLA-S-2.5GR-0.5EDTA, PLA-S-2.5GR-0.5SNC and PLA-S-2.5GR-0.5Alb, respectively with respect to PLA-S-2.5GR. Figure 6.6 depicts the influence of the different components towards the chain relaxation of PLA for the composites. Table 6.1 conveys a comparative representation of thermal behavior of the composites. Secondary relaxation behavior (glass transition temperature) is found to be unaltered even after incorporation of the additives into the system. The marginal decrement in crystallization temperature in case of SNC and albumin maybe because of the hindrance effect of protein chains towards the chain folding of PLA (Tripathi & Katiyar, 2016a). In case of PLA-S-2.5GR-0.5EDTA crystallization temperature is marginally improved to 121 ºC from 119 ºC, which may be due to nucleation effect of EDTA (Battegazzore et al., 2011a). The presence of shouldering in the melting peak of the PLA-S-2.5GR-0.5SNC and PLA-S-2.5GR-0.5Alb is noticed indicating the presence of both primary and secondary crystal (Pal & Katiyar, 2016).

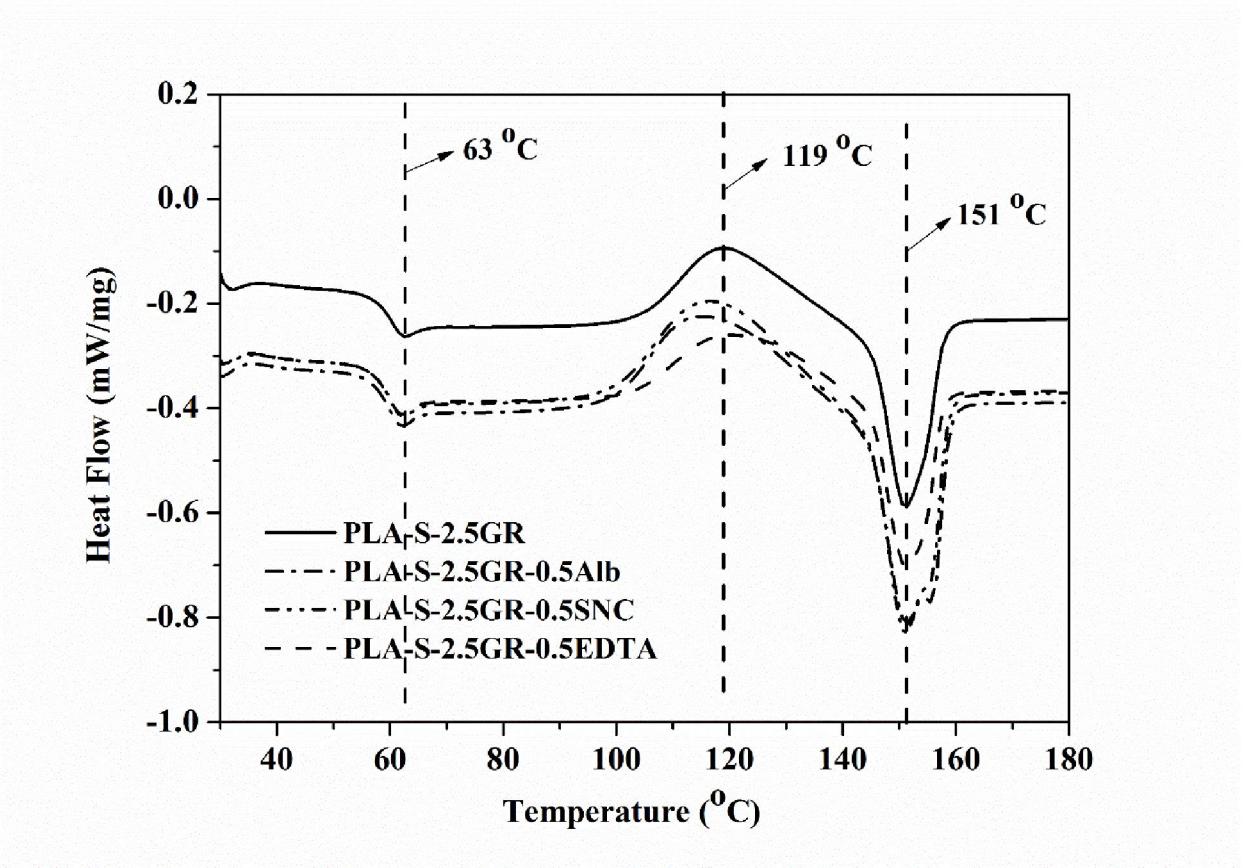

Fig. 6.6 DSC plot of PLA-S-2.5GR, PLA-S-2.5GR-0.5Alb, PLA-S-2.5GR-0.5EDTA, PLA-S-2.5GR-0.5SNC nanocomposites

6.3.6 DMA

DMA is one of the major thermal analysis technique for materials to know about the deformation nature under a constant load when subjected to change in temperature within the viscoelastic domain. From Fig. 6.7, it can be seen that storage modulus (E′) value is decreased upon incorporation of additives EDTA, SNC and albumin. At 40 ºC, E′ values are 2473.58 MPa, 2326.42 MPa, 2166.98 MPa and 1308.49 for PLA-S-2.5GR, PLA-S-2.5GR-0.5EDTA, PLA-S-2.5GR-0.5Alb and PLA-S-2.5GR-0.5SNC, respectively. At the temperature of 70 ºC, (above the glass transition temperature, i.e., ≥63ºC in the present case, Table 6.1) the storage modulus is slightly higher for PLA-S-2.5GR-0.5EDTA (222.64 MPa) and PLA-S-2.5GR-0.5Alb (124.53) as compared to PLA-S-2.5GR (50.94 MPa) and PLA-S-2.5GR-0.5SNC (50.94 MPa). This again establishes good compatibility between PLA and SNC, which is less in case of PLA-

EDTA and PLA-albumin systems. Tan δ value, which is due the branch relaxation behavior of the composites, shows a maximum at 61 ºC for PLA-S-2.5GR, PLA-S-2.5GR-0.5Alb, and PLA-S-2.5GR-0.5SNC. However in case of PLA-S-2.5GR-0.5EDTA, it shows the maximum at 65 ºC. This may be because of EDTA being highly branched compound makes branch relaxation faster compared to other additives.

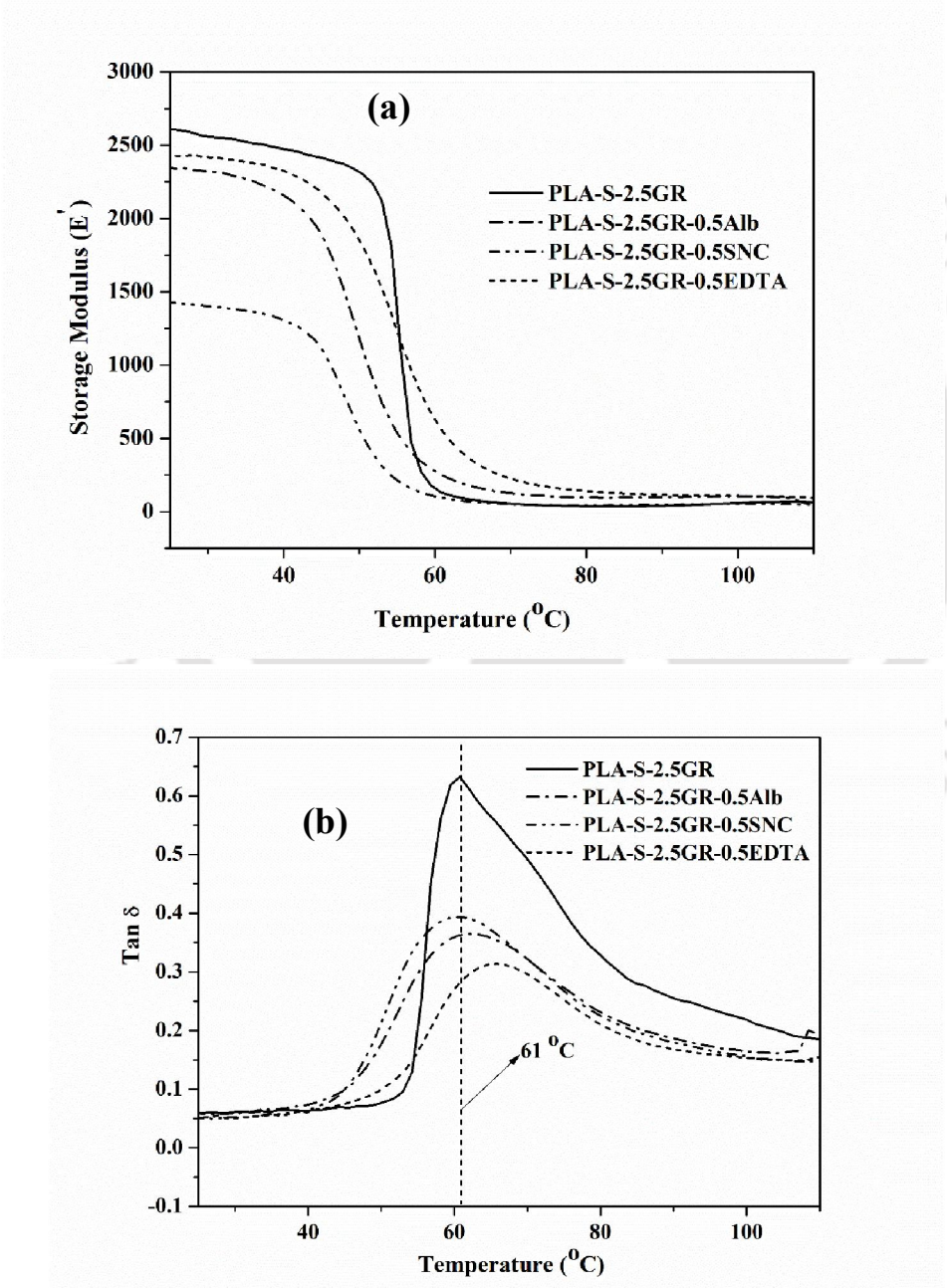

Fig. 6.7 DMA plot of PLA-S-2.5GR, PLA-S-2.5GR-0.5Alb, PLA-S-2.5GR-0.5EDTA and PLA-S-2.5GR-0.5SNC nanocomposites

6.3.7. Impedance analysis

Frequency response analysis (Potentiostatic) was conducted for the composites PLA-S-2.5GR, PLA-S-2.5GR-0.5Alb, PLA-S-2.5GR-0.5EDTA, and PLA-S-2.5GR-0.5SNC in order to get the impedance values. In chapter 4 of the thesis optimization of GR loading was carried out and 2.5 wt. % loading was selected for ethanol sensing because of stable network. In this work, effect of the additives like EDTA, SNC and albumin on the present networks of GR inside the PLA matrix was examined. It can be seen from Fig. 6.8 that the impedance response is resistive in nature and similar to that of PLA-S-2.5GR. However, the value of impedance decreases upon incorporation of additives. At 0.1 Hz frequency, the impedance values are 18770, 12129, 11034 and 10204 Ω for PLA-S-2.5GR, PLA-S-2.5GR-0.5SNC, PLA-S-2.5GR-0.5EDTA and PLA-S-2.5GR-0.5Alb, respectively. This indicates that electrical mobility of the composite system is substantially enhanced upon incorporation of the additives because of the ionic nature of the compounds.

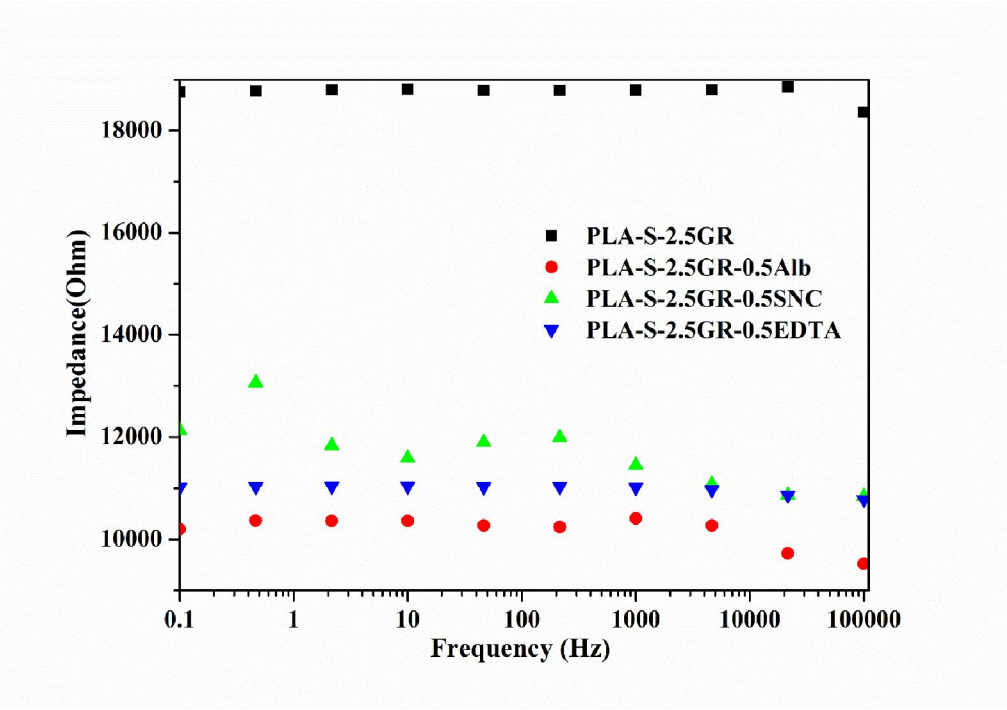

Fig. 6.8 Impedance plot of PLA-S-2.5GR, PLA-S-2.5GR-0.5Alb, PLA-S-2.5GR-0.5EDTA and PLA-S-2.5GR-0.5SNC nanocomposites

6.3.8 Metal ion detection

This section discusses the results of detection experiments for various metal ions using different composites fabricated in the present work. First of all, the performance of fabricated composite PLA-S-2.5GR as electrode (using Autolab) is compared with that of commercial conductivity meter where different concentrations of $CuCl_2$ solution (5-100 ppm) was used for both the cases. Secondly, results of PLA-S-2.5GR based electrode for detection of various metal ions are analyzed. Thereafter, impact of different anions in the electrolyte solution is examined using same PLA-S-2.5GR based electrode. This section also discusses the repeatability of such results. It also examines the changes in response, if any upon variation of the scan rate. Finally, performances of the composites with additives EDTA, SNC and Albumin are compared for detection of a representative metal ion, Cu (II) in the present case. An attempt is made to substantiate the results through mechanistic analysis

Comparison of performance between PLA-S-2.5GR (Autolab) and conductivity meter

This sub-section discusses the performance comparison study between conventional conductivity meter and Autolab using PLA-S-2.5GR. $CuCl_2$ solution of concentration rangeing between 5 to 100 ppm was taken in this regard and I-V study was done for eleven concentrations within the range selected for the study. The I-V response for different concentrations of Cu^{2+} shows a hysteresis between forward and backward path of the working electrode in the voltage range of -1.0 V to +1.0 V (Fig. 6.9). With increase in voltage and also concentration of Cu^{2+}, current is more till a voltage of 0.75V. After applying positive voltage when the working electrode is performing as anode, the Cu^{2+} ions move more towards the reference electrode acting as cathode. Then, particularly for higher concentrations of Cu^{2+} and after applied voltage of 0.75V

or above, there is a sharp drop of current. This could be because of accumulation of Cu^{2+} near the reference electrode due to high voltage, which in effect retards the Cu^{2+} movement towards the anode and thus reduces the current substantially. This again can be understood from the slow decrease in current for relatively lower concentration of Cu^{2+} for the same applied voltages. In addition, this accumulation reduces the backward current compared to forward current when the voltage is started decreasing from +1.0 V to 0.0 V. This, in turn, makes the hysteresis loop. FESEM image of PLA-S-2.5GR (Fig 6.10) indicates formation of Cu layer over PLA-S-2.5GR, which reveals the formation of stern layer over the composite. These findings establish the fact that PLA-S-2.5GR is acting as electrode material with similar characteristics of metal or glassy carbon electrode. In order to compare the functionality of the PLA-S-2.5GR, conductivity of the same solutions were also estimated by using conventional conductivity meter (Fig. 6.11a).The conductivity is found to increase linearly with increasing concentration of Cu^{2+}. From I-V response analysis (Fig. 6.9) taking 0.5V as reference voltage the corresponding currents for different concentrations of Cu^{2+} are plotted in Fig. 6.11b (Feier et al., 2015). It is found that with an increase in the concentration of Cu^{2+}, current through the working electrode (PLA-S-2.5GR) also increases linearly. Prediction of unknown concentration in the range (5-100 ppm) by both the cases is compared through Fig. 6.12, where 25, 50 and 70ppm solutions were considered as unknown concentrations. Fig. 6.12 clearly indicates that PLA-S-2.5GR predicts the Cu^{2+} concentration very well and at par with the results obtained from the conventional conductivity meter. This establishes the fact that PLA-S-2.5GR has the potential to sense and precisely detect Cu^{2+} ion.

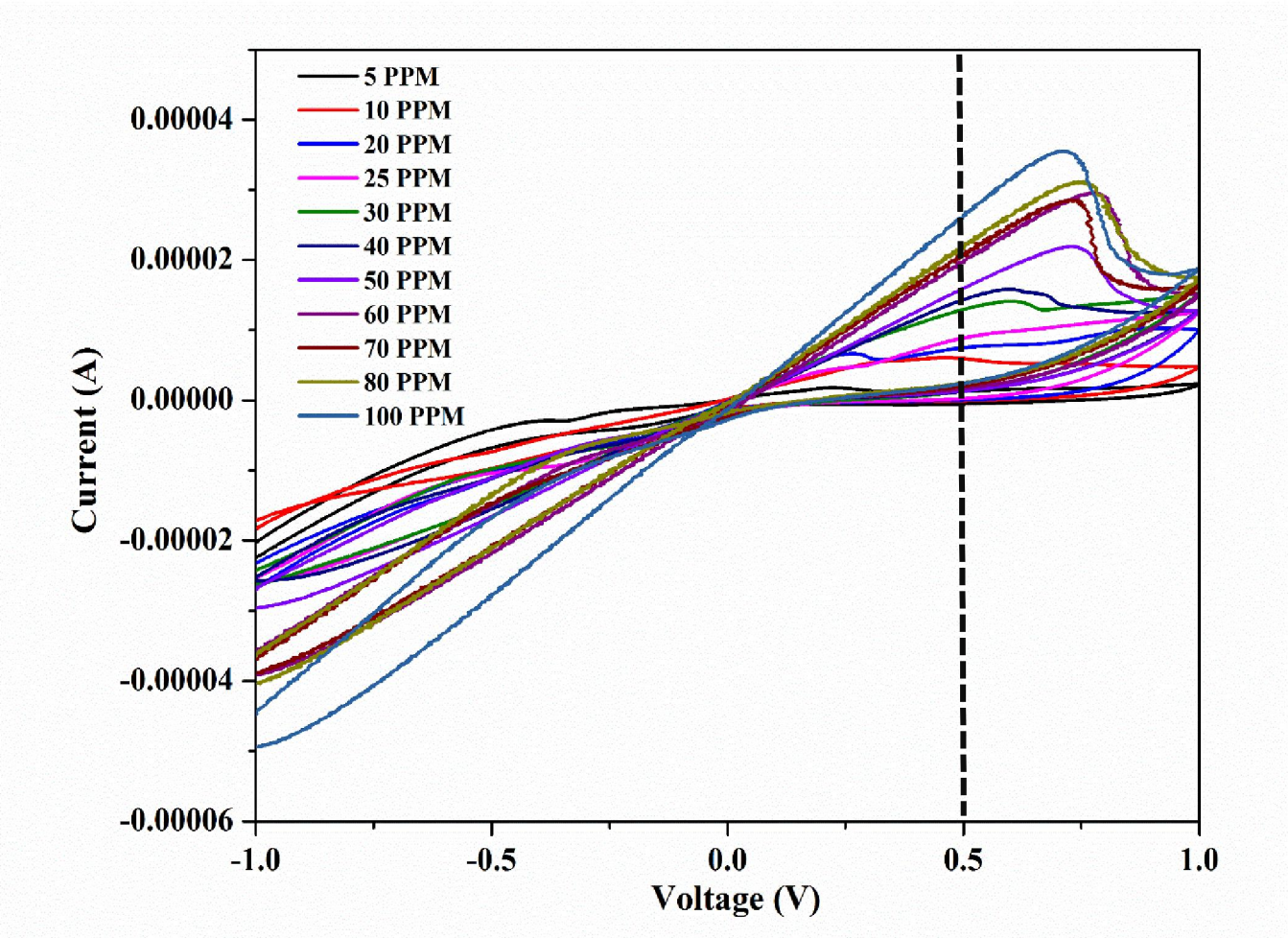

Fig. 6.9 Copper ion detection by PLA-S-2.5GR (Autolab)

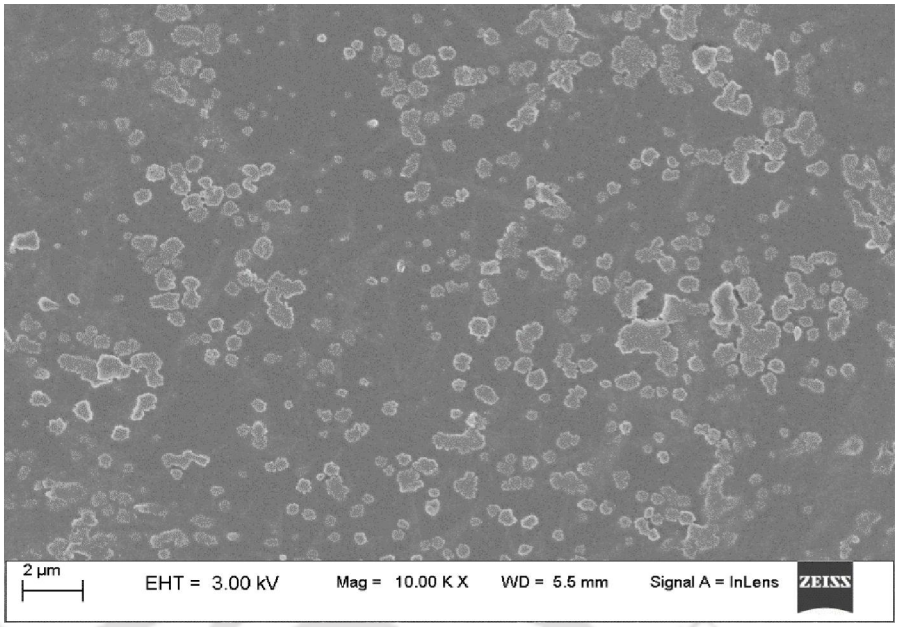

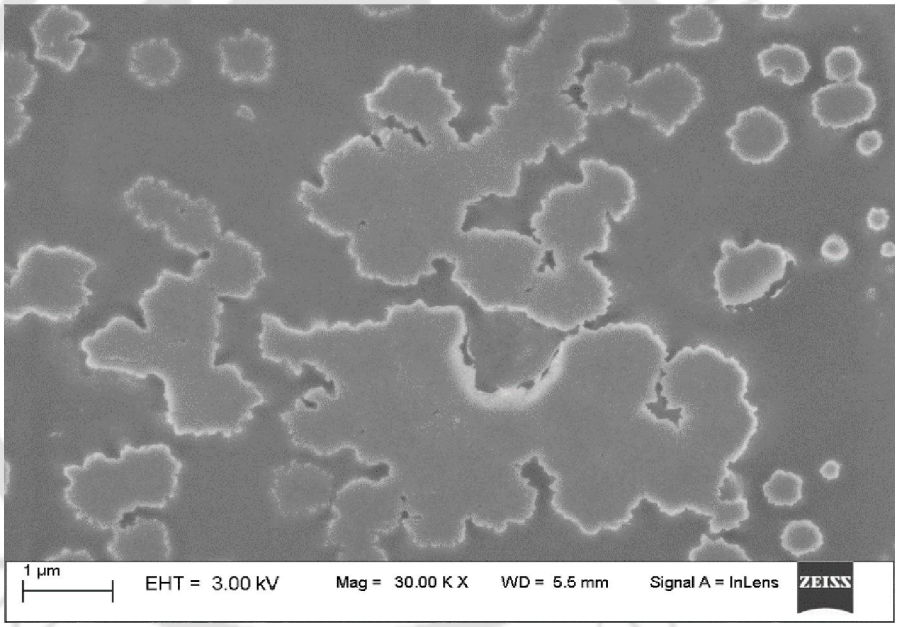

Fig. 6.10 FESEM images of PLA-S-2.5GR after dipping in Cu solution (Different magnification)

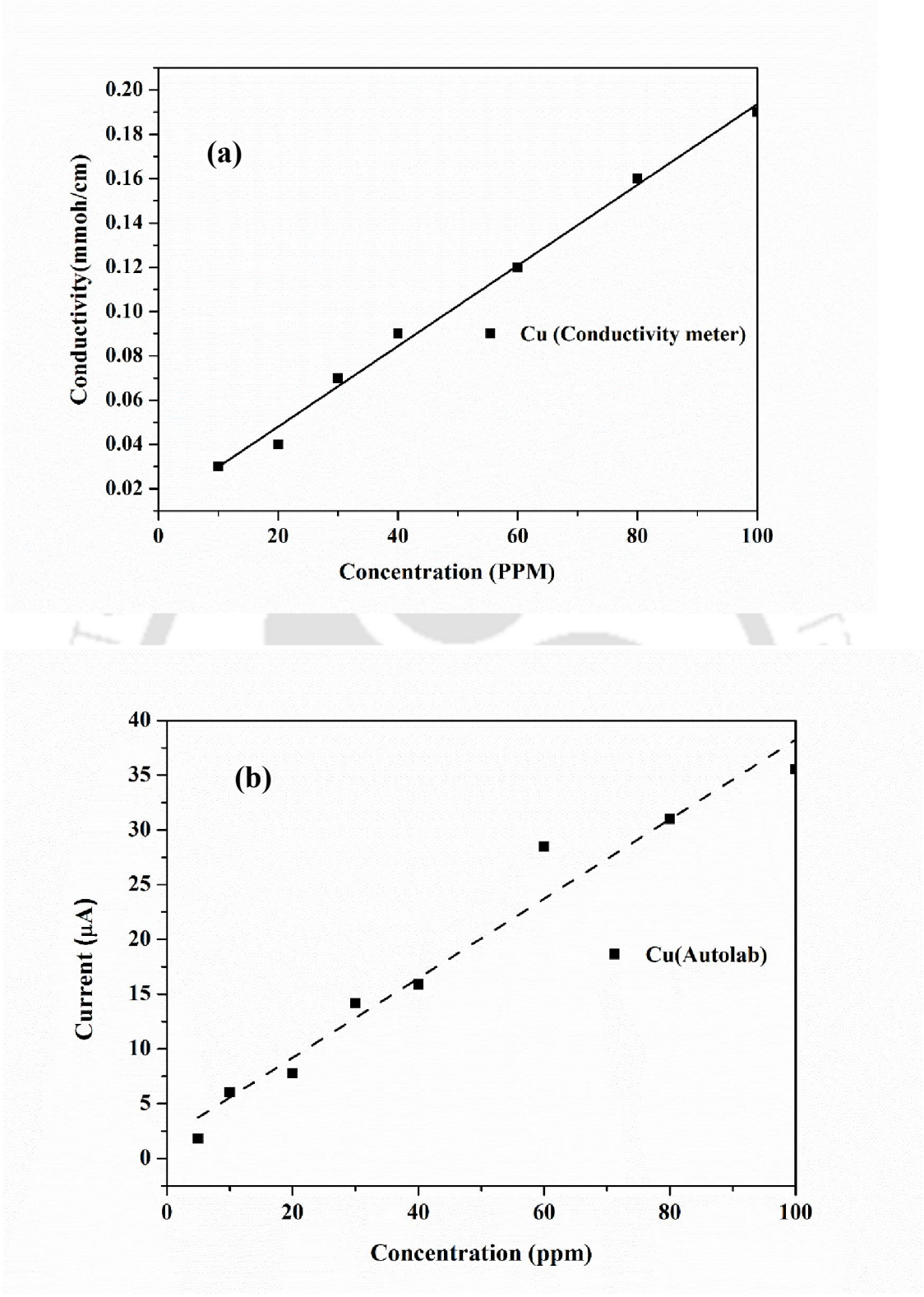

Fig. 6.11 Copper ion calibration plot in conductivity meter and Autolab (PLA-S-2.5GR)

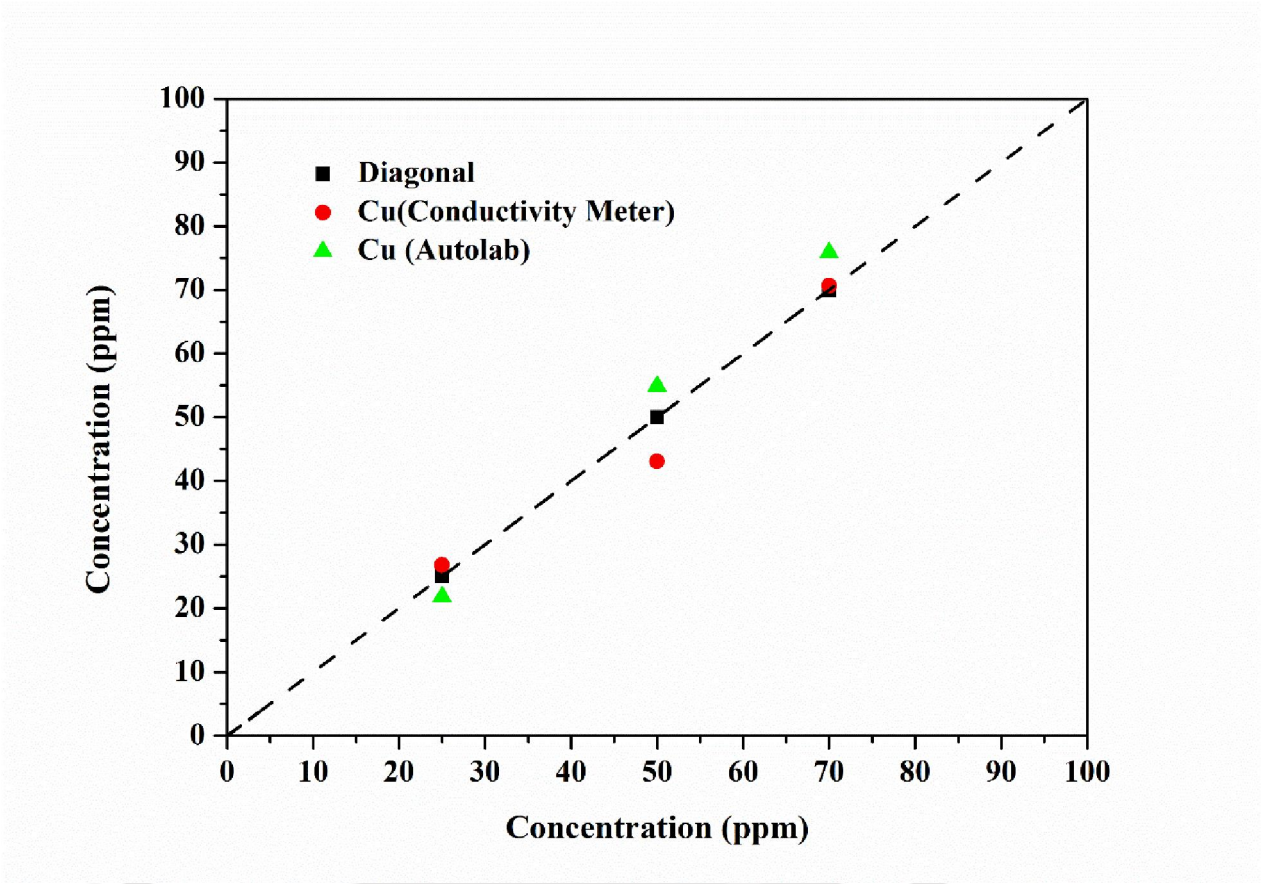

Fig. 6.12 Comparison of concentrations (25, 50 and 70 ppm $CuCl_2$ solution) in conductivity meter and Autolab (PLA-S-2.5GR)

Detection of other metal ion

In order to examine the effect of cation on the I-V response of PLA-S-2.5GR, chloride salts of metal ions Mg, Zn, Co, Fe were tested along with Cu of 25 ppm concentration within the voltage range of -0.5V to +0.5V. It can be seen from Fig. 6.13 that electrode response pattern of PLA-S-2.5GR is dependent on the type of the metal ion. All the cases of metal ions show hysteresis loop indicating quasi-reversible phenomena and possibly of diffusion-controlled electrode process. The current for a particular applied voltage, the pattern and the width of the hysteresis loop are different for the different metal ions. The conductivity of the working electrode is different for various metal ions depending on their effective charge and mobility (Heitzmann et al., 2007). The analysis

of the results so obtained i.e. variation in conductivity can be exploited to distinguish and detect the different metal ions. This, in turn, establishes the immense potential of application of PLA-S-2.5GR based electrode as a sensor for metal ion detection.

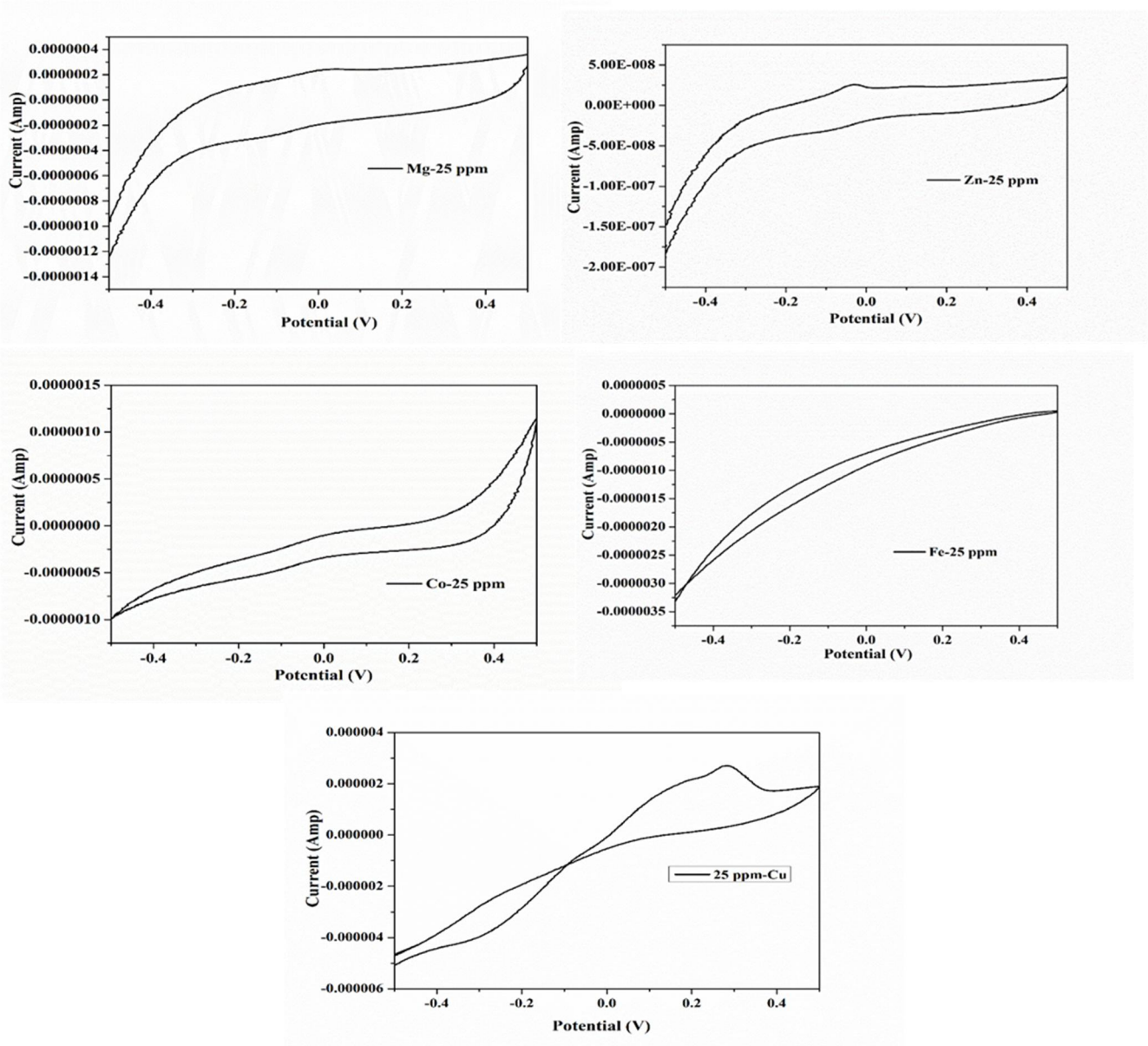

Fig. 6.13 Effect of metal ion on PLA-S-2.5GR

Impact of different anions

The working electrode current depends on the electron flow from bulk ions to the stern layer. Thus anionic environment of the metal ions also influences the electromobility of the electrode. In order to examine this fact, the chloride and sulfate salt of Cu of different concentrations were subjected as stimuli for PLA-S-2.5GR. The concentrations of 20 ppm, 40 ppm and 60 ppm of Cu salt were studied for both the cases. From Fig. 6.14 it can be noticed that with an increase in the concentration from 20 ppm to 60 ppm, current increases for both the cases. However, hysteresis loop pattern is found to be dependent on the anion environment around Cu. SO_4^{2-} being more electronegative compared to Cl^- reduces the effective electro positivity of the Cu^{2+}. It causes more loss in current between the forward and backward path. Thus, different anions provide distinguishing I-V response for the metal ion. Hence, the change in anionic part of the metallic compound doesn't prohibit the use of the composite as electrode material for sensing and detecting metal ions.

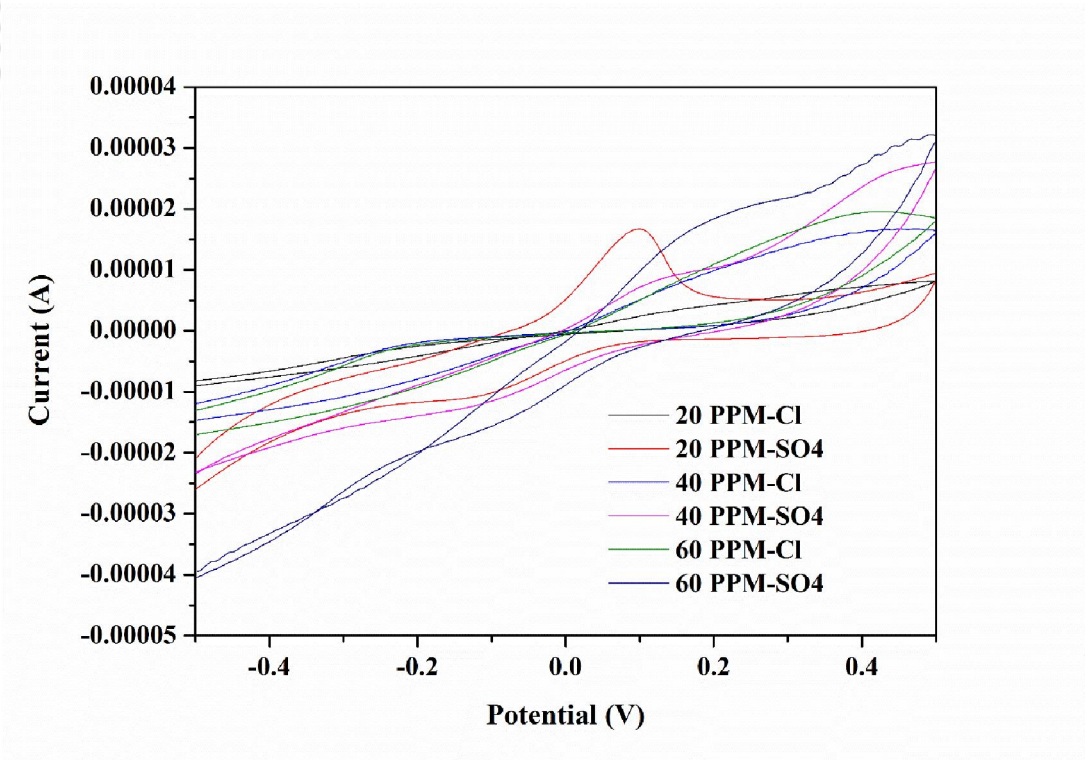

Fig. 6.14 Effect of anions on PLA-S-2.5GR

Repeatability Study

Response analysis of PLA-S-2.5GR from different batch samples was carried out to examine the repeatability of I-V response within same voltage range for 20 ppm solution of $CuCl_2$. It can be seen from Fig. 6.15a that same batch samples (S-1, S-2) are showing similar I-V response. Whereas for different batch samples (S_1/S_2, S_3) little variation in response is found which could be due to possible variation in dispersion during casting and associated experimental error. The repeatability of same sample for 10 consecutive cycles suggests that I-V response remains unaltered even after 10 cycles (Fig. 6.15b).

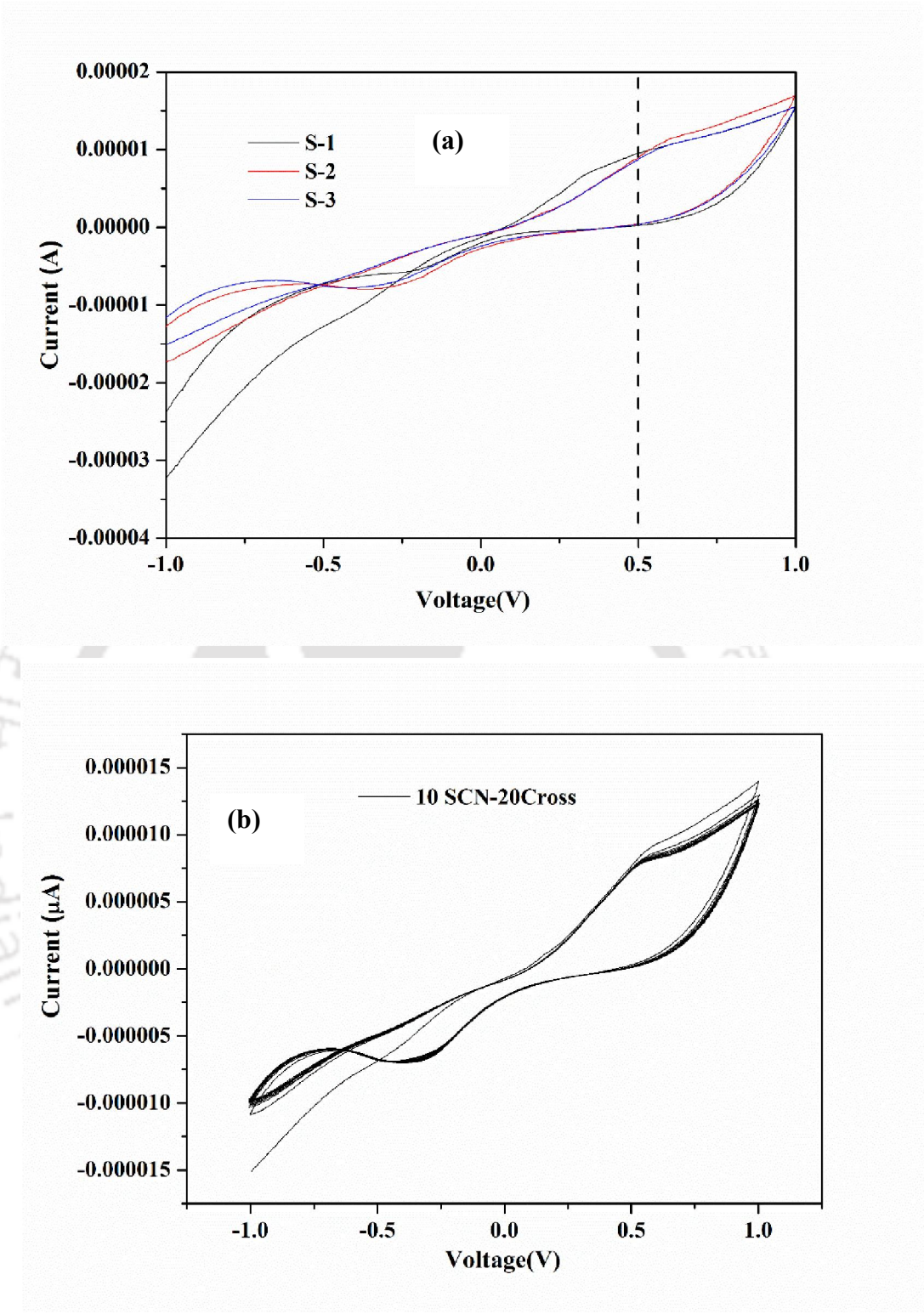

Fig. 6.15 (a) Repeatability analysis of different batch sample and (b) Repeatability analysis of the same sample for 10 consecutive cycle

Scan rate variation study

The impact of scan rate (ν) on the current-voltage (I-V) response of the PLA-S-2.5GR electrode was investigated in different scan rate varying from 0.1000 to 0.0400 V/s. It is found that over the domain, current is proportional to the square root of scan rate (Feier et al., 2015) (Fig. 6.16) and root mean square (r-square) value as 0.99 is indicative of little variance.

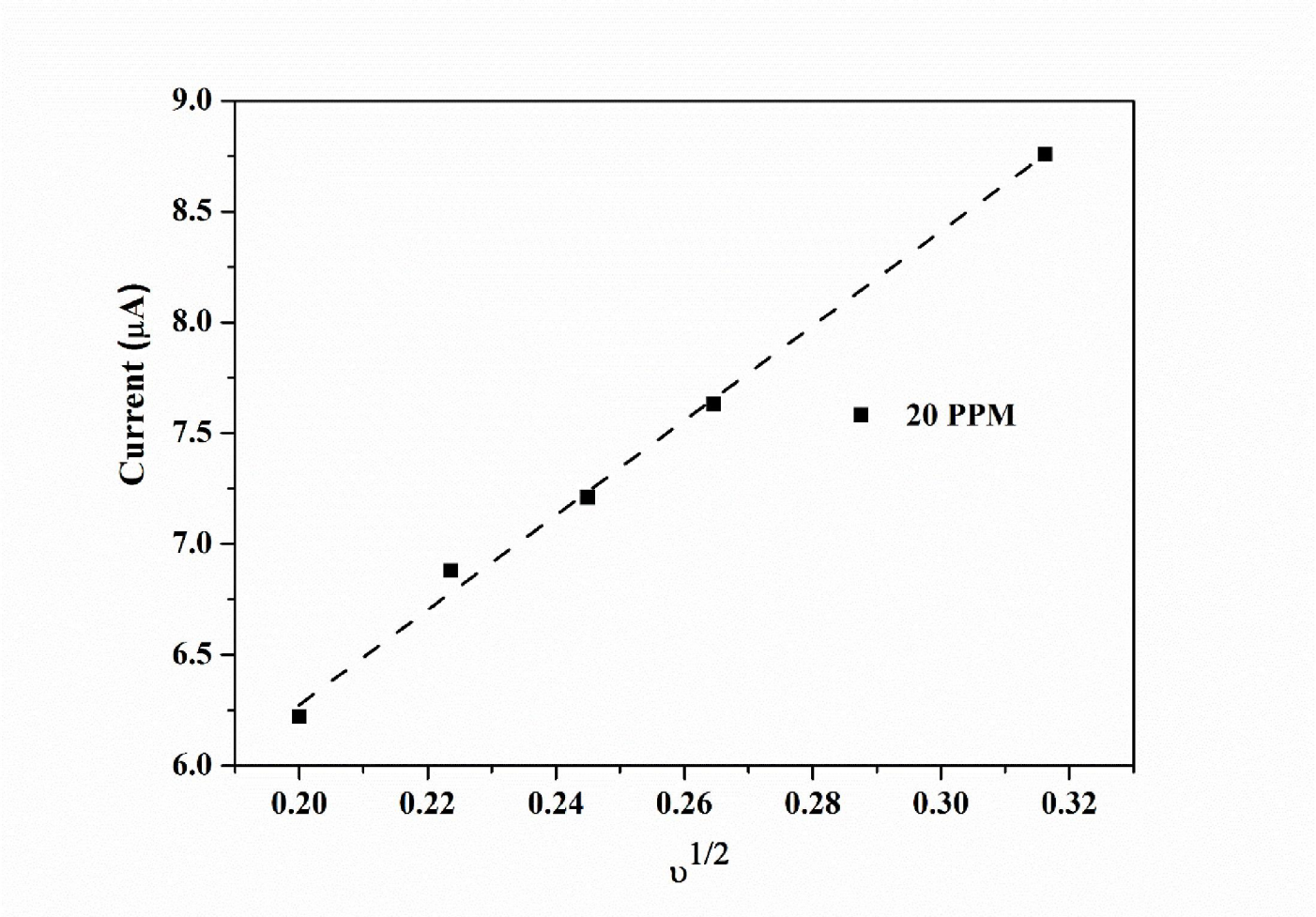

Fig. 6.16 Effect of scan rate on 20 ppm Cu solution

Detection ability of modified composites

XRD, morphological, FTIR, and DMA analyses indicate successful incorporation of the additives (EDTA, SNC, and Albumin) in the PLA/GR composite system. Thermal

analysis confirms that stability of the composites is not altered. Impedance analysis reveals improvement in the conductivity of electron in the system due to incorporation of ionic compounds EDTA, SNC, and electron-rich compound albumin. Therefore, these composites were further utilized for detection of metal ion, Cu^{2+}.

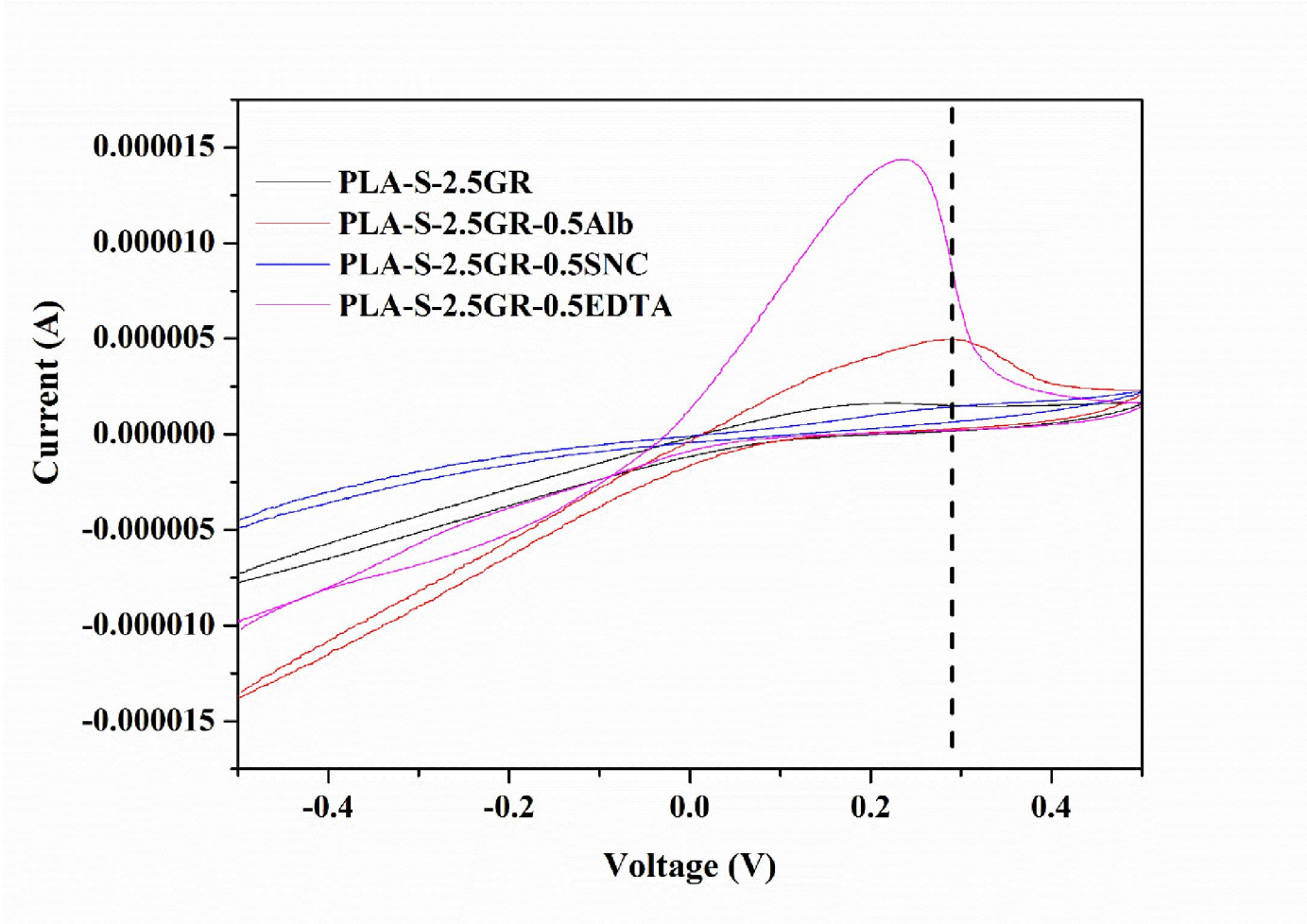

Fig. 6.17 I-V characteristics study of 20 ppm Cu solution using different components

Additionally, according to the literature, Lin et al., (2009) showed selective Cu^{2+} detection using EDTA modified copolythiophene electrode by selective binding at 0.30 V. Therefore, the modified composites as electrodes were investigated in this work in the voltage range of 0.5 V to -0.5 V using a scan rate 0.10 V/s. Further, Feier et al., (2015) reported that Cu^{2+} has strong interaction with EDTA in the pH range of 6-7. In view of this, the present study was conducted at neutral pH.

Fig. 6.17 compares the I-V response for the different composites where 20 ppm $CuCl_2$ solution is used as electrolyte. It can be seen from the figure that depending on the compound present in the PLA-GR system, the binding nature is different and reduction peak appears at different voltages. In the case of PLA-S-2.5GR and PLA-S-2.5GR-0.5SNC, there is no reduction peak of Cu^{2+} observed whereas for PLA-S-2.5GR -0.5Alb and PLA-S-2.5GR-0.5EDTA, the reduction peak appears at 0.29V and 0.24V, respectively. When Cu^{2+} solution was subjected to different strips for single-use, it was observed that peak current shifted to higher voltage and higher current. Fig 6.18a and Fig 6.18b are representative plots for PLA-S-2.5GR-0.5EDTA and PLA-S-2.5GR-0.5Alb in three different concentrations 20 ppm, 40 ppm and 60 ppm of $CuCl_2$. In case of PLA-S-2.5GR-0.5EDTA, both voltage and current were shifted to higher value with an increase in the concentration. In case of EDTA, peak current is shifted to low voltage because of presence of two binding sites –C=O and –N. Peak shifting to higher voltage in case of higher concentration indicating complexation that taking place at higher potential. PLA-S-2.5GR-0.5Alb shows that from 20ppm to 40 ppm, there is a shift in both voltage and current to higher values. However, further increment in concentration doesn't affect the peak current and voltage is shifted to higher value. This may be due to presence of single binding site of albumin and beyond $CuCl_2$ concentration of 40 ppm, availability of binding site becomes less, which is reflected through similar I-V response even with an increase in concentration. The higher peak current for EDTA loaded composite may be due to higher available site allowing to form the stern layer and thus increasing the current as compared to Alb loaded composite.

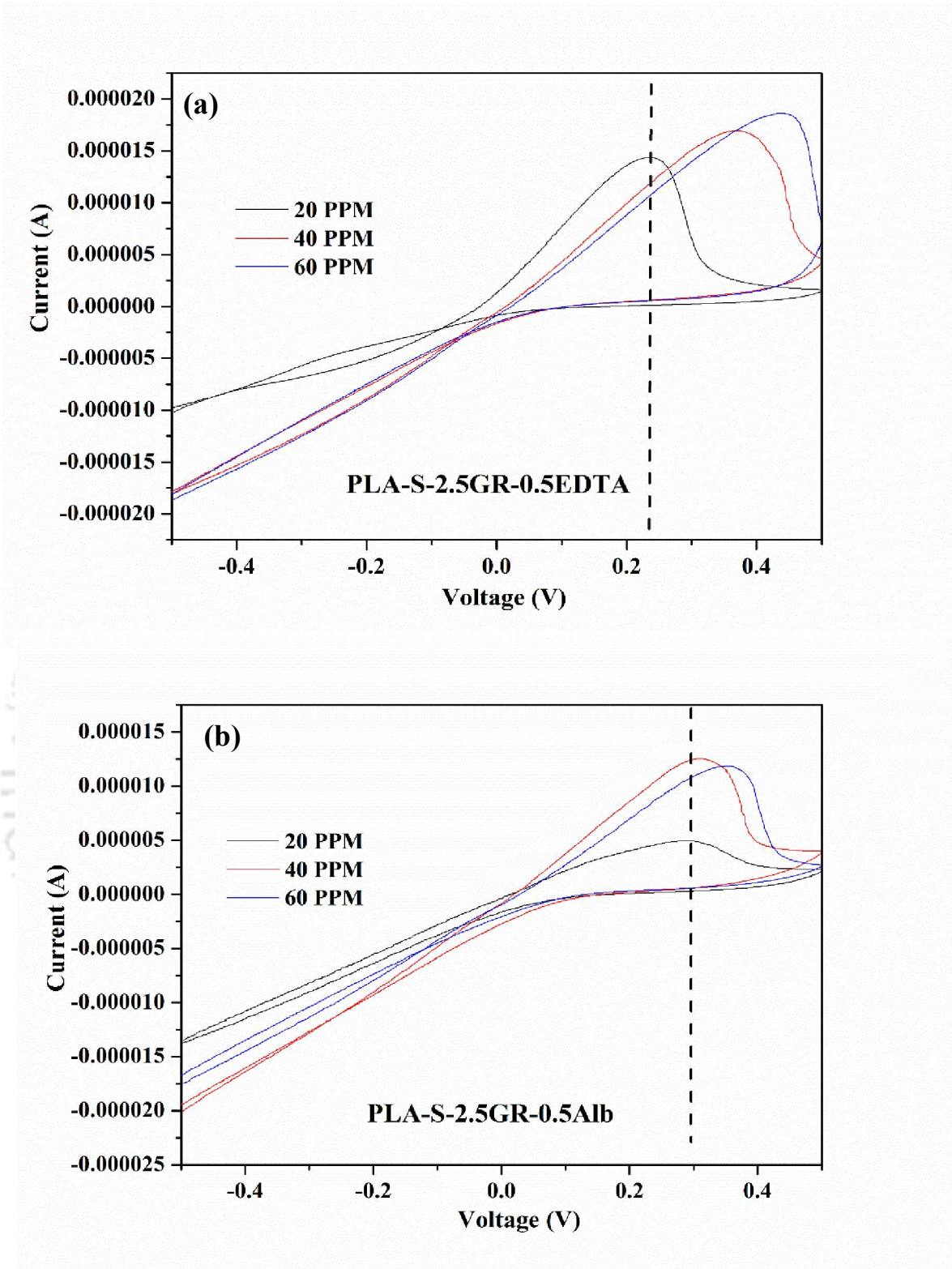

Fig. 6.18 I-V characteristics study of (a) PLA-S-2.5GR-0.5EDTA and (b) PLA-S-2.5GR-0.5Alb in different concentration (Single strip- Single concentration)

The modified PLA-S-2.5GR electrode surfaces contain SNC, Alb or EDTA based on the modification Fig. 6.19a. SNC because of higher hydrophobicity, is not open to the metal ions thus restricting it to form a complex with Cu ion. So, in spite of being protein in nature, SNC is not effective towards metal binding. EDTA has more than one binding sites to form complexes with Cu ion. Feier et al., (2015) reported formation of square planer complex with Cu ion when four binding sites are present in case of amine derived additive. Fisher et al., (2006) reported for Cu ion formation of distorted octahedron complex with EDTA exhibiting Jhan-Teller effect. So, it increases the ion mobility and thus working current for the case of PLA-S-2.5GR-0.5EDTA. In case of albumin modification, –CONH, –COOH and $–NH_2$ are the binding sites available. However, in the neutral pH condition, only the terminal amine group acts as binding site to Cu. Thus the number of available sites are less in case of PLA-S-2.5GR-0.5Alb (Fig 7.18b) (Sokolowska et al., 2002).

Fig. 6.20 is indicative of the usability of single strip for multiple concentration applications between 5-100 ppm using previously mentioned representative samples. It showed that in case of PLA-S-2.5GR and PLA-S-2.5GR-0.5Alb, the peak current increases with an increase in the concentration and the pattern can be divided into two linear subsections; up to 25 ppm, there is a sharp increment and after that, it follows a marginally increasing trend. In case of EDTA modified composite, the peak current is almost linear in the studied concentration for both 0.5% and 1% EDTA though the latter shows little higher current. SNC loaded composite (PLA-S-2.5GR-0.5SNC) displays decreasing current with an increase in the concentration and response pattern indicates that SNC modified composite is comparatively less suitable for metal ion detection. The current data beyond the reported concentration for respective composites are not presented as film failure was observed during experimentation under such condition.

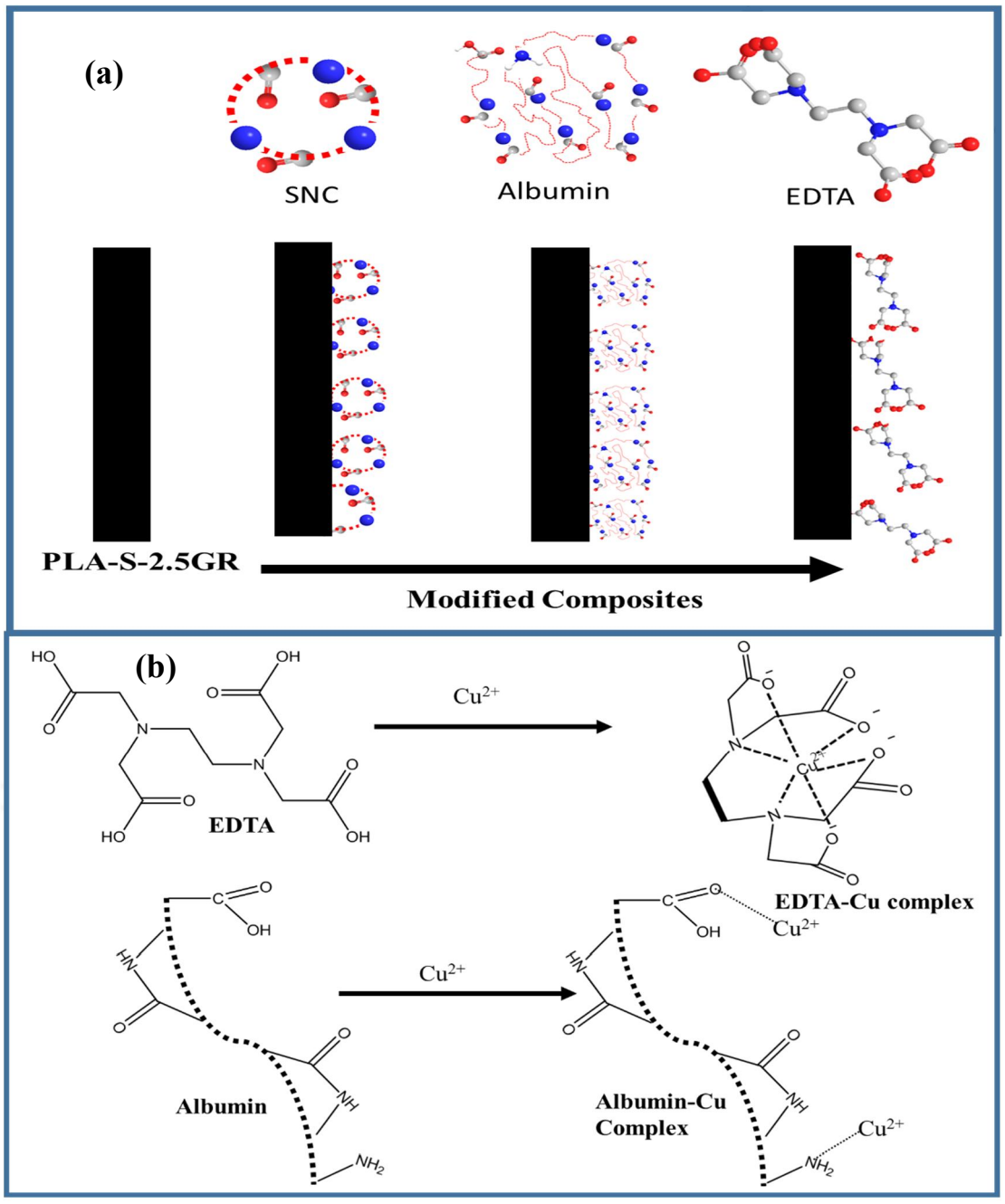

Fig. 6.19 (a) Modifications of PLA-S-2.5GR composite and (b) Probable complexation of Cu with EDTA and Albumin

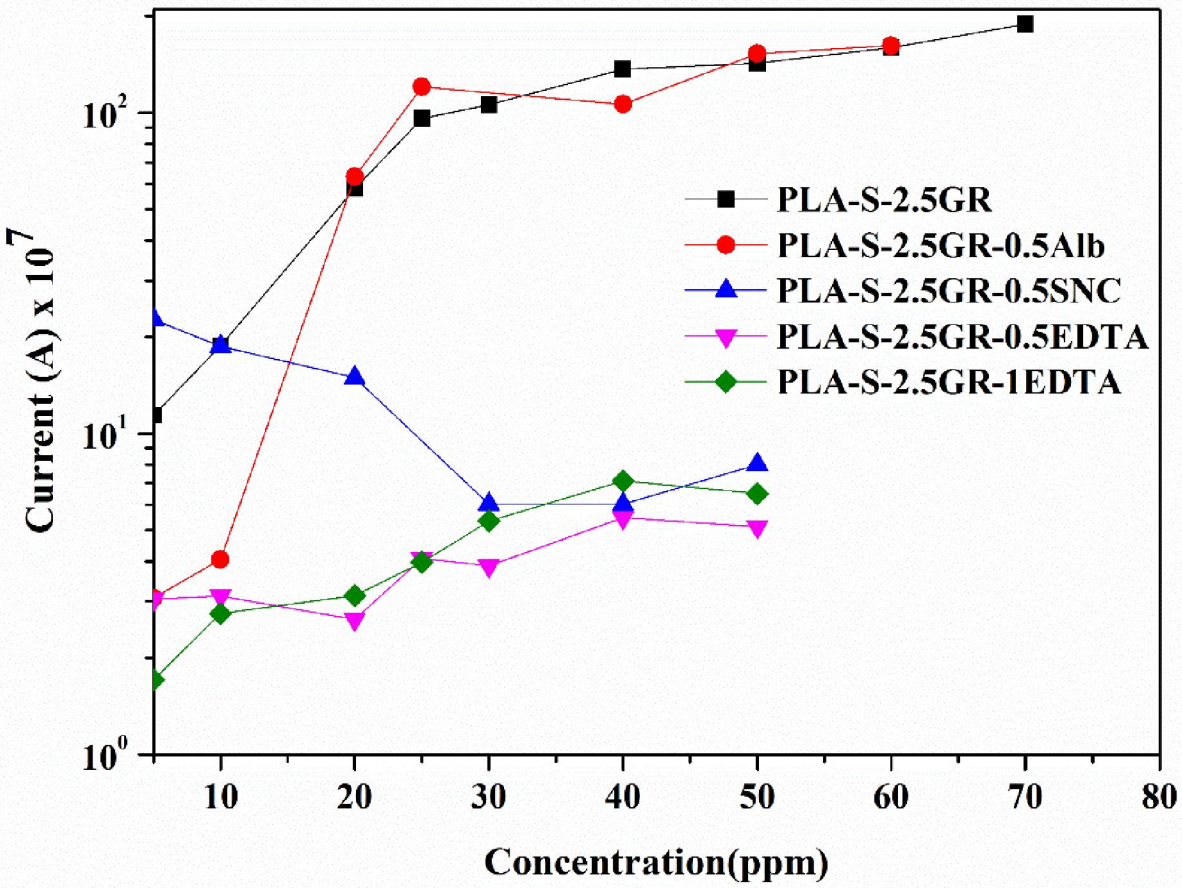

Fig. 6.20 I-V characteristics study up to stability of strip (Single strip- multi concentration)

6.4 Summary

PLA based conductive composite PLA-S-2.5GR was successfully explored for the detection of metal ions. In a comparison study, it gave similar performance as that by a conventional conductivity meter. Different additives like EDTA, SNC, and Albumin were successfully incorporated into the PLA/GR, system which was confirmed through FTIR and XRD analysis. Incorporation of filler decreased the thermal stability of the film, which is marginal decrease for PLA-S-2.5GR-0.5EDTA. Dynamic mechanical analysis also indicated slight decrement in strength of film because of additives.

However, PLA-S-2.5GR composite showed good sensitivity for Cu^{2+} ion detection within the concentration range of 5-100 ppm. Hysteresis loop of I-V response was found to be dependent on scan rate, type of cation and type of anion and electrode type. It confirms the behaviour of PLA-S-2.5GR film as possible future material for the electrode. In case of modified composites a reduction peak of Cu^{2+} was found for PLA-S-2.5GR -0.5EDTA and PLA-S-2.5GR -0.5Alb at 0.24 and 0.29 V, respectively. It indicates that ion binding with the additives depends on the ligand sites available. Single strip use for multiple concentration indicated dependence of stability on modifier. Application domain found to be higher for PLA-S-2.5GR-0.5Alb whereas for PLA-S-2.5GR-0.5EDTA linearity in response is higher compared to other compositions.

Chapter 7

Synthesis of Magnetic Nanomaterials and Studies on Magneto-Rheological and Vapour Sensing Behavior of PLA based Nanocomposites

Abstract

This chapter includes fabrication of magnetic nanoparticle from graphene oxide (GO) and oxidised carbon fibre (CF). Co-precipitation technique was adopted to prepare magnetic materials like GO-Fe (GO-Fe_3O_4), GO-FC (GO-$CoFe_2O_4$), and CF-Fe (CF-Fe_3O_4). These magnetic materials are found to have good ferromagnetic properties. Impact on the different properties like morphology, thermal stability, crystallization nature, magnetic rheological behaviour, impedance was analysed using fabricated PLA based composites of 0.5-2 wt. % loading. Magnetic rheology indicates that the presence of field increases the storage modulus and viscosity of the composite melts. An ethanol vapour detection setup was fabricated by combining 3D-printing and interdigital electrode. Representative materials were tested for ethanol sensing under nitrogen flow. Response is found to be increasing within 10 sec. A comparison of performance for ethanol sensing is carried out between the present composites and the previously used composites.

Graphical abstract

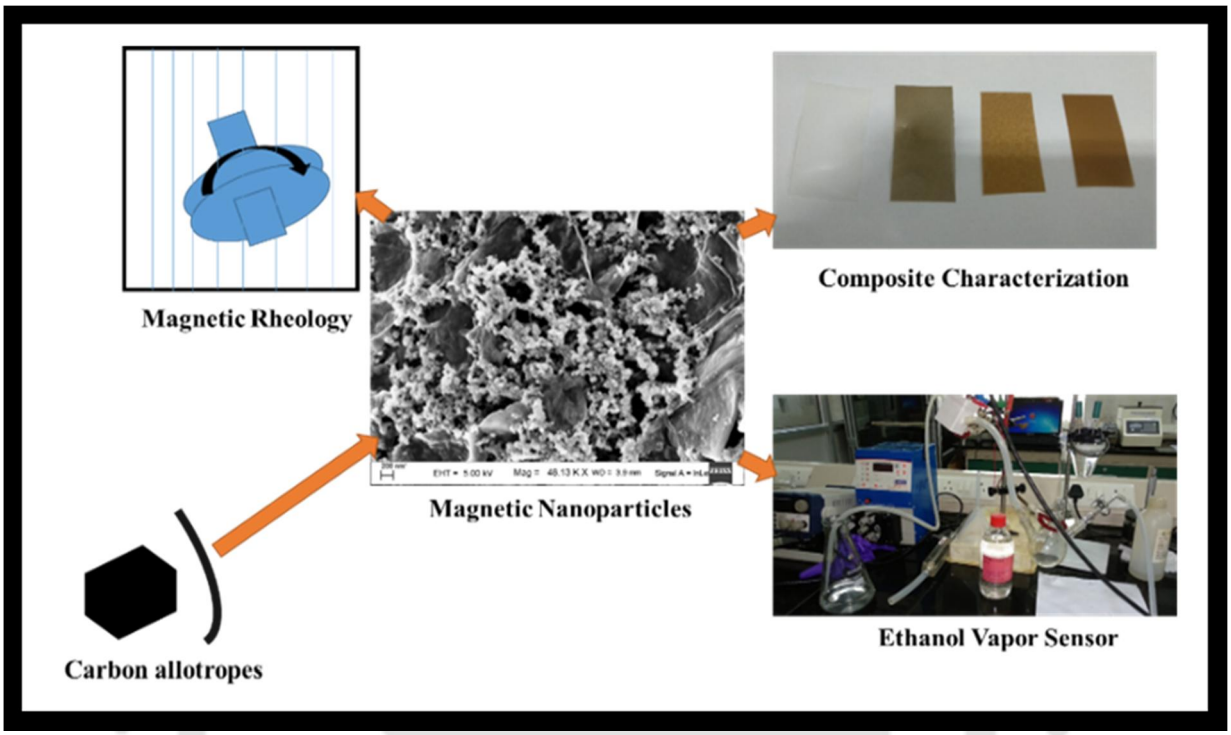

7.1 Introduction

Magnetic nanoparticle-based hybrids in combination with carbon materials like graphene, carbon nanotube, are utilized in waste-water treatment, drug delivery, catalysis, biomedical and packaging applications (He et al., 2010; Lu et al., 2007; Patwa et al., 2018). Utilization of templates like graphene, carbon fibre, increases the surface area because of plate-like morphology (He et al., 2010). Magnetic material reinforcement into polymers also makes it field sensitive and thus opens its application arena towards smart electronics, smart magneto fluids and active packaging with self-heating and antimicrobial properties (Biji et al., 2015; WU KT & YAO, 2001; Xu et al., 2015). Kassaee et al., (2011) fabricated iron oxide decorated graphene oxide and polystyrene composite with magnetization of 2.2 emu/g with a loading of 1.2 wt. % which was sensitive to magnetic field (Kassaee et al., 2011). Ferromagnetic materials are sensitive to magnetic field. Flow behaviour and optical transparency can be altered by varying the preparation condition or under external field (Filali et al., 2018; Rinaldi et al., 2005). Wu et al., (2001) synthesized ferromagnetic particle-based fluid with different particle dimensions and observed that the transparency is dependent on pH and magnetic field. Biodegradable polymers are already being utilized in several advanced applications apart from short term packaging applications. Incorporation of magnetic particles into biodegradable polymers can improve the mechanical, magnetic, thermal and electrical properties (Dhar et al., 2016). Dhar et al., (2016) prepared polylactic acid magnetic cellulose nanocrystal nanocomposite by solution casting. Magnetic cellulose nanocrystals (FeCNC) reinforcement into PLA matrix improved the tensile strength and elongation by 70% and 240%, respectively. Orientation of FeCNC into PLA matrix is also found to play important role in the mechanical and electrical properties of PLA. Carbon filler template-based magnetic materials can impart both

conductive nature as well as magnetic behaviour into the biodegradable polymers like PLA and convert it into smart conductive composites, which makes it suitable for the application as vapour sensor (Kumar et al., 2012).

In this chapter graphene oxide and carbon fibre based magnetic nanomaterials were synthesized by co-precipitation method. Initially, compatibility of the magnetic particles with PLA system was determined by making solution cast films. X-ray diffraction analysis, Raman analysis, morphological investigation and vibrating sample magnetism analysis were conducted in order to notice the nature and properties of the magnetic nanoparticles, FTIR, morphology analysis, thermogravimetric analysis, differential scanning calorimetric studies, impedance analysis, and magnetism investigation were carried out to study the effect of incorporation of magnetic nanoparticles into PLA matrix in the loading range of 0.5-2.0 wt. %. Rheological behaviour of the composite melts was investigated under magnetic field. In order to fabricate vapour sensor , one custom made 3D-printed gas chamber was fabricated in lab. Interdigital electrode (IDE) with 1mm spacing was taken and inserted into the casing. GO-Fe and CF-Fe were used to cast conductive film over IDE for detection of ethanol vapour. PLA was used as binder. Initially loading of the filler was optimized which was followed by testing towards ethanol vapour under constant nitrogen flow rate. Effect of nitrogen flow rate towards the ethanol vapour detection also tested. A normal multimeter was also utilized for representative case to compare the detection in comparison to Autolab.

7.2 Materials & Methods

7.2.1 Materials

2003D grade of PLA was supplied from NatureWorks® LLC (USA) have the properties like density of 1.24 g/cm^3, M_n and M_w of 150000 and 200000 g/mol respectively and of granular appearance. Methanol (extra pure AR), chloroform, ethanol and ammonium solution required for the research work were provided by SISCO Research Laboratories (SRL Chemicals, India). Carbon fiber (CF) from Sigma Aldrich, USA. Ferric chloride, sodium nitrate and potassium permanganate were supplied by Merck Specialities Pvt. Ltd. (MERCK). HPLC grade chloroform was purchased from Merck Specialities Pvt. Ltd. (MERCK). Millipore water (Metrohm) was used as solvent for some of the cases. Expanded graphite was purchased from Asbury Carbons, USA. Sulphuric acid and nitric acid were purchased from HiMedia Laboratory. Hydrogen peroxide was purchased from Fisher Scientific. Ferrous chloride was supplied by Loba chemie, India.

7.2.2 Experimental Section

7.2.2.1 Preparation of graphene oxide (GO) from graphite

GO was synthesized from graphite by following Hummers method (Shahriary & Athawale, 2014). In order to oxidise graphene stacks, 0.5 gm of graphite along with 0.5 gm $NaNO_3$ were subjected to stirring for 4 h. in presence of 23 ml of 98% H_2SO_4. Then it was continuously stirred with $KMnO_4$ and 30 w/w % H_2O_2 in successive stages. Finally, the mixture was kept for dialysis (GO kept inside a dialysis bag, which was kept immersed in a water bath and the water was changed at times) in order to make the pH ~7 and then centrifuged and dried.

7.2.2.2 Functionalization of carbon fiber (CF)

CF was functionalized by HNO_3 refluxing. 69% HNO_3 (100 ml) was added into 100 mg CF and refluxed for 10 hr at 120 ^oC. After that, it was treated with 30 w/w % H_2O_2 and kept for dialysis and dried to get functionalized CF (CF-CH).

7.2.2.3 Preparation of GO and CF based magnetic particles

In order to prepare magnetic particle of different morphology and composition, 5 mg of GO was taken in 20 mL of water and kept under sonication for 45 min to get uniform solution. $FeCl_3$ (20mg) and $FeCl_2$ (10 mg) were mixed with water and added to the above-mentioned solution and stirred for 2 hr. Then at 85 ^oC, ammonia solution (1mL in 20 mL water) was added dropwise under vigorous stirring at 900 rpm for 4 h. Finally, it was centrifuged and dried at 60 ^oC to get GO-Fe (1:4). In place of GO, CF-CH was used to get CF-Fe particles. $CoCl_2$ was used in place of $FeCl_2$ in order to prepare GO-FC (GO-FC-W). In order to check difference in magnetism one GO based magnetic particle (GO-FC-M) was synthesized taking 1: 2 mole ratio of $FeCl_3$ and $CoCl_2$ in place of weight ratio.

7.2.2.4 Fabrication of magnetic particle based PLA composite

Magnetic particle incorporated PLA nanocomposites were fabricated in the loading range 0.5 to 2 wt. % to extract information about compatibility and interaction with PLA. In order to cast the composites, 2 g. of PLA was taken in 20 mL chloroform and was stirred in a conical flask till the dissolution. GO-Fe (10 mg) was taken in 30 mL chloroform and sonicated for 1 h using probe sonicator (55% power) till the solution became uniform with no residue left in the bottom. The two solutions were mixed and stirred overnight (10 h) and cast on Teflon Petri dish to get 0.5% PLA/GO-Fe composite (PLA-GFe-0.5). Similarly, PLA-GFe-1 and PLA-GFe-2 were cast for 1 wt.

% and 2 wt. % loading of GO-Fe. Following the similar procedure PLA-GFC-0.5 was prepared by taking 0.5% GO-FC and PLA-CFe-0.5, PLA-CFe-1 were cast taking 0.5 and 1 wt.% CF-Fe, respectively.

7.2.2.5 Magnetic particle based nanocomposite for vapour sensing

In order to study the vapour sensing behaviour of magnetic particles. GO-Fe and CF-Fe were taken in the wt. % of 10, 20 and 50 wt. % and 5, 10 and 20 wt. % along with PLA to make conductive thin film of thickness between 30-50 μm over the IDE of ethanol vapour sensor.

7.2.3 Characterization

7.2.3.1 XRD analysis

Instrument details and operating conditions are mentioned in Chapter 2.

7.2.3.2 Raman spectroscopy

The Raman spectra for magnetic nanoparticles were carried out using a spectrometer (Make: Lab Ram HR Model: Horiba Jobin Vyon) equipped with a Nd: YAG diode-pumped laser (1W, 1064 nm) and operated at an excitation wavelength of 488 nm. The materials were scanned in the wavenumber ranging from 3000 to 500 cm^{-1}.

7.2.3.3 Morphological analysis

Instrument details and operating conditions are mentioned in Chapter 2.

7.2.3.4 Magnetism analysis (VSM)

Magnetic moment of the samples were measured by using vibrating sample magnetometer (Make: Lakeshore, Model: 7410 series). In the case of powder sample, 10 mg of sample was taken for individual cases and for magnetic particle loaded composite film a dimension of 10 mm length with width 5mm and thickness 0.1 mm was taken.

7.2.3.5 FTIR analysis

Instrument details and operating conditions are mentioned in Chapter 2.

7.2.3.6 TGA

Instrument details and operating conditions are mentioned in Chapter 4.

7.2.3.7 DSC analysis

Instrument details and operating conditions are mentioned in Chapter 4.

7.2.3.8 Impedance analysis

Instrument details and operating conditions are mentioned in Chapter 2.

7.2.3.9 Magnetic rheology analysis

The rheological measurements of PLA and the nanocomposites were carried out by using a controlled stress rheometer (Make: Anton Parr, Model: MCR 102) having cone and plate arrangement (20 mm in diameter) in the melt state. The dynamic frequency sweep test was performed with a strain level of 5% in the linear viscoelastic region (LVE) which was predetermined experimentally by the amplitude sweep test. Current sweep was conducted in the range of 0.1 to 0.6 A.

7.2.3.10 Ethanol vapour sensing

Ethanol vapour sensor set up was fabricated in lab. It was composed of mainly two parts one is interdigital electrode (IDE) another one was 3D-printed outer case. IDE was fabricated in lab with 1mm gap between each layer. Outer case was cast by 3D-Printing machine using polymeric filament. Finally, this set up was connected to a three-neck flask. One end of it was connected to nitrogen gas line. During measurement magnetic particle or magnetic particle/PLA composite was cast over IDE and kept inside the case and measured amount of ethanol kept inside the flask (Fig. 7.1). Impedance of the electrode was measured and relative change of impedance was calculated with respect to zero time. Similarly, in some of the cases for comparison

digital multimeter also used for measurement of reading. Detailed about the setup and sensing is mentioned in the section 7.3.3.

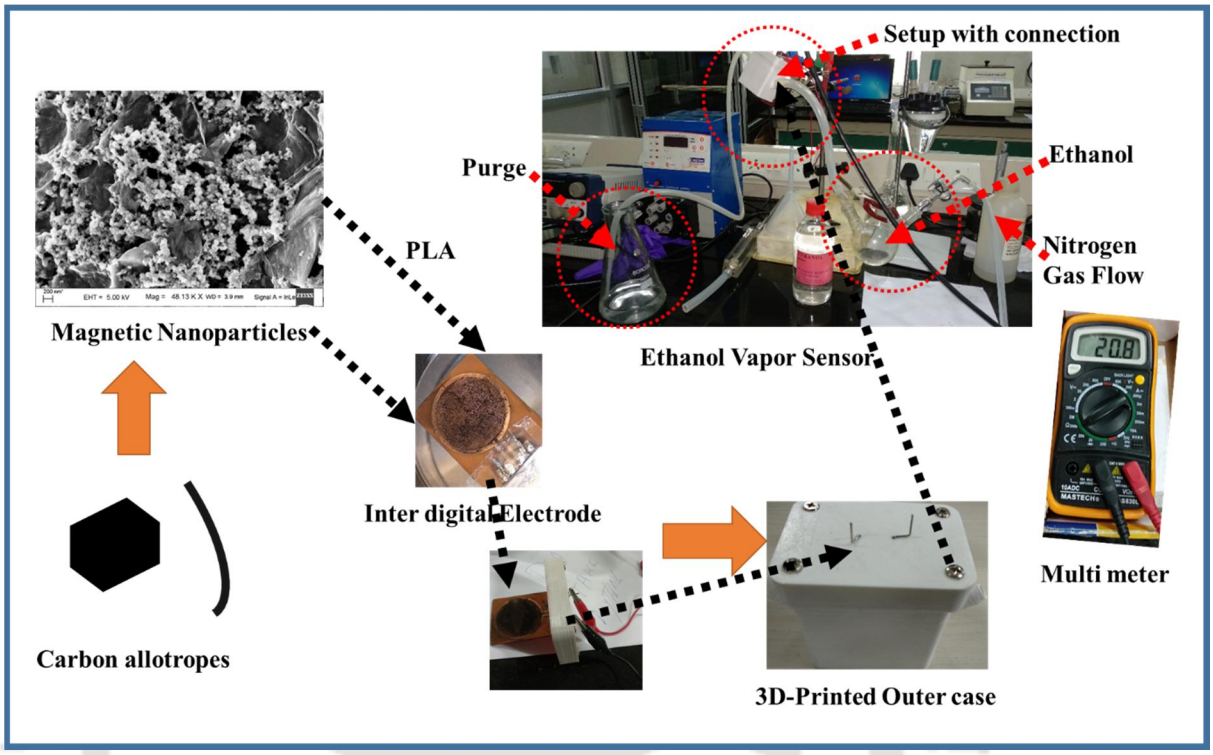

Fig. 7.1 Ethanol vapour sensing set up

7.3 Results & Discussion

7.3.1 Magnetic particle characterization

7.3.1.1 XRD analysis

XRD of graphene oxide (GO) showed peak at 2θ=9.6° corresponding to d=0.92 nm and the functionalized carbon fibre (CF-CH) at 2θ=25.6° corresponding to d=0.35 nm. The magnetized nanoparticle, GO-Fe displays peaks at 2θ=30.3, 35.6, 43.4, 56.9 and 62.8°, corrosponding to the (220), (311), (400), (511) and (440) crystallographic planes of Fe_3O_4, respectively (Fig. 7.2) (El-Okr et al., 2011; Kassaee et al., 2011). For GO-FC samples, the peaks at 2θ=18.8, 31.1, 36.6, 44.5, 58.6 and 64.6°corrosponding to the (111), (220), (311), (400), (511) and (440) crystallographic planes of $CoFe_2O_4$, respectively (Fig. 7.2) (Zhang et al., 2010). The marginal increment of 2θ values for GO-FC compared to that of GO-Fe indicates the decrement of d-spacing due to smaller

atomic radius of Co compared to that of Fe (Zhang et al., 2010). In case of CF-Fe, all the peaks corresponding to CF-CH and Fe_3O_4 can be seen from Fig 7.2. The above results indicate successful fabrication of the desired carbon template-based magnetic nanoparticles.

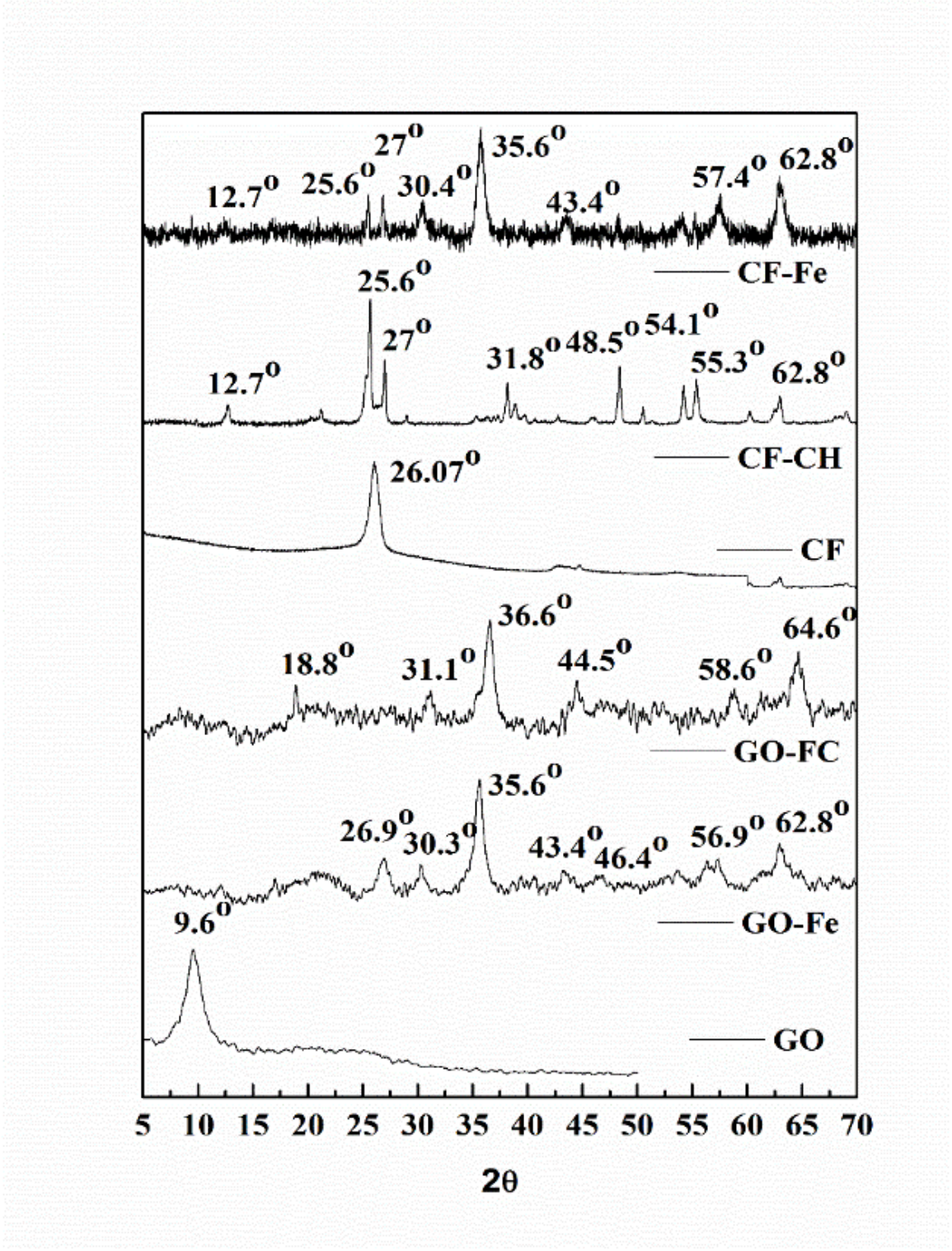

Fig. 7.2 XRD analysis of the GO, GO-Fe, GO-FC, CF, CF-CH and CF-Fe

7.3.1.2 Raman spectroscopy

Raman spectroscopy of the magnetic particles showed presence of peaks at ~1360 cm^{-1} corresponding to D-band (measure of disorder and edge oxidation in the sp^2 carbon structure) and at ~1580 cm^{-1} corresponding to G-band (measure of sp^2 moiety of carbon) of the carbon templates (Fig. 7.3) (Sasaki, Tokura, & Sogawa, 2013). Vibrations due to Fe_3O_4 (vibrations of hematite formed from magnetite) below 1000 cm^{-1} are suppressed because of high intensity of I_D and I_G band of carbon allotropes (Zhang et al., 2010). I_D/I_G ratio for GO is found to be 0.71. In case of GO-Fe and GO-FC, this ratio is increased compared to that of GO (Table 7.1), which is indicative of generation of more disorders and participation of oxidised sites binding towards Fe. In case of CF-Fe, it is decreased as compared to that of CF. It is due to decrement of intensity of D-band (I_D) as probably oxidation caused the decrement of thickness of fibre and reduced edge disorders during the process i.e., oxidation followed by magnetization. This observation is similar to the case where single-wall carbon nanotube (SWCNT) has lower intensity in D-band as compared to multiwall carbon nanotube (MWCNT) (Hodkiewicz & Scientific, 2010) .

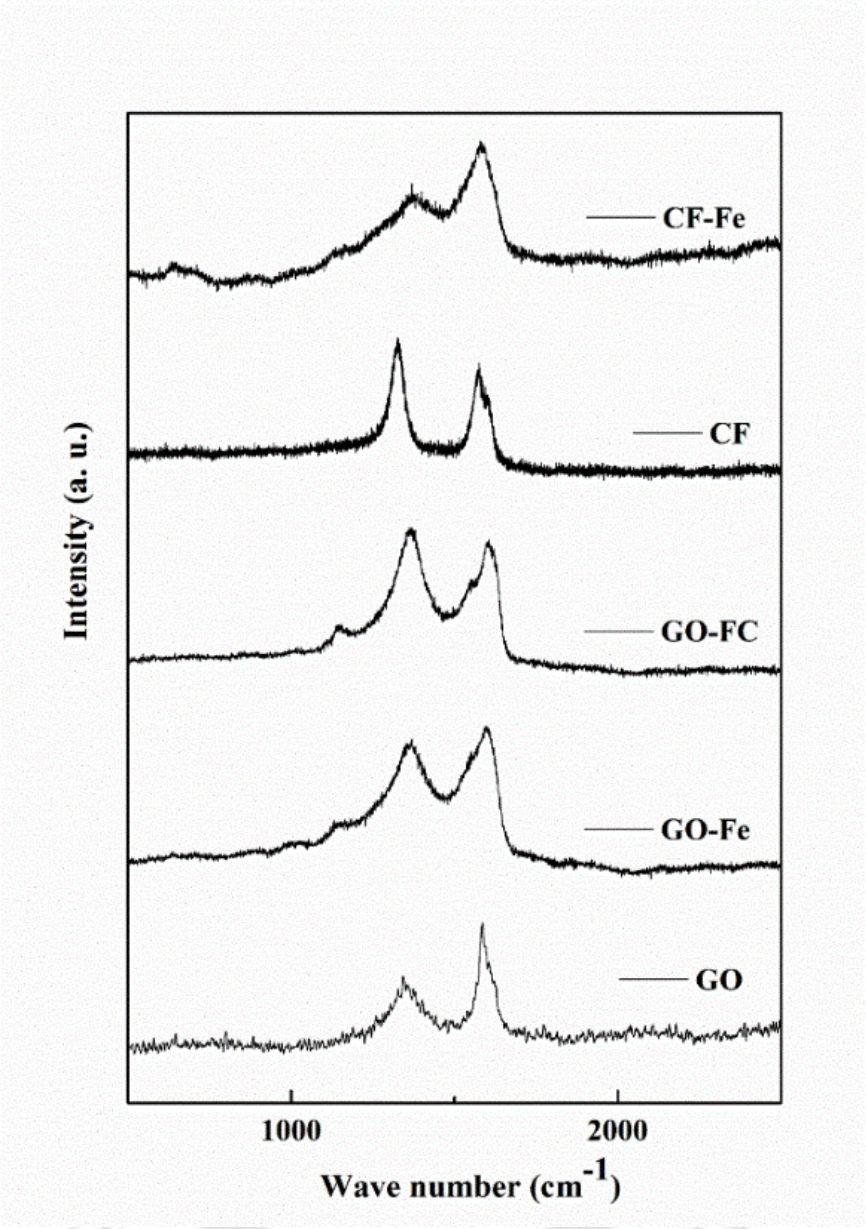

Fig. 7.3 Raman analysis of the GO, GO-Fe, GO-FC, CF and CF-Fe

Table 7.1 Raman analysis parameters of GO, GO-Fe, GO-FC, CF and CF-Fe

Component	I_D (cm^{-1})	I_G (cm^{-1})	I_D/I_G
GO	1370	1583.2	0.71
GO-Fe	1356.5	1589.9	0.93
GO-FC	1360.9	1596.5	1.10
CF	1325.3	1576.5	1.26
CF-Fe	1374.2	1583.2	0.76

7.3.1.3 Morphological analysis

TEM images, of the magnetic nanomaterials indicated that the carbon templates for GO-Fe, GO-FC and CF-Fe are decorated with discrete Fe_3O_4 nanoparticles (Fig. 7.4). Magnetic nanoparticles diameters are observed to be less than 20 nm and are uniformly distributed over the carbon templates with less agglomeration.

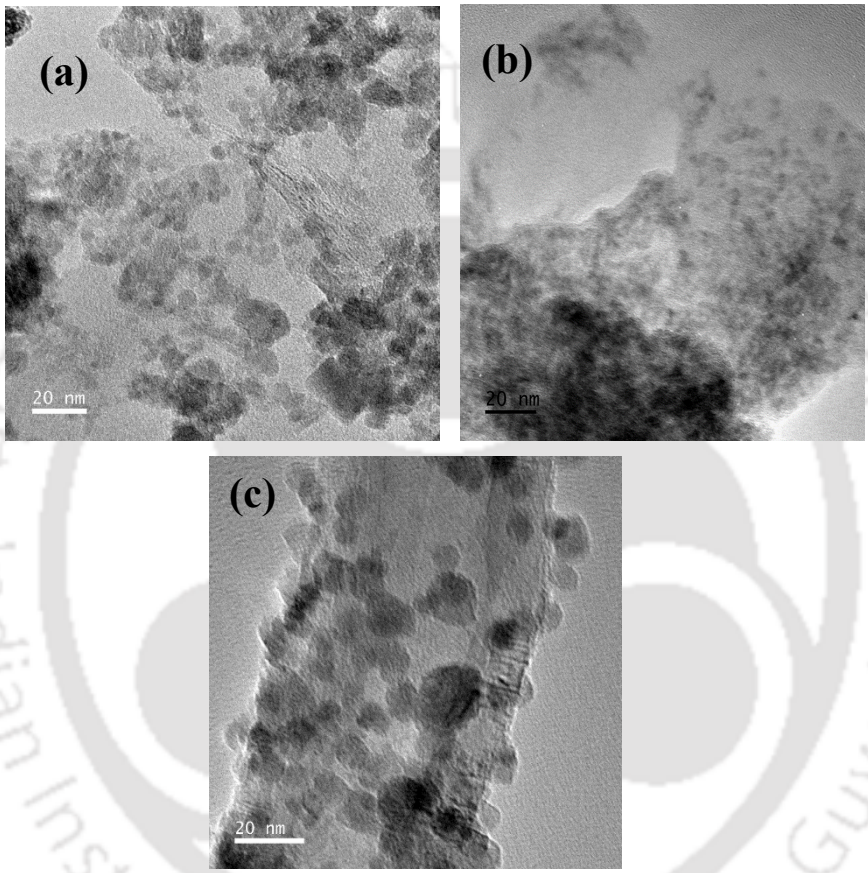

Fig. 7.4 TEM images of (a) GO-Fe, (b) GO-FC and (c) CF-Fe

Morphological investigation through FESEM also indicates presence of Fe_3O_4 over the surface of the templates (Fig. 7.5). Iron oxide has almost covered the surface of carbon templates to give magnetic nanomaterial along with increased effective surface area. In case of GO template-based magnetic nanomaterials (GO-Fe and GO-FC), the decorated particles are observed to be plate-like magnetic nanomaterials (Fig. 7.5 (a-b)) whereas

CF-based magnetic nanomaterial (CF-Fe), fiber like morphology was noticed (Fig. 7.5(c-d)).

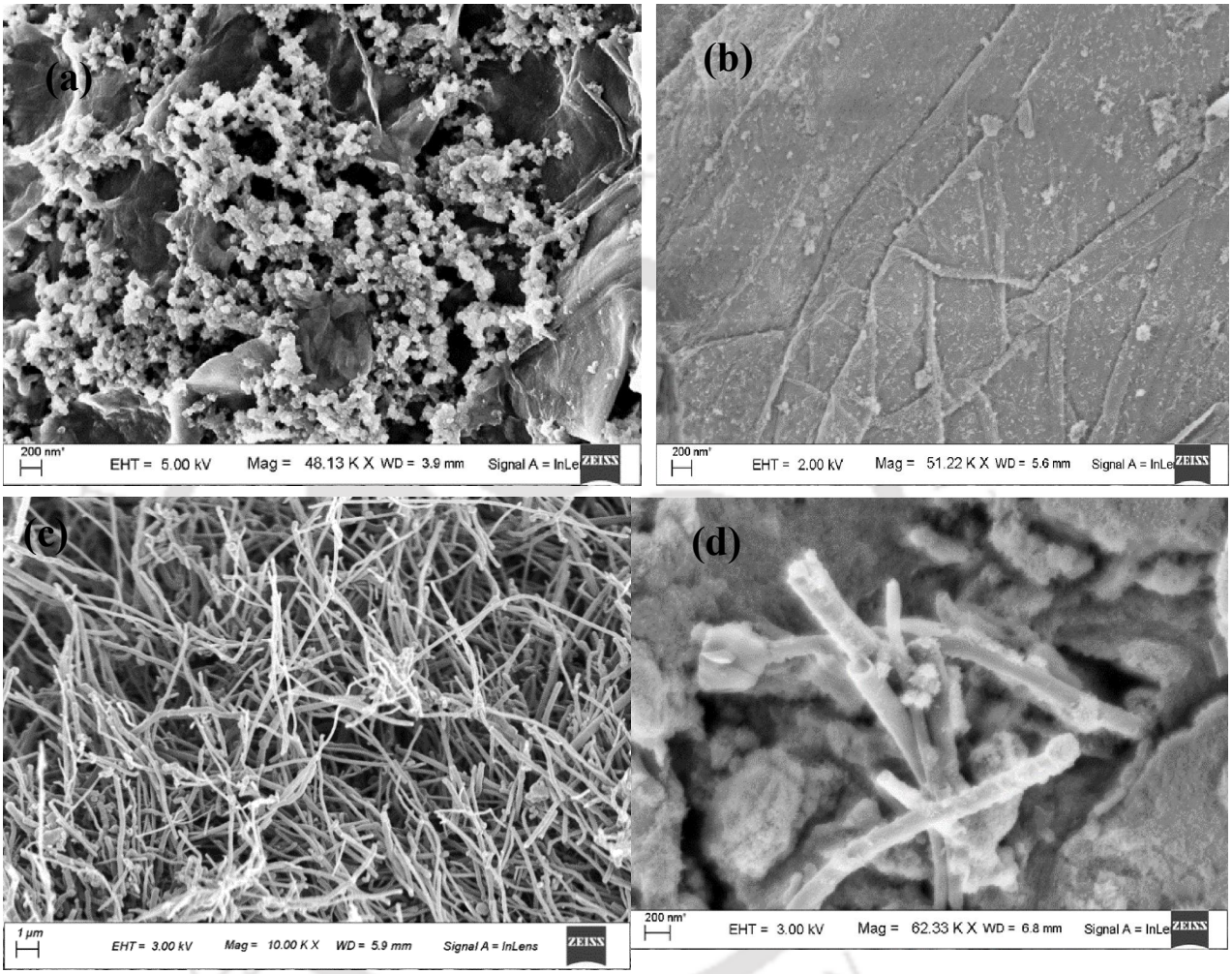

Fig. 7.5 FESEM images of (a) GO-Fe, (b) GO-FC, (c) CF and (d) CF-Fe

7.3.1.4 VSM analysis

Magnetic measurements of GO-Fe, GO-FC and CF-Fe were examined by VSM analysis. Magnetic hysteresis loop of the magnetic particles implies that all the synthesized magnetic particles are ferromagnetic in nature (El-Okr et al., 2011). Under identical condition CF-Fe is found to have more magnetism compared to GO-Fe (Fig. 7.6) that may be due to higher loading of iron oxide on the surface. $CoFe_2O_4$ loaded

GO has less magnetism compared to Fe_3O_4 loaded GO. It is also observed that GO-FC prepared by taking iron and cobalt salt in 1:2 wt. ratio (GO-FC-W) has higher magnetism compared to that prepared by mole ratio 1:2 (GO-FC-M). It may be due to higher relative amount of Co is for the former case compared to the latter. Saturation magnetism is higher for GO-Fe (14.3 emu/g) and that for GO-FC-W and CF-Fe are 6.2 and 42.10 emu/g, respectively. Coercivity values are found to be 27.56, 17.12 and 27.73 Oe for GO-Fe, GO-FC-W and CF-Fe, respectively. Retentivity values for GO-Fe, GO-FC-W and CF-Fe are observed to be 0.4156, 0.1015 and 1.1209 emu/g, respectively. Thus the above findings imply high magnetic nature of the synthesized template-based magnetic particles GO-Fe, GO-FC (GO-FC-W) and CF-Fe.

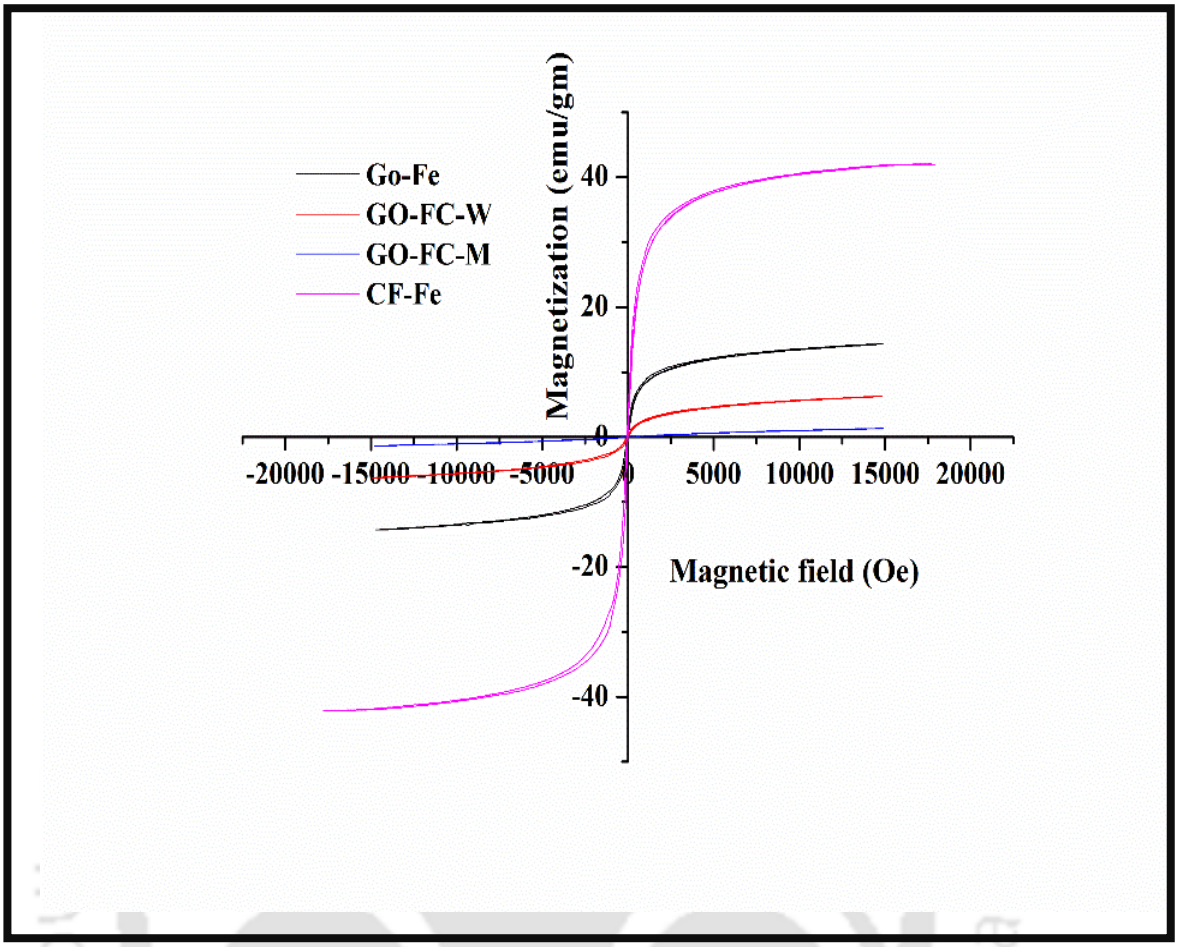

Fig. 7.6 VSM analysis of (a) GO-Fe, (b) GO-FC and (c) CF-Fe

7.3.2 Magnetic particle-PLA interaction

From the previous results, it is found that Fe_3O_4 is successfully decorated over the carbon templates. XRD, morphology and VSM investigation implied formation of well-structured oxides over the carbon allotropes. However, prior to application of such materials as ethanol sensing elements, compatibility and interaction of these materials with PLA matrix was investigated by fabricating composite using solution casting method. Since GO-Fe showed the highest magnetism, the composites were fabricated by loading of GO-Fe in the range of 0.5 to 2 wt. % in the PLA matrix. However, in order to make comparison of performance of the magnetic nanocomposites GO-FC (0.5

wt. % loading) and CF-Fe (0.5 and 1 wt. % loading) loaded PLA based magnetic nanocomposite were also fabricated. Effect of reinforcement of the different morphology magnetic nanomaterials in the structural, thermal, crystallization and conductivity properties and the flow behaviour was studied in order to examine the interaction of the magnetic particles with PLA.

7.3.2.1 XRD analysis

XRD analysis of the PLA based composite films can be seen from Fig. 7.7. The presence of peaks corresponding to 2θ= 14.7, 16.5, 18.9 and 22.3º represent (010), (110)/ (200), (203) and (015) planes of PLA (Tripathi & Katiyar, 2016a).The presence of identical crystal structure of the composites PLA-GFe-0.5, PLA-GFe-1, PLA-GFe-2, PLA-GFC-0.5, PLA-CFe-0.5 and PLA-CFe-1 reveals that the reinforcement of the nanoparticles does not alter the crystallographic structure of PLA.

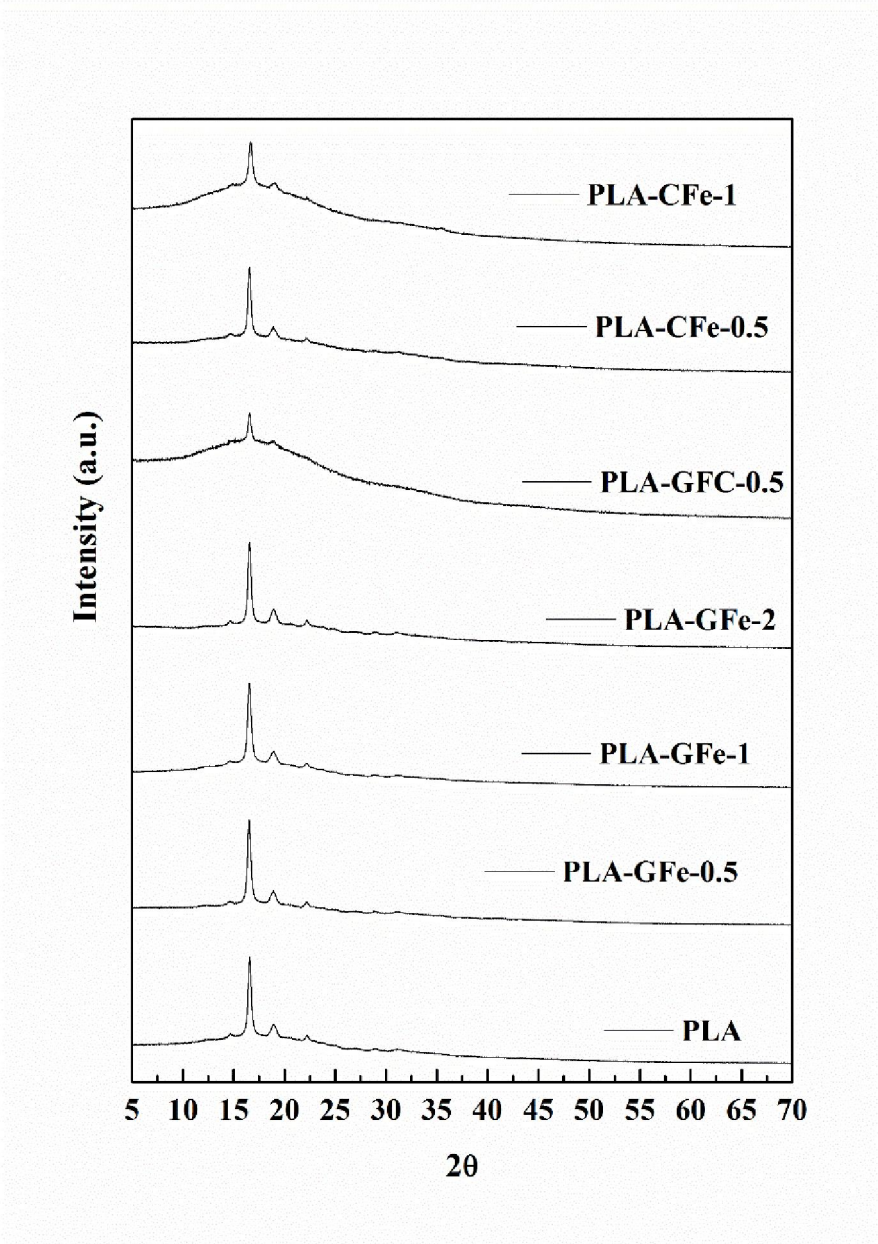

Fig. 7.7 XRD analysis of the PLA and magnetic composite samples

7.3.2.2 FTIR analysis

FTIR spectra of PLA, PLA-GFe-0.5, PLA-GFe-1, PLA-GFe-2, PLA-GFC-0.5, PLA-CFe-0.5 and PLA-CFe-1 can be seen from Fig. 7.8. Structural vibration at 800 cm^{-1} implies to –C-C- stretching; those at 1026 cm^{-1} and 1216 cm^{-1} implies to -C-O- stretching of –CH-O- group; and band at 1748 cm^{-1} corrospond to –C=O stretching of carbonyl group and bands at 2853 cm^{-1} and 2934 cm^{-1} implies to symmetric and asymmetric stretching of $–CH_2$ (Pal & Katiyar, 2016; Tripathi & Katiyar, 2016a). After

incorporation of magnetic nanomaterials into the PLA matrix, the peak at 1748 cm^{-1} shifted to ~1742 cm^{-1} due to the interaction of –C=O with Fe ions (Dhar et al., 2016). Similar structural vibration of the composites as compared to PLA (Fig. 7.8) implies that reinforcement of magnetic nanomaterial didn't alter the structural uniformity of PLA.

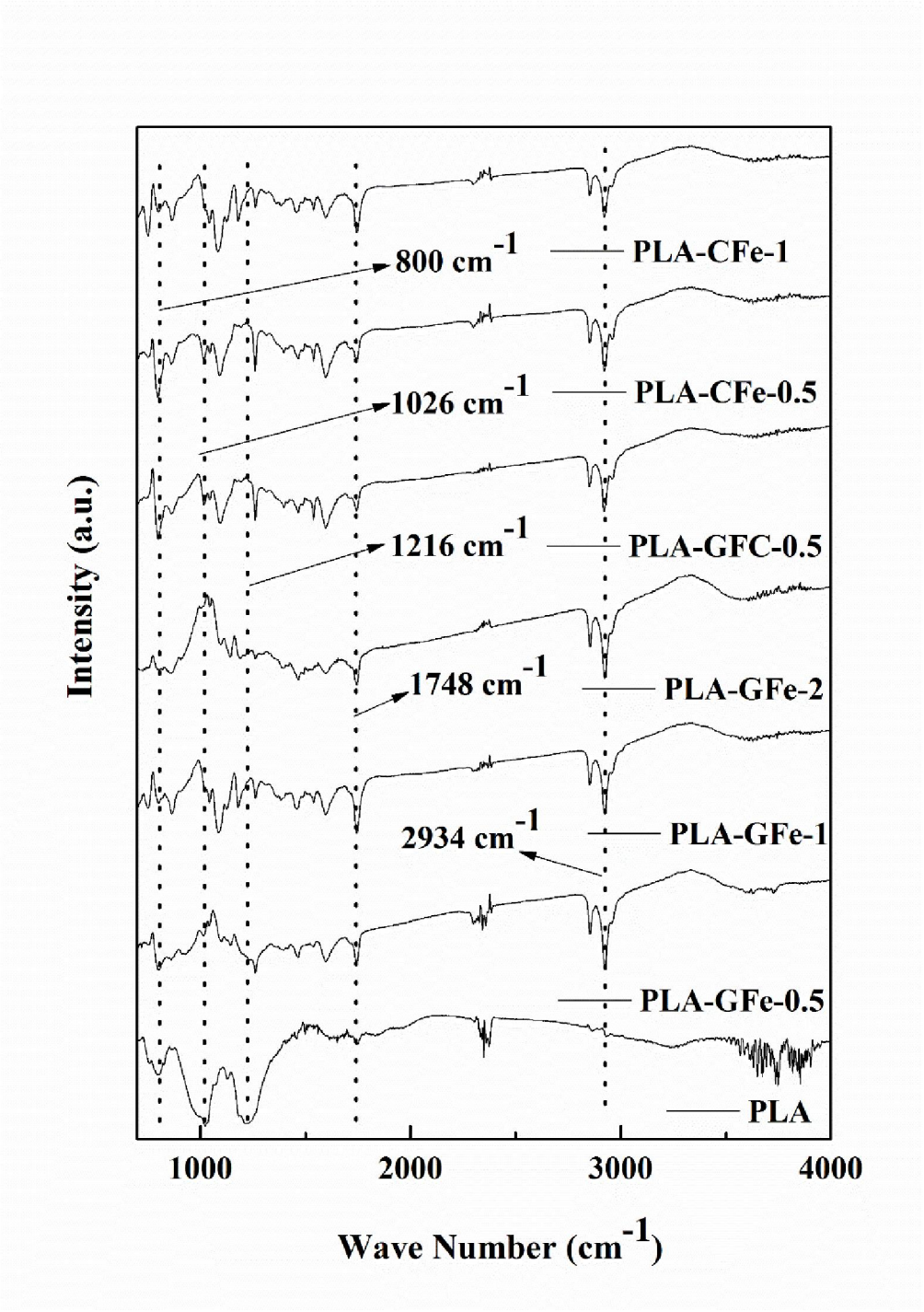

Fig. 7.8 FTIR analysis of PLA and magnetic composite samples

7.3.2.3 Morphological analysis

FESEM analysis of the representative composites PLA-GFe-0.5, PLA-GFe-2, PLA-GFC-0.5 and PLA-CF-0.5 were carried out in order to examine the distribution of particles into the matrix of the PLA. Fig. 7.9 (a & b) depicts distribution of the GO-Fe into PLA matrix, which reveals that with an increase in loading from 0.5 to 2 wt. % of GO-Fe, agglomeration sites are increased. Distribution of GO-FC into PLA matrix can be seen from Fig.7.9(c), which is similar to that of PLA-GFe-0.5 indicating the presence of uniformly distributed GO-FC with lesser agglomeration sites. In case of PLA-CFe-0.5 (Fig. 7.9d), the presence of fibre like morphology of CF in the PLA matrix can be seen with less agglomeration.

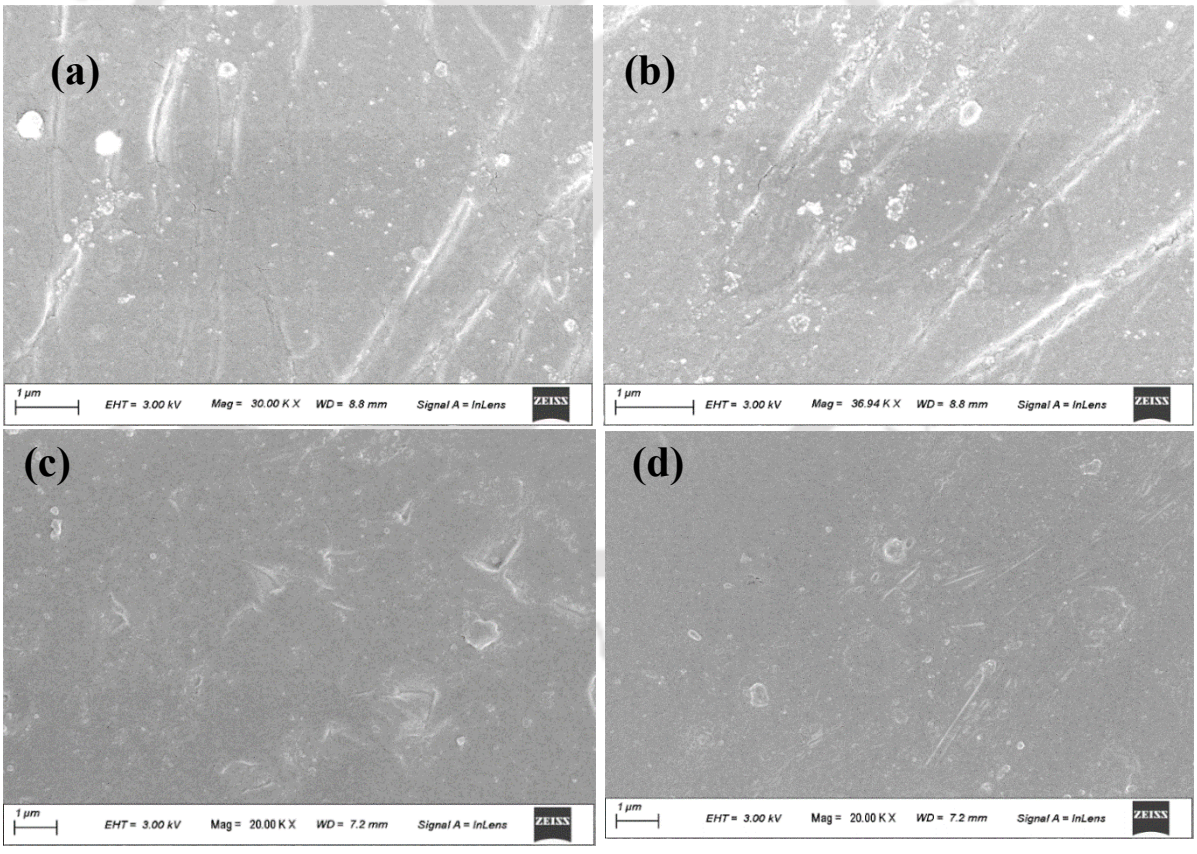

Fig. 7.9 FESEM images of (a) PLA-GFe-0.5, (b) PLA-GFe-2, (c) PLA-GFC-0.5 and (d) PLA-CFe-0.5

7.3.2.4 TGA

Thermal stability of the composites was evaluated by TGA analysis of the components (Fig. 7.10). The onset degradation temperature is found to be improved by 36, 20 and 19 °C for 0.5 wt. % loading of GO-Fe, GO-FC and CF-Fe, respectively into the PLA matrix. With further increase of loading, it is decreased for both GO-Fe and CF-Fe (Table 7.2). The temperature at 50% degradation (T_{50}) is observed to be increased by 30 °C for PLA-GFe-0.5 but with further increase in loading of GO-Fe, it again decreased. Similarly, in case of PLA-GFC-0.5 and PLA-CFe-0.5, T_{50} is increased by 20 °C and 5 °C, respectively. The maximum degradation temperature (T_{max}) is found to be increased by 5.5 °C for PLA-GFe-0.5 as compared to PLA. Whereas, with an increase in loading of GO-Fe, it is found to be decreased by 38 and 40.4°C as seen for PLA-GFe-1 and PLA-GFe-2, respectively. In case of PLA-GFC-0.5 and PLA-CFe-0.5, T_{max} is decreased by 6.6 and 28.4 °C, respectively. The above results imply that GO-based filler having plate-like morphology hinders the flow of the gas generated from degradation and increases the thermal stability at low loading as compared to the CF-based one, which has fibre like morphology (Murariu et al., 2010; Valapa et al., 2015a). At higher loading, the possible catalytic effect of iron oxide towards the degradation of PLA is responsible for the decrease in thermal stability (Liu et al., 2015). Fe_3O_4 decorated GO is found to have better thermal stability compared to that of $CoFe_2O_4$ one. Catalytic effect of iron oxide is more prominent at maximum rate of degradation, because of higher temperature at T_{max}.

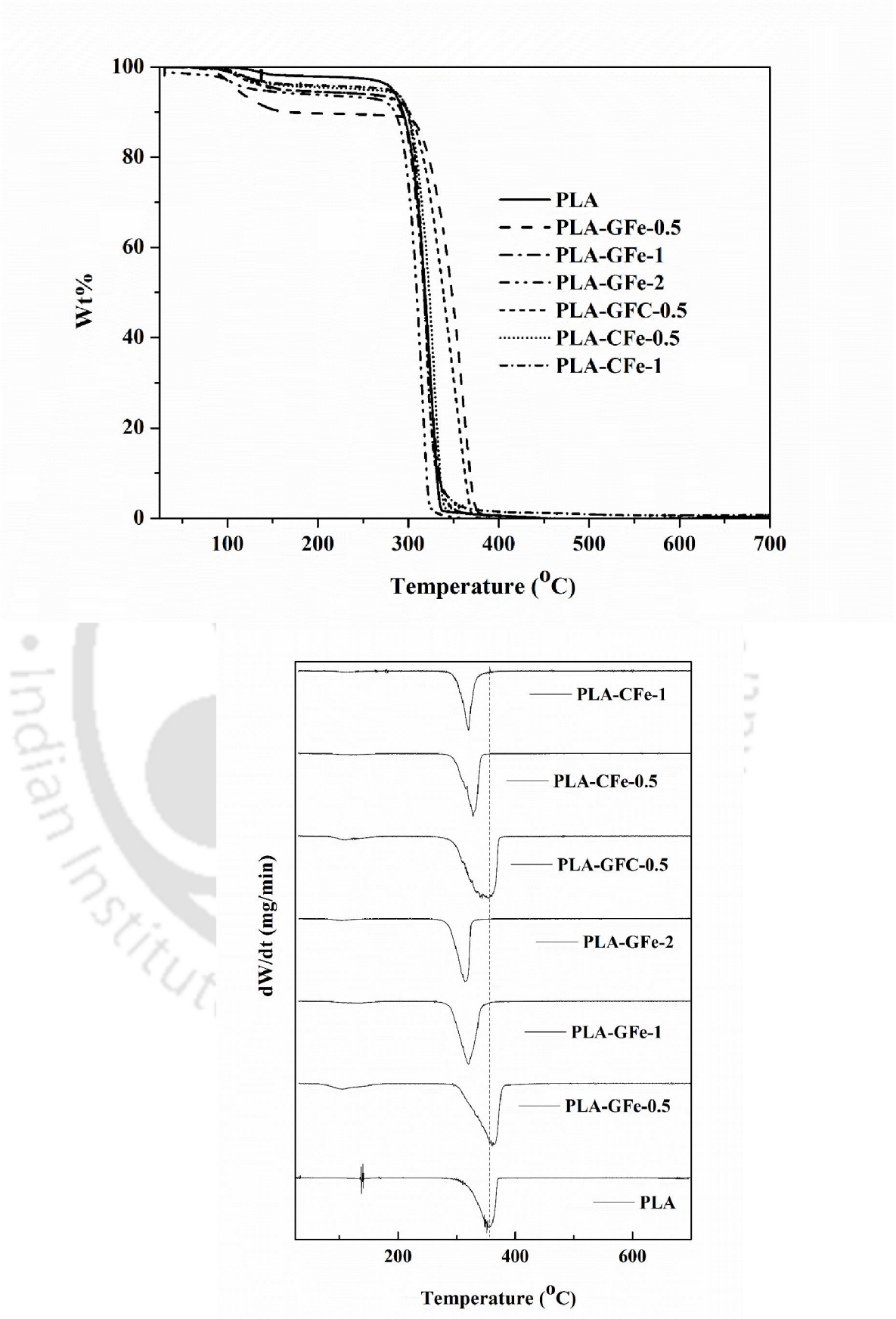

Fig. 7.10 TGA and DTG analysis of the PLA and magnetic composite samples

7.3.2.5 DSC analysis

Chain folding behaviour of PLA and magnetic nanoparticle reinforced composites during cold crystallization can be seen from Fig. 7.11. Glass transition temperature (T_g) is found to be similar for all the composites fabricated in this work as well as PLA (~61°C). Cold crystallization temperature (T_{cc}) of the composites is found to be higher compared to PLA (114 °C). In case of PLA-GFe-0.5 and PLA-CFe-0.5, improvement in T_{cc} are 9.9 and 9.8 °C, respectively (Table 7.2). Further increase in loading for PLA-GFe-1 and PLA-GFe-2 caused decrement in T_{cc}. Melting temperature (T_m) is not altered much due to incorporation of the magnetic materials. This result implies that magnetic nanomaterials acted as nucleating substance, which is responsible for increment of the cold crystallization temperature (Battegazzore et al., 2011a; Valapa et al., 2015b). Effect on chain folding nature is almost similar for GO-Fe and CF-Fe, which implies that nature of morphology does not significantly affect the chain folding of PLA.

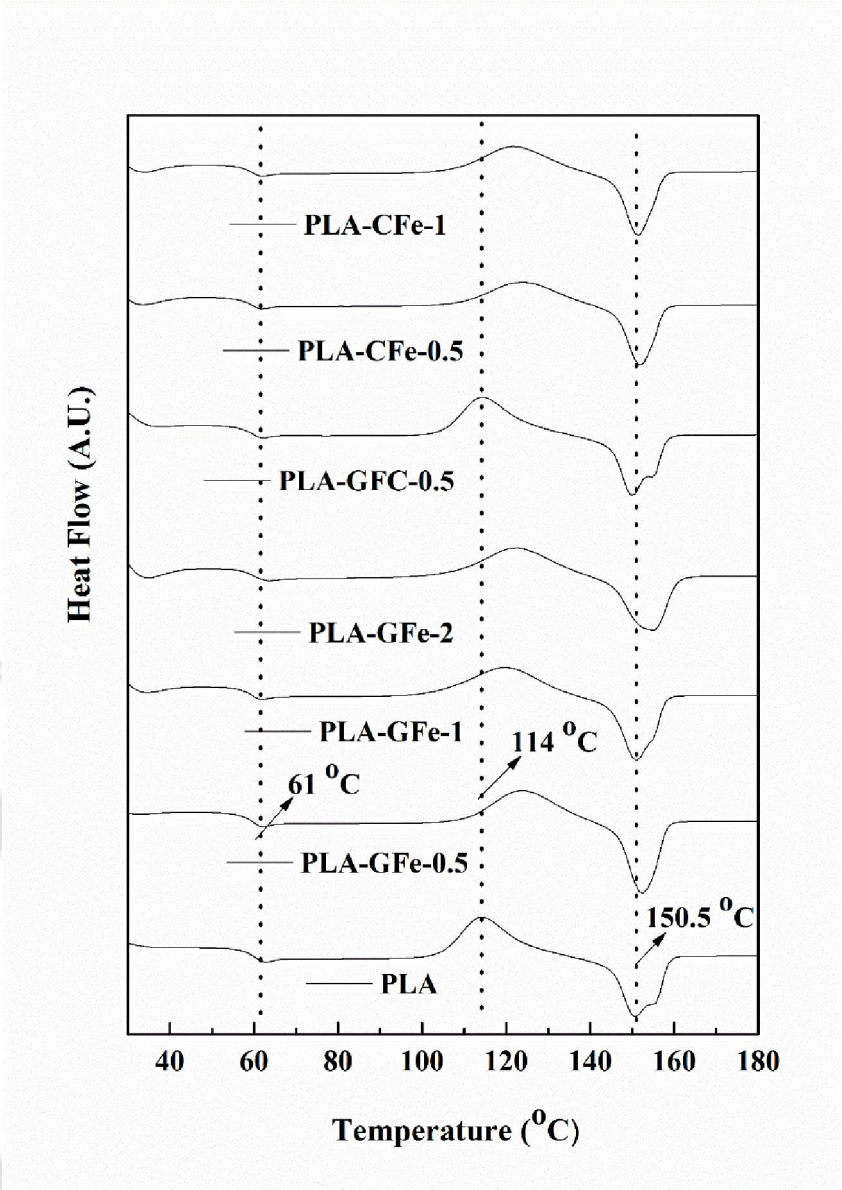

Fig. 7.11 DSC analysis of the PLA and magnetic composite samples

Table 7.2 Thermal analysis data of PLA and magnetic composite samples

Components	T_{Onset}	T_{50}	T_{max}	T_g(°C)	T_{cc} (°C)	T_m (°C)
PLA	293	318	356.3	61	114	150.5
PLA-GFe-0.5	328.9	348.2	361.8	60.7	123.9	152.6
PLA-GFe-1	305.8	317.6	318.3	61.1	119.8	151
PLA-GFe-2	298.1	309.2	315.9	62.3	122.6	153.4
PLA-GFC-0.5	312.8	338.8	349.7	61.1	114.6	150.2
PLA-CFe-0.5	311.9	323.1	327.9	61.1	123.8	151.9
PLA-CFe-1	307.9	317.6	318.3	61.1	121.4	151.4

7.3.2.6 Impedance analysis

In order to examine the impact of the magnetic nanomaterials on the conductive nature of the composite, impedance of the composite was measured within the frequency range of 0.1 to 10^5 Hz (Fig. 7.12). With an increase in frequency from 0.1 Hz to 10^5 Hz, the impedance decreased from 10^{10} Ω to 10^5 Ω. The nature of the impedance response indicates capacitive loss associated with the composites, which is due to improper dispersion of the fillers into the PLA matrix. With incorporation of GO-Fe and CF-Fe, impedance decreased marginally for the composites as compared to PLA in the studied loading range and film thickness was ~0.1mm. Thus, the impedance value is not found to be attractive for application in sensing studies (Kobashi et al., 2008). Thus, magnetic nanomaterials has an impact on the conductive nature of the composites, however in order to use those filler based composites in sensing application, either the loading of

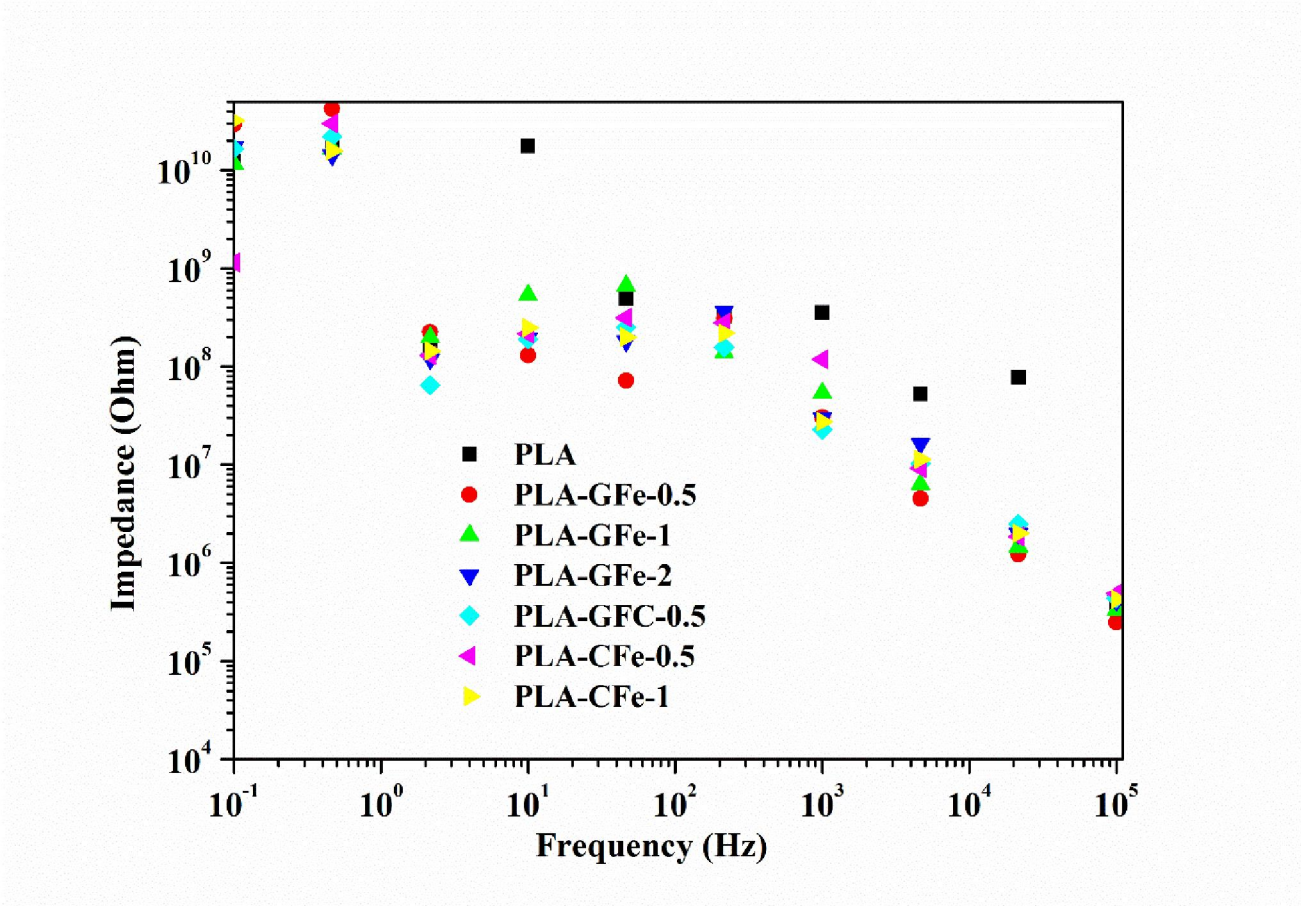

Fig. 7.12 Impedance analysis of the PLA and magnetic composite samples

7.3.2.7 VSM analysis

Magnetically active materials have properties such as self-heating nature in the presence of magnetic field and can act as a bioactive compound. In this regard, magnetic hysteresis of the composites was examined under magnetic field. Fig. 7.13 depicts the nature of hysteresis loop for the magnetic particle loaded composites, which reveals that with an increase in field, the magnetism is increased. In the lower loading range of 0.5 to 1 wt. % range the increment in magnetism is less. In case of PLA-GFe-2, saturation magnetism is 0.4 emu/cm^3 which is much higher compared to the almost magnetically inactive PLA. This indicates that based on the requirement, loading of this magnetic nanoparticles can be changed to make suitable magnetically active material for different applications, particularly in the field of sensitive active packaging and in bioactive applications (Laurent et al., 1989; Pyun, 2007).

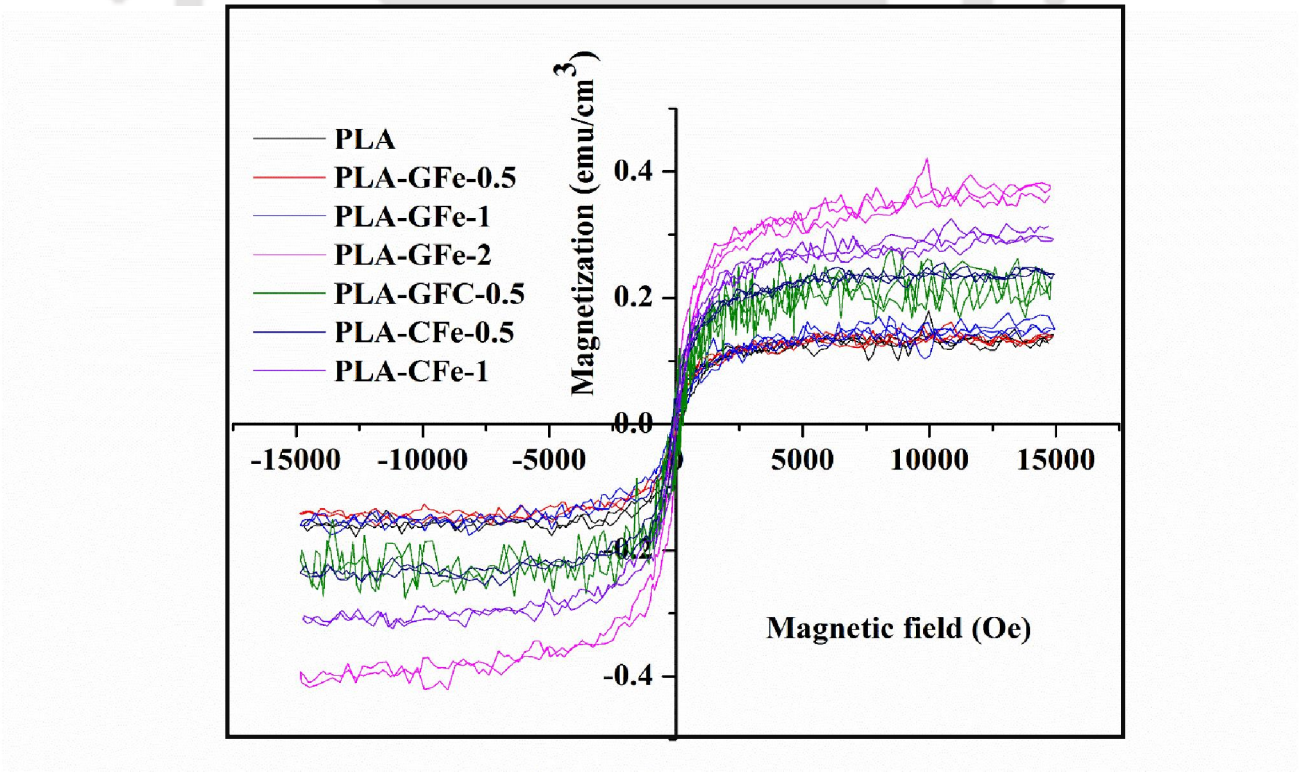

Fig 7.13 Magnetic property analysis of the PLA and magnetic composite samples

7.3.2.8 Magnetic rheology analysis

Rheological investigation of the composites gives information about polymer chain flow behaviour, branching, crosslinking, uniformity in dispersion and homogeneity. This indirectly sets the processing conditions of the particular polymer reinforcement system. Melt rheology is thus very important property of the thermoplastic polymer, required to be studied for effective processing (Al-Itry et al., 2014; Chen et al., 2013). Ferromagnetic particle incorporation is imparting magnetic nature into the composite, which can be seen from section 8.3.2.7. Ferrofluids are used in several technical and clinical application, which opens up the probable application of the present composites in molten condition (Kaloni & Mahajan, 2010). In this context, flow behaviour investigation of the composite melts were conducted under different magnetic fields. Field strength was varied by varying the current from 0.2 to 0.6 A.

Strain sweep analysis

Storage modulus and loss modulus of the composites were examined under strain conditions of 0.01 to 100 % at constant frequency of 10 Hz in order to check the effect of different morphology magnetic nanomaterials as well as the loading, on the flow behaviour at a constant current of 0.2 A. It can be seen from Fig. 7.14 that under magnetic field, the storage modulus (G′) and loss modulus (G″) values are higher for PLA-GFe-0.5 as compared to PLA-CFe-0.5 and PLA-GFC-0.5 at 170 °C. The trend of G′ and G″ with strain is quite similar in nature with almost steady value up to 10%. Then there is a sharp decrement in value for both the cases. This is because in the steady region, the strain rate is not high enough as well as the structural deformation of the polymer melt, whereas in the high stain region, non-linear nature can be seen as material deformation occurs in the direction of shear and melt is unable to absorb the strain energy (Aranguren et al., 1992; Cassagnau & Melis, 2003). In case of GO-Fe, with

increasing loading, the modulus value is increased for PLA-GFe-2 as compared to that for PLA-GFe-0.5. This is possibly because of GO-Fe hindering the PLA chain relaxation. Whereas in case of CF-Fe loading, the modulus values decrease with an increase in the loading. Impact of the magnetic particles is more prominent in the steady region compared to the nonlinear region where the flow of material is more dependent on the shear.

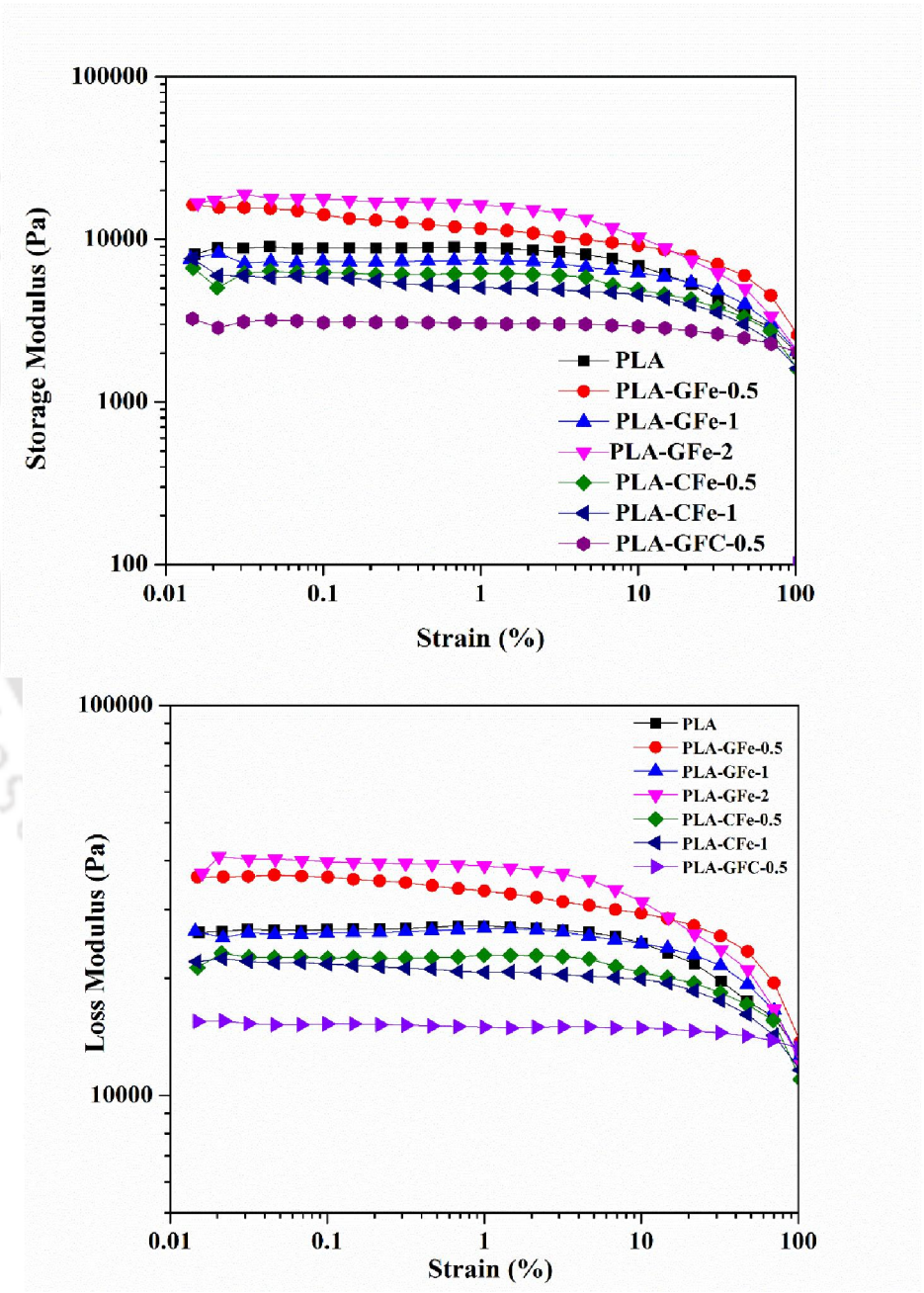

Fig. 7.14 Strain sweep study of the PLA and magnetic composite samples at a fix current (0.2A)

In order to examine the impact of magnetic field on the flow behaviour of magnetic nanoparticle loaded composites, magnetic field strength was varied by changing current from 0.2 A to 0.6 A for the representative composite PLA-GFe-0.5 under strain deformation of 0.01-100%. In case of PLA-GFe-0.5, with an increase in field strength, the modulus values are almost linear up to 5% and beyond that strain dependent flow can be seen (Fig. 7.15). This implies that beyond 5 strain%, the structural deformations take place and it is almost identical in presence of low field strength, whereas in higher field the modulus value decrease compared to zero field. This signifies that in presence of higher field, array of nanomaterials promotes structural deformation. With increasing the field strength, both the modulus are increased in the steady range. The value is higher at 0.2A and with further increment in current, the values are decreased, and at very high current ~0.6A, the value is even lower to zero field. This may be because of very strong field causing magnetic particle orient in the flow direction or some phase separation due to agglomeration of magnetic particles. The above results imply that magnetic particle-based melt is field sensitive and the strain deformation is influenced in presence of the external field. Loss modulus values are also indicating hindered chain mobility in presence of magnetic field up to current of 0.4A and the same is further increased remarkably. This is possibly because of orientation of particles in the flow direction or phase separation as explained above.

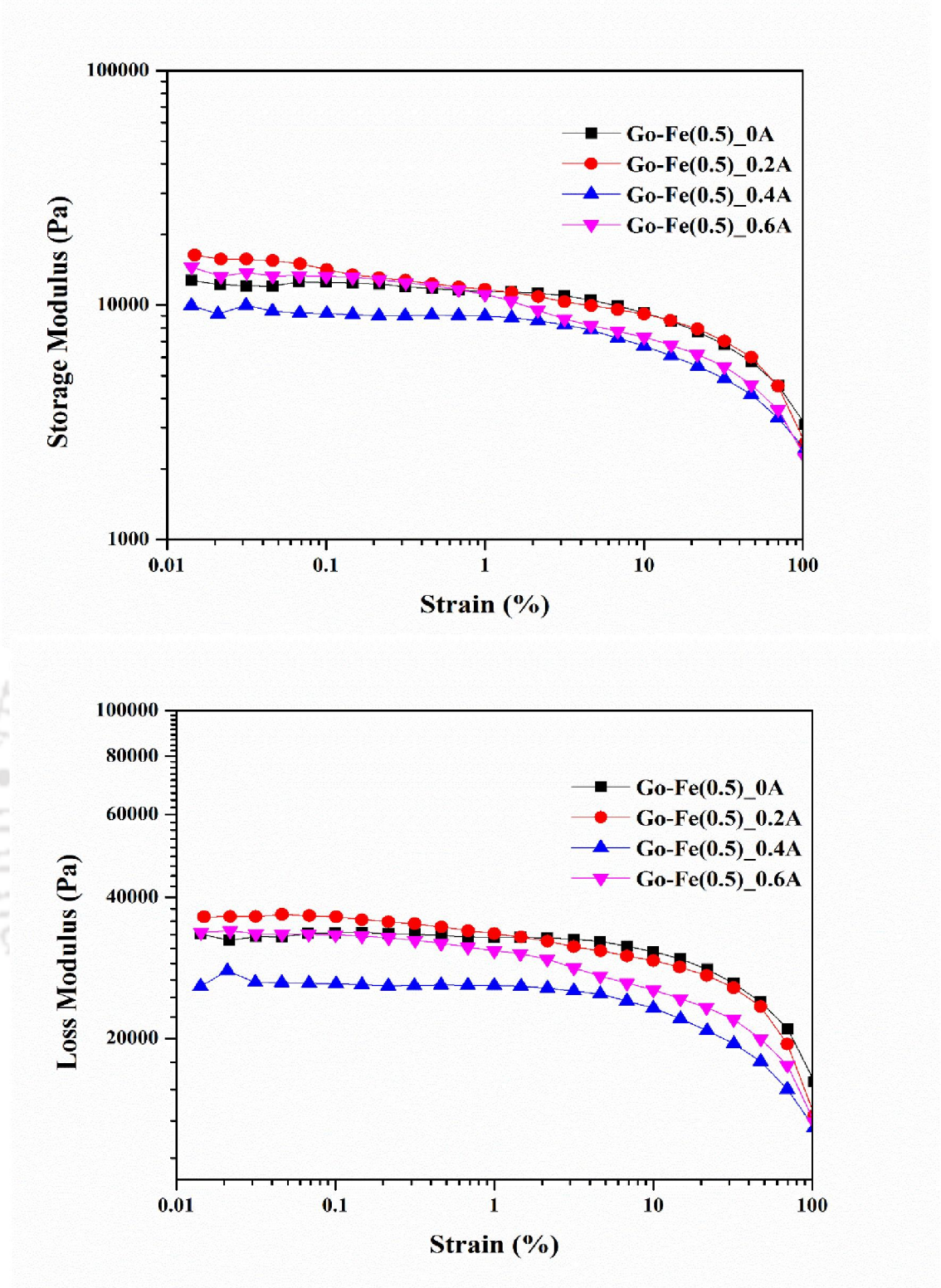

Fig. 7.15 Strain sweep study of PLA-GFe-0.5 in different current (at 170°C)

Frequency sweep analysis

Frequency sweep analysis of the composites at molten state at 170 °C at a constant strain deformation of 5% can be seen from Fig. 7.16. For the components, the trend is

similar i.e. increasing with increase of frequency (Al-Itry et al., 2014; Tesfaye et al., 2017). Storage modulus and loss modulus values are found to be higher for GO-Fe loaded composites at a constant magnetic field corresponding to current of 0.2A. With increase in loading of GO-Fe, the modulus value is decreasing. In case of CF-Fe loaded composites, modulus values are quite similar to PLA. Complex viscosity (η^*) value is higher for GO-Fe loaded composites at a particular magnetic field as compared to other components (Fig. 7.16). 'η^*' decreases with increasing GO-Fe loading from 0.5 to 2 wt. %. This may be due to the presence of more agglomeration sites in the PLA matrix in case of higher loading and this is less active towards orientation in presence of magnetic field. In case of CF-Fe, η^* values are much lower compared to that of PLA, which may be due to fibre-like morphology and orientation in the direction of flow.

Changes in 'G′', 'G″' and 'η^*' are recorded in Fig. 7.17 in case of PLA-GFe-0.5 when magnetic field strength is increased by increasing the current from 0.05-0.6A in order to check the impact of magnetic field on the flow behaviour of PLA under frequency sweep. With increase in field strength, the modulus values are found to be increased and viscosity is found to be decreased compared to the melt of the composite without field. This indicates that the nature of the melts are similar to ferrofluid (Filali et al., 2018; Pan et al., 2005). GO-Fe orients itself under magnetic field, which provides additional resistance towards flow of PLA chains resulting in increment of the modulus values. η^* value is found to be higher at 0.6A for the PLA-GFe-0.5 which suggests that orientation of the magnetic nanomaterial increases with an increase in field strength (Fig. 7.17).

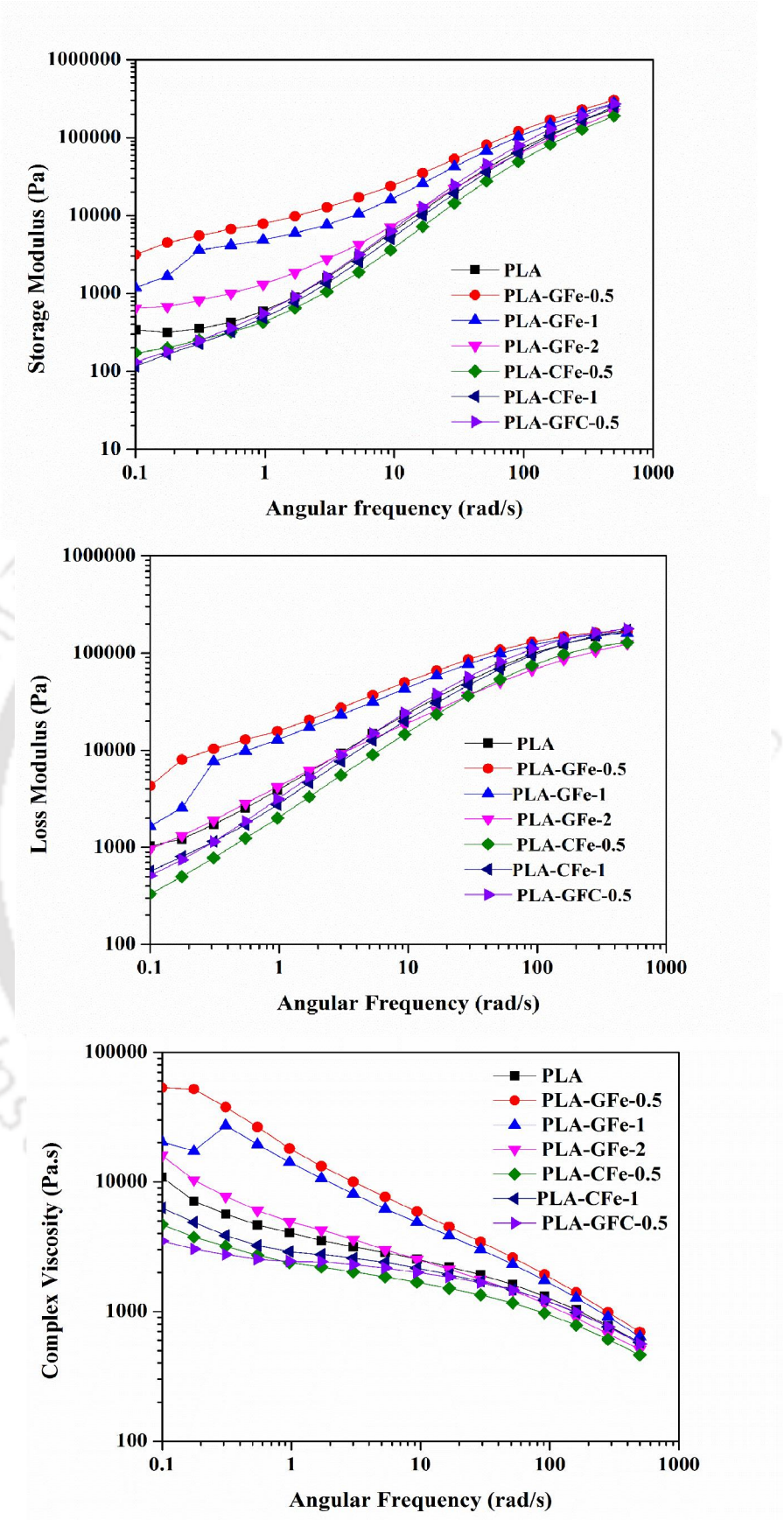

Fig. 7.16 Frequency sweep study of the PLA and magnetic composite samples at a fixed current (0.2A)

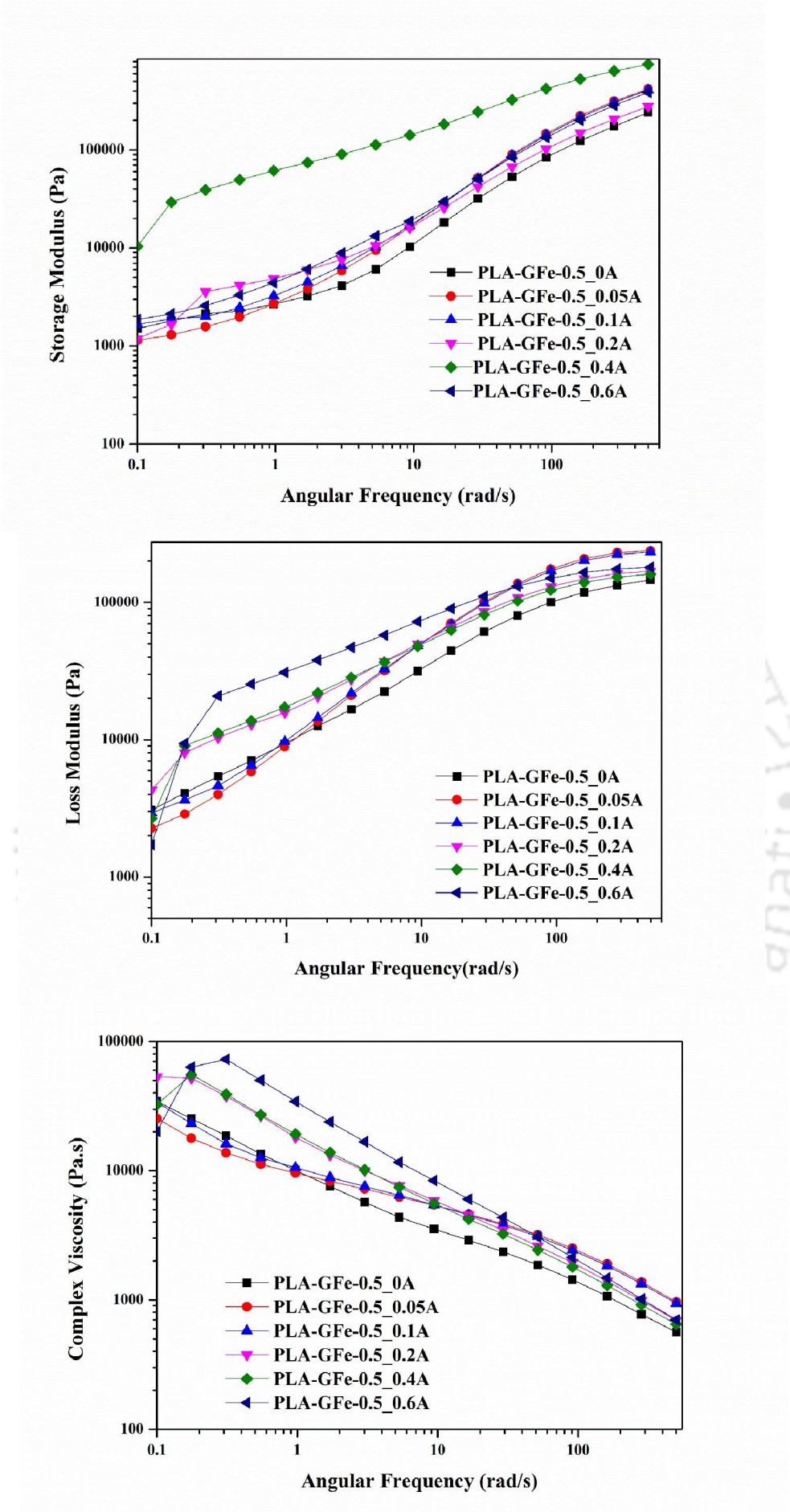

Fig. 7.17 Frequency sweep study of PLA-GFe-0.5 at different current (at 170°C)

Effect of Temperature on frequency sweep

Impact of temperature on the flow behaviour of the polymeric chains of PLA can be seen from Fig. 7.18 for the nanocomposite PLA-GFe-0.5. As expected, ‘G′’ and ‘G″’ values are noticed to be higher for melts at lower temperature (170 °C) in the frequency range of 0.1 to 10 Hz as the polymer chains are getting enough time for chain relaxation. However, in the higher frequency range, the difference between ‘G′’ and ‘G″’ for two different temperatures becomes lower as polymer chains are not getting enough time for structural relaxation. This is due to more liquid-like nature of the composite at higher temperature (175°C). Accordingly, η^* value is lower for the composite at 175°C reflecting the melt to be more fluidic and relaxation to be higher compared to that at 170°C (Al-Itry et al., 2014; Chen et al., 2013).

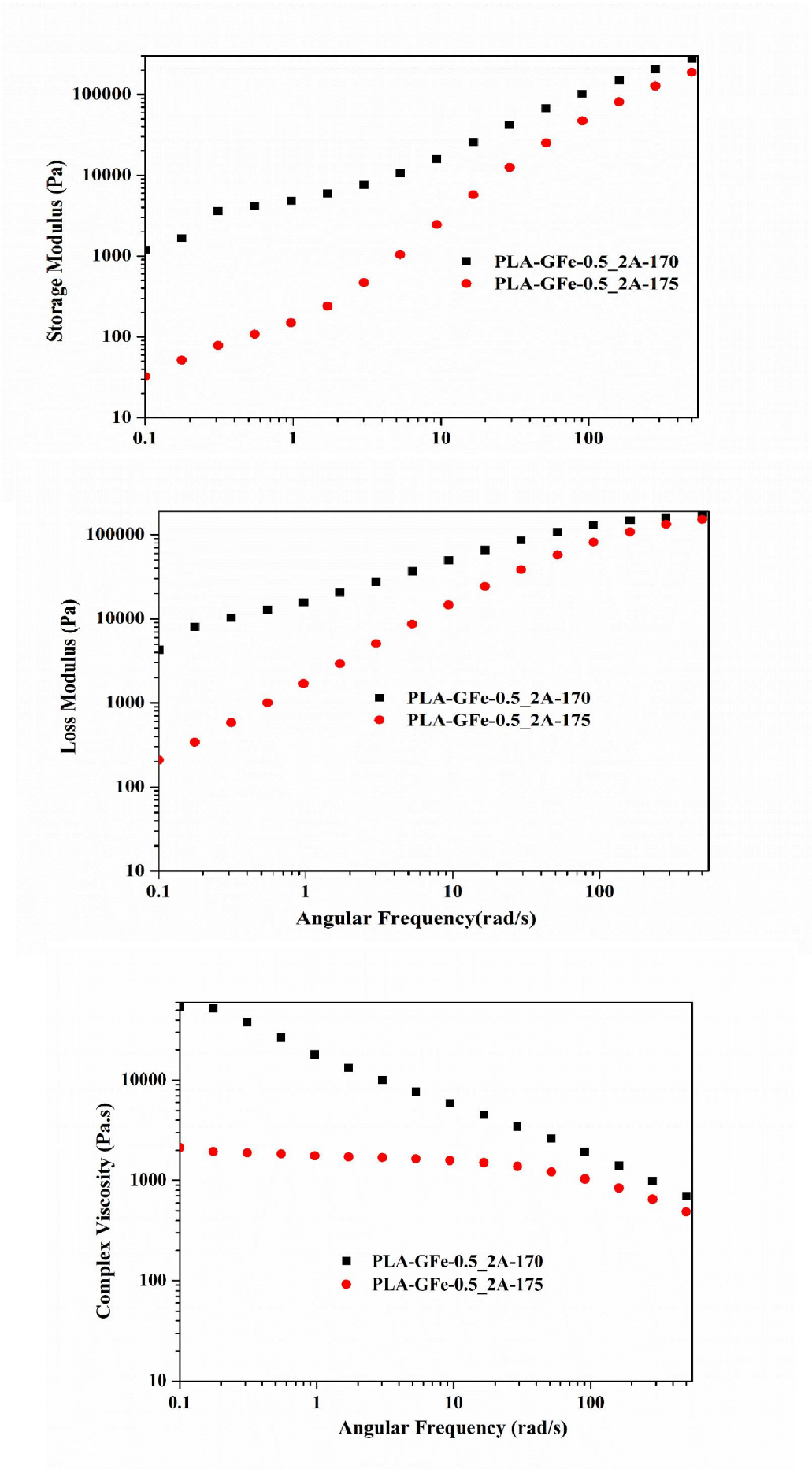

Fig. 7.18 Effect of temperature on storage and loss modulus of PLA-GFe-0.5

7.3.3 Ethanol vapour sensing

In the previous sections, fabrication of magnetic nanoparticles and compatibility of different morphology magnetic particle reinforcement into PLA matrix was thoroughly investigated. It is observed that at low loading of magnetic particles irrespective of their morphology, some of the properties of PLA such as thermal stability, crystallization, magnetism, and flow behaviour are improved. Consequently, the applicability of the magnetic particles as vapour sensing element was studied and details of which are presented below.

Impedance analysis of the composites fabricated doesn't reflect enough conductivity even after addition of magnetic particles in the loading range 0.5 to 2 wt. % as discussed in section 7.3.2.6. In view of this, further investigation was carried out in order to apply magnetic nanoparticles in combination with PLA for sensing application particularly the vapour. Accordingly, from the results in the earlier section, where GO-Fe and CF-Fe were found to be more compatible and had significant impact on the conductive nature and sensing behaviour of PLA, the concept of polymeric binder approach was adopted instead of polymeric composite that, reduces the thickness of the sensing element, reduces the experimental error during casting and also reduces the impedance. This approach provides sophisticated ways for fabrication and vapour sensing. In order to examine the applicability of the magnetic nanoparticles towards vapour sensing through this modified approach, ethanol was taken as representative component for detection. The overall work was divided into the following steps

(i) Development of custom made gas sensing chamber

(ii) Inter-digital electrode (IDE) preparation

(iii) Assembling of vapour sensing set up and

(iv) Ethanol vapour sensing using PLA as binder

(i) Development of custom made gas sensing chamber

3D-printing technique was utilized in order to cast the electrode holding chamber, which can also be termed as gas chamber (Fig. 7.19). It is a closed set up with one inlet and one outlet for vapour. The lid is leak-free and at the centre, a provision is kept to attach the IDE electrode. The entire chamber was first designed using software and then was cast using polymeric thread. In order to ensure no leakage, gasket is used between the lid and the chamber.

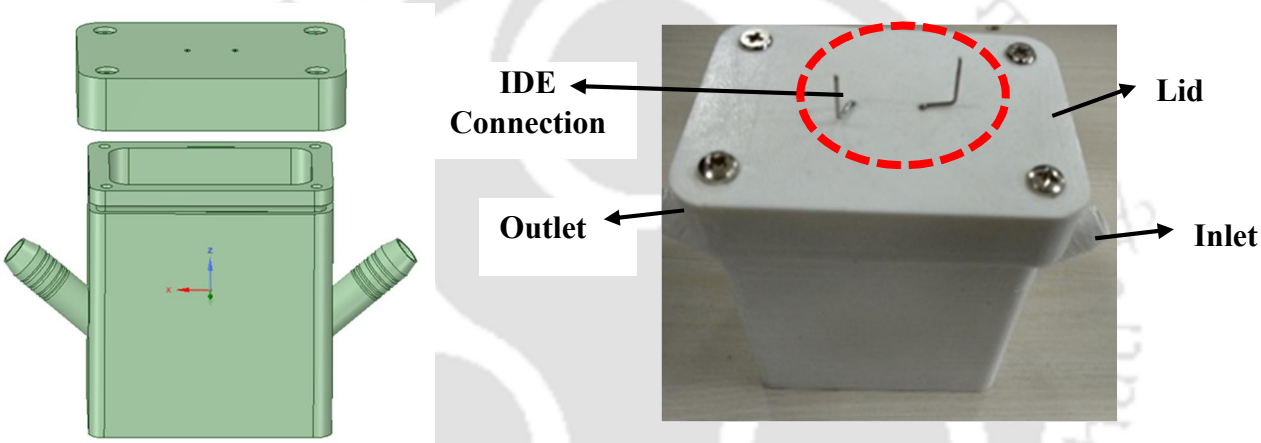

Fig. 7.19 3D-printed custom made gas chamber

(ii) Interdigital electrode (IDE) preparation

Interdigital electrode was cast over breadboard using Cu deposition followed by etching. The gap between the successive electrodes was kept at 1 mm (Fig.7.20). The IDE has two probes which are attached to the gas chamber lid.

Fig. 7.20 Interdigital electrode

(iii) Assembling of vapour sensing set up

The previously mentioned two parts are the major components of the vapour sensor set up. The gas chamber inlet was alternately connected with ethanol vapour or nitrogen source depending on detection experiment or purging. Outlet of the chamber was connected to a rotameter followed by purge. Nitrogen was used as carrier gas for the ethanol vapour. Nitrogen flow rate was maintained using the rotameter between 6NL-20NL/min (NL/min indicates flow in L/min at N.T.P). Purpose of change in flow rate of the carrier is to change the concentration of ethanol in the ethanol-nitrogen mixture. Concentration of ethanol inversely varies with the gas flow rate. Two probes of the chamber were connected to either autolab or multimeter based on requirement and nature of investigation.

A thin film of magnetic nanoparticle in combination with PLA was deposited to make the IDE electrically conductive. PLA was used as binder to make the film uniformly

deposited over the IDE. Use of PLA makes deposition more uniform over the plate (Fig. 7.21). The overall vapour sensing set up can be seen in Fig. 7.22.

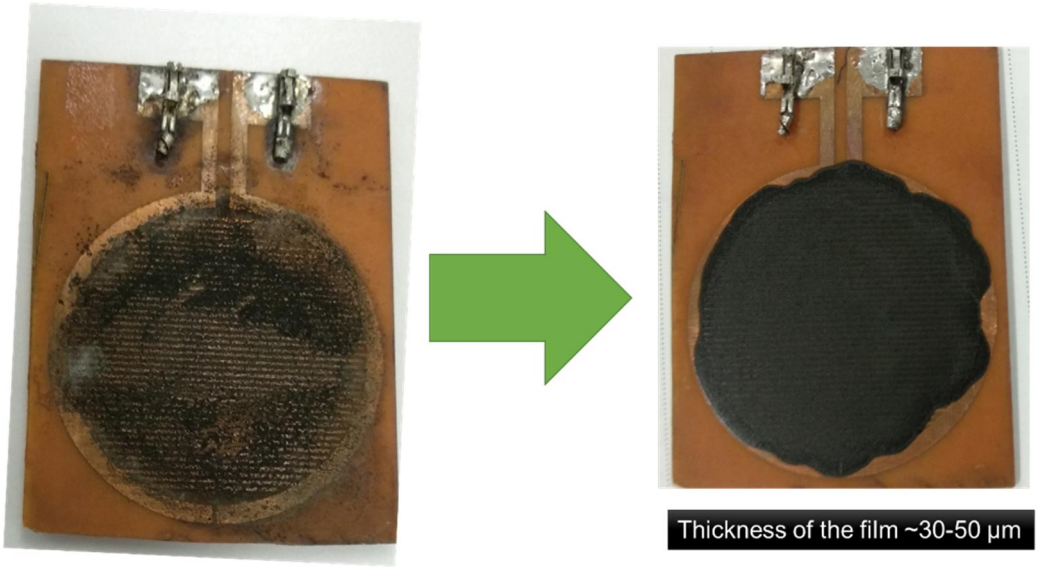

Fig. 7.21 Interdigital electrode before and after using PLA as binder

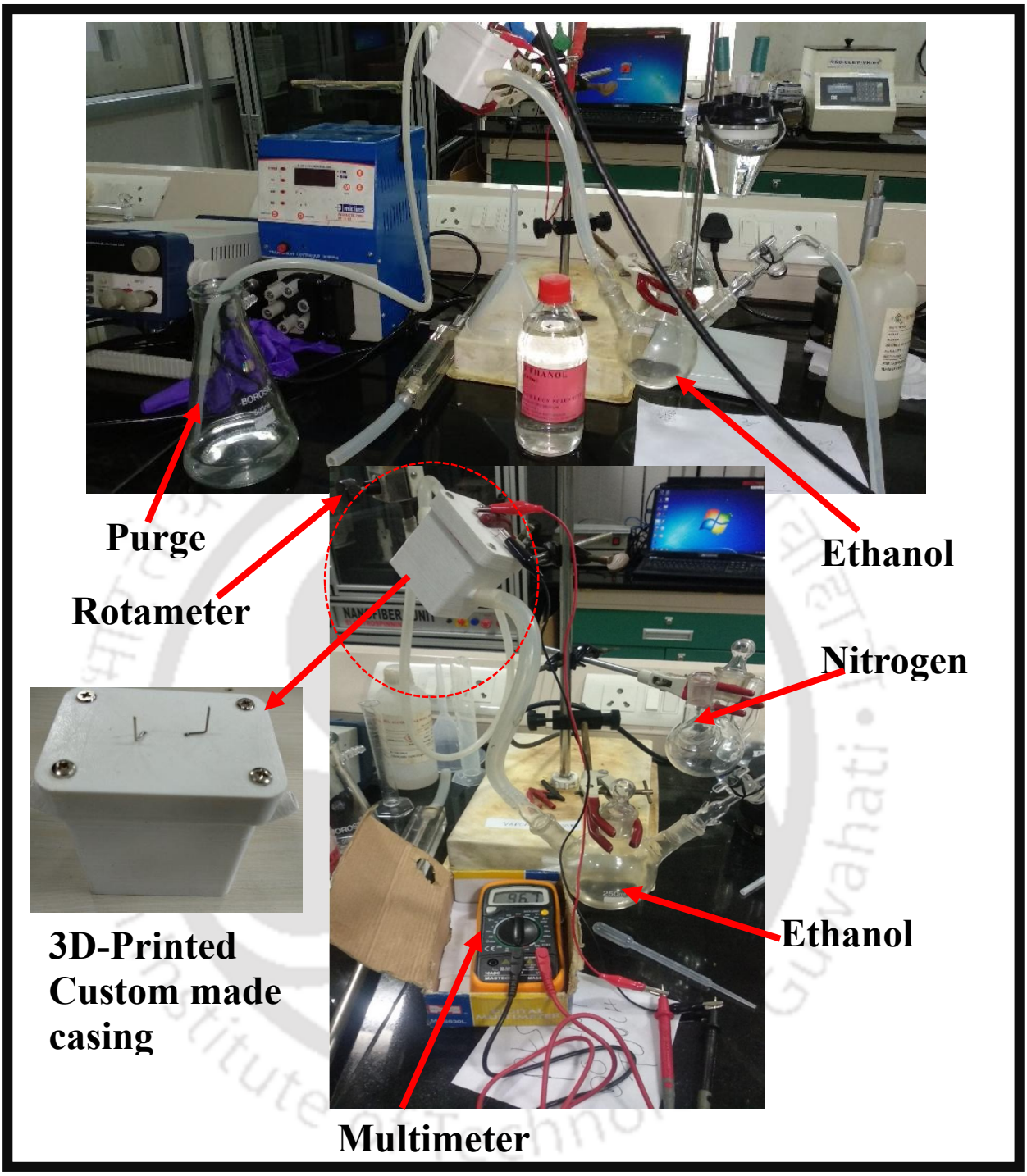

Fig. 7.22 Ethanol vapour sensing set up

(iv) Ethanol vapour sensing using PLA as binder

Initially, prior to investigation of the magnetic particles for ethanol vapour sensing, impedance of the composites were tested using autolab for different loading of magnetic particles within the frequency range of 0.1 to10^5 Hz. Thickness of the films was maintained between 30-50 μm. It can be seen from Fig. 7.23 that impedance is decreasing for both GO-Fe and CF-Fe with an increase in the loading. In the case of CF-Fe loading of 20 wt. %, the impedance value is reduced to ~10Ω. Whereas in case of GO-Fe loading (50 wt. %), the impedance value is reduced to ~10^4 Ω. This is possibly because of higher conductivity and length of carbon fibre (CF) as compared to graphene oxide (GO).

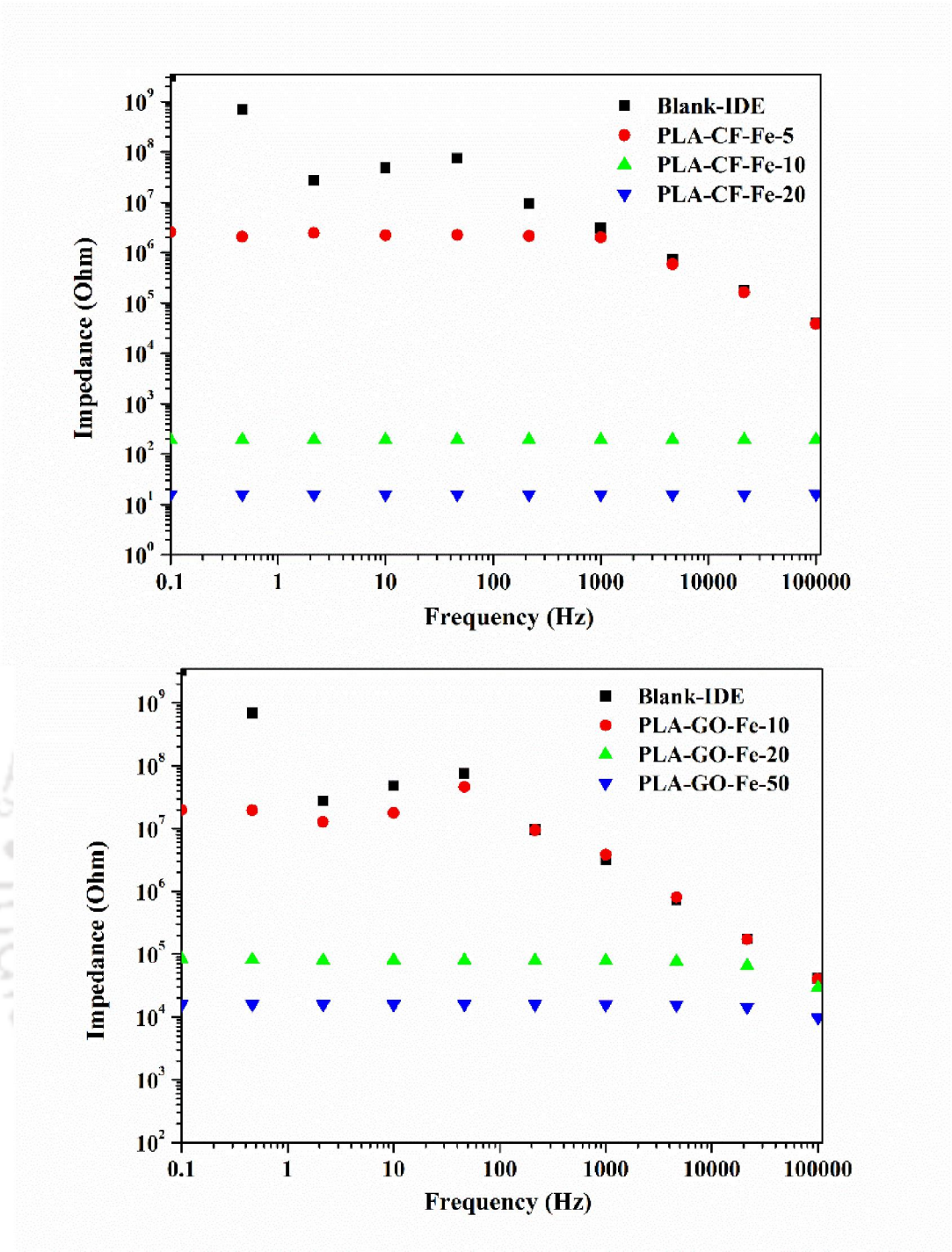

Fig. 7.23 Change in impedance for different loading of GO-Fe and CF-Fe

Ethanol vapour detection was carried out using PLA-GO-Fe-20, PLA-GO-Fe-50 and PLA-CF-Fe-20 by exposing towards ethanol vapour under steady nitrogen flow rate of 6 NL/min. It can be seen from Fig. 7.24 (a) that with exposure time change in relative response is increasing (impedance at 0.1Hz frequency was taken for calculation of change in response). In case of higher loading of GO-Fe (50 wt. %), the nature of

response is similar to CF-Fe (20 wt. %). However, in lower loading of the GO-Fe (20 wt. %), the response is higher compared to that of higher loading. This may be due to higher impedance value of the composite, which means less number of conductive pathways due to capacitive loss within the composite (Kobashi et al., 2008). Figure 7.24 (b) depicts a representative case of PLA-CF-Fe-20 towards ethanol vapour detection in two successive cycles using a drying condition (after 10 min exposure to vapour, drying at 50°C for 5 min followed by 5min at 25°C) in between two cycles. The response is found to be almost similar for the two successive cycles.

Figure 7.25 (a) represents the effect of change of gas flow rate towards change in response. For this study, PLA-GO-Fe-50 and PLA-CF-Fe-20 were taken as sensing element and two nitrogen gas flow rates were maintained viz. 6NL and 10NL. It can be seen that response is higher in case of lower gas flow rate. These findings indicate that this material has sensitivity towards different concentration of ethanol vapour (Kumar et al., 2012). However, further work like calibration for gas flow rate with concentration can determine the sensing range of this sensor, which is a scope of future work of the thesis.

PLA-GO-Fe-50 was taken as representative sensing element for detection by both autolab as well as normal multimeter. In the former case, the relative change in impedance was recorded as response whereas for multimeter, the relative change in resistance was recorded as response. Figure 7.25(b) represents the comparative curve, which suggests that in both the cases, nature of response is quite identical. Continuous measurement using multimeter suggests that the sensing system is responsive within 30 sec of vapour exposure.

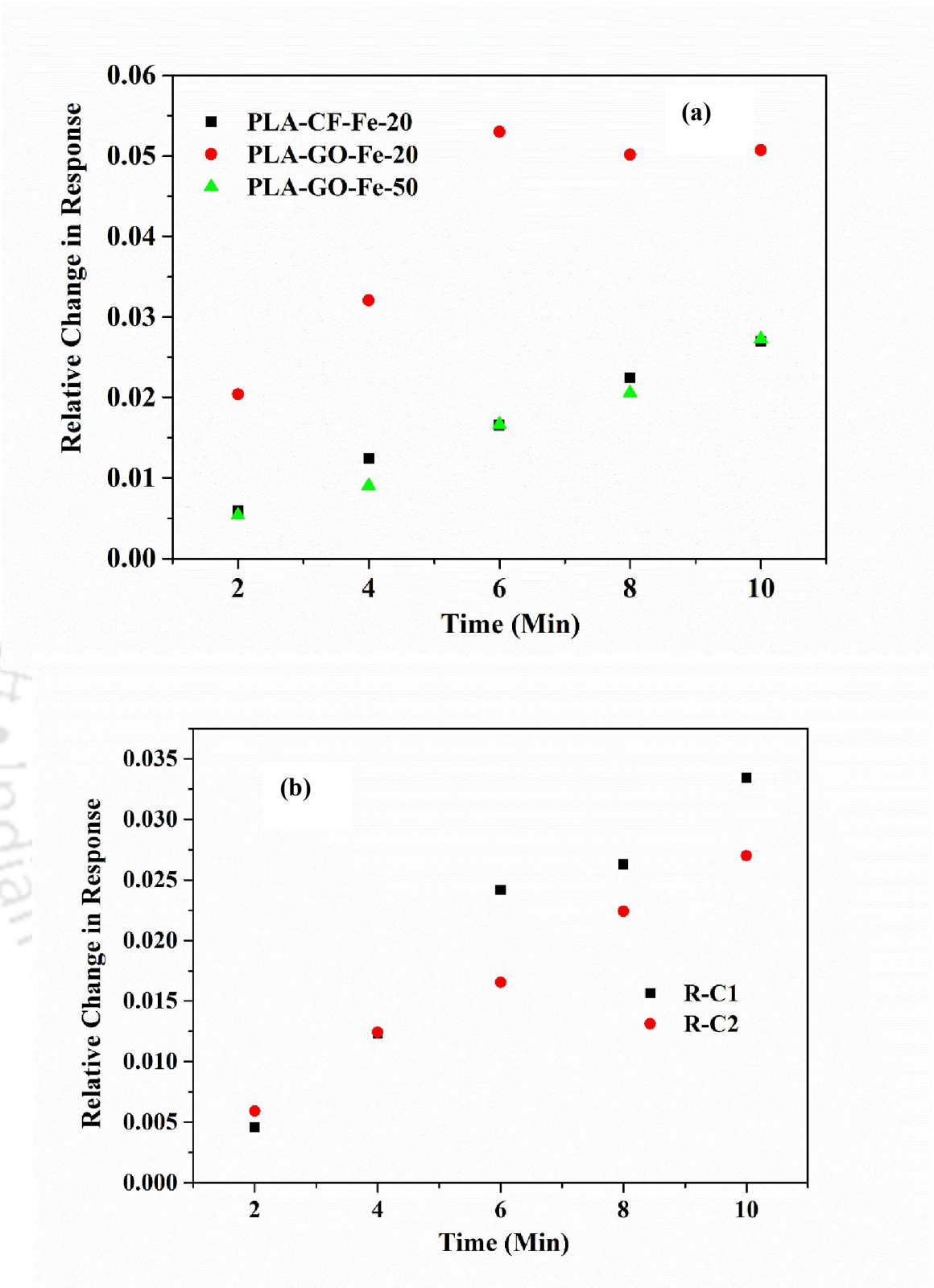

Fig. 7.24 Ethanol vapour sensing (a) Different magnetic material at 6NL nitrogen flow and (b) Repeatability study of PLA-CF-Fe-20

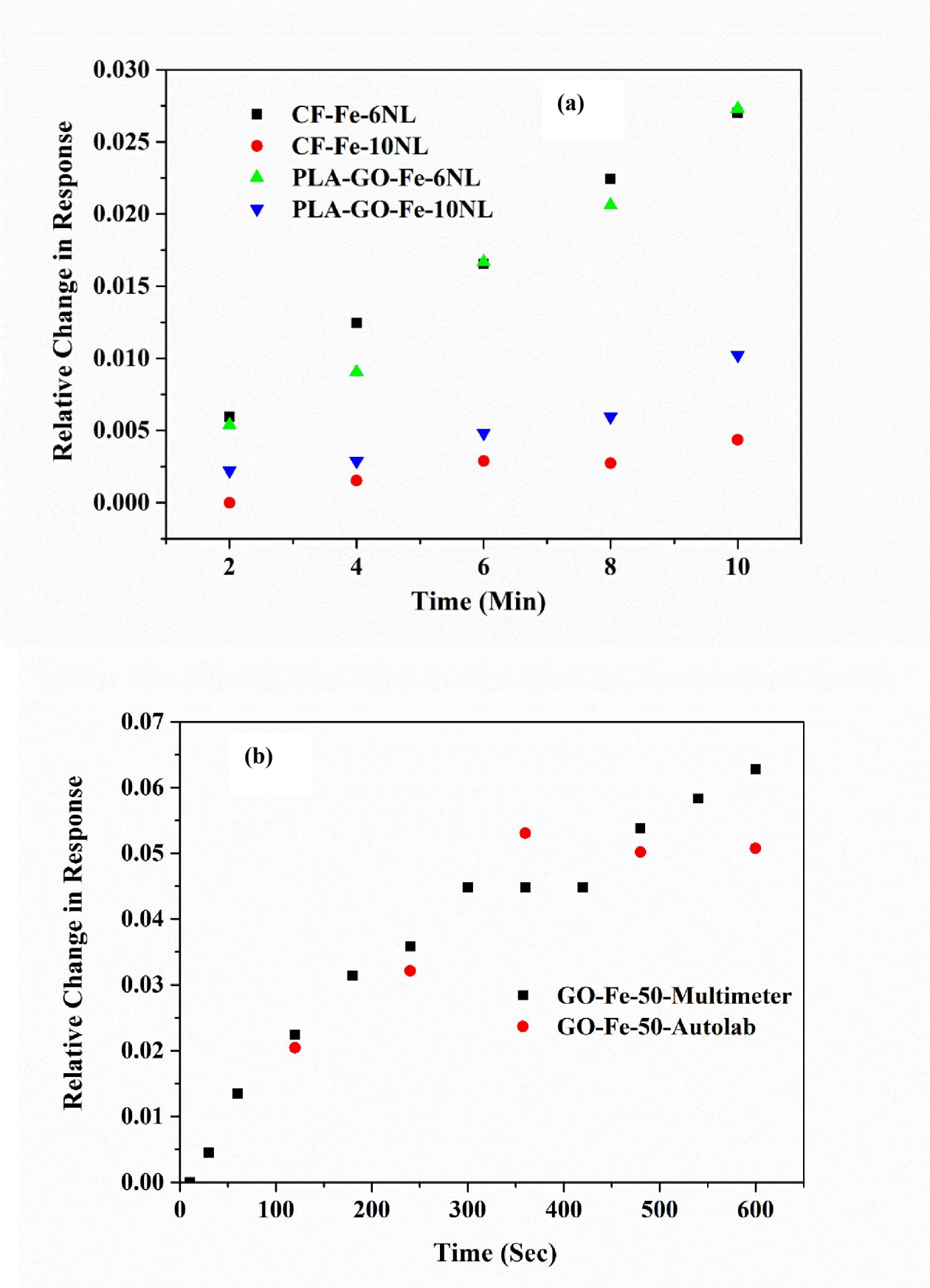

Fig. 7.25 Ethanol vapour sensing (a) Effect of gas flow rate and (b) Comparison with multimeter

Performance comparison of components used for liquid ethanol sensing in this thesis towards ethanol vapour sensing using Autolab

In order to compare the ethanol vapour sensing ability (response and sensitivity) of the compositions used for liquid ethanol sensing in this thesis, a comparison is also made alongside magnetic material based sensing. PLA along with GR was used for liquid ethanol sensing in Chapter 4 and PLA along with GR in presence of low amount of FeCNC was used for sensing for liquid ethanol in Chapter 5 and both were found to have selectivity and sensitivity towards liquid ethanol. Here two compositions i.e. PLA-S-2.5GR (Chapter 4) and PLA-S-2.5GR-0.5Fe (Chapter 5) were cast over IDE in similar way as PLA-GO-Fe and PLA-CF-Fe in order to check vapour sensing ability of the compositions (30-50 μm film). Figure 7.26 depicts the findings where PLA/GR is found to be less responsive towards ethanol vapour and PLA/GR/FeCNC system is found to be responsive towards ethanol vapour sensing, but the response is lower and sensitivity towards variation in concentration is lower as compared to that of the GO-Fe/CF-Fe based compositions. This may be because of the fact that PLA-GR has no additive to promote ethanol vapour adsorption to surface and only diffusion through the film can change the impedance of existing GR networks in the PLA matrix. So in low vapour concentration, the change is small and almost identical for 6NL and 10NL flow rates of nitrogen (Kobashi et al., 2008; Pötschke et al., 2010). In case of PLA/GR/FeCNC, the additive loading is 0.5 wt.% which is distributed in matrix alongside GR networks and increases the response compared to PLA/GR. Whereas, in case of GO-Fe and CF-Fe based compositions, both conductivity and selectivity are imparted by the same filler and as PLA is used as binder, adsorption effectivity towards ethanol vapour is much higher compared to the other two (Barsan & Weimar, 2012;

Huang & Wan, 2009). This may be the possible reason for the higher response and the better sensitivity towards concentration change of ethanol vapour.

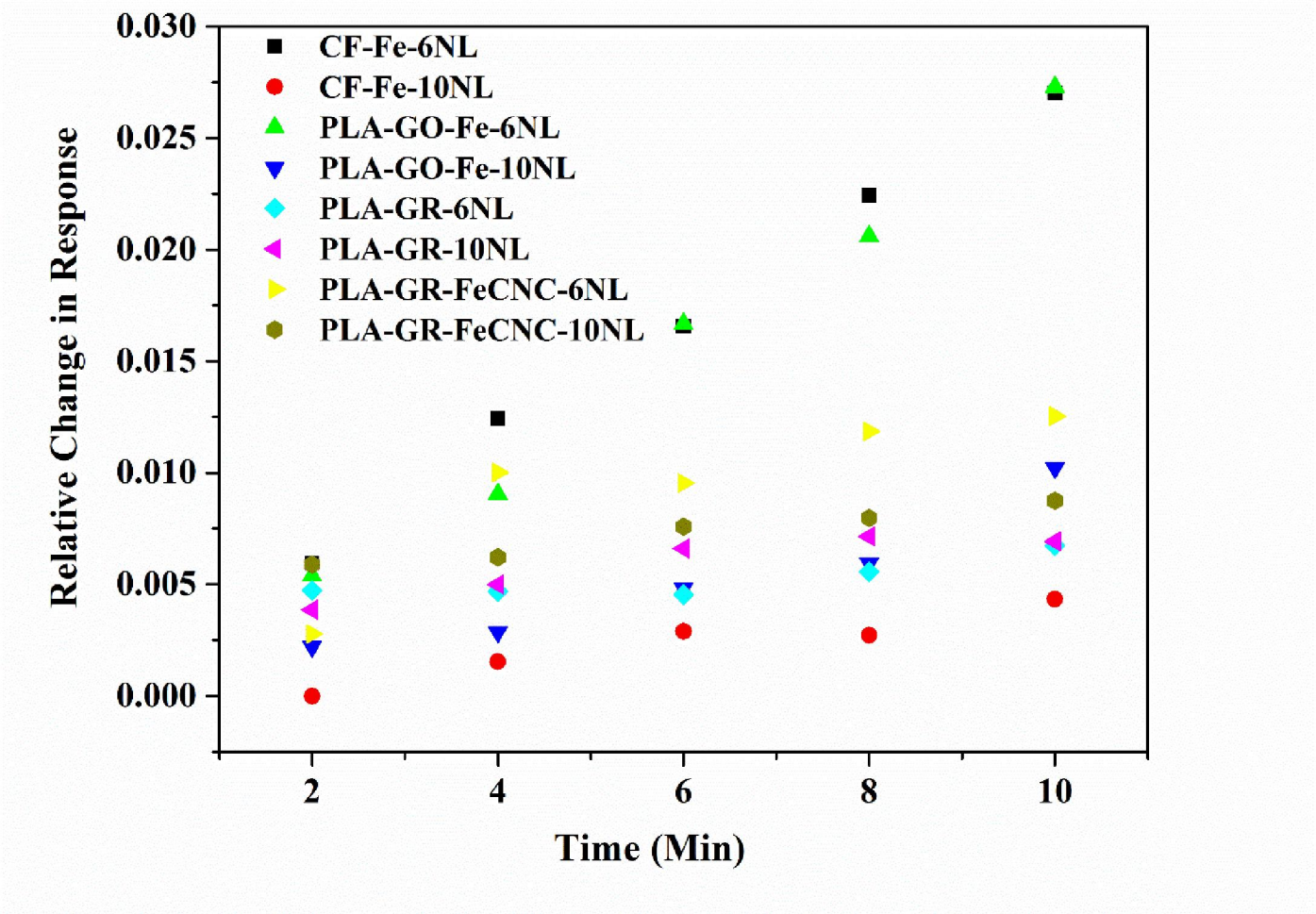

Fig. 7.26 Ethanol vapour sensing using different composition used for the detection of ethanol

7.4 Summary

Successful fabrication of templated magnetic nanomaterials is achieved in this work with uniform dispersion and crystalline nature. Ferromagnetic nature is also observed for the magnetic nanomaterials through VSM analysis.

Incorporation of magnetic nanomaterials in the PLA matrix in the loading range of 0.5 to 2 wt. % doesn't alter the structural nature of PLA. Presence of agglomeration is noticed for the composites, which is higher in case of higher loading. GO-Fe improves the thermal stability of PLA more in comparison to that of CF-Fe due to higher surface area. Catalytic effect of Fe_3O_4 is noticed particularly at maximum degradation temperature. Composite melts are found to be responsive towards change in the magnetic field of the surroundings. Frequency sweep study indicates improvement in melt strength due to application of magnetic field.

Impedance of the PLA composite system reduced to in the order of 10 Ω which is remarkable. Vapour sensing study indicates that magnetic nanoparticle PLA based composites has the capability for ethanol vapour sensing. At higher loading of magnetic nanoparticles, response is found to be reproducible. The response is also found to be sensitive to gas flow rate. These observations suggest that with due calibration and suitable modification, the entire set up can be more applicable for practical purpose. Response time of the sensor observed to be less than 30 sec. The setup is capable of running using normal multimeter indicating potential of practical applicability of the vapour sensor.

Chapter 8
Conclusions and Future Scope

This chapter includes the findings and conclusions of the research work and also indicates the future direction of the work

8.1 Conclusions

Findings of the research works are assembled to get the overall conclusion as follows:

- Well dispersed graphene/PLA composite was fabricated without altering the structure of graphene by solvent coating approach and non-covalent master batch. Both these techniques promoted dispersion of graphene. Environmental hazard due to nanoparticle in surrounding atmosphere was absent during processing.
- Incorporation of graphene improved the thermal stability, hydrophobicity, mechanical strength, storage modulus of the composites significantly compared to that of PLA-M. Dispersion of exfoliated graphene and thermal stability were improved in PLA-M-0.05GR compared to that of both PLA-M and PLA-M-0.2GR. A marginal improvement in electrical conductivity leaves a scope for future research in order to get significant conductivity of PLA/GR composites. Melt rheology revealed that storage modulus (G′) is lower than loss modulus (G″) for the PLA-M and composites; however, storage modulus value is higher for the GR loaded composites (PLA-M-0.05GR and PLA-M-0.2GR) as compared to PLA-M. Excellent dispersion of GR in PLA-M and single phase behaviour of the composites were observed from the Han plot, which is

substantiated by Cole-Cole plot and Van Gurp-Palmen's plot. Polydispersity of PLA was not disturbed much due to incorporation of GR as reinforcement.

- XRD, FESEM and Raman studies revealed better dispersion and interaction of reinforcement in case of the MB diluted composites (PLA-MB-0.05GR and PLA-MB-0.2GR) compared to that of normal coated composite (PLA-M-0.2GR). Thermal stability was found to be higher for PLA-MB-0.2GR compared to that for PLA-MB-0.05GR due to effect of graphene loading. Tensile strength decreased for the MB diluted composites when compared with normal coated composite. Young's modulus was higher for PLA-MB-0.05GR signifying better compatibility of the reinforcement with the matrix due to similar polymer interaction. Elongation at break increased for 0.05 wt. % loading and it was 17% higher than PLA-M. Even though there is no major improvement in some of the mechanical properties of the GR-dispersed PLA composite compared to the ordinary PLA-M, other properties such as dynamic mechanical, thermal and rheological properties are significantly improved for the MB dispersed GR composites.
- Ethanol of varied concentration was used for detection test by the fabricated composite with optimized GR content. Impedance of the PLA/GR composites was reduced from $10^{11}\Omega$ for PLA to $10^{4}\Omega$ range due to the incorporation of GR. The normalized effective polymer length of the composite responsible for the resistive response was reduced to a very low value of 10^{-6}. The composite PLA-S-2.5GR with 2.5 wt. % GR loading was successfully applied for the detection of ethanol with varied concentration. The composite film was reused at least five times without any significant change in response. Repeatability study of the composites from different batches suggested that controlled fabrication of the

composite in terms of crystallinity and uniform thickness is necessary to make it an application ready material. Solvent diffusion is the main governing phenomena and the composites demonstrated desired ethanol selectivity and sensitivity. Overall, the PLA/GR composite with suitable GR loading has proved itself as a potential material for sensor application and would open up a new arena for development of sustainable material for sensor application.

- Fe-CNC was added to the optimized PLA-S-2.5GR composite to improve the sensing capability of PLA/GR composite for ethanol as well as biomolecules like D-glucose and glycine. Firstly, optimization of Fe-CNC loading was done by taking two different loading of Fe-CNC i.e. 0.5 wt. % of Fe-CNC (PLA-S-2.5GR-0.5Fe) and 1 wt. % Fe-CNC (PLA-S-2.5GR-1Fe). The former showed better dispersion, lesser agglomeration, better mechanical strength and comparable thermal stability. Conductive network was not altered due to incorporation of Fe-CNC. Thus, considering the above findings, PLA-S-2.5GR-0.5Fe turns out to be the better composite, which was used for electrochemical sensing for ethanol, D-glucose and glycine. PLA-S-2.5GR-0.5Fe displayed better response towards 25% ethanol detection. It reflects that incorporation of Fe-CNC increases the driving force of ethanol diffusion and thus change in response is higher. Stability analysis of the composite film after use also confirmed the ethanol diffusion through composite film and also indicated that the films are stable even after used for third cycles. The performance of the composites was also found to be repeatable, reusable and consistent. D-glucose and Glycine sensing studies demonstrated that the PLA-S-2.5GR-0.5 Fe film has selectivity and sensitivity toward these components. Thus appropriate selection of metallic filler followed by fabrication of the composite and sensing

study with proper thermo-physical condition can effectively and efficiently be applied for various types of biomolecules.

- Different additives like EDTA, SNC and Albumin were successfully incorporated into the PLA/GR system, which was confirmed through FTIR and XRD. Incorporation of filler decreased the thermal stability of the film, but for PLA-S-2.5GR-0.5EDTA, the decline was less.. PLA-S-2.5GR composite displayed good sensitivity for Cu^{2+} ion detection within the concentration range of 5-100 ppm. Hysteresis loop of I-V response was found to be dependent on the scan rate, type of cation and anion and electrode type. It confirms behaviour of PLA-S-2.5GR film as ideal material for electrode. In case of modified composites, a reduction peak of Cu^{2+} is found for PLA-S-2.5GR-0.5EDTA and PLA-S-2.5GR-0.5Alb indicating that ion binding with the additives depends on the available ligand sites. Application domain is found to be higher for PLA-S-2.5GR-0.5Alb whereas for PLA-S-2.5GR-0.5EDTA linearity in response is higher compared to the other composition.
- In view of fabricating PLA based smart conductive material, GO and carbon fiber based magnetic nanomaterials were successfully synthesized by co-precipitation method. Ferromagnetic nature is observed for the magnetic nanomaterials. Incorporation of magnetic nanomaterials in the PLA matrix in the loading range of 0.5 to 2 wt. % doesn't alter the structure of PLA. Owing to larger surface area of GO-Fe the thermal stability of PLA is improved more in comparison to that of CF-Fe. Composite melts are found to be responsive towards change in the magnetic field of the surroundings and improvement in melt strength is noticed on application of magnetic field. Magnetic nanoparticle PLA based composites has the capability for ethanol vapour sensing. At higher

loading of magnetic nanoparticles, response is found to be reproducible and sensitive to gas flow rate. These observations suggest that with due calibration and suitable modification, the entire set up can be made applicable for practical purpose.

- In order to investigate the sensing nature of the PLA based conductive composites, three different type of sensing system was investigated and two of them were prepared in lab as discussed in Chapter 4 and Chapter 7. Vapour sensor setup was prepared by lab made 3D-printed gas chamber and interdigital electrode printed in Lab. Different additives are utilized in order to enhance the sensitivity and selectivity of the composites and significant improvement is noticed for the respective cases, which promotes applicability of PLA based conductive composites in electronics application particularly in the field of electrochemical and biosensing. Magnetic particle incorporation followed by rheological investigation in presence of magnetic field reflects the potential of PLA to be applicable for preparation of smart magnetic fluid and smart composites. The first hand results from ethanol vapour sensing study indicate that PLA has the capability to be applicable as binder along with magnetic particle for vapour sensing application.

8.2 Scope for Future Work

- Non-covalent wrapping technique for GR dispersion in PLA can be done using conductive polymers.
- Other metallic compounds along with PLA/GR can be studied for improvement of ethanol detection.
- Calibration of gas flow rate with concentration of ethanol vapour is necessary to get sensitivity range of the ethanol vapour sensor.
- Further reduction of the thickness of the bulk modified composites and application towards glucose, glycine and metal ions can be done.

References

Abrosimova, K., Shulenina, O., & Paston, S. (2016). FTIR study of secondary structure of bovine serum albumin and ovalbumin. *Journal of Physics: Conference Series* (Vol. 769, p. 012016): IOP Publishing.

Aboulkas, A., & El Harfi, K. (2008). Study of the kinetics and mechanisms of thermal decomposition of Moroccan Tarfaya oil shale and its kerogen. *Oil Shale*, 25(4), 426-443.

Ahmed, J., Varshney, S. K., Auras, R., & Hwang, S. W. (2010a). Thermal and Rheological Properties of L-Polylactide/Polyethylene Glycol/Silicate Nanocomposites Films. *Journal of Food Science*, 75(8).

Al-Itry, R., Lamnawar, K., & Maazouz, A. (2014). Reactive extrusion of PLA, PBAT with a multi-functional epoxide: Physico-chemical and rheological properties. *European Polymer Journal*, 58, 90-102.

Al-Mulla, A., & Shaban, H. (2008). Thermal degradation of poly (trimethylene terephthalate) and acrylonitrile butadiene styrene blends: Kinetic analysis of thermogravimetric data. *International Journal of Polymeric Materials*, 57(3), 275-287.

Al-Mulla, E. A. J., Suhail, A. H., & Aowda, S. A. (2011). New biopolymer nanocomposites based on epoxidized soybean oil plasticized poly (lactic acid)/fatty nitrogen compounds modified clay: Preparation and characterization. *Industrial Crops and Products*, 33(1), 23-29.

Antić, V. V., Pergal, M. V., Antić, M. P., & Đonlagić, J. A. (2010). Rheological behaviour of thermoplastic poly (ester-siloxane) s. *Hemijska industrija*, 64(6), 537-545.

Apaydin-Varol, E., Polat, S., & Putun, A. E. (2014). Pyrolysis kinetics and thermal decomposition behavior of polycarbonate-a TGA-FTIR study. *Thermal Science*, 18(3), 833-842.

Appendini, P., & Hotchkiss, J. H. (2002). Review of antimicrobial food packaging. *Innovative Food Science & Emerging Technologies,* 3(2), 113-126.

Aranguren, M. I., Mora, E., DeGroot Jr, J. V., & Macosko, C. W. (1992). Effect of reinforcing fillers on the rheology of polymer melts. *Journal of Rheology,* 36(6), 1165-1182.

Araújo, A., Botelho, G., Oliveira, M., & Machado, A. (2014). Influence of clay organic modifier on the thermal-stability of PLA based nanocomposites. *Applied Clay Science,* 88, 144-150.

Arsat, R., Breedon, M., Shafiei, M., Spizziri, P., Gilje, S., Kaner, R.,Wlodarski, W. (2009). Graphene-like nano-sheets for surface acoustic wave gas sensor applications. *Chemical Physics Letters,* 467(4-6), 344-347.

Auras, R., Harte, B., & Selke, S. (2004). An overview of polylactides as packaging materials. *Macromolecular Bioscience,* 4(9), 835-864.

Babu, R. P., O'connor, K., & Seeram, R. (2013). Current progress on bio-based polymers and their future trends. *Progress in Biomaterials,* 2(1), 8.

Bair, S., Yamaguchi, T., Brouwer, L., Schwarze, H., Vergne, P., & Poll, G. (2014). Oscillatory and steady shear viscosity: The Cox–Merz rule, superposition, and application to EHL friction. *Tribology International,* 79, 126-131.

Bakker, E., & Telting-Diaz, M. (2002). Electrochemical sensors. *Analytical Chemistry,* 74(12), 2781-2800.

Bansod, B., Kumar, T., Thakur, R., Rana, S., & Singh, I. (2017). A review on various electrochemical techniques for heavy metal ions detection with different sensing platforms. *Biosensors and Bioelectronics,* 94, 443-455.

Baran, E. J., Wagner, C. C., & Torre, M. H. (2002). Synthesis and characterization of EDTA complexes useful for trace elements supplementation. *Journal of the Brazilian Chemical Society,* 13(5), 576-582.

Barsan, N., & Weimar, U. (2012). 7.3. 3 Fundamentals of Metal Oxide Gas Sensors. *Proceedings IMCS 2012*, 618-621.

Battegazzore, D., Bocchini, S., & Frache, A. (2011). Crystallization kinetics of poly (lactic acid)-talc composites. *Express Polymer Letters,* 5(10), 849-858.

Biji, K., Ravishankar, C., Mohan, C., & Gopal, T. S. (2015). Smart packaging systems for food applications: a review. *Journal of Food Science and Technology,* 52(10), 6125-6135.

Boncel, S., Brzeziński, M., Mrowiec-Białoń, J., Janas, D., Koziol, K. K., & Walczak, K. Z. (2013). Oxidised multi-wall carbon nanotubes–(R)-polylactide composite with a covalent β-d-uridine filler-matrix linker. *Materials Letters,* 91, 50-54.

Bondeson, D., & Oksman, K. (2007). Polylactic acid/cellulose whisker nanocomposites modified by polyvinyl alcohol. *Composites Part A: Applied Science and Manufacturing,* 38(12), 2486-2492.

Borkotoky, S. S., Dhar, P., & Katiyar, V. (2018). Biodegradable poly (lactic acid)/Cellulose nanocrystals (CNCs) composite microcellular foam: Effect of nanofillers on foam cellular morphology, thermal and wettability behavior. *International Journal of Biological Macromolecules,* 106, 433-446.

Bose, S., Kuila, T., Uddin, M. E., Kim, N. H., Lau, A. K., & Lee, J. H. (2010). In-situ synthesis and characterization of electrically conductive polypyrrole/graphene nanocomposites. *Polymer,* 51(25), 5921-5928.

Buys, Y. F., Aoyama, T., Akasaka, S., Asai, S., & Sumita, M. (2010). Utilization of polymer degradation to modify electrical properties of poly (l-lactide)/poly (methyl methacrylate)/carbon filler composites. *Composites Science and Technology,* 70(1), 200-205.

Buzea, C., Pacheco, I. I., & Robbie, K. (2007). Nanomaterials and nanoparticles: sources and toxicity. *Biointerphases,* 2(4), MR17-MR71.

Cao, Y., Feng, J., & Wu, P. (2010). Preparation of organically dispersible graphene nanosheet powders through a lyophilization method and their poly (lactic acid) composites. *Carbon,* 48(13), 3834-3839.

Carrasco, F., Pagès, P., Gámez-Pérez, J., Santana, O., & Maspoch, M. L. (2010). Processing of poly (lactic acid): characterization of chemical structure, thermal stability and mechanical properties. *Polymer Degradation and Stability,* 95(2), 116-125.

Cassagnau, P., & Melis, F. (2003). Non-linear viscoelastic behaviour and modulus recovery in silica filled polymers. *Polymer,* 44(21), 6607-6615.

Castro-Aguirre, E., Iñiguez-Franco, F., Samsudin, H., Fang, X., & Auras, R. (2016). Poly (lactic acid)—Mass production, processing, industrial applications, and end of life. *Advanced drug delivery reviews,* 107, 333-366.

Chaudhry, Q., & Castle, L. (2011). Food applications of nanotechnologies: an overview of opportunities and challenges for developing countries. *Trends in Food Science & Technology,* 22(11), 595-603.

Chen, G. G.-Q. (2009). *Plastics from bacteria: natural functions and applications*: Springer Science & Business Media.

Chen, J.-L., Yan, X.-P., Meng, K., & Wang, S.-F. (2011). Graphene oxide based photoinduced charge transfer label-free near-infrared fluorescent biosensor for dopamine. *Analytical Chemistry,* 83(22), 8787-8793.

Chen, K., Zhao, Y., & Yuan, X. (2014). Grafting of poly (lauryl acrylate) onto nano-silica by 'click chemistry'. *Chemical Research in Chinese Universities,* 30(2), 339-342.

Chen, Y., Zou, H., Liang, M., & Liu, P. (2013). Rheological, thermal, and morphological properties of low-density polyethylene/ultra-high-molecular-weight polyethylene and linear low-density polyethylene/ultra-high-molecular-weight polyethylene blends. *Journal of Applied Polymer Science,* 129(3), 945-953.

Chieng, B., Ibrahim, N., Yunus, W., Hussein, M., Then, Y., & Loo, Y. (2014). Effects of graphene nanoplatelets and reduced graphene oxide on poly (lactic acid) and plasticized poly (lactic acid): a comparative study. *Polymers,* 6(8), 2232-2246.

Chieng, B. W., Ibrahim, N. A., Yunus, W. M. Z. W., Hussein, M. Z., & Loo, Y. Y. (2014). Effect of graphene nanoplatelets as nanofiller in plasticized poly (lactic acid) nanocomposites. *Journal of Thermal Analysis and Calorimetry,* 118(3), 1551-1559.

Chu, Z., Zhao, T., Li, L., Fan, J., & Qin, Y. (2017). Characterization of antimicrobial poly (lactic acid)/nano-composite films with silver and zinc oxide nanoparticles. *Materials,* 10(6), 659.

Chung, M. G., Kim, D.-H., Seo, D. K., Kim, T., Im, H. U., Lee, H. M., Kim, Y. H. (2012). Flexible hydrogen sensors using graphene with palladium nanoparticle decoration. *Sensors and Actuators B: Chemical,* 169, 387-392.

Cox, W., & Merz, E. (1959). Rheology of Polymer Melts—A Correlation of Dynamic and Steady Flow Measurements. *International Symposium on Plastics Testing and Standardization*: ASTM International.

De Azeredo, H. M. (2009). Nanocomposites for food packaging applications. *Food Research International,* 42(9), 1240-1253.

Djurdjevic, P (1990). The complexation between iron (III) ion and glycine in nitrate medium. *Transit. Met. Chem*.15, 345-350

Dhar, P., Kumar, A., & Katiyar, V. (2016). Magnetic cellulose nanocrystal based anisotropic polylactic acid nanocomposite films: influence on electrical, magnetic, thermal, and mechanical properties. ACS Applied Materials & Interfaces, 8(28), 18393-18409.

Dhar, P., Tarafder, D., Kumar, A., & Katiyar, V. (2015). Effect of cellulose nanocrystal polymorphs on mechanical, barrier and thermal properties of poly (lactic acid) based bionanocomposites. *Rsc Advances,* 5(74), 60426-60440.

Dong, H., Esser-Kahn, A. P., Thakre, P. R., Patrick, J. F., Sottos, N. R., White, S. R., & Moore, J. S. (2011). Chemical treatment of poly (lactic acid) fibers to enhance the rate of thermal depolymerization. *ACS Applied Materials & Interfaces,* 4(2), 503-509.

Drumright, R. E., Gruber, P. R., & Henton, D. E. (2000). Polylactic acid technology. *Advanced Materials,* 12(23), 1841-1846.

Dua, V., Surwade, S. P., Ammu, S., Agnihotra, S. R., Jain, S., Roberts, K. E., . . . Manohar, S. K. (2010). All-organic vapor sensor using inkjet-printed reduced graphene oxide. *Angewandte Chemie International Edition,* 49(12), 2154-2157.

Duncan, T. V. (2011). Applications of nanotechnology in food packaging and food safety: Barrier materials, antimicrobials and sensors. *Journal of Colloid and Interface Science,* 363(1), 1-24.

El-Okr, M., Salem, M., Salim, M., El-Okr, R., Ashoush, M., & Talaat, H. (2011). Synthesis of cobalt ferrite nano-particles and their magnetic characterization. *Journal of Magnetism and Magnetic Materials,* 323(7), 920-926.

Faruk, O., Bledzki, A. K., Fink, H.-P., & Sain, M. (2012). Biocomposites reinforced with natural fibers: 2000–2010. *Progress in Polymer Science,* 37(11), 1552-1596.

Feier, B., Bajan, I., Fizesan, I., Floner, D., Cristea, C., Geneste, F., & Sandulescu, R. (2015). Highly selective electrochemical detection of copper (II) using N, N'-bis (acetylacetone) ethylenediimine as a receptor. *International Journal of Electrochemical Science* 10, 121-139.

Feig, V. R., Tran, H., & Bao, Z. (2018). Biodegradable polymeric materials in degradable electronic devices. *ACS Central Science,* 4(3), 337-348.

Filali, Y., Er-Riani, M., & El Jarroudi, M. (2018). The deformation of a ferrofluid drop under a uniform magnetic field. *International Journal of Non-Linear Mechanics,* 99, 173-181.

Fisher, A., & Naughton, D. (2006). Copper (II) complex of the chelating agent EDTA bis (tyrosine). *Journal of Structural Chemistry,* 47(1), 87-90.

Flory, P. J. (1953). *Principles of Polymer Chemistry*: Cornell University Press.

Furlan, P. Y., Scott, S. A., & Peaslee, M. H. (2007). FTIR-ATR Study of pH Effects on Egg Albumin Secondary Structure. *Spectroscopy Letters,* 40(3), 475-482.

Gan, T., & Hu, S. (2011). Electrochemical sensors based on graphene materials. *Microchimica Acta,* 175(1-2), 1.

Gao, F. (2004). Clay/polymer composites: the story. *Materials today,* 7(11), 50-55.

Gao, X., Du, C., Zhuang, Z., & Chen, W. (2016). Carbon quantum dot-based nanoprobes for metal ion detection. *Journal of Materials Chemistry C,* 4(29), 6927-6945.

Gerard, M., Chaubey, A., & Malhotra, B. (2002). Application of conducting polymers to biosensors. *Biosensors and bioelectronics,* 17(5), 345-359.

Girija, T., & Sangaranarayanan, M. (2006). Analysis of polyaniline-based nickel electrodes for electrochemical supercapacitors. *Journal of Power Sources,* 156(2), 705-711.

Gómez, H., Ram, M. K., Alvi, F., Villalba, P., Stefanakos, E. L., & Kumar, A. (2011). Graphene-conducting polymer nanocomposite as novel electrode for supercapacitors. *Journal of Power Sources,* 196(8), 4102-4108.

Gorghiu, L., Jipa, S., Zaharescu, T., Setnescu, R., & Mihalcea, I. (2004). The effect of metals on thermal degradation of polyethylenes. *Polymer Degradation and Stability,* 84(1), 7-11.

Gwon, H., Kim, H.-S., Lee, K. U., Seo, D.-H., Park, Y. C., Lee, Y.-S.,Kang, K. (2011). Flexible energy storage devices based on graphene paper. *Energy & Environmental Science,* 4(4), 1277-1283.

Han, H. S., You, J.-M., Jeong, H., & Jeon, S. (2013). Synthesis of graphene oxide grafted poly (lactic acid) with palladium nanoparticles and its application to serotonin sensing. *Applied Surface Science,* 284, 438-445.

He, F., Fan, J., Ma, D., Zhang, L., Leung, C., & Chan, H. L. (2010). The attachment of Fe3O4 nanoparticles to graphene oxide by covalent bonding. *Carbon,* 48(11), 3139-3144.

Heitzmann, M., Bucher, C., Moutet, J.-C., Pereira, E., Rivas, B. L., Royal, G., & Saint-Aman, E. (2007). Complexation of poly (pyrrole-EDTA like) film modified electrodes: Application to metal cations electroanalysis. *Electrochimica Acta,* 52(9), 3082-3087.

Hernández, J. C. R., Sánchez, M. S., Ribelles, J. L. G., & Pradas, M. M. (2007). Polymer–silica nanocomposites prepared by sol–gel technique: nanoindentation and tapping mode AFM studies. *European Polymer Journal,* 43(7), 2775-2783.

Hirsch, A. (2002). Functionalization of single-walled carbon nanotubes. *Angewandte Chemie International Edition,* 41(11), 1853-1859.

Hodkiewicz, J., & Scientific, T. (2010). Characterizing carbon materials with Raman spectroscopy. *application note,* 51946.

Huang, J., & Wan, Q. (2009). Gas sensors based on semiconducting metal oxide one-dimensional nanostructures. *Sensors,* 9(12), 9903-9924.

Huang, L., Huang, Y., Liang, J., Wan, X., & Chen, Y. (2011). Graphene-based conducting inks for direct inkjet printing of flexible conductive patterns and their applications in electric circuits and chemical sensors. *Nano Research,* 4(7), 675-684.

Huang, L., Zhuang, X., Hu, J., Lang, L., Zhang, P., Wang, Y., Jing, X. (2008). Synthesis of biodegradable and electroactive multiblock polylactide and aniline pentamer copolymer for tissue engineering applications. *Biomacromolecules,* 9(3), 850-858.

Ibupoto, Z., Khun, K., Beni, V., & Willander, M. (2013). Non-enzymatic glucose sensor based on the novel flower like morphology of nickel oxide. *Soft Nanoscience Letters,* 3(04), 46.

Jamshidian, M., Tehrany, E. A., Imran, M., Jacquot, M., & Desobry, S. (2010). Poly-Lactic Acid: production, applications, nanocomposites, and release studies. *Comprehensive Reviews in Food Science and Food Safety,* 9(5), 552-571.

Jang, H., Park, Y. J., Chen, X., Das, T., Kim, M. S., & Ahn, J. H. (2016). Graphene-based flexible and stretchable electronics. *Advanced Materials,* 28(22), 4184-4202.

Jem, K. J., van der Pol, J. F., & de Vos, S. (2010). *Microbial lactic acid, its polymer poly (lactic acid), and their industrial applications*. In *Plastics from bacteria* (pp. 323-346): Springer

Jiang, L., Zhang, J., & Wolcott, M. P. (2007). Comparison of polylactide/nano-sized calcium carbonate and polylactide/montmorillonite composites: reinforcing effects and toughening mechanisms. *Polymer,* 48(26), 7632-7644.

Jing, Y., Lin, E., Su, X., Liu, Y., Li, H., Yuan, X.,Fan, Y. (2016). Electrodeposition of Au nanoparticles on poly (diallyldimethylammonium chloride) functionalized reduced graphene oxide sheets for voltammetric determination of nicotine in tobacco products and anti-smoking pharmaceuticals. *RSC Advances,* 6(31), 26247-26253.

Joseph, P., Joseph, K., Thomas, S., Pillai, C., Prasad, V., Groeninckx, G., & Sarkissova, M. (2003). The thermal and crystallisation studies of short sisal fibre reinforced polypropylene composites. *Composites Part A: Applied Science and Manufacturing,* 34(3), 253-266.

Kaloni, P., & Mahajan, A. (2010). Stability and uniqueness of ferrofluids. *International Journal of Engineering Science,* 48(11), 1350-1356.

Kassaee, M., Motamedi, E., & Majdi, M. (2011). Magnetic Fe3O4-graphene oxide/polystyrene: fabrication and characterization of a promising nanocomposite. *Chemical Engineering Journal,* 172(1), 540-549.

Keeley, G. P., O'Neill, A., McEvoy, N., Peltekis, N., Coleman, J. N., & Duesberg, G. S. (2010). Electrochemical ascorbic acid sensor based on DMF-exfoliated graphene. *Journal of Materials Chemistry,* 20(36), 7864-7869.

Kim, I. H., & Jeong, Y. G. (2010). Polylactide/exfoliated graphite nanocomposites with enhanced thermal stability, mechanical modulus, and electrical conductivity. *Journal of Polymer Science Part B: Polymer Physics,* 48(8), 850-858.

Khalid, W. E. F. W., Heng, L. Y., & Arip, M. N. M. (2018). Surface modification of cellulose nanomaterial for urea biosensor application. *Sains Malaysiana,* 47(5), 941-949.

Kobashi, K., Villmow, T., Andres, T., & Pötschke, P. (2008). Liquid sensing of melt-processed poly (lactic acid)/multi-walled carbon nanotube composite films. *Sensors and Actuators B: Chemical,* 134(2), 787-795.

Kochmann, S. (2014). Graphene as a sensor material.

Kolb, E. S., Gaudiana, R. A., & Mehta, P. G. (1996). A new polymeric triarylamine and its use as a charge transport layer for polymeric LEDs. *Macromolecules,* 29(7), 2359-2364.

Kopinke, F.-D., Remmler, M., & Mackenzie, K. (1996). Thermal decomposition of biodegradable polyesters—I: Poly (β-hydroxybutyric acid). *Polymer Degradation and Stability,* 52(1), 25-38.

Krikorian, V., & Pochan, D. J. (2003). Poly (L-lactic acid)/layered silicate nanocomposite: fabrication, characterization, and properties. *Chemistry of Materials,* 15(22), 4317-4324.

Kruck, T. P., Lau, S.-J., & Sarkar, B. (1976). Molecular design to mimic the copper (II) transport site of human albumin: studies of equilibria between copper (II) and glycylglycyl-L-histidine-N-methyl amide and comparison with human albumin. *Canadian Journal of Chemistry,* 54(8), 1300-1308.

Kuilla, T., Bhadra, S., Yao, D., Kim, N. H., Bose, S., & Lee, J. H. (2010). Recent advances in graphene based polymer composites. *Progress in Polymer Science,* 35(11), 1350-1375.

Kumar, A., & Gupta, R. K. (2018). *Fundamentals of Polymer Engineering*: CRC Press.

Kumar, B., Castro, M., & Feller, J.-F. (2012). Poly (lactic acid)–multi-wall carbon nanotube conductive biopolymer nanocomposite vapour sensors. *Sensors and Actuators B: Chemical,* 161(1), 621-628.

Lasprilla, A. J., Martinez, G. A., Lunelli, B. H., Jardini, A. L., & Maciel Filho, R. (2012). Poly-lactic acid synthesis for application in biomedical devices—A review. *Biotechnology Advances,* 30(1), 321-328.

Laurent, C., Mauri, D., Kay, E., & Parkin, S. (1989). Magnetic properties of granular Co-polymer thin films. *Journal of Applied Physics,* 65(5), 2017-2020.

Lee, S.-H., & Wang, S. (2006). Biodegradable polymers/bamboo fiber biocomposite with bio-based coupling agent. *Composites Part A: Applied Science and Manufacturing,* 37(1), 80-91.

Lewandowska, K., Staszewska, D. U., & Bohdanecký, M. (2001). The Huggins viscosity coefficient of aqueous solution of poly (vinyl alcohol). *European Polymer Journal,* 37(1), 25-32.

Labanowski, J., Monna, F., Bermond, A., Cambier, P., Fernandez, C., Lamy, I., & Van Oort, F. (2008). Kinetic extractions to assess mobilization of Zn, Pb, Cu, and Cd in a metal-contaminated soil: EDTA vs. citrate. *Environmental Pollution,* 152(3), 693-701.

Lei, L., Qiu, J., & Sakai, E. (2012). Preparing conductive poly (lactic acid)(PLA) with poly (methyl methacrylate)(PMMA) functionalized graphene (PFG) by admicellar polymerization. *Chemical Engineering Journal,* 209, 20-27.

Lei, W., Si, W., Xu, Y., Gu, Z., & Hao, Q. (2014). Conducting polymer composites with graphene for use in chemical sensors and biosensors. *Microchimica Acta,* 181(7-8), 707-722.

Li, B., Dong, F.-X., Wang, X.-L., Yang, J., Wang, D.-Y., & Wang, Y.-Z. (2009). Organically modified rectorite toughened poly (lactic acid): Nanostructures, crystallization and mechanical properties. *European Polymer Journal,* 45(11), 2996-3003.

Li, W., Xu, Z., Chen, L., Shan, M., Tian, X., Yang, C., Qian, X. (2014). A facile method to produce graphene oxide-g-poly (L-lactic acid) as an promising reinforcement for PLLA nanocomposites. *Chemical Engineering Journal,* 237, 291-299.

Li, Z., Xie, C., Wang, J., Meng, A., & Zhang, F. (2015). Direct electrochemistry of cholesterol oxidase immobilized on chitosan–graphene and cholesterol sensing. *Sensors and Actuators B: Chemical,* 208, 505-511.

Lim, L.-T., Auras, R., & Rubino, M. (2008). Processing technologies for poly (lactic acid). *Progress in Polymer Science,* 33(8), 820-852.

Lin, M., Cho, M., Choe, W.-S., Son, Y., & Lee, Y. (2009). Electrochemical detection of copper ion using a modified copolythiophene electrode. *Electrochimica Acta,* 54(27), 7012-7017.

Lin, W.-Y., Shih, Y.-F., Lin, C.-H., Lee, C.-C., & Yu, Y.-H. (2013). The preparation of multi-walled carbon nanotube/poly (lactic acid) composites with excellent conductivity. *Journal of the Taiwan Institute of Chemical Engineers,* 44(3), 489-496.

Liu, L., Zachariah, M. R., Stoliarov, S. I., & Li, J. (2015). Enhanced thermal decomposition kinetics of poly (lactic acid) sacrificial polymer catalyzed by metal oxide nanoparticles. *RSC Advances,* 5(123), 101745-101750.

Liu, M., Liu, R., & Chen, W. (2013). Graphene wrapped Cu2O nanocubes: non-enzymatic electrochemical sensors for the detection of glucose and hydrogen peroxide with enhanced stability. *Biosensors and Bioelectronics,* 45, 206-212.

Llorens, E., Armelin, E., del Mar Pérez-Madrigal, M., del Valle, L., Alemán, C., & Puiggalí, J. (2013). Nanomembranes and nanofibers from biodegradable conducting polymers. *Polymers,* 5(3), 1115-1157.

Long, F., Zhu, A., Shi, H., Wang, H., & Liu, J. (2013). Rapid on-site/in-situ detection of heavy metal ions in environmental water using a structure-switching DNA optical biosensor. *Scientific Reports,* 3, 2308.

Lopes, M. S., Jardini, A., & Maciel Filho, R. (2012). Poly (lactic acid) production for tissue engineering applications. *Procedia Engineering,* 42, 1402-1413.

Lu, A. H., Salabas, E. e. L., & Schüth, F. (2007). Magnetic nanoparticles: synthesis, protection, functionalization, and application. *Angewandte Chemie International Edition,* 46(8), 1222-1244.

Lu, C. H., Yang, H. H., Zhu, C. L., Chen, X., & Chen, G. N. (2009). A graphene platform for sensing biomolecules. *Angewandte Chemie International Edition,* 48(26), 4785-4787.

Lü, K., Zhao, G., & Wang, X. (2012). A brief review of graphene-based material synthesis and its application in environmental pollution management. *Chinese Science Bulletin,* 57(11), 1223-1234.

Lu, T., Zhang, Y., Li, H., Pan, L., Li, Y., & Sun, Z. (2010). Electrochemical behaviors of graphene–ZnO and graphene–SnO2 composite films for supercapacitors. *Electrochimica Acta,* 55(13), 4170-4173.

Ma, X., & Pawlik, M. (2007). Intrinsic viscosities and Huggins constants of guar gum in alkali metal chloride solutions. *Carbohydrate Polymers,* 70(1), 15-24.

Mahobia, S., Bajpai, J., & Bajpai, A. K. (2016). An in-vitro investigation of swelling controlled delivery of insulin from egg albumin nanocarriers. *Iranian journal of pharmaceutical research: IJPR,* 15(4), 695.

Mai, F., Habibi, Y., Raquez, J.-M., Dubois, P., Feller, J.-F., Peijs, T., & Bilotti, E. (2013). Poly (lactic acid)/carbon nanotube nanocomposites with integrated degradation sensing. *Polymer,* 54(25), 6818-6823.

Mani, V., Dinesh, B., Chen, S.-M., & Saraswathi, R. (2014). Direct electrochemistry of myoglobin at reduced graphene oxide-multiwalled carbon nanotubes-platinum nanoparticles nanocomposite and biosensing towards hydrogen peroxide and nitrite. *Biosensors and Bioelectronics,* 53, 420-427.

Maniar, K. K. (2004). Polymeric nanocomposites: A review. *Polymer-Plastics Technology and Engineering,* 43(2), 427-443.

McKeon, K., Lewis, A., & Freeman, J. (2010). Electrospun poly (D, L-lactide) and polyaniline scaffold characterization. *Journal of Applied Polymer Science,* 115(3), 1566-1572.

Mehta, R., Kumar, V., Bhunia, H., & Upadhyay, S. (2005). Synthesis of poly (lactic acid): a review. *Journal of Macromolecular Science, Part C: Polymer Reviews,* 45(4), 325-349.

Misra, R., Fu, B. X., & Morgan, S. E. (2007). Surface energetics, dispersion, and nanotribomechanical behavior of POSS/PP hybrid nanocomposites. *Journal of Polymer Science Part B: Polymer Physics,* 45(17), 2441-2455.

Miyata, T., & Masuko, T. (1998). Crystallization behaviour of poly (L-lactide). *Polymer,* 39(22), 5515-5521.

Mohanty, S. P., & Kougianos, E. (2006). Biosensors: a tutorial review. *Ieee Potentials,* 25(2), 35-40.

Molinaro, S., Romero, M. C., Boaro, M., Sensidoni, A., Lagazio, C., Morris, M., & Kerry, J. (2013). Effect of nanoclay-type and PLA optical purity on the characteristics of PLA-based nanocomposite films. *Journal of Food Engineering,* 117(1), 113-123.

Mori, T., Nishida, H., Shirai, Y., & Endo, T. (2004). Effects of chain end structures on pyrolysis of poly (L-lactic acid) containing tin atoms. *Polymer Degradation and Stability,* 84(2), 243-251.

Mortazavi, B., Hassouna, F., Laachachi, A., Rajabpour, A., Ahzi, S., Chapron, D., Ruch, D. (2013). Experimental and multiscale modeling of thermal conductivity and elastic properties of PLA/expanded graphite polymer nanocomposites. *Thermochimica Acta,* 552, 106-113.

Murariu, M., Dechief, A. L., Bonnaud, L., Gallos, A., Fontaine, G., Bourbigot, S., & Dubois, P. (2010). The production and properties of polylactide composites filled with expanded graphite. *Polymer Degradation and Stability,* 95(5), 889-900.

Murariu, M., & Dubois, P. (2016). PLA composites: From production to properties. *Advanced Drug Delivery Reviews,* 107, 17-46.

Murariu, M., Ferreira, A. D. S., Degée, P., Alexandre, M., & Dubois, P. (2007). Polylactide compositions. Part 1: Effect of filler content and size on mechanical properties of PLA/calcium sulfate composites. *Polymer,* 48(9), 2613-2618.

Nampoothiri, K. M., Nair, N. R., & John, R. P. (2010). An overview of the recent developments in polylactide (PLA) research. *Bioresource Technology,* 101(22), 8493-8501.

Narimissa, E., Gupta, R. K., Kao, N., Nguyen, D. A., & Bhattacharya, S. N. (2014). Extensional Rheological Investigation of Biodegradable Polylactide-Nanographite Platelet Composites via Constitutive Equation Modeling. *Macromolecular Materials and Engineering,* 299(7), 851-868.

Neppalli, R., Causin, V., Marega, C., Modesti, M., Adhikari, R., Scholtyssek, S.,Marigo, A. (2014). The effect of different clays on the structure, morphology and degradation behavior of poly (lactic acid). *Applied Clay Science,* 87, 278-284.

Norazlina, H., & Kamal, Y. (2015). Graphene modifications in polylactic acid nanocomposites: A review. *Polymer Bulletin,* 72(4), 931-961.

Ojijo, V., & Ray, S. S. (2013). Processing strategies in bionanocomposites. *Progress in Polymer Science,* 38(10-11), 1543-1589.

Okada, A., Fukushima, Y., Kawasumi, M., Inagaki, S., Usuki, A., Sugiyama, S.,Kamigaito, O. (1988). Composite material and process for manufacturing same. Google Patents.

Oksman, K., Skrifvars, M., & Selin, J.-F. (2003). Natural fibres as reinforcement in polylactic acid (PLA) composites. *Composites Science and Technology,* 63(9), 1317-1324.

Okubo, K., Fujii, T., & Yamamoto, Y. (2004). Development of bamboo-based polymer composites and their mechanical properties. *Composites Part A: Applied Science and Manufacturing,* 35(3), 377-383.

Pal, A. K., & Katiyar, V. (2016). Nanoamphiphilic chitosan dispersed poly (lactic acid) bionanocomposite films with improved thermal, mechanical, and gas barrier properties. *Biomacromolecules,* 17(8), 2603-2618.

Pan, H.-j., Huang, H.-j., Zhang, L.-z., Qi, J.-y., & Cao, S.-k. (2005). Rheological properties of magnetorheological fluid prepared by gelatin—carbonyl iron composite particles. *Journal of Central South University of Technology,* 12(4), 411-415.

Patwa, R., Soundararajan, N., Mulchandani, N., Bhasney, S. M., Shah, M., Kumar, S., Katiyar, V. (2018). Silk nano-discs: A natural material for cancer therapy. *Biopolymers,* 109(11), e23231.

Pinto, A. M., Moreira, S., Gonçalves, I. C., Gama, F. M., Mendes, A. M., & Magalhães, F. D. (2013). Biocompatibility of poly (lactic acid) with incorporated graphene-based materials. *Colloids and Surfaces B: Biointerfaces,* 104, 229-238.

Pluta, M., Jeszka, J., & Boiteux, G. (2007). Polylactide/montmorillonite nanocomposites: structure, dielectric, viscoelastic and thermal properties. *European Polymer Journal,* 43(7), 2819-2835.

Pötschke, P., Andres, T., Villmow, T., Pegel, S., Brünig, H., Kobashi, K.,Häussler, L. (2010). Liquid sensing properties of fibres prepared by melt spinning from poly

(lactic acid) containing multi-walled carbon nanotubes. *Composites Science and Technology,* 70(2), 343-349.

Potts, J. R., Dreyer, D. R., Bielawski, C. W., & Ruoff, R. S. (2011). Graphene-based polymer nanocomposites. *Polymer,* 52(1), 5-25.

Pumera, M., Ambrosi, A., Bonanni, A., Chng, E. L. K., & Poh, H. L. (2010). Graphene for electrochemical sensing and biosensing. *TrAC Trends in Analytical Chemistry,* 29(9), 954-965.

Pyun, J. (2007). Nanocomposite materials from functional polymers and magnetic colloids. *Polymer Reviews,* 47(2), 231-263.

Qi, H., Mäder, E., & Liu, J. (2013). Unique water sensors based on carbon nanotube–cellulose composites. *Sensors and Actuators B: Chemical,* 185, 225-230.

Qureshi, A., Kang, W. P., Davidson, J. L., & Gurbuz, Y. (2009). Review on carbon-derived, solid-state, micro and nano sensors for electrochemical sensing applications. *Diamond and Related Materials,* 18(12), 1401-1420.

Rajeswari, N., Selvasekarapandian, S., Prabu, M., Karthikeyan, S., & Sanjeeviraja, C. (2013). Lithium ion conducting solid polymer blend electrolyte based on bio-degradable polymers. *Bulletin of Materials Science,* 36(2), 333-339.

Rahman, M., Ahammad, A., Jin, J.-H., Ahn, S. J., & Lee, J.-J. (2010). A comprehensive review of glucose biosensors based on nanostructured metal-oxides. *Sensors,* 10(5), 4855-4886.

Ramachandran, R., Mani, V., Chen, S.-M., Saraswathi, R., & Lou, B.-S. (2013). Recent trends in graphene based electrode materials for energy storage devices and sensors applications. *International Journal of Electrochemical Science,* 8(10), 11680-11694.

Raquez, J.-M., Habibi, Y., Murariu, M., & Dubois, P. (2013). Polylactide (PLA)-based nanocomposites. *Progress in Polymer Science,* 38(10-11), 1504-1542.

Ray, S. S., Yamada, K., Okamoto, M., Ogami, A., & Ueda, K. (2003). New polylactide/layered silicate nanocomposites, 4. Structure, properties and biodegradability. *Composite Interfaces,* 10(4-5), 435-450.

Reddy, M. M., Vivekanandhan, S., Misra, M., Bhatia, S. K., & Mohanty, A. K. (2013). Biobased plastics and bionanocomposites: Current status and future opportunities. *Progress in Polymer Science,* 38(10-11), 1653-1689.

Rhim, J.-W., Hong, S.-I., & Ha, C.-S. (2009). Tensile, water vapor barrier and antimicrobial properties of PLA/nanoclay composite films. *LWT-Food Science and Technology,* 42(2), 612-617.

Rhim, J.-W., Park, H.-M., & Ha, C.-S. (2013). Bio-nanocomposites for food packaging applications. *Progress in Polymer Science,* 38(10-11), 1629-1652.

Rinaldi, C., Chaves, A., Elborai, S., He, X. T., & Zahn, M. (2005). Magnetic fluid rheology and flows. *Current Opinion in Colloid & Interface Science,* 10(3-4), 141-157.

Rizvi, R., Kim, J.-K., & Naguib, H. (2010). The effect of processing and composition on the properties of polylactide–multiwall carbon nanotube composites prepared by solvent casting. *Smart Materials and Structures,* 19(9), 094003.

Russo, P. A., Donato, N., Leonardi, S. G., Baek, S., Conte, D. E., Neri, G., & Pinna, N. (2012). Room-temperature hydrogen sensing with heteronanostructures based on reduced graphene oxide and tin oxide. *Angewandte Chemie International Edition,* 51(44), 11053-11057.

Sabzi, M., Jiang, L., Liu, F., Ghasemi, I., & Atai, M. (2013). Graphene nanoplatelets as poly (lactic acid) modifier: Linear rheological behavior and electrical conductivity. *Journal of Materials Chemistry A,* 1(28), 8253-8261.

Sanchez-Garcia, M. D., Lopez-Rubio, A., & Lagaron, J. M. (2010). Natural micro and nanobiocomposites with enhanced barrier properties and novel functionalities for food biopackaging applications. *Trends in Food Science & Technology,* 21(11), 528-536.

Sasaki, K.-i., Tokura, Y., & Sogawa, T. (2013). The origin of Raman D band: bonding and antibonding orbitals in graphene. *Crystals,* 3(1), 120-140.

Seligra, P. G., Nuevo, F., Lamanna, M., & Famá, L. (2013). Covalent grafting of carbon nanotubes to PLA in order to improve compatibility. *Composites Part B: Engineering,* 46, 61-68.

Shahriary, L., & Athawale, A. A. (2014). Graphene oxide synthesized by using modified hummers approach. *International Journal of Renewable Energy and Environmental Engineering*, 2(01), 58-63.

Shayeh, J. S., Ehsani, A., Ganjali, M., Norouzi, P., & Jaleh, B. (2015). Conductive polymer/reduced graphene oxide/Au nano particles as efficient composite materials in electrochemical supercapacitors. *Applied Surface Science,* 353, 594-599.

Shen, Y., Jing, T., Ren, W., Zhang, J., Jiang, Z.-G., Yu, Z.-Z., & Dasari, A. (2012). Chemical and thermal reduction of graphene oxide and its electrically conductive polylactic acid nanocomposites. *Composites Science and Technology,* 72(12), 1430-1435.

Silvestre, C., Duraccio, D., & Cimmino, S. (2011). Food packaging based on polymer nanomaterials. *Progress in Polymer Science,* 36(12), 1766-1782.

Singh, V., Joung, D., Zhai, L., Das, S., Khondaker, S. I., & Seal, S. (2011). Graphene based materials: past, present and future. *Progress in Materials Science,* 56(8), 1178-1271.

Slezakova, K., Morais, S., & do Carmo Pereira, M. (2013). Atmospheric nanoparticles and their impacts on public health. InTech.

Södergård, A., & Stolt, M. (2002). Properties of lactic acid based polymers and their correlation with composition. *Progress in Polymer Science,* 27(6), 1123-1163.

Sokolowska, M., Krezel, A., Dyba, M., Szewczuk, Z., & Bal, W. (2002). Short peptides are not reliable models of thermodynamic and kinetic properties of the N-terminal metal binding site in serum albumin. *European Journal of Biochemistry,* 269(4), 1323-1331.

Sun, H., Wu, L., Wei, W., & Qu, X. (2013). Recent advances in graphene quantum dots for sensing. *Materials Today,* 16(11), 433-442.

Sundberg, M. W., Meares, C. F., Goodwin, D. A., & Diamanti, C. I. (1974). Selective binding of metal ions to macromolecules using bifunctional analogs of EDTA. *Journal of Medicinal Chemistry,* 17(12), 1304-1307.

Tamm, J., Hallik, A., Alumaa, A., & Sammelselg, V. (1997). Electrochemical properties of polypyrrole/sulphate films. *Electrochimica Acta,* 42(19), 2929-2934.

Taubner, V., & Shishoo, R. (2001). Influence of processing parameters on the degradation of poly (L-lactide) during extrusion. *Journal of Applied Polymer Science,* 79(12), 2128-2135.

Tesfaye, M., Patwa, R., Gupta, A., Kashyap, M. J., & Katiyar, V. (2017). Recycling of poly (lactic acid)/silk based bionanocomposites films and its influence on

thermal stability, crystallization kinetics, solution and melt rheology. *International Journal of Biological Macromolecules*, 101, 580-594.

Tesfaye, M., Patwa, R., Kommadath, R., Kotecha, P., & Katiyar, V. (2016). Silk nanocrystals stabilized melt extruded poly (lactic acid) nanocomposite films: Effect of recycling on thermal degradation kinetics and optimization studies. *Thermochimica Acta*, 643, 41-52.

Tong, X.-Z., Song, F., Li, M.-Q., Wang, X.-L., Chin, I.-J., & Wang, Y.-Z. (2013). Fabrication of graphene/polylactide nanocomposites with improved properties. *Composites Science and Technology,* 88, 33-38.

Tripathi, N., & Katiyar, V. (2016). PLA/functionalized-gum arabic based bionanocomposite films for high gas barrier applications. *Journal of Applied Polymer Science,* 133(21).

Valapa, R., Hussain, S., Iyer, P. K., Pugazhenthi, G., & Katiyar, V. (2015). Influence of graphene on thermal degradation and crystallization kinetics behaviour of poly (lactic acid). *Journal of Polymer Research,* 22(9), 175.

Valapa, R. B., Pugazhenthi, G., & Katiyar, V. (2015a). Effect of graphene content on the properties of poly (lactic acid) nanocomposites. *Rsc Advances,* 5(36), 28410-28423.

Valapa, R. B., Pugazhenthi, G., & Katiyar, V. (2015b). Fabrication and characterization of sucrose palmitate reinforced poly (lactic acid) bionanocomposite films. *Journal of Applied Polymer Science,* 132(3).

Van Gurp, M., & Palmen, J. (1998). Time-temperature superposition for polymeric blends. *Rheology Bulletin,* 67(1), 5-8.

Walha, F., Lamnawar, K., Maazouz, A., & Jaziri, M. (2016). Rheological, morphological and mechanical studies of sustainably sourced polymer blends based on poly (Lactic acid) and polyamide 11. *Polymers,* 8(3), 61.

Wall, M. (2011). The Raman Spectroscopy of Graphene and the Determination of Layer Thickness. *Thermo Scientific-Application Note,* 52252.

Wang, C., Zhang, L., Guo, Z., Xu, J., Wang, H., Zhai, K., & Zhuo, X. (2010). A novel hydrazine electrochemical sensor based on the high specific surface area graphene. *Microchimica Acta,* 169(1-2), 1-6.

Wang, G., Zhang, L., & Zhang, J. (2012). A review of electrode materials for electrochemical supercapacitors. *Chemical Society Reviews,* 41(2), 797-828.

Wang, H., & Qiu, Z. (2011). Crystallization behaviors of biodegradable poly (l-lactic acid)/graphene oxide nanocomposites from the amorphous state. *Thermochimica Acta,* 526(1-2), 229-236.

Wang, H., & Qiu, Z. (2012). Crystallization kinetics and morphology of biodegradable poly (l-lactic acid)/graphene oxide nanocomposites: Influences of graphene oxide loading and crystallization temperature. *Thermochimica Acta,* 527, 40-46.

Wang, N., Zhang, X., Ma, X., & Fang, J. (2008). Influence of carbon black on the properties of plasticized poly (lactic acid) composites. *Polymer Degradation and Stability,* 93(6), 1044-1052.

Wen, X., Zhang, K., Wang, Y., Han, L., Han, C., Zhang, H., . . . Dong, L. (2011). Study of the thermal stabilization mechanism of biodegradable poly (L-lactide)/silica nanocomposites. *Polymer International,* 60(2), 202-210.

Wu, D., Wu, L., Wu, L., Xu, B., Zhang, Y., & Zhang, M. (2007). Nonisothermal cold crystallization behavior and kinetics of polylactide/clay nanocomposites. *Journal of Polymer Science Part B: Polymer Physics,* 45(9), 1100-1113.

Wu, D., Wu, L., Zhang, M., & Zhao, Y. (2008). Viscoelasticity and thermal stability of polylactide composites with various functionalized carbon nanotubes. *Polymer Degradation and Stability,* 93(8), 1577-1584.

WU KT, K., & YAO, Y. (2001). Magnetic and optical properties of Fe 3 O 4 nanoparticle ferrofluids prepared by coprecipitation technique [J]. *IEEE Transactions on Magnetics,* 37(4), 2651-2653.

Xiao, L., Wang, B., Yang, G., & Gauthier, M. (2012). Poly (lactic acid)-based biomaterials: synthesis, modification and applications. *Biomedical Science, Engineering and Technology,* 11.

Xiao, Q., & Zhou, X. (2003). The study of multiwalled carbon nanotube deposited with conducting polymer for supercapacitor. *Electrochimica Acta,* 48(5), 575-580.

Xu, J.-Z., Chen, T., Yang, C.-L., Li, Z.-M., Mao, Y.-M., Zeng, B.-Q., & Hsiao, B. S. (2010). Isothermal crystallization of poly (l-lactide) induced by graphene nanosheets and carbon nanotubes: a comparative study. *Macromolecules,* 43(11), 5000-5008.

Xu, S., Habib, A. H., Pickel, A. D., & McHenry, M. E. (2015). Magnetic nanoparticle-based solder composites for electronic packaging applications. *Progress in Materials Science,* 67, 95-160.

Xu, X., Chen, X., Liu, A., Hong, Z., & Jing, X. (2007). Electrospun poly (L-lactide)-grafted hydroxyapatite/poly (L-lactide) nanocomposite fibers. *European Polymer Journal,* 43(8), 3187-3196.

Xu, X., Yang, Q., Wang, Y., Yu, H., Chen, X., & Jing, X. (2006). Biodegradable electrospun poly (L-lactide) fibers containing antibacterial silver nanoparticles. *European Polymer Journal,* 42(9), 2081-2087.

Yáñez-Sedeño, P., Campuzano, S., & Pingarrón, J. M. (2017). Electrochemical sensors based on magnetic molecularly imprinted polymers: A Review. *Analytica Chimica Acta,* 960, 1-17.

Yogeswaran, U., & Chen, S.-M. (2008). A review on the electrochemical sensors and biosensors composed of nanowires as sensing material. *Sensors,* 8(1), 290-313.

Yoon, J. T., Lee, S. C., & Jeong, Y. G. (2010). Effects of grafted chain length on mechanical and electrical properties of nanocomposites containing polylactide-grafted carbon nanotubes. *Composites Science and Technology,* 70(5), 776-782.

Yoon, O. J., Jung, C. Y., Sohn, I. Y., Kim, H. J., Hong, B., Jhon, M. S., & Lee, N.-E. (2011). Nanocomposite nanofibers of poly (D, L-lactic-co-glycolic acid) and graphene oxide nanosheets. *Composites Part A: Applied Science and Manufacturing,* 42(12), 1978-1984.

Yu, L., Wu, H., Wu, B., Wang, Z., Cao, H., Fu, C., & Jia, N. (2014). Magnetic Fe 3 O 4-reduced graphene oxide nanocomposites-based electrochemical biosensing. *Nano-Micro Letters,* 6(3), 258-267.

Yu, T., Ren, J., Li, S., Yuan, H., & Li, Y. (2010). Effect of fiber surface-treatments on the properties of poly (lactic acid)/ramie composites. *Composites Part A: Applied Science and Manufacturing,* 41(4), 499-505.

Yuan, Q., Awate, S., & Misra, R. (2006). Nonisothermal crystallization behavior of polypropylene–clay nanocomposites. *European Polymer Journal,* 42(9), 1994-2003.

Yuan, W., Liu, A., Huang, L., Li, C., & Shi, G. (2013). High-performance NO2 sensors based on chemically modified graphene. *Advanced materials,* 25(5), 766-771.

Yuzay, I. E., Auras, R., Soto-Valdez, H., & Selke, S. (2010). Effects of synthetic and natural zeolites on morphology and thermal degradation of poly (lactic acid) composites. *Polymer Degradation and Stability,* 95(9), 1769-1777.

Zaidi, L., Kaci, M., Bruzaud, S., Bourmaud, A., & Grohens, Y. (2010). Effect of natural weather on the structure and properties of polylactide/Cloisite 30B nanocomposites. *Polymer Degradation and Stability,* 95(9), 1751-1758.

Zhang, Y., Liu, Y., Su, L., Zhang, Z., Huo, D., Hou, C., & Lei, Y. (2014). CuO nanowires based sensitive and selective non-enzymatic glucose detection. *Sensors and Actuators B: Chemical,* 191, 86-93.

Zhang, Y., Li, H., Pan, L., Lu, T., & Sun, Z. (2009). Capacitive behavior of graphene–ZnO composite film for supercapacitors. *Journal of Electroanalytical Chemistry,* 634(1), 68-71.

Zhang, Y., Yang, Z., Yin, D., Liu, Y., Fei, C., Xiong, R., . . . Yan, G. (2010). Composition and magnetic properties of cobalt ferrite nano-particles prepared by the co-precipitation method. *Journal of Magnetism and Magnetic Materials,* 322(21), 3470-3475.

Zhao, N., Shi, S., Lu, G., & Wei, M. (2008). Polylactide (PLA)/layered double hydroxides composite fibers by electrospinning method. *Journal of Physics and Chemistry of Solids,* 69(5), 1564-1568.

Zheng, G., Wu, J., Wang, W., & Pan, C. (2004). Characterizations of expanded graphite/polymer composites prepared by in situ polymerization. *Carbon,* 42(14), 2839-2847.

Research Outputs

Book Chapter

1. G. Chakraborty, P. Bhagabati and V. Katiyar, Author's viewpoint on the developments of biodegradable polymers to improve their versatility in food packaging, , Biobased plastics for food packaging applications, Smithers Pira, 2017, (eBook ISBN: 978-1-91024-259-9, Hardback: 978-1-91024-258-2)

2. G. Chakraborty, V. Katiyar, Biobased Polymeric Conductive Materials for Advanced Applications, Advances in sustainable polymers: Processing and Applications, Springer (Under Review)

Journal Publication

1. Chakraborty, G., Valapa, R. B., Pugazhenthi, G., & Katiyar, V. (2018). Investigating the properties of poly (lactic acid)/exfoliated graphene based nanocomposites fabricated by versatile coating approach. *International Journal of Biological Macromolecules*, 113, 1080-1091.

2. Chakraborty, G., Gupta, A., Pugazhenthi, G., & Katiyar, V. (2018). Facile dispersion of exfoliated graphene/PLA nanocomposites via in situ polycondensation with a melt extrusion process and its rheological studies. *Journal of Applied Polymer Science*, 135(33), 46476.

3. Chakraborty, G., Pugazhenthi, G., & Katiyar, V. (2019). Exfoliated graphene-dispersed poly (lactic acid)-based nanocomposite sensors for ethanol detection. *Polymer Bulletin*, 76(5), 2367-2386.

4. Borkotoky, S. S., **Chakraborty, G.,** & Katiyar, V. (2018). Thermal degradation behaviour and crystallization kinetics of poly (lactic acid) and cellulose nanocrystals

(CNC) based microcellular composite foams. *International Journal of Biological Macromolecules*, 118, 1518-1531.

5. Chakraborty, G., Dhar, P., Pugazhenthi, G., & Katiyar, V. (2019). Applicability of Fe-CNC/GR/PLA Composite as Potential Sensor for Biomolecules. Journal of Materials Science: Materials in Electronics (Under Review)

6. Chakraborty, G., Pugazhenthi, G., & Katiyar, V, Improvisation of Polylactic acid (PLA)/Exfoliated graphene (GR) Nanocomposite for Detection of Metal ions (Cu^{2+}) (to be communicated).

7. Chakraborty, G., Narendren, S., Pugazhenthi, G., & Katiyar, V, Development of vapour sensor by IDE electrode using 3D-printed chamber (to be communicated).

Conference Proceedings

1. Gourhari Chakraborty, Ravi Babu Valapa, Gopal Pugazhenthi, Vimal Katiyar, Review on PLA based nanocomposites for versatile application, *Advances in sustainable polymers (ASP-15)*, January 21-22, 2015, Guwahati, India

2. Gourhari Chakraborty, Ravi Babu Valapa, Gopal Pugazhenthi, Vimal Katiyar. Properties of PLA/Graphene Nanocomposite Prepared by Melt Processing Technique, *CHEMCON 2015*, December 27-30, 2015, Guwahati, India

3. Gourhari Chakraborty, Gopal Pugazhenthi, Vimal Katiyar, PLA based conductive biomaterial for the detection of liquid solvents, *Advances in sustainable polymers (ASP-16)*, August 3-6, 2016, Kyoto, Japan

4. Gourhari Chakraborty, Gopal Pugazhenthi, Vimal Katiyar, Poly lactic acid (PLA) based conductive biomaterial for the detection of Alcohols, *MACRO-2017*, January 9-11, 2017, Thiruvananthapuram, Kerala, India

5. Gourhari Chakraborty, Prodyut Dhar, Gopal Pugazhenthi, Vimal Katiyar, Developement of Fe-Cellulose Nanocrystal (Fe-CNC) based thin polymeric film for

ethanol sensing, *International Symposium on Advances in Sustainable Polymers, ASP-17*, January 8-11, 2018, Guwahati, India (2nd Best Poster Award)

6. Gourhari Chakraborty, Gopal Pugazhenthi, Vimal Katiyar, Developement of thin Bio based polymeric film sensor for detection of sucrose, *Indo-Japan Bilateral Symposium on Future Perspective of Bioresource Utilization in North-East India (IJBS-17)*, February 1-4, 2018, Guwahati, India.

7. Gourhari Chakraborty, Gopal Pugazhenthi, Vimal Katiyar, Studies on melt rheology of biodegradable polymeric composite fabricated by extrusion technique, *Indo-Japan Bilateral Symposium on Future Perspective of Bioresource Utilization in North-East India (IJBS-17)*, February 1-4, 2018, Guwahati, India, (2nd Best Poster award)

8. Gourhari Chakraborty, Gopal Pugazhenthi, Vimal Katiyar, Development of Thin Polymeric Film sensor for Ethanol Sensing, *Research Conclave-18(RC-18)*, Guwahati, India, March 8-11, 2018.

9. Gourhari Chakraborty, Gopal Pugazhenthi, Vimal Katiyar, Development of biobased thin film sensor for biochemicals, *Kathmandu Symposia on Advanced Materials-2018 (KaSAM-2018)*, October 26-29, 2018, Kathmandu, Nepal (Onyx Group Nutriset Award for best poster presentation)

10. Gourhari Chakraborty, Gopal Pugazhenthi, Vimal Katiyar, Poly (lactic acid)/Graphene based thin film Sensors for Ethanol Detection, *Kathmandu Symposia on Advanced Materials-2018 (KaSAM-2018)*, October 26-29, 2018, Kathmandu, Nepal

11. Gourhari Chakraborty, Gopal Pugazhenthi, Vimal Katiyar, Effect of dispersion of graphene on thermal stability and dynamic mechanical properties of melt processed PLA*, 257th ACS National Meeting*, March 31- April 04, 2019, Orlando, Florida.